Study of the hydrodynamic characteristics, COD elimination and nitrification in a new multi-section bioreactor

Haoran Pang

Université de Toulouse

THÈSE

En vue de l'obtention du

DOCTORAT DE L'UNIVERSITÉ DE TOULOUSE

Délivré par :
Institut National des Sciences Appliquées de Toulouse (INSA Toulouse)

Discipline ou spécialité :

Génie des Procédés et Environnement

Présentée et soutenue par :
PANG HAORAN

le : mercredi 19 mars 2014

Titre :

Etude de l'hydrodynamique, de l'élimination de la DCO et de la nitrification d'un nouveau lit bactérien segmenté

JURY

Michel ROUSTAN, Professeur, Président du Jury
Alain GRASMICK, Professeur, Rapporteur
Nicolas BERNET, Professeur, Rapporteur
Gilles HEBRARD, Professeur, Examinateur

Ecole doctorale :
Mécanique, Energétique, Génie civil et Procédés (MEGeP)

Unité de recherche :
LISBP EAD9

Directeur(s) de Thèse :
Etienne PAUL, Professeur, Directeur de thèse
Valérie LETISSE, Professeur, Co-Directeur de thèse

Rapporteurs :
Nicolas BERNET, Professeur, INRA
Alain GRASMICK, Professeur, Université de Montpellier II

Study of the hydrodynamic characteristics, COD elimination and nitrification in a new Multi-section Bioreactor

Thesis submitted to the
National Institute of Applied Science, Toulouse
for award of the degree
of

Doctor of Environmental Engineering

By

Haoran PANG

March, 2014

Résumé:

L'objectif principal de ce travail de thèse concerne l'étude de l' élimination de la DCO et de la nitrification dans une nouveau lit bactérien Multi-Section (MSB) . Après une caractérisation de l'hydrodynamique et du transfert d'oxygène de ce lit bactérien, les expériences biologiques menées sous des conditions opératoires contrastées (fortes et faibles charges organiques et eaux usées contenant ou pas des matières particulairs) ont été menées. En parallèle, des simulations avec le logiciel Biowin® ont été réalisées. Les principaux résultats sont résumés en suivant :

- La rétention de liquide statique est majoritaire par rapport à la rétention dynamique que ce soit en présence ou en absence de biofilm. Le biofilm joue le rôle d'une "éponge" permettant un maintien de l'humidité du lit même à faible débit. Les expériences de DTS ont montré que le biofilm accroit le temps de séjour du liquide et conduit à une diminution de l'épaisseur du film liquide permettant ainsi de promouvoir le transfert de l'oxygène.
- Le réacteur MSB montre une élimination efficace de la DCO (> 95 %) et de la nitrification (> 60 % de l'azote entrant), mais une accumulation de DCO particulaire a lieu dans le filtre ce qui conduira à un colmatage à terme. La nitrification cohabite avec l'élimination de la DCO même dans la première section et pour une charge organique élevée ce qui implique une bonne capacité d'oxygénation du MSB par l'aération naturelle.
- Un modèle dynamique de MSB a été utilisé implémenté sur le simulateur - BioWin® , afin d'obtenir la répartition des biomasses au sein du réacteur et d'évaluer le processus limitant dans chaque section. Le modèle partiellement calibré peut aider à estimer les besoins minimum d'oxygène pour la nitrification et peut rendre compte de la compétition entre la croissance hétérotrophe et la nitrification.

Mots-Clés:

Traitement décentralisé des eaux usées, lit bactérien, hydrodynamique, distribution des temps de séjour (DTS), épaisseur de film liquide, transfert d'oxygène, nitrification, élimination de l'azote, simulation

Abstract:

The main objective of this PhD work focused on the study of the COD removal and nitrification in a new designed Multi-Section Bioreactor (MSB). Hydrodynamic characterization of the reactor, biological experiments under contrasted conditions and simulations by Biowin® software were carried out:

- Firstly, it was found that static liquid retention is the predominant part both without and with the presence of biofilm. Biofilm acts like a "sponge". RTD experiments showed that biofilm can promote liquid residence time, decrease the liquid film and promote the oxygen transfer consequently.
- Secondly, the MSB operated at contrasted organic loading rate (OLRs) and nitrogen loading rate (NLRs) showed that COD can be effectively removed (removal efficiency > 95%) and nitrification (> 60% of the N removal) occurred in this biofilter. Nitrification is efficient even in the first section implying no drastic oxygen limitation though only natural aeration is occurring.
- Thirdly, a TF dynamic model has been used from a simulator - BioWin, in order to get more insights on the biomass distribution in the pilot and to assess the limiting process in each section of the bioreactor. Calibration of the model can help us to estimate the minimum oxygen requirement for nitrification for each zone inside the pilot and it can well represent the competition between heterotrophic growth and nitrification.

Key words:

Decentralized wastewater treatment, trickling filter, hydrodynamic, residence time distribution (RTD), oxygen transfer, nitrification, nitrogen removal, simulation, Biowin® software

Acknowledgement

I would like to express my deep and sincere gratitude to my Supervisors Prof. Etienne PAUL and Prof. Valerie LETISSE for their valuable guidance, inspiration, constant encouragement and heartfelt good wishes. Their genuine interest in the research topics, free accessibility for discussion sessions, thoughtful and timely suggestions has been the key source of inspiration for this work. I feel indebted to both my supervisors for giving abundant freedom to me for pursuing new ideas. It was overall a great experience of working with both of them.

I record my sincere thanks and gratitude to Prof. Gilles HEBRARD, for his cordial advice and suggestions on hydrodynamic experiments and simulations, and continued encouragement throughout all this work. Not to mention those valuable guidance, inspiration, constant encouragement and heartfelt good wishes for my publications and for the presentations during my works.

My special thanks to my colleagues Mañas Angela., Irene Mozo., Yoan Pechaud, Matthieu Peyrela for their help in performing various experiments and modeling work.

I express my special thanks to my friend Chengcheng LI for his readiness to help for anything and everything for the current work.

I remain ever grateful to our technical staffs Mr. Mansour Bounouba and Mr. Evrard Mengelle for their assistance in experimental work.

Finally, I would like to thank my family in China, for their patience and support for this thesis, I owe them so much. The thesis would remain incomplete without mentioning the contributions of my parents for making me what I am today.

(Haoran PANG)

Nomenclature

Greek letter

φ_{cb}:	Apparent packing-bed void fraction	(-)
ε:	Total packed bed void fraction	(-)
ε' :	Particle porosity	(-)
d_p:	Equivalent sphere diameter	(cm)
Φ:	Sphericity of particle	(-)
σ:	Liquid surface tension	($N \cdot m^{-1}$)
σ^2:	Variance of calculated RTD from experimental RTD	(-)
ρ_L:	Liquid density	($kg \cdot m^{-3}$)
$\rho_{particle}$:	Particle density	($kg \cdot m^{-3}$)
α:	Contact angle between the liquid and solid sphere	(°)
δ_L:	Liquid film thickness	(mm)
β_d:	Liquid dynamic retention (dynamic volume/pure solid volume)	(-)
β_s:	Liquid static retention (static volume/pure solid volume)	(-)
β_t:	Total liquid retention (total liquid volume/pure solid volume)	(-)
τ:	Theoretical liquid residence time	(s)
τ_H:	Hydraulic residence time	(s)
τ_p:	Shear stress	(Pa)
μ:	Mean liquid residence time from RTD curves	(s)
μ_{max}:	Maximum specific heterotrophic/autotrophic growth rate	(d^{-1})
μ_H:	Specific heterotrophic growth rate	(d^{-1})
μ_A:	Specific autotrophic growth rate	(d^{-1})
θ:	Dimensionless time	(-)
ν :	Kinematic viscosity	(m^2/s)
θ_d:	Sludge retention time	(d)

Latin letter

b_H:	Heterotrophic decay rate	(d^{-1})
b_A:	Autotrophic decay rate	(d^{-1})
h_{Lt}:	Total liquid holdup	(m^3)
h_{LS}:	Liquid static holdup	(m^3)
h_{Ld}:	Liquid dynamic holdup	(m^3)
hl_{pore}:	Pore holdup	(-)
hl_{cap}:	Capillary rise holdup	(-)
hl_{res}:	Residual holdup	(-)
h_{cap}:	Liquid capillary rise height	(m)
$h_{in.cap}$:	Internal capillary rise height of single particle	(m)
$h_{ex.cap}$:	External capillary rise height of single particle	(m)
$m_{in.cap}$:	Liquid internal capillary mass of the packed bed	(kg)
$m_{ex.cap}$:	Liquid external capillary mass of the packed bed	(kg)
h_{cb}:	Height of packed bed	(m)
m_{DP}:	Total dry packing mass	(kg)
$m_{LS:}$	Liquid static holdup mass	(kg)
m_{fd}:	Fast dynamic holdup mass	(m^3)
m_{sd}:	Slow dynamic holdup mass	(m^3)
F_{ad}:	Liquid adsorption fraction of the medium volume	(-)

Q:	Volumetric flow rate	($m^3 \cdot h^{-1}$)
V_{Lt}:	Total liquid holdup volume	(m^3)
V_{LS}:	Liquid static holdup volume	(m^3)
V_{Ld}:	Liquid dynamic holdup volume	(m^3)
V_{solid}:	Pure solid volume	(m^3)
$V_{p,L}$:	Liquid volume around single particle	(m^3)
$V_{effective}$:	Effective liquid volume involved in RTD curves	(m^3)
$N_{particles}$:	Number of particles	(-)
m:	Fraction of active zone in packed bed	(-)
f_W	Wetting fraction of the packed bed	(-)
f_{LSE}	Fraction of partial static holdup volume of tracer exchange	(%)
L_f:	Biofilm thickness	(mm)
Sh:	Sherwood number	(-)
Re:	Reynolds number	(-)
Sc:	Schmidt number	(-)
S	Soluble substrate concentration	(g/m^3)
X:	Biomass concentration	(g/m^3)
Ks:	Substrate half-saturation coefficient	(g/m^3)
b_H:	Decay rate of heterotrophic biomass	(d^{-1})
K_H:	Hydrolysis rate	(d^{-1})
K_S:	Carbon substrate half saturation coefficient	($gCOD/m^3$)
K_O:	Oxygen half saturation coefficient	(gO_2/m^3)
K_{NH}:	Ammonia half saturation coefficient	(gN/m^3)
Ds :	Mass diffusivity coeffecient	(m^2/s)
D_O :	Oxygen diffusivity coeffecient	(m^2/s)
D_{NH} :	Ammonia diffusivity coeffecient	(m^2/s)
Su	Soluble inert organics	(mg/L)
S_B	Readily biodegradable substrate	(mg/L)
Xu	Particulate inert organics	(mg/L)
X_B	Slowly biodegradable substrate	(mg/L)
Xoho	Active heterotrophic biomass	(mg/L)
Xba	Active autotrophic biomass	(mg/L)
Xu,e	Unbiodegradable particulates from cell decay	(mg/L)
Xsto	Cell internal storage product	(mg/L)
ISS	Cell internal storage product	(mg/L)
So	Dissolved oxygen	(gO_2/m^3)
Sno	Nitrate and nitrite N	(gN/m^3)
Snh	Free and ionized ammonia	(gN/m^3)
Snd	Soluble biodegradable organic nitrogen (in S_B)	(gN/m^3)
Xnd	Particulate biodegradable organic nitrogen (in X_B)	(gN/m^3)
Snn	Dinitrogen	(gN/m^3)
salk	Alkalinity	($mole/m^3$)
Xii	Inert inorganic suspended solids	(g/m^3)
Y_H:	Heterotrophic yield coefficient	-
Y_A:	Autotrophic yield coefficient	(gCOD/gN)
Yg,obs	Observed growth yield coefficient	-

Abbreviation

P.E.:	Per Equivalent	
SA:	Total surface area of packed bed	(m^2)
SSA:	Specific surface area	(m^2/m^3)
SA_{eff}:	Effective surface area of packed bed	(m^2)
S.H.L:	Surface hydraulic loads	($m \cdot h^{-1}$)
HLR:	Hydraulic loading rate	($m \cdot h^{-1}$)
OLR:	Organic loading rate	($m \cdot h^{-1}$)
OUR:	Oxygen Uptake Rate	(mgO/L/h)
WWTP:	Waste Water Treatment Plant	
CWWTP	Central Waste Water Treatment Plant	
OWTS:	On-site Wastewater Treatment System	
STEP:	Septic Tank Effluent Pumping System	
SP:	Stabilization Ponds	
SBR:	Sequence Batch Reactor	
BFR:	Biofilm Fluidized Bed reactors	
UASB:	Upflow Anaerobic Sludge Blanket reactor	
BASR:	Biofilm Airlift Suspension Reactor	
AS:	Activated Sludge	
TF:	Trickling Filter	
TFC:	Trickling Fixed-bed Column	
MSB:	Multi-Section Bioreactor	
RTD:	Residence Times Distribution	
PF:	Plug Flow	
CSTR:	Continuous Stirred-Tank Reactor	
HRT:	Hydraulic Retention Time	(h or s)
LRT:	Liquid Residence Time	(h or s)
SRT:	Sludge Retention Time	(d or h)
COD:	Chemical Oxygen Demand	
CODt:	Total COD	
CODs:	Soluble COD	
CODp:	Particulate COD	
BOD:	Biological Oxygen Demand	
BOM:	Biological Organic Matter	
EPS:	Extracellular Polymeric Substances	
TKN:	Total Kjeldahl Nitrogen	
TKNt:	Total Kjeldahl Nitrogen	
TKNs:	Soluble Kjeldahl Nitrogen	
N-NOx:	Nitrite and nitrate nitrogen	
OHO:	Ordinary Heterotrophic Organisms	
AOB:	Ammonia Oxidizing Biomass	
NOB:	Nitrite Oxidizing Biomass	

List of Tables and Figures

Contents

Preface

What is a "Decentralized" wastewater system?

The terms "Decentralized" and "Onsite" are often used interchangeably. However, a "Decentralized" system also refers to the use of onsite or cluster systems to treat all of the wastewater collectively generated by many homes or an entire community. Rather than operating a centralized wastewater treatment system where all sewage flows to one treatment plant, most rural communities today still use a decentralized wastewater treatment approach, traditionally with one onsite system per household, though few local leaders would ever think of their community as having a decentralized system.

What is the state of the art of decentralized treatment approach?

In the introduction to the book “Small and decentralized wastewater management systems”, Crites and Tchobanoglous (1998), the authors wrote: “A decentralized approach towards wastewater management is increasingly recognized to offer an affordable and appropriate solution to the collection and disposal of wastewater for peri-urban and small rural communities. The wide range of technologies that are appropriate for decentralized systems enables flexibility in the planning and design process which may result in a solution that is more appropriate to local conditions and resources. These technologies can form important components of environmental control strategies to mitigate pollution and improve the quality of the environment and natural water resources.”

What are the technologies available for decentralized treatment systems?

A decentralized system employs a combination of onsite and/or cluster systems and is used to treat and dispose of wastewater from dwellings and businesses close to the source.
Decentralized wastewater systems allow for flexibility in wastewater management, and different parts of the system may be combined into “treatment trains,” or a series of processes to meet treatment goals, overcome site conditions, and to address environmental protection requirements. Managed decentralized wastewater systems are viable, long-term alternatives to

centralized wastewater treatment facilities, particularly in small and rural communities where they are often most cost-effective.

Onsite systems now include a number of alternatives that surpass conventional septic tank and drain field systems in their ability to treat waste water. Alternative onsite processes, such as sand filters, peat filters, aerobic treatment units, pressure distribution systems, drip irrigation, and disinfection systems, can be employed in a wide range of soil and site conditions. Alternative systems require more monitoring and maintenance, making a strong case for these systems to be managed.

Is the Trickling filter a potential effective reactor for treatment of WW in rural and decentralized systems?

Trickling Filters (TF) were a common technology for treating municipal wastewater before cities began using activated sludge aeration systems. Now, many homes and businesses use trickling filters in on-site wastewater treatment systems. TF is suitable in areas where large tracts of land are not available for a treatment system. It may qualify for equivalent secondary discharge standards; they are effective in treating high concentrations of organic material depending on the type of medium used. They provide high performance reliability and ability to handle and recover from shock loads. This technology requires relatively low power. The level of skill and technical expertise needed to manage and operate the system.

The advantages for TF applied for on-site/decentralized wastewater treatment are: Low maintenance costs; Low energy usage; Small footprint; Modular design enables phased construction; Durable fiberglass construction; Can be sealed and insulated for seasonal conditions;

What is known in the field of TF technologies and what remains to be investigated?

For a conventional TF, it is known now that the mass transfer is the main limiting factor for biological substrate biodegradation. Furthermore, physiochemical factors that affect the mass transfer such as liquid film thickness, liquid residence time, wetting fraction, biofilm thickness, substrate diffusion rate have sometimes been investigated. In addition, the hydrodynamic characteristics and models of TF have been widely investigated; it is known

that the liquid distribution inside a TF is close to Plug Flow pattern and that the liquid residence time is correlated with the dynamic retention. The ASM models are widely applied in the TF simulators and modeling. However, some drawbacks still exist to represent the actual processes in a TF because this system is usually more complex than activated sludge systems.

The closed structure makes it necessary to be combined with a forced aeration device to fulfill the oxygen demand for substrate biodegradation and effective nitrification if the organic loads are relative high, causing more energy consumption. The disadvantage is that trickling filters contain less surface area per unit volume for attached growth of aerobic organisms. This means that greater depth of filter or recirculation of the waste back through the filter may be necessary to achieve adequate treatment of the waste. Alternatively, forced aeration may be combined with the coarser medium to create what is termed an aerobic packed bed bioreactor.

What are the objectives of this PhD?

The aim of this thesis is to characterize and better understand a new type of Trickling Filter (called in this PhD, the Multi-Section Bioreactor (MSB) to treat rural or decentralized wastewaters, taking as objectives both organic substrate removal and full nitrification. To treat this type of wastewater by a MSB, the characteristics of rural wastewater should first be investigated in terms of its constituents, flow and mass loading fluctuation.

In this PhD thesis, Chapter 1 reviewed the techniques applied in rural wastewater treatment, the Trickling Filter approach in particular. The physical processes and kinetics of mass transformation were then recalled. Based on classic design criterion, a Multi-Section Bioreactor pilot for this PhD study was dimensioned. Biowin simulator was introduced to modeling the MSB performance. Finally, typical rural wastewater characteristics were reviewed.

Chapter 2 represents the methods to determine the physical properties of Concrete Brick medium applied in this study, such as volumetric method. Then the hydrodynamic experiments, such as drainage method, RTD were applied, to investigate the liquid holdup and retention behaviors inside our pilot in the cases with and without biofilm. The methods that investigate both COD removal and nitrification performances were then introduced. Parameters setting and adjustments by Biowin software were then detailed described.

Chapter 3 reported the hydrodynamic behaviors of our pilot, such as liquid static and dynamic holdup fractions, static holdup modeling, liquid residence time, RTD curves, liquid film thickness estimation, and oxygen transfer coefficient estimation.

Chapter 4 investigates the COD removal and nitrification performances of 3 different periods, under different OLRs, but at same flowrate. Both global and local performances were reported, for COD and nitrogen. Then the connection between hydrodynamic behaviors and biological experiments was proposed, recalled the biofilm thicknesses and LRTs.

In Chapter 5, 3 groups of simulations for MSB and mono-stage TF were carried out, including a group of simulations with same OLR and NLR, but at different input substrate concentrations and flowrates to investigate the organic and hydraulic conditions on the carbon removal and nitrification performances of our pilot; a group under different air input flow rates and oxygen input concentrations for oxygen modeling to understand the oxygen limitation conditions for our pilot; another group was attempt to fit the biological experiments by adjusting oxygen effect to better understand how the Biowin simulator can predict the real biological performance, to promote the carbon removal and nitrification.

Chapter 1

Bibliography

Part 1: Treatment systems used for macro-pollutants removal in decentralized area

1. Overview of treatment techniques

Wastewater treatment can be based on physical, chemical or biological treatment. For rural or decentralized wastewater treatment, typically systems serve usually fewer than 10,000 people located in rural or remote location. Because in these areas it is not feasible to connect to a larger centralized Publically-Owned Treatment Works (POTW), simple wastewater treatment systems and land disposal systems are usually applied.

1.1 Technologies for rural wastewater treatment

Technologies currently employed for rural wastewater treatment in different countries are summarized in Table I-1.

In this table, the treatment systems can be divided into two main domains: The first one uses mechanical means to create the contact between wastewater, microbial cells and oxygen, such as Activated Sludge (AS), Trickling filter (TF), Rotating Bioreactor (RBC) and their developed approaches; A second are those where natural or ecological transformations occur (Burkhard et al. 2000), such as Constructed Wetland, Ponds. Concerning their application in the rural or decentralized wastewater treatment field, these technical alternatives have to be evaluated regarding plant size, operation safety, reliability, demand for skilled personnel, investment and operation costs (Boller, 1997).

Another division criterion is based on the state of the biomass that can be in suspension in the liquid or attached on supports. Attached film (Fixed-film) systems are usually biological processes that employ a medium such as rock, plastic, wood and other natural or synthetic solid material that support biomass on its surface and within its porous structure.

Generally, the selection of treatment system is normally based on several factors: 1. Community layout; 2. Housing density; 3. Terrain (topography); 4. Financial constraints; 5. Political constraints.

Table I- 1: Technologies currently employed in rural wastewater treatment

Country	Ref.	Tech. currently applied	Status
China	(ZHOU et al, 2010)	STEPs, SP, CW, MBR, Earthworm Biofilter	3% of village and 12% of towns treated by 2005
France	(Payne, 1993) (Payne et al, 1995)	STEPs, OWTS, CW, WSP, ISF, RBF	17% are treated by 2002
U.K.	(Arja, 2007) (Roland et al, 2000)	RBC, AS, lagoons, cesspools, STEPs, SABF,SBR, CW, Sand Filter	98% of the national population connected to WWTP, 2% adoptable to OWTS
Germany	(Qin, 1998)	STEPs, SP, AP, RBC, SBR, MBR	93% of the national population connected to WWTP
U.S.A.	(Susan, 2008)(Don et al, 2007)	OWTS，RBF, RBC	25% connected to OWTS by 1997
Finland	(Arja, 2007)	STEPs, AS, SF, RBC, package-plant,	350 000 OWTS serving permanent dwellings by 2004
Hungary	(Arja, 2007)	SF, STEPs	40% connected to WWTP
Poland	(Jerzy)	STEPs, AS, SBR, TF, RBC, Biofilter,	48.3% applied STEPs.
Japan	(ZENG et al, 2001) (Hiroshi et al, 2003)	Johkasou system, MBR, SP, FBR	More than 92.2% treated by 1992
Korean	(Kwun et al, 2000) (Yoon et al, 2008)	ABS, NEWS,CW	Less than 20% treated by 2002

CW: Constructed wetland; ISF: Intermittent Sand Filters; RBF: Reed Bed Filters; WSP: Waste Stabilization Ponds; STEPS: Septic Tank Effluent Pumping System; SP: Stabilization Ponds; SBR: Sequence Batch Reactor; ABS: Absorbent Biofilter System; NEWS: Natural and Ecological Wastewater treatment System; WWTP: Waste Water Treatment Plant; OWTS: On-site Wastewater Treatment System

A recommended application domain in France is presented in Figure I-1.

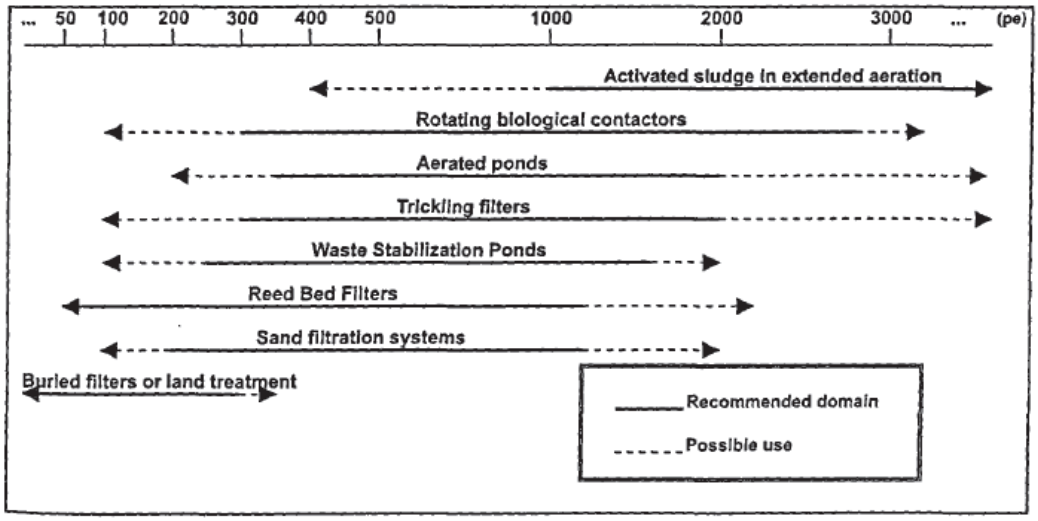

Figure I- 1: Recommended and possible domain of utilization of different types of wastewater treatment plants (Catherine et Alain. 2003)

pe represents per equivalent, also noted as P.E. in the following paragraph

From Figure I-1, trickling filter best application is in the range of 300-2000 P.E. for urban wastewater treatment in France. Currently in China, it's also usually applied in the range of 300-2000 P.E. for village wastewater treatment. However in urban areas, this range is always higher than 2000 P.E. These prescriptions are directly related to the level of quality assigned to the receiving water and particularly to the dilution of the treated effluent at low water levels (Équip, 1997).

1.2 Attached growth & Suspended growth systems

(Nicolella et al. 2000) gave a distribution of the use of biological processes depending on substrate concentration and flow rate of the WW (Figure I-2). The processes that were considered are static biofilms (e.g. in trickling filters (TF)), particulate biofilms (e.g. in biofilm fluidized bed reactors (BFR), upflow anaerobic sludge blanket reactors (UASB) and biofilm airlift suspension reactors (BASR)), and flocs (in activated sludge processes (AS)).
In Figure I-2, some lines define different regions of applicability in the diagram:

1. Retention time is so short and substrate concentration so high that microorganisms grow in suspension because of the high substrate concentrations.

2. At high flow rates, particulate biofilms and flocs are washed-out and only static biofilms can be retained in the reactors, or the reactors have a very flat and extended shape.
3. Low flowrate and high organic loading conditions are suitable for application of particulate biofilm reactors.
4. Low flowrate and low loading conditions are suitable for applications of flocs, provided that separation and biomass recycle are used (e.g. activated sludge processes). This region partially overlaps the particulate biofilm region.
5. For high strength and low flow wastewater, upflow sludge blanket reactors can be used and also granular sludge.
6. The sludge is retained in the reactor without need for external separation and recycles.

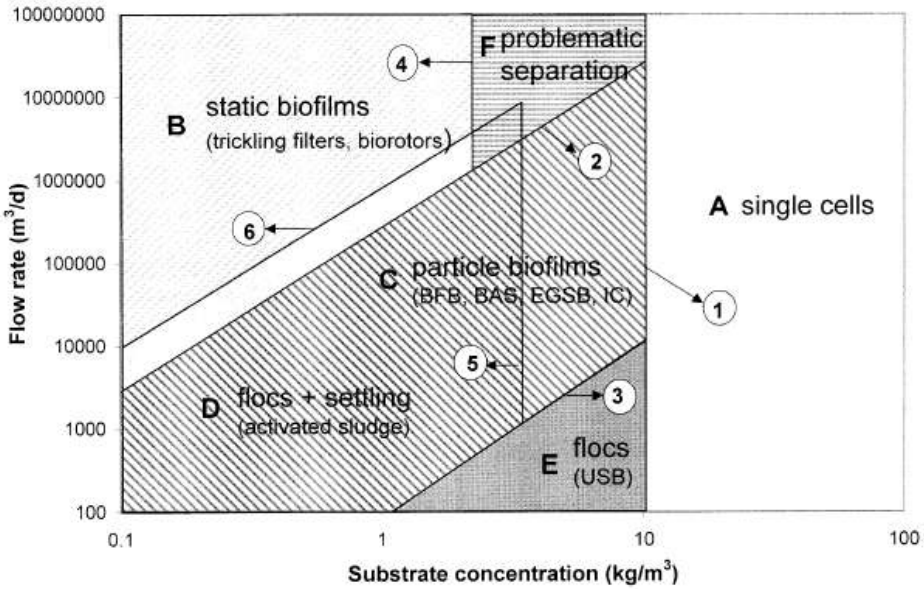

Figure I- 2：Concentration- flow rate phase diagram for application of flocs and biofilm bioreactors (Nicolella et al. 2000)

Both static (Flowrate>10000m^3/d, substrate concentration<10 kg/m^3) and particle biofilm systems can resist higher hydraulic loads than suspended growth systems (active sludge) and can treat low strength wastewater.

2. Overview of Trickling Filter process

The trickling filter system has been widely used in municipal and industrial wastewater treatment for over 100 years (Norris et al., 1982; Logan et al., 1987a; Logan et al, 1987b; Logan et al., 1989; Hinton et al., 1989; Logan et al., 1990). TF is often combined with other processes to enhance the treatment efficiency. As an example the combination Trickling Filter/Activated Sludge (TF/AS) is used to accomplish treatment requiring advanced nitrogen removal.

In general, a single-stage TF has to remove organic carbon in the upper portion of the unit and provide nitrifying bacteria for nitrification in the lower part. For two-stage TFs: reduction of organic carbon occurs in the first treatment stage; nitrification occurs in the second stage.

2.1 Single-stage TF

A conventional single-stage TF is usually composed of a distributor, a tank packed with medium, an under-draining system, a settling device with recycle pipe and/or air pump and also a settling device if needed. A typical configuration of TF is shown in Figure I-3.

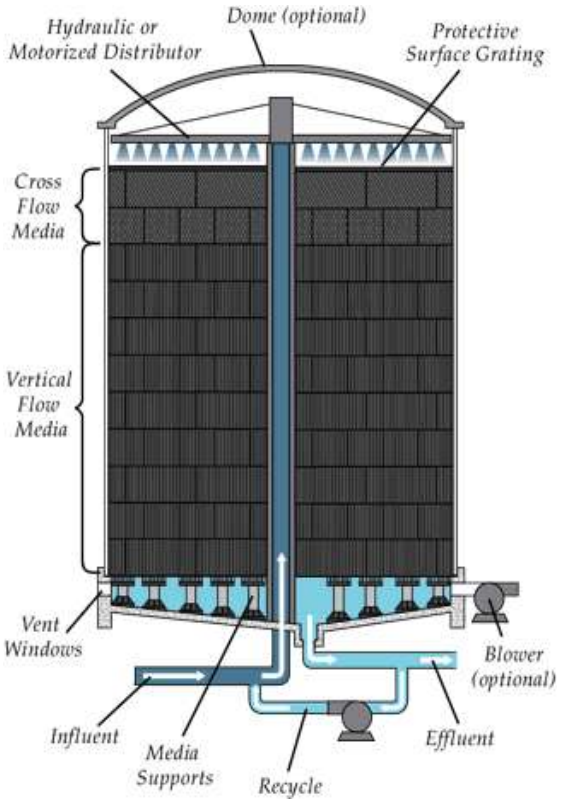

Figure I- 3: Diagram of a conventional Trickling filter (BRENTWOOD-INDUSTRIE)

2.2 General Principal in TF

In a TF, microorganisms establish a strong attachment to the uneven surface of the medium (rocks, stones or plastic) and biofilms develop above the plane of the medium (Rittmann and McCarty, 1980). Small organic molecules diffuse into microbial cells in the biofilm, providing carbon and nutrients for microbial cell growth. To remove larger molecules and particulate COD, these particles must be trapped in the biofilm, so that they can be degraded into small enough particles for diffusion to occur. The larger molecules and particulates become trapped in the biofilm by a 'glue' (Extracellular Polymeric Substances –EPS) secreted by the microbial cells. The EPS also allow the attachment of the micro-organisms to the medium (Boltz et al 2006).

The biological reaction is exothermic and the released heat warms the interstitial air by convection inducing air renewal.

Hydraulic conditions must be carefully controlled in order to equally distribute the waste water to treat on the carrier.

Part 2: Description of a biofilm and of biological processes

1. Brief of biofilm

A biofilm is any group of microorganisms in which cells stick to each other on a surface. These adherent cells are frequently embedded within a self-produced matrix of extracellular polymeric substance (EPS). Biofilm EPS, which is also referred to as slime (although not everything described as slime is a biofilm), is a polymeric conglomeration generally composed of extracellular DNA, proteins, and polysaccharides. Biofilms may form on living or non-living surfaces and can be prevalent in natural, industrial and hospital settings. The microbial cells growing in a biofilm are physiologically distinct from planktonic cells of the same organism, which, by contrast, are single-cells that may float or swim in a liquid medium. Figure I-4 shows the processes occurring on the surface of biofilm and in the biofilm.

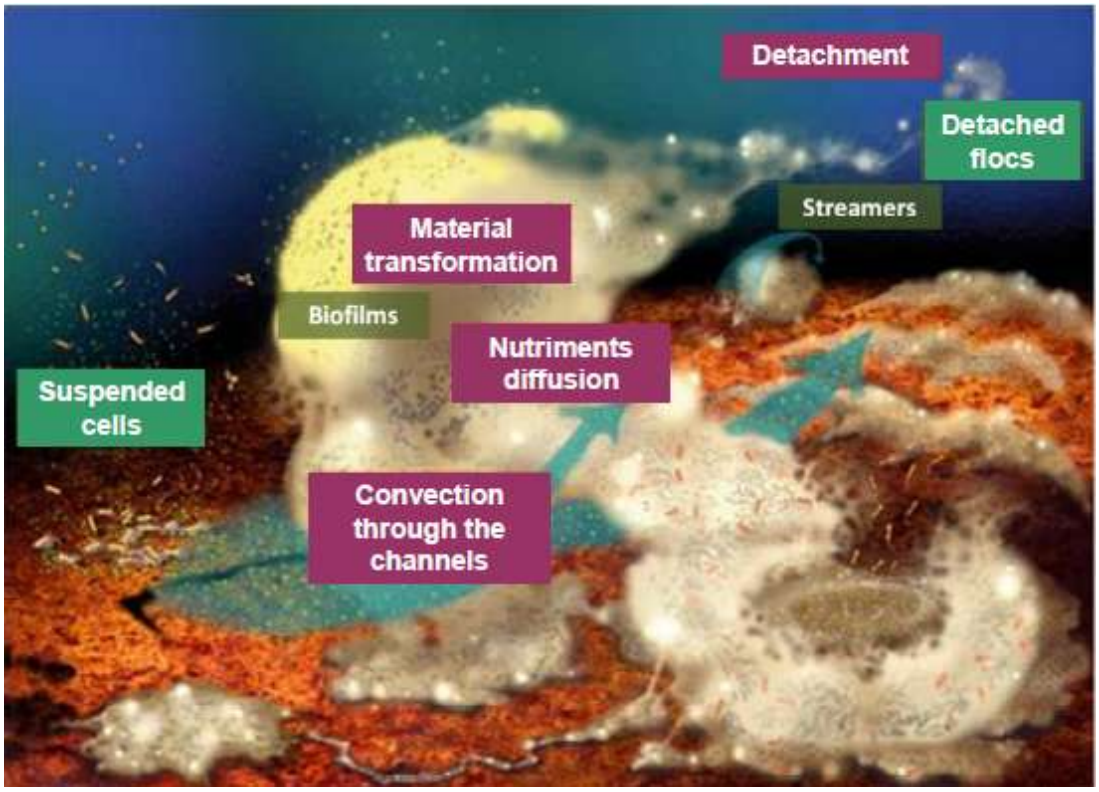

Figure I- 4: Schematic representation of the different processes and different morph-types of bacterial aggregates. (Hall-Stoodley et al. 2004).

Both biological and physical processes occur in biofilms. These processes are next briefly described.

2. Biological reactions

2.1 Principal of COD removal

The total COD removal derives from both the consumption of biodegradable fraction and the removal of non-biodegradable fraction in a TF.

For biodegradable fraction

The consumption of biodegradable COD (COD_{bio}) is mainly consumed by heterotrophic growth for bacterial synthesis with a maximal heterotrophic growth yield (Y_H, the classic value is 0.63g COD/gCOD); additionally, part ($1-Y_H$) of biodegradable COD is oxidized into CO_2 which supply energy for bacterial synthesis. Death of bacteria also occur leading to the release of both biodegradable and non biodegradable COD. All these processes are illustrated in Figure I-5.

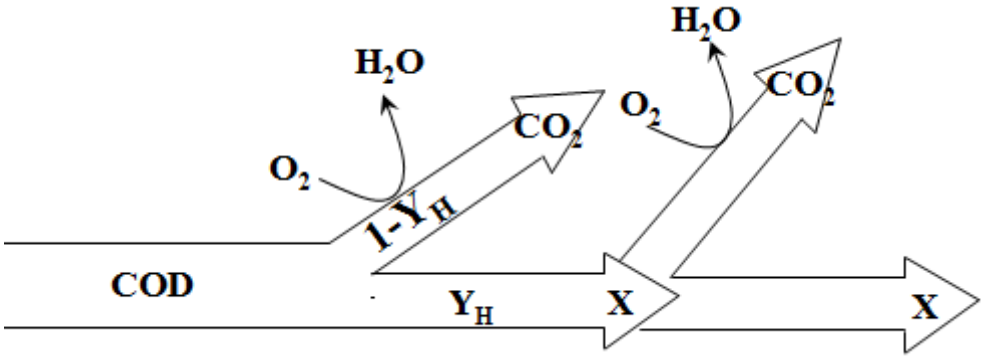

Figure I- 5: Consumption of biodegradable COD

2.2 Principal of nitrification

Nitrification is a process in which ammonia nitrogen in wastewater is oxidized first to nitrite nitrogen and then to nitrate nitrogen by autotrophic bacteria. Nitrification starts when the soluble Biological Oxygen Demand (BOD) concentration in the wastewater is low enough for nitrifiers to compete with heterotrophs, which derive energy from the oxidation of organic matter. There are two steps involved in the nitrification process:

1) Nitritation. Ammonia is oxidized to nitrite (NO_2^-) by *Nitrosomonas* bacteria.

$$2NH_4^+ + 3O_2 \rightarrow 2NO_2^- + 4H^+ + 2H_2O$$

2) Nitratation. The nitrite is converted to nitrate (NO_3^-) by *Nitrobacter* bacteria.

$$2NO_2^- + O_2 \rightarrow 2NO_3^-$$

These two reactions supply the energy that the nitrifying bacteria need for growth. Additionally, the *Nitrobacter* bacteria develop faster than the *Nitrosomonas* bacteria, so the nitritation is the limiting step. Hence in theory, the nitrite ions do not accumulate in nitrification. The equation for ammonia oxidization into nitrate can be written as:

$$NH_4^+ + 2O_2 \rightarrow NO_3^- + 2H^+ + H_2O$$

From this equation, the theoretical oxygen demand for oxidizing the ammonia-nitrogen into nitrate is 4.57 $gO_2/gN_{nitrified}$. Nevertheless, this equation does not take the bacteria synthesis into account. Considering the chemical formula $C_5H_7NO_2$ as the living biomass, the general relation of nitrification is written as:

$$NH_4^+ + 1.86O_2 + 1.98HCO_3^- \rightarrow 0.02C_5H_7NO_2 + 0.98NO_3^- + 1.98H^+ + 0.094H_2O$$

Correspondingly, the removal of ammonia is plotted in Figure I-6.

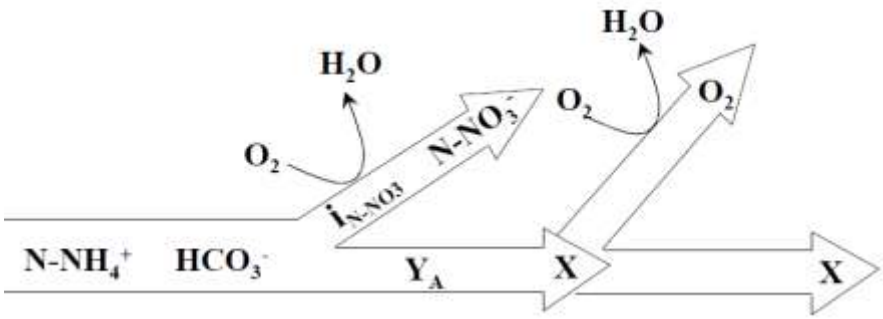

Figure I- 6: Removal of ammonia

Autotrophic bacteria derive their carbon and energy from carbonates (HCO_3^-) and ammonia (NH_4^+), respectively. From this equation, the theoretical oxygen demand for nitrification is 4.33 $gO_2/gN_{nitrified}$. The autotrophic yield rate Y_A from this equation is calculated as 0.24 $gCOD_{biomass}$ production/$gN_{nitrified}$. Nitrification is therefore a reaction with low energy generation per N-NH_4^+ oxidized (1-Y_A).

Additionally, ammonia removal is not isolated reactions, ammonia will also be consumed by heterotrophic growth, and ammonia is also assimilated for bacterial syntheses as the source of nutrient. The relation of assimilation reaction is usually written as:

$$C_{18}H_{19}O_9N + 0.74NH_3 + 8.8O_2 \rightarrow 1.74C_5H_7NO_2 + 9.3CO_2 + 4.52H_2O$$

There are several major factors that influence the kinetics of nitrification. These are organic loading, hydraulic loading, temperature, pH, dissolved oxygen concentration, and filter medium. The influence of these factors on nitrification will be discussed in the following part on the bio-kinetics of modeling the biofilm system.

3. Bio-kinetics of modeling a biofilm system

3.1 Mass balance kinetic of overall system

The mass balance is a quantitative description of all the material that enters, leaves and accumulates in a system with defined physical boundaries. All the outlet fractions (in flow effluent and gas phase release) and accumulated fraction in the system are all generated from the inlet. The diagram of mass balance in the entire system of a TF is shown in Figure I-7.

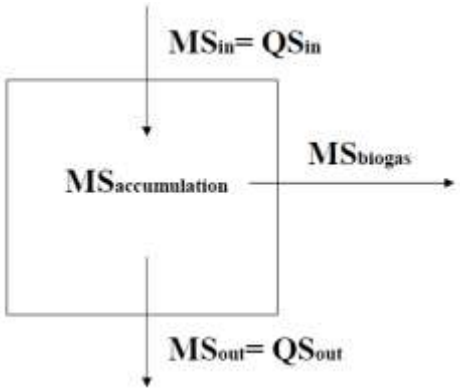

Figure I- 7: Diagram of mass balance in the pilot

The general principal of mass balance on the liquid is

$$\frac{dS}{dt}V = QS_0 - QS_e - r_S V \qquad \text{(I-1)}$$

where r_s is substrate reaction rate; V is the volume of liquid present in the TF; Q is volumetric flowrate; S_e denotes the substrate concentration in effluent; S_0 is the substrate concentration in influent; MS_{in} and MS_{out} is the inlet and outlet biomass concentration.

The modeling of the system can be structured for two distinct conditions: steady-state and dynamic-state.

3.1.1 Steady-state

In a long term operated TF, the system can reach a pseudo steady-state, the mass accumulation in the entire system equals 0 (dS/dt=0) and the removal of substances is assumed to follow the first-order reaction (r_S=-kS). Eq. I-1 can be modified into Eq. I-2.

$$r_S = -kS = \frac{Q}{V}(S_0 - S_e) = \frac{1}{\tau_H}(S_0 - S_e) \qquad \text{(I-2)}$$

where τ_H is the liquid Hydraulic Retention Time (HRT)

In the design of a TF system, it is more usual to use the simplified steady state equations. Previous design models such as NRC, Velz equations were all based on the bio-kinetics from the mass balance analysis, which assumed the microbial kinetics limited substrate removal (Logan et al., 1987b).

3.1.2 Dynamic-state

The dynamic state is the state when there is mass accumulation of components in the system. The accumulation rate dS/dt≠0, the concentrations of components in the system is therefore variable with time and can increase or decrease, depending on the balance between the positive and negative terms. Usually in a treatment plant, the input flow and the concentration are variable, besides the possibility of having other stimulus to the system (temperature changes) that causes a transient in the concentrations of the components. Dynamic conditions are prevailing conditions in actual treatment plant. The steady-state is only a particular case of the dynamic state. The dynamic models are based on the generalized mass balance equation from Eq. I-1. Although the dynamic models is more complex in the solution of the equations and the greater requirements of values for models coefficients and variables, simulators such as Hydromantis GPS-X, Aquasim, BIOWIN makes it easier to be well analyzed.

3.2 Mass transformation kinetics

The transformation processes are generally the biochemical reactions that produce or consume one or more components according to the hypothesis of models. The main transformation processes include the bacterial synthesis (heterotrophic growth), decay of biomass, ammonification of soluble organic nitrogen and hydrolysis of particulate substrate.

3.2.1 Monod equation

Monod proposed the saturation-isotherm type of function to estimate the specific growth rate, which was developed by many authors to relate the heterotrophic or autotrophic growth to the prevailing feeding concentration. The specific growth rate depends on the maximum growth rate, and the substrate concentration.

$$\frac{dX}{dt} = \mu_{\max}\left(\frac{S}{K_S + S}\right) \qquad \text{(I-3)}$$

where X is the biomass concentration (g/m³); μ_{max} is the maximum specific heterotrophic/autotrophic growth rate (d^{-1}); S is substrate concentration (g/m³); K*s* is the half-saturation coefficient of substrate (g/m³);

Many authors develop the Monod equation, it for both heterotrophic and autotrophic growth, especially for COD removal and nitrification.

3.2.2 Growth for COD removal

In a biofilm system, the dominant process is the bacterial syntheses which consume Biological Organic Matter (BOM) and produce biomass. The Monod equation and the models developed from the Monod equation are widely applied to describe the bacterial syntheses. The expression of heterotrophic growth is as follows:

$$r_{BH} = \frac{dX_{BH}}{dt} = (\mu_{H,\max}\left(\frac{S_S}{K_S + S_S}\right)\left(\frac{S_O}{K_{OH} + S_O}\right) - b_H)X_{BH} \qquad \text{(I-4)}$$

where r_{BH} is the heterotrophic growth rate; X_{BH} is the heterotrophic biomass concentration; $\mu_{max,H}$ is the maximum specific heterotrophic growth rate; Ss is readily biodegradable substrate concentration; So is the oxygen concentration; Ks and K_{OH} are the half-saturation coefficient of readily biodegradable substrate and oxygen, respectively; b_H is the decay rate of heterotrophic biomass.

When the substrate concentration is higher than the half-saturation coefficient, Ss>>Ks, Eq. I-4 can be rewrite as follows:

$$r_{BH} = \frac{dX_{BH}}{dt} = (\mu_{H,\max}\left(\frac{S_O}{K_{OH} + S_O}\right) - b_H)X_{BH}$$

This indicates that oxygen concentration could be the limiting factor for biodegradation of COD.

3.2.3 Hydrolysis of particulate matter

Hydrolysis reaction usually means the cleavage of chemical bonds by the addition of water; usually it is a step in the degradation of a substance. Biodegradable particulate matter should be firstly hydrolyzed into soluble substrate, and then it can be biodegraded. The hydrolysis process is considered as a process limited by the reaction surface. The hydrolysis rate is maximum and independent of the substrate concentration X_S only if it is in large excess relative to the concentration of cells X_H (as $X_S/X_H >> K_X$). Everything happens as if all the cells were saturated with substrate.

$$\frac{dX_S}{dt} = -k_H \frac{X_S / X_H}{K_X + X_S / X_H} \cdot X_H \qquad \text{(I-5)}$$

Activated-sludge in the cell concentration X_H is in excess compared to X_S. The hydrolysis rate is independent of the concentration of cells (there is an excess of hydrolytic enzymes). So this equation is often simplified and replaced by a reaction of order 1 with respect to X*s*.

$$\frac{dX_S}{dt} = -k_H X_S$$

The k_H ranges from 1.5 to10 d^{-1}. The classical value is 3.6 d^{-1}.

3.2.4 For nitrification

Some Swiss investigators (Gujer et al., 1984; Gujer et al., 1986; Logan et al., 1987) proposed an approximation that could be integrated for nitrification rate dC_N/dt with the ammonia nitrogen concentration:

$$r_{BA} = \frac{dX_{BA}}{dt} = (\mu_{\max,A} \frac{S_{NH}}{K_{NH} + S_{NH}} \times \frac{S_O}{K_O + S_O} - b_A) X_{BA} \qquad \text{(I - 6)}$$

where:

S_{NH}-Bulk liquid ammonia nitrogen concentration, mg/L; $\mu_{max,A}$- maximum nitrification rate at high ammonia levels, g N/m^2d; S_{NH} is the concentration of ammonia; K_{NH}- Half-saturation coefficient of ammonia; b_A is the decay rate of autotrophic biomass; X_{BA}- Concentration of autotrophic biomass.

When $S_{NH} >> K_{NH}$, Eq.I-6 can be rewrite as follows:

$$r_{BA} = \frac{dX_{BA}}{dt} = (\mu_{\max,A} \frac{S_O}{K_O + S_O} - b_A) X_{BA}$$

This implies that when ammonia nitrogen concentration is very higher than half-saturation coefficient, the oxygen concentration is the limit factor of nitrification process.

Those Swiss investigators also studied the nitrification rate along the filter depth. The "line fit equation" for the decline of nitrification rate versus depth is as follows. However, this formula was usually applied in NTF:

$$jn(z) = \frac{E \cdot jO_{2\max}}{4.3} \cdot \frac{S_{NH}}{K_{NH} + S_{NH}} \cdot e^{-kz} \qquad \text{(I - 7)}$$

where jn (z)- nitrification rate at depth z, g of N/m^2d; z- depth in Trickling Filter, m; E- Medium effectiveness factor; jO_2 –maximum surface oxygen-transfer rate (with respect to temperature), g O_2/ m^2d; S_{NH}-Bulk liquid ammonia nitrogen concentration, mg/L; k- Empirical parameter describing decrease of nitrification rate with depth.

From those investigations, both for COD removal and nitrification, oxygen concentration is a key limiting factor for biodegradation process and nitrogen removal. To provide enough oxygen concentration for biodegradation and nitrification, in our experiments, we should improve the efficiency of oxygen supply if we adopt the natural aeration. Hence, we decided to change the close structure of conventional TF to an open structure, in order to optimize the oxygen supply.

Part 3: Description of physical processes

1. Physical processes

Additionally, modeling development of bio-systems has challenged the assumption that microbial kinetics limited substrate removal as proposed by Monod. However, diffusion through the biofilm could be the limiting step in substrate removal in a TF (Swilley and Atkinson 1963; Maier et al., 1967; Kissel 1986; Logan et al., 1987b).

1.1 Mechanisms of mass transfer and transport

Soluble biodegradable COD, Total Ammonia Nitrogen (TAN) and dissolved oxygen (DO) consumption of an attached biofilm at steady-state can be described as a two-step process: external mass transfer between the liquid/biofilm interface and internal mass diffusion inside the biofilm. The conceptual schema is shown in Figure I-8.

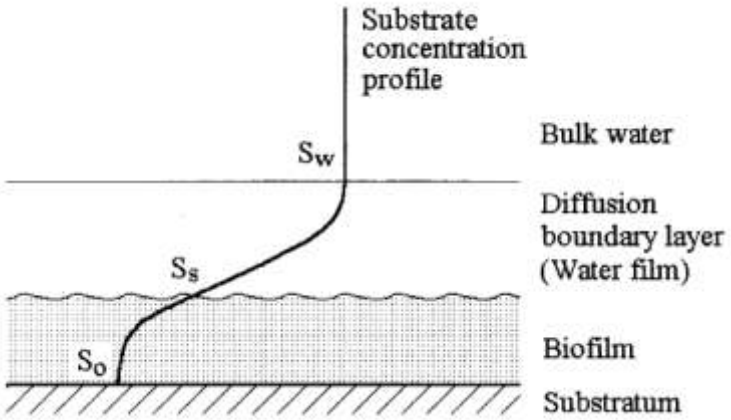

Figure I- 8: Conceptual profile of a fixed biofilm (Lin, 2008)

The following paragraph focuses on a description of the different phenomena involved in component diffusion from the substrate to the biofilm.

1.1.1 External mass transfer

External mass transfer of soluble components

The transport of substrate in moving liquid is governed by molecular diffusion and advection (Lewandowski et al., 1992). The substrate transfer rate to the biofilm interface is due to the

combination of these processes and can be expressed (Hamdi, 1995; Chen and Huang, 1996) :

$$J_S = \frac{D_W}{\delta_{L,\lim}}(S_W - S_S) = \frac{ShD_W}{L}(S_W - S_S) \qquad \text{(I-8)}$$

where J_S is the biodegradable substrate transport flow rate or removal rate (g /m^2 d), D_W is the biodegradable substrate diffusion coefficient in liquid (m^2/d), $\delta_{L,\lim}$ is the thickness of water film layer (m), S_W is the substrate concentration in bulk liquid (g/m^3), S_S is the substrate concentration at liquid-biofilm interface (g/m^3), Sh is the Sherwood number (dimensionless), which is defined as the ratio of actual mass flow to the rate of mass transfer that would occur if the same concentration difference were established across a still water layer with the thickness of characteristic length ***L***.

Moreover, the Sherwood number, *Sh* (also called the mass transfer Nusselt number) is a dimensionless number used in mass-transfer. It represents the ratio of convective to diffusive mass transport.

It is defined as follows:

$$Sh = \frac{KL}{D} = \frac{Convective mass\ transfer coefficient}{Diffusive mass\ transfer coefficient}$$

where ***L*** is a characteristic length (m); D is mass diffusion coefficient in liquid (m^2.s^{-1}); K is the external mass transfer coefficient (m.s^{-1}).

Using dimensional analysis for given geometry, *Sh* can also be defined as a function of the Reynolds and Schmidt numbers:

$$Sh = f(\mathrm{Re}, Sc)$$

For example, for a single sphere it can be expressed as:

$$Sh = Sh_0 + C\,\mathrm{Re}^m\, Sc^{\frac{1}{3}}$$

where Sh_0 is the Sherwood number due only to natural convection and not forced convection; C, m are constants.

In this relation, the Schmidt number, S_C, is a dimensionless number defined as the ratio of momentum diffusivity (viscosity) to mass diffusivity, and is used in fluid flows in which there are simultaneous momentum and mass diffusion convection processes.

Schmidt number is the ratio of the shear component for diffusivity viscosity/density to the diffusivity for mass transfer D. It physically relates the relative thickness of the hydrodynamic layer and mass-transfer boundary layer.

It is defined as:

$$Sc = \frac{\upsilon}{D} = \frac{\mu}{\rho D} = \frac{viscous\,diffusion\,rate}{molecular\,diffusion\,rate}$$

where ν is the kinematic viscosity or (μ/ρ) in units of (m^2/s); D is the mass diffusivity (m^2/s); μ is the dynamic viscosity of the fluid (Pa·s or N·s/m² or kg/m·s); ρ is the density of the fluid (kg/m^3).

The Reynolds number is a dimensionless number that gives a measure of the ratio of inertial forces to viscous forces and consequently quantifies the relative importance of these two types of forces for given flow conditions. It is defined by:

$$\mathrm{Re} = \frac{Ud_p}{\nu} \qquad \text{(I-9)}$$

where U is the liquid velocity; $\mathbf{d_p}$ is the diameter of particle; and **ν** is the kinematic viscosity (**ν**=μ/ρ)

In the expressions of external mass transfer, it can be found that the hydraulic factor $\delta_{L,\,lim}$ influences the external transfer significantly, which leads to the consideration of investigating the hydrodynamic behavior of the new designed system, especially to estimate the liquid film thickness.

Regardless the configuration of the reactor, the Sherwood number is proportional to the Reynolds number to some positive power. Therefore the faster the flow, the higher the Sherwood number is and therefore the less the resistance to external transport is.

The inclusion of external transport is the key in the field of biofilms. Indeed, even if in many reactor configurations, limiting the external transport is negligible compared to the internal transport, it can significantly boost low Re limitations by transport. Strong resistance to external transport reduces substrate concentrations seen by the biofilm and tends to the formation of high surface roughness with the presence of "towers" inflexible (Eberl et al. 2000).

Recognizing the importance of surface properties of the biofilm, Picioreanu et al. (2000) introduced a shape factor (α) in the expression which defines the *Sh* developed by the biofilm on a solid surface determined surface. The constants ψ and n, determine the activity of the biofilm. For low activity, ψ = 0.478 and n = 1.12, whereas at high activity, ψ= 0.45 and n = 1.034. By numerical simulations, they showed that rough biofilms engendered a halving

transfer coefficient compared to that obtained for a flat biofilm resulting in a reduction of over 10% conversion rate.

Similarly, from experimental measurements through microprobes, Washe et al. (2002) introduces another factor structure (Ω) to the classical formulas involving the Sherwood number for tubular reactors. This factor depends on the conditions under which the biofilm was developed (Re, μ).

Table I- 2: Summary of significant relationships between the numbers of Sherwood (Sh) or Reynolds (Re) and Schmidt (Sc), ε (porosity of the fluidized bed), d (pipe diameter), L (length of pipe) n1, n2, m (experimental constants). Adapted from (Ochoa et al, 2009)

Configuration	Conditions	Relation	Reference
Flow cell	Re<1	$1.8 < n_1 < 2.3$ $0.22 < n_2 < 0.28$ $Sh = n_1 + n_2 \,\mathrm{Re}^m \, Sc^{1/3}$ $0.22 < m < 0.60$	(Stoodley et al. 1997)
Tubular reactor	1668<Re<66710	$Sh = 0.13\mathrm{Re}^{0.63} \, Sc^{1/3}$	(Zhu and Chen 2001)
Tubular reactor	Re<2000	$Sh = 2\,\mathrm{Re}^{0.5} \, Sc^{1/2} \left(\frac{d}{l}\right)^{0.5} \cdot \left(1 + 0.0021\mathrm{Re}\right)$	(Horn and Hempel 1995)
Fluidized bed	1.6<Re<1320	$Sh = \frac{0.8}{\varepsilon} \mathrm{Re}^{0.5} \, Sc^{1/3}$	(Koloini et al. 1977)
Fluidized bed	-	$K = \frac{0.81}{\varepsilon} \left(\frac{D_w \nu^{1/3}}{\mu_l^{1/3} d_p} \right)^{1/2}$	(Shieh and Keenan 1986)
Fluidized bed	0.0016<Re<55	$\frac{1}{K} = \frac{\varepsilon}{1.09 v} \mathrm{Re}^{2/3} \, Sc^{2/3}$	(Manem and Rittmann 1990)
Tubular reactor	750<Re<1000 3000<Re<6000	$Sh_{lam} = 8.7 \cdot \mathrm{Re}^{0.5} \cdot Sc^{0.5} \left(\frac{d}{L}\right)^{0.5} \cdot \Omega^{-1}$ $Sh_{turb} = 0.16 \cdot \mathrm{Re}^{0.75} \cdot Sc^{0.5} \cdot \Omega^{-1}$ $\Omega = e^{6\mu^*} \cdot \mathrm{Re}_{croiss}^{-\frac{\mu^*}{1.5}}$	(Wasche et al. 2002)
Biofilms with surface roughness (modeling)	-	$Sh = \frac{\psi}{\alpha^n} \mathrm{Re}^{1/3} \, Sc^{1/3}$ $0.45 < \psi < 0.478$ $1.034 < n < 1.12$	(Picioreanu et al. 2000)
Surface plane	Re<30000 350<Sc<100000	$Sh = 0.01\mathrm{Re}^{0.9} \, Sc^{1/3}$	(Ochoa 2009)

External mass transfer of particulate components: attachment and detachment

Enzymes bound to the microorganism cells in the EPS break down the particulates through hydrolysis, into smaller and smaller units (Confer and Logan, 1998), until the compounds are small enough to diffuse across the cell membrane and used by heterotrophic growth.

The external mass transfer of particulate components occurs at the interface of liquid/biofilm. The suspended particulate components attach to the biofilm surface with rate $\mathbf{r_{att}}$, where the biomass detaches from the biofilm surface at rate $\mathbf{r_{det.}}$ The attachment and detachment rates were found proportional to the square of the particulate components concentration at the surface of biofilm (X_{surf}) (Plattes et al., 2008).

$$R_{att} = r_{att}(X_{surf})^2$$

$$R_{\det} = r_{\det}(X_{surf})^2$$

Detachment is a random process caused by local instabilities within the physical biofilm structure with external forces (shear forces caused by fluid flow or random collisions of particles during backwashing) (Morgenroth and Wilderer, 2000). Usually, the detachment process is determined in the biofilm modeling.

Literature sources that reported biofilm detachment are shown in Table I-3.

Table I- 3: Models of detachment in literatures

Processes relative to detachment models	Expressions of detachment models	Reference
Unrestricted growth	0 (no detachment)	(Fruhen et al. 1991)
		(Kissel et al., 1984)
	Constant biofilm thickness defined	(Wanner and Gujer 1985)
Biofilm thickness	$k_d(\rho_f L_f)^2$	(Wanner and Gujer 1985) (Kissel et al., 1984) (Fruhen et al. 1991) (Trulear and Characklis 1982) (Bryers 1984)
	$k_d \rho_f {L_f}^2$	(Wanner and Reichert 1996) (Kreikenbohm and Stephan 1985)
	$k_d \rho_f L_f$	(Chang and Rittmann 1987)
	$k_d(L_f - L_{basethickness})^2$ during backwash	(Morgenroth and Wilderer 2000)

	0 during operation	(Elenter et al. 2007)
	$U_f(\frac{L_f}{L_{f\max}})^2 d$	(Lackner et al. 2008)
Shear Stress	$k_d \rho_f \tau_P$	(Bakke et al. 1984)
	$k_d \rho_f L_f \tau_P^{0.58}$	(Rittmann and McCarty 1980)
Growth rate or substrate consumption	$L_f(k_d + k_d^{'}\mu)$	(Speitel and Digiano 1987)
	$k_d r_S L_f$	(Tijhuis et al. 1995) (Peyton and Characklis 1993)
Distance to the biofilm surface Z	$k_d z^2$	(Xavier et al. 2005) (Alpkvist et al. 2006) (Picioreanu et al. 2000)

ρ_f- mean biofilm volumetric density; L_f- biofilm thickness; Kd- detach rate coefficient; τp- shear stress (Pa); $L_{basethickness}$- biofilm thickness after backwashing.

1.1.2 Internal mass transport

Internal mass diffusion of soluble components

Solute transport in biofilm is the result of diffusion in the denser aggregates and potentially convective transport within pores and water channels, diffusion has been shown to dominate mass transport in many biofilm systems. The soluble substrate is transported in the biofilm by molecular diffusion due to the concentration gradient, from the higher concentration to the lower concentration. It is usually modeled by the first Fick's law (Eberl et al., 2006):

$$\frac{dS}{dt} = -D_F \frac{d^2S}{dz^2} = -f_d D_W \frac{d^2S}{dz^2} \qquad \text{(I-10)}$$

Where D_F is the effective Permeability (m^2/d) and f_d is the diffusion factor within a biofilm; z is the biofilm depth perpendicular to the support medium (m), S is the oxygen concentration within a biofilm (g/m^3); Dw is the diffusion coefficient of mass in the pure water.

Effective permeability in biofilm (D_f)

Biofilm are mainly composed of water and the diffusion coefficient of mass in the biofilm D_F is often related to the diffusion coefficient of mass in the pure water D_w and the relative diffusivity coefficient f_d reported by (Hinson and Kocher, 1996):

$$D_f = f_d D_W \qquad \text{(I-11)}$$

The f_d value are reported (Fan et al., 1990, Hinson and Kocher, 1996) to be in the range from 0.1-1.0 depending on characteristics of the biofilm and of the solutes.

Some researchers have associated this coefficient (f_d) with the biofilm density (ρ_f) or biofilm porosity (ε) and tortuosity (τ) shown in Table I-4:

Table I- 4: Biofilm density and f_d in literatures

Reference	**Substrate**	**ρ_f (kg/m³)**	**Relations**	**f_d**
(Horn et al,. 2006)	oxygen	10-20	$f_d = 1.112 - 0.019\rho_f$	0.5-1
	Sodium nitrate	20-35	$f_d = 1.152 - 0.022\rho_f$	0.8-0.4
	Sodium chloride	>35	$f_d = 1.006 - 0.016\rho_f$	<0.6
	All data	3-40	$f_d = 1.119 - 0.021\rho_f$	-
(Fan et al. 1990)	Phenol	182-130	$f_d = 1 - \frac{0.43\rho_f^{0.92}}{11.19 + 0.27\rho_f^{0.99}}$	0.26-0.38
(Yano et al. 1961)	Citric acid	170-30	-	0.11-0.9
(Beyenal et al. 1997)	phenol	47-107	-	0.17-0.44
	oxygen	47-107	-	0.09-0.24
(Smith et al., 1984)	oxygen	29.4-84	-	0.61-0.25
(Zhang and Bishop, 1994) (Westrin and Axelsson, 1991)			$f_d = \frac{\varepsilon}{\tau^2}$ where $\tau = \frac{\pi^2}{4}(1 - 1.32\frac{r}{h})$ $\varepsilon = \frac{\pi^4}{8}\left(\frac{r}{h}\right)^2\left(1 - 1.32\frac{r}{h}\right)$	
(Fujie et al. 1977)	oxygen	23.5	-	0.5

In general, to well determine the effective diffusion coefficient D_F, f_d is very important in the biofilm diffusion and limitation conditions study, and this coefficient is associated mainly with the biofilm density (ρ_f) and biofilm porosity (ε').

Internal mass diffusion of particulate components

The internal mass diffusion of particulate components in the biofilm is normally expressed by different models. For example, (Wanner and Reichert, 1996) proposed the transport of particulate components in a mixed cultured biofilm like the molecular diffusion.

$$\frac{dC_X}{dt} = -f_d D_{WX} \frac{dC_X}{dz^2} \qquad \text{(I-12)}$$

where D_{WX} is the particulate components diffusion coefficient.

The diffusion coefficient of particulate components D_{WX} is much smaller than the soluble components diffusion in pure water. This diffusion flux caused the mixing of particulate components in the solid matrix of biofilm, as the result of biofilm deformation by hydraulic forces. This deformation caused the particulate components to first detach and then reattach to another zone different from original zone in biofilm matrix. However, only the final result is modeled by diffusion.

Figure I-9 represents the different processes occurring in a biofilm system.

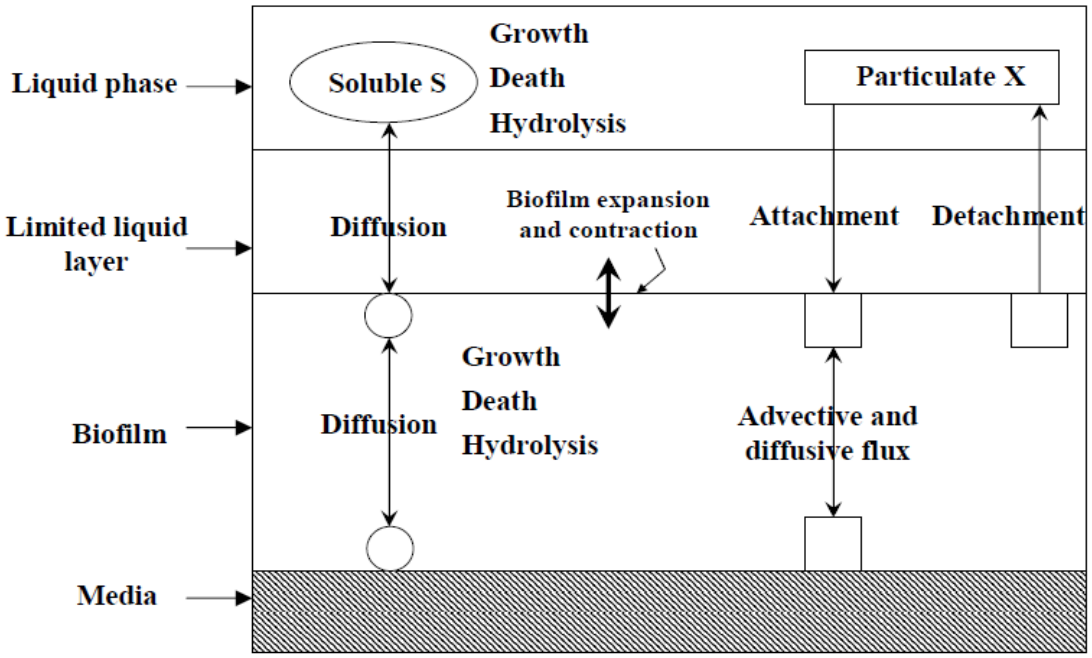

Figure I- 9: Schematic diagram of general mechanisms in a biofilm system (Wanner and Morgenroth, 2004)

2. Partial conclusion

The number of elements influencing the performances of substrates removal and nitrification were divided into two levels by (Boller et al., 1994) in their investigation of a nitrifying TF:

1) The parameters which describe the hydraulics and nutrients transport conditions to the biofilm surface, gas exchange processes, reactor configuration and operational conditions, the reactor specific conditions mainly focus on the bioreactor-level;

2) The parameters including transport and reaction processes within the biofilm. Those important elements are summarized in Table I-5.

Table I- 5: Elements affecting the performance of nitrifying biofilms on a biofilm oriented and a reactor specific level (Boller et al. 1994)

Reactor specific elements	Biofilm Specific parameters
Reactor configuration (completely stirred, plug flow, mixed)	Concentration of dissolved nutrients at and in the biofilm: COD, NH_4^+, NO_2^-, NO_3^-,O_2
Reactor hydraulics (laminar, turbulent flow)	Concentration of particulate substances: TSS, COD, heterotrophy
Oxygen transfer= function (℃)	Concentration of substances toxic to nitrifier
Biofilm sloughing	Diffusion coefficients f(℃) of: COD, NH_4^+, NO_2^-, NO_3^-, HCO_3^-, O_2
	Maximum specific growth rate μ_{max} of microbial species= f(℃): heterotrophy, Nitrosomonas, Nitrobacterium
Biofilm grazing	Saturation coefficients= f(℃) for: COD, NH_4^+, NO_2^-, NO_3^-, HCO_3^-, O_2
	Biofilm density and thickness

Part 4: Pilot design

1. Design criteria

In the following paragraph, conventional modeling for COD and nitrogen removal is reviewed. We designed our pilot-scale MSB set-up based on a conventional method for combined COD removal and effective nitrification.

1.1 For COD removal

Classification of T.F. is based on their organic loading, hydraulic loading and filter height. The T.F. is usually divided into Low-rate/standard-rate; Intermediate-rate; High-rate; Super-rate/Roughing filter. Classification criteria proposed by (EPA, 2000; Metcalf and Eddy, 1991) is shown in Table I-6:

Table I- 6: TF classification from EPA criteria

Types	Hydraulic loads (m^3/m^2d)	Organic loads ($kgBOD/m^3d$)	Height (m)
Low rate	1-4	0.08-0.32	1.5-3
Intermediate rate	4-10	0.24-0.48	1-2.5
High rate	10-40	0.32-1	1-2
Super rate	40-200	0.8-6	4-12

Because of the improvements of construction material in recent decades, technically no limit exists for the TF height if the costs are not taken into account. Additionally it is now recognized that the height of packing bed has less importance on Biological Organic Matter (BOM) removal efficiency than the mass transfer. Continuous use of various kinetic models requires the kinetic “constants” be adjusted as a function of filter height to correct their models (WEF Manual of Practice, 2000).

Early TF design models for BOD removal, such as U.S. National Research Council (**NRC**) and **Velz** Equation were based on the assumption that microbial kinetics limited the substrate removal (Logan et al., 1987). In those empirical relations, the organic loads affected the biodegradable substrate removal efficiency. An empirical relation for BOD removal efficiency and organic loading rate reported by (Gordon et al. 1948) from the NRC equation is shown in Eq. I-13:

$$E = \frac{100}{1 + 0.505 \times \left(\frac{C_{vBOD}}{F}\right)^{0.5}} \qquad \text{(I - 13)}$$

where:

E-BOD removal efficiency(%)

C_{vBOD}-Volumetric BOD loads (kg/d)

F-Recycle factor (1, no recycle)

(Logan et al., 1987) reported that BOD removal can exceed oxygen transfer if a sufficient pool of alternate electron acceptors is available.

The empirical relation of ***Velz Model*** shows that microbial kinetics limited the BOD removal. The BOD outlet/inlet ratio (C_{out}/C_{in}) versus the reaction coefficient ***k***, filter depth ***D*** and hydraulic loads ***q*** for those trickling filters with plastic medium is present in Eq. I-14:

$$\frac{C_{out}}{C_{in}} = e^{\frac{-k\,D}{q^n}} \qquad \text{(I -14)}$$

When a recirculation factor ***R*** was applied into operation, and to reform the BOD concentration ratio **(C_{out}/C_{in})** with respect to BOD removal efficiency ***E***, the classic Eq. I-14 of *Velz Model* can be rewritten as follows:

$$Ln(1-E) = \frac{D}{((1+R)q)^n} \qquad \text{(I -15)}$$

Furthermore, the temperature is a very important parameter because of its effect on chemical reactions and reaction rates, aquatic life, and the suitability of the water for beneficial uses. In addition, temperature of the wastewater can affect the dissolved oxygen concentrations in wastewater. Additionally, (Eckenfelder et al, 1963) developed the Velz equation by adding the special surface area $\boldsymbol{A_s}$ of the packing, the recirculation factor ***R*** and temperature correction coefficient $\boldsymbol{\theta}$ in Eq. I-16.

$$\frac{C_{out}}{C_{in}} = \frac{1}{(R_f + 1)\left(\frac{k_{20} A_s D \theta^{T-20}}{\left[q(R_f+1)\right]^n}\right) - R_f} \qquad \text{(I - 16)}$$

where:

C_{out}-BOD concentration in outlet, mg/L;

C_{in}-BOD concentration in inlet, mg/L;

D- Depth of the trickling filter media, m;

q- Surfacial hydraulic loads, m/h.

n- A constant with respect to the medium properties.

R_f -recirculation factor; proposed by (Sorrels and Zeller, 1955)

From NRC and Velz equation, with the assumption that the microbial kinetics limit the organic substrate removal; several hydraulic (Q, q and R), organic (C_{vBOD}), physical (medium constant *n*, packing bed depth *D*, specific surface area of medium *SSA*) and environmental elements (T and θ) should be taken into account when dimensioning a pilot.

1.2 For nitrification

(Logan et al., 1998) found that at low Organic Loading Rate (OLR), a single-stage TF can also reach high nitrification efficiency. The typical OLR applied for nitrification efficiency in a single-stage TF reported by (EPA, 2000) is shown in Table I-7.

Table I- 7: Typical OLR for single-stage nitrification (Metcalf and Eddy, 1991)

TF medium	Nitrification efficiency %	Typical organic loading rate kgBOD/m³d
Rock	75-85	0.1-0.2
	85-95	0.05-0.1
Rock	90	<0.08
	<50	>0.22
Plastic	75-85	0.2-0.3
Tower TF	85-95	0.1-0.2

From Table I-7, if we want to achieve effective nitrification (higher than 50%), the typical organic loading rate should be lower than 0.2 kgBOD/m³d.

1.3 Competition between heterotrophs and autotrophs in biofilm systems

Nitrification efficiency is strongly impacted by the addition of particulate organic matter. The Total Ammonia Nitrogen (TAN) removal rate was significantly lower at C/N≥0.5 than at C/N=0 (Michaud et al., 2006). The easily biodegradable organic carbon enrichment supporting the heterotrophic activity resulted in the establishment of a competition between autotrophic nitrifiers and heterotrophs for oxygen, nutrients and space inside the multi-specific biofilms, causing the reduction of nitrification rate. This competition between

the different microbial populations can result in a spatial distribution of microorganisms within the biofilm matrix that affects mass transfer processes and thus the performance of nitrification (Fdz-Polanco et al., 2000). Okabe et al., (1996) showed that heterotrophs and nitrifiers coexisted in the outermost biofilm for C/N=0. At C/N=1.5 heterotrophs dominated in the outermost biofilm and nitrifiers were present only in the deeper biofilm. Siebritz et al. (1983) found that the nitrification process is strongly inhibited by the heterotrophic processes when organic carbon was present, and when the ratio of COD/TKN (BOD/TKN) was higher than 20 (10), no nitrification process occurred. To decrease the inhibitory impact of the heterotrophic process on nitrifying bacteria, one should reduce the particulate fraction and enhance the removal of soluble organic carbon.

- Even the soluble fraction of typical rural wastewater is higher than 30% (Ze et al., 2010), whether the nitrification is effective and still can be inhibited by particulate substrate should be investigated in this study.

Additionally, (Zhu et al., 2001) found that the hydraulic condition of the biofilm surface was a major factor affecting TAN removal rate. Furthermore, liquid film diffusion of nutrients and oxygen has a considerable influence on the performance of nitrification (Tanaka and Dunn, 1982).

- It leads to the further study of hydraulic behaviors in the bioreactor, nutrients and oxygen transfer and transport in this thesis.

Besides the operating conditions, the medium is a very important element for treatment performance.

The next paragraph provides an overview of medium and their correlation with the hydrodynamic behaviours, also the performance difference depending on medium properties.

2. Medium selection

2.1 Types of medium

Medium is an important element for trickling filter design and operation. The characteristics of a medium can be analyzed in terms of its physical configuration, bulk density, material

density, porosity and specific surface area (West, 2008). Several typical medium widely employed in Trickling Filter approach are shown in Figure I- 10.

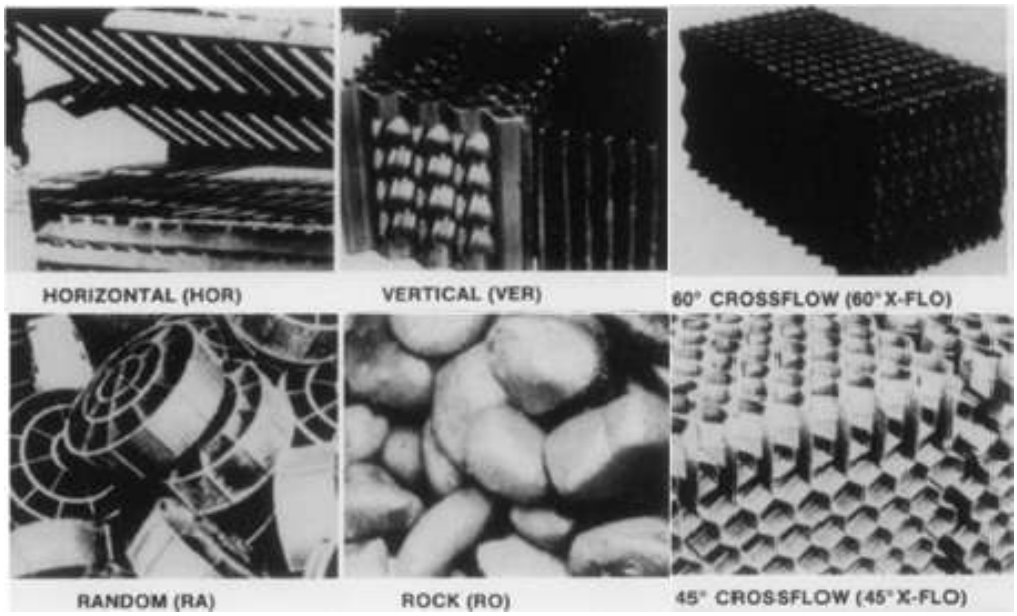

Figure I- 10: Typical Medium employed in Trickling Filter (Harrison and Daigger, 1987)

In the specialized studies of TF medium by (Harrison and Daigger, 1987), they investigated six typical medium in a TF under different hydraulic and organic loads. The characteristics of these medium are shown in Table I-8.

Table I- 8: Filter Medium characteristics in research of Harrison and Daigger, (1987)

Medium types	Medium physical characteristics				
	Material	Specific surface area (m^2/m^3)	Porosity (%)	Dry unit weight (kg/m^3)	Medium cross-sectional area (m^2)
Horizontal	Redwood slats	46	94	160	1.486
Vertical	Polyvinyl chloride	88	97	30	1.486
60°crossflow	PVC	98	95	30	1.486
45°crossflow	PVC	98	95	30	1.486
Random	cylinders	105	92	50	1.745
Rock	River rock	50	35	1280	1.745

2.2 Performance based on Medium configuration

To analyze the effect of medium configuration on the treatment performance, the liquid-surface contact time ***t*** and the packing azimuthal angle **α** were taken into account as reported by (Howland, 1958). For a TF, especially those packed with plastic medium, when the wastewater as a laminar flowing over the medium surface, the relation between the local contact time t and the flowrate Q over an inclined plane or a sphere firstly derived from (Don et al., 1959; Howland, 1959), are shown in Figure I- 11.

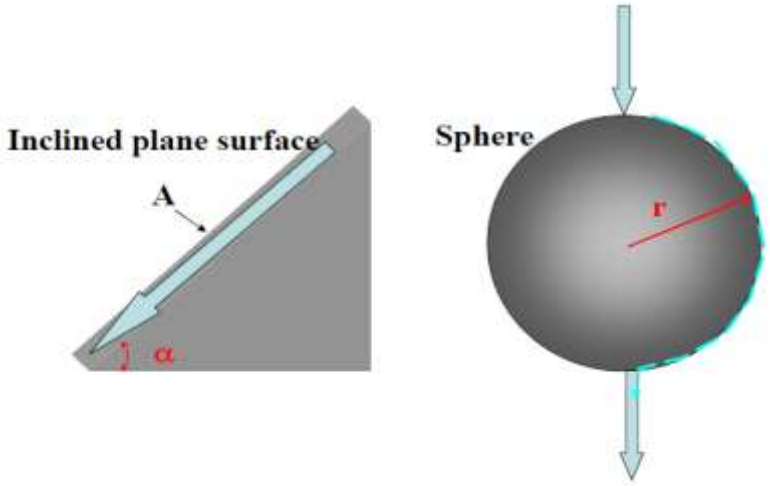

Figure I- 11: Diagram of the theoretical relation between contact time and flow

For an inclined plane, the local contact time is:

$$t = \left(\frac{3\upsilon}{g}\right)^{1/3} \frac{A}{S^{1/3}Q^{2/3}} \qquad \text{(I - 17)}$$

For a spherical medium, local contact time derives:

$$t = 2.6\left(\frac{3\upsilon}{g}\right)^{1/3} \frac{(2\pi)^{2/3} r^{5/3}}{Q^{2/3}} \qquad \text{(I - 18)}$$

where:

A-Area of inclined plane surface (m^2);

g- Gravitational acceleration (m/s^2);

Q- Flow rate (m^3/s);

r- Radius of sphere (m);

S- Slope of plane expressed as sinα;

t- Contact time of flow over medium surface (s);

v- Kinematic viscosity of water (m^2 /s).

Bird (1979) investigated the liquid film thickness on an inclined plane medium by falling liquid film analysis for the ideal laminar flow:

$$\delta_L = \left(\frac{3Q\mu}{\rho g W \sin\alpha} \right)^{1/3} \qquad \text{(I - 19)}$$

where:

δ_L- Liquid film thickness (m);

μ- Liquid viscosity (m^2 /s);

ρ- Liquid film density (g/ m^3);

g- Gravitational acceleration (m/s^2);

W- Width of the plane (m);

α - Angle of inclination of the plane

Q- Volumetric flow rate down the inclined plane (m^3/s).

As the configuration of the plastic medium shown in Figure I- 10 all contain inclined plane surface and considering the flow contact time ***t*** on the medium surface and the liquid film thickness $\boldsymbol{\delta_L}$ in Eq. I-19; the **α** of Vertical Medium (VE), Horizontal medium (HO), 60°Cross-Flow (CF) medium and 45° CF are 90°, 0°, 60° and 45°, respectively, HO medium has longest contact time (t) and thickest liquid film (δ) which results in the worst oxygen-transfer capability through the liquid film. In contrary, VE medium has best oxygen-transfer capability because of the thinnest liquid film and shortest contact time, and followed by 60°and 45°CF medium.

The BOD removal efficiency and the nitrification versus different hydraulic and organic loads in trickling filters by applying different medium have been reported by numerous researchers (Norris et al., 1982; Logan et al., 1987a; Logan et al, 1987b; Logan et al., 1989; Hinton et al., 1989; Logan et al., 1990).

A detailed research by (Harrison and Daigger, 1987) are shown in Figure I-12 for BOD removal and Figure I-13 for nitrification (where HO-Horizontal medium; CF-Cross-Flow medium; VE- Vertical medium).

The BOD removal performance related to operation conditions in a TF based on Eq. I-15 is shown in Figure I-12.

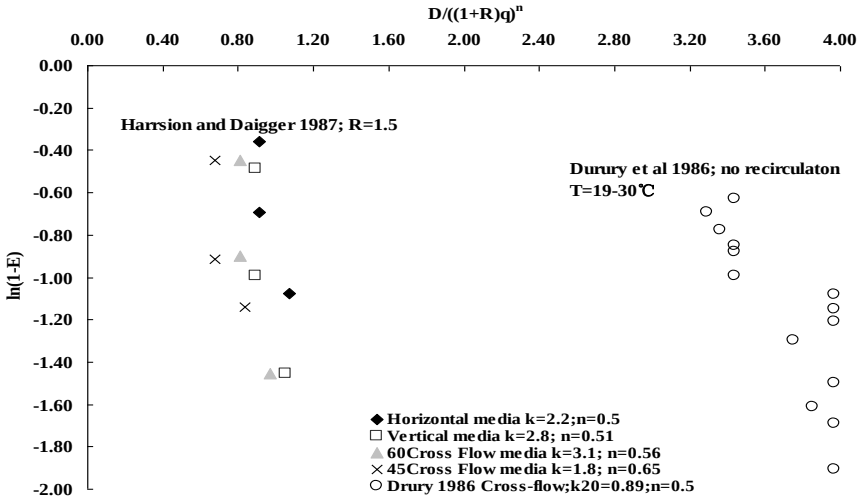

Figure I- 12: Comparison of different media accounting for relations of filter depth and hydraulic loads with BOD removal efficiency based on modified Velz equation.

In Figure I-12, the BOD removal performances depend on medium configuration under different hydraulic loads and organic loads. This indicates that medium types and configurations influence the treatment efficiencies. Generally, under the same hydraulic and organic conditions, vertical medium has better BOD removal performance than other medium whose reaction rate ***k*** is greater than that of other medium; However, Trickling filter with cross-flow medium can sustain higher hydraulic loading and lower packing depth and probably offer longer Hydraulic Retention Time (HRT) and more space for nitrification.

Figure I-13 present the nitrification performance of 6 different medium under different OLR.

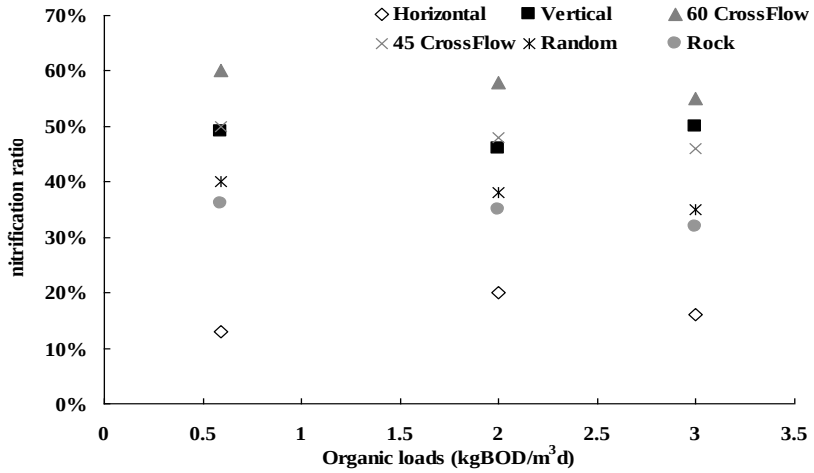

Figure I- 13: Medium configuration effect on nitrification versus volumetric organic loads (Harrison and Daigger 1987)

Figure I-13 indicates 60° CF media has the best nitrification efficiency under different organic loads. This resulted from the better oxygen transfer of 60° CF media. However, in Harrison and Daigger's research (Harrison and Daigger, 1987), they didn't find any significant difference in the oxygen transfer when comparing CF with other medium. Rock media have lower SSA and lower porosity; HO media have the worst oxygen-transfer capability because of both the low SSA and thickest liquid film.

To sum up, different types of media lead to different substrate removal efficiencies depending on their different configurations, which lead to different SSA, porosity, oxygen-transfer capacity, liquid film thickness and Liquid Residence Time (LRT) consequently. In order to employ different medium into a TF to treat rural wastewater, we should analyze the physical properties such as SSA of packing a_p, solid density ρ_p, porosity of solid ε'. These physical properties are in correlation with the medium type coefficient n, and their hydrodynamic characteristics, such as the liquid-surface local contact time t and overall LRT in the filter, also the liquid film thickness δ_L.

3. Dimensioning a pilot

3.1 Particular consideration of new structure

All the previous discussion about the design criteria of TF pilot and medium selection were mainly for conventional TF and conventional media. In order to apply natural aeration for our lab-scale pilot to minimize the energy consumption and to improve the oxygen supply for pilot, we decided to apply an open structure for our pilot design, which changes the close structure of a conventional TF into an open structure for better oxygen supply. Meanwhile, in order to improve the air supply at the bottom of each section, the interval space between sections were also decided to be applied in our pilot design.

Due to the cooperation between LISBP of INSA and SJTU of China, we decided to use a new Concrete-Brick Medium into our lab-scale pilot; this is a new type of medium recently developed for wastewater treatment. Though as discussed in the previous paragraph, different

type of media will effect the COD removal and nitrification performance, we only focus on this new type of medium for its effect on final performance.

3.2 Dimensioning our pilot for lab-scale experiments

The dimensioning lab-scale pilot for both COD removal and effective nitrification is presented in Appendix 1 in detail. The design of pilot was mainly based on the Manuel of U.S. Environment Protection Agency (EPA, 2000) (EPA, 2002) with respect to the carbon removal and nitrification also considering the rural wastewater characteristics as discussed in following part. The detailed discussion of the interval space determination is also calculated in Appendix 1. Generally, in order to maintain at least 50% of the liquid droplet at the splash edge, an interval distance H$\leqslant$0.1m is necessary.

Additionally, the interval distance less than 10 cm is sufficient to avoid droplet splash from both edges of the section.

Finally, the pilot we selected to validate all the requirements is shown in Figure II-1 in Chapter 2 of M&M.

4. Partial conclusion

1. The Trickling Filter process is reviewed in this chapter and the main affecting elements both the physical and biological are overviewed and discussed.
2. Attempts were made to design a pilot based on the BOD removal and nitrogen removal which derives from the discussion of medium and physical and biological aspects.
3. The interval distance/space between adjacent sections was roughly discussed. Approximately 0.1 m of this interval distance will avoid partial feeding loss from the section edges.
4. Those parameters and value ranges are summarized from design criteria and also literature references for the simulation and analysis works in the next Chapter are shown as follows:

For bioreactor and medium aspect, we will study their physical properties and hydrodynamic aspect. These parameters should include SSA of packing $\boldsymbol{a_p}$, solid density $\boldsymbol{\rho_p}$, porosity of solid $\boldsymbol{\varepsilon'}$, that are in correlation with the medium type coefficient $\boldsymbol{n}$, and their

hydrodynamic characteristics, such as the liquid-surface local contact time $\boldsymbol{t}$ and overall LRT in the filter, also the liquid film thickness $\boldsymbol{\delta_L}$. Moreover, in order to better understand how the hydraulic characteristics affect the treatment performance, the liquid distribution form in the bioreactor such Completely Stirred Tank Reactor (CSTR), Plug Flow (PF) along with the modeling method such as Retention Time Distribution (RTD) will be applied.

For biofilm aspect, from above all discussion, we will mainly focus on the biodegradation of Biological Organic Matter (BOM) and nitrogen removal processes, such as biological transformations, attachment, detachment, oxygen transfer, liquid repartition. Then we will provide information for a better design and operation of this type of TF

5. Those parameters discussed above in the simulation works might not be well associated with the models within a simulator; hence pre-simulation is needed to verify how this software works on the Trickling filter systems also make calculation of those parameters and processes with the software to see whether there is a need to calibrate these parameters.

Part 5: Modeling of TF

1. Introduction of the software BIOWIN

BioWin is a wastewater treatment process simulator that ties together biological, chemical, and physical process models. BioWin is used world-wide to design, upgrade, and optimize wastewater treatment plants of all types. The core of BioWin is the proprietary biological model which is supplemented with other process models (e.g. water chemistry models for calculation of pH, mass transfer models for oxygen modeling and other gas-liquid interactions). The BioWin model is owned, developed, and supported exclusively by Enviro-Sim, the original “whole plant” model.

1.1BioWin in Brief

The user can define and analyze behavior of complex treatment plant configurations with single or multiple wastewater inputs. Most types of wastewater treatment systems can be configured in BioWin using many process modules. These include:

- A range of activated sludge bioreactor modules – suspended growth reactors (diffused air or surface aeration), various SBRs, medium reactors for IFAS and MBBR systems, variable volume reactors.
- Trickling Filter module.
- Anaerobic and aerobic digesters.
- Various settling tank modules – primary, ideal and 1-D model settlers.
- Different input elements – wastewater influent (COD- or BOD-based), user-defined (state variable concentrations), metal addition for chemical phosphorus precipitation (ferric or alum), methanol for denitrification.
- Other process modules – holding tanks, equalization tanks, dewatering units, flow splitters and combiners.

The program has the look and feel of many Windows applications. When it is launched it comes up with the familiar interface and menu structure. Complex treatment plant schemes can be configured rapidly through "drag and drop" mouse actions. Functions are selected from

the pull-down menus, using short cut keys, or by pointing the mouse and clicking on icons in the toolbar. The user can also access many of the Windows functions usually embedded in a Windows application; for example, selecting and configuring the printer setup. Context-sensitive Help is built into BioWin to provide on-line assistance, particularly for new users.

Careful consideration has gone into the design of the package; for example, the hardware and software platforms, the object oriented software development system, the data structures, the user interface, and so on. A primary aim has been the production of a package structured to allow on-going development in years to come.

The BioWin simulator suite presently includes two modules:

- A steady state module for analyzing systems based on constant influent loading and/or flow weighted averages of time-varying inputs. This unit is also very useful for mass balancing over complex plant configurations.
- An interactive dynamic simulator where the user can operate and manipulate the treatment system "on the fly". This module is ideal for training and for analyzing system response when subjected to time-varying inputs or changes in operating strategy.

1.2 TF Module

A new trickling filter (TF) element is now included into the BioWin model library. The TF element can be configured for various packing types such as Rock, Horizontal, Structured Plastic (cross-flow), Loose Medium (random), and Custom. The depth of the filter unit is modeled in three equal layers to simulate oxygen levels and removal gradients from top to bottom. The number of layers for modeling the biofilm, the thickness of the liquid layer on the biofilm, and the boundary layer thickness can all be configured to closely match the existing filter unit.

The TF element aeration can be specified by the dissolved oxygen concentration or air flow rate, at constant or scheduled pattern values. Gas phase modeling can be used to determine Dissolved Oxygen (DO) concentrations throughout TF model depth from the top to the

bottom. Local unit parameters such as temperature, biofilm and kinetic parameters can all be user specified. The new TF element allows user to explicitly model a trickling filter unit and further expands the flexibility of BioWin.

The Trickling Filter model can predict the extent of carbon and nitrogen removal. The profiles of the various components through the biofilm were modeled so that different environments (aerobic, anoxic) can exist within the biofilm. The limitations of this model concern mainly the hydraulics of Trickling Filter and the biofilm itself. It is assumed that the flowrate and organic loads to the filter can always be processed, which means the clogging and headlosses through the filter are not modeled. Moreover, the max thickness of the biofilm cannot be calculated automatically. Rather the user should specify it. This assumption was primarily made because there are few data available for calibration of the maxi biofilm thickness calculation. Generally, it is assumed that there is uniform flow distribution over the entire surface area of the packing medium in a TF. However, there is no possibility that users specify the porosity of medium and the void space of packing bed in the TF which should be considered in the physical variables.

1.2.1 Conceptual model of TF

The TF is divided into 3 horizontal sections. Each section represents a cross-section of the TF at a different depth. The transfer of the state variables between each of these horizontal sections is through liquid flow. The biofilm in each of these horizontal sections is modeled as a number of layers (default is first layer as the liquid film on the top and other two layers as the biofilm). The transfer of soluble substrates between those layers is only by diffusion. Particulate substrates can be displaced into the adjacent layer by growth processes. Biofilm layers are modeled as a CSTR with the same biological reactions. Attachment and detachment coefficients are used to provide for a means of transfer of particulate components between the biofilm surface and liquid film. When the biofilm thickness starts to approach the maximum value, detachment of biofilm will occur. The conceptual diagram of TF model is depicted in Figure I-14.

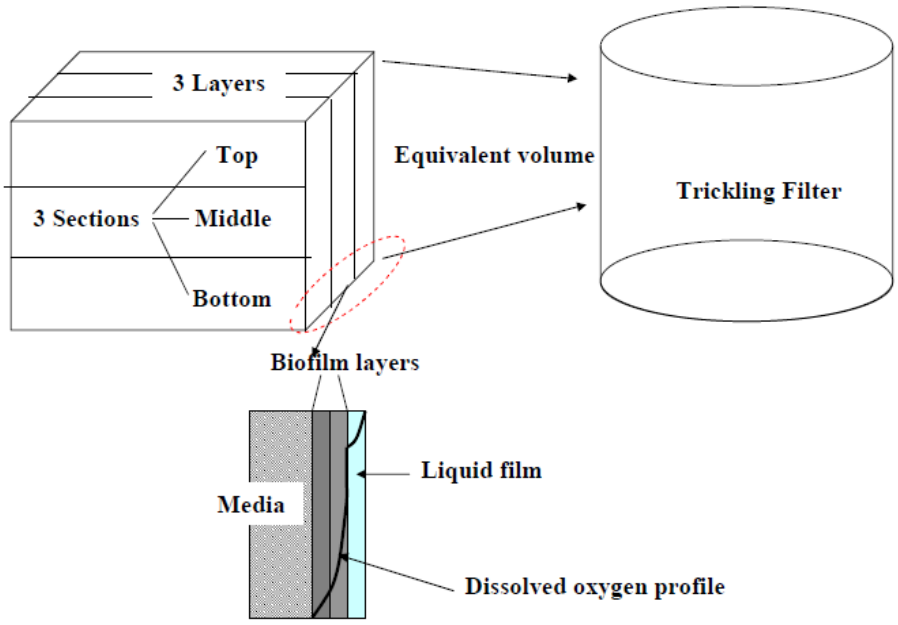

Figure I- 14: Conceptual diagram of the TF model

1.2.2 Biological models

A crucial component of BioWin is the biological process model. The BioWin model is unique in that it merges both activated sludge and anaerobic biological processes. Additionally, the model integrates pH and chemical phosphorus precipitation processes.

Biofilm thickness

The evolution of the biofilm thickness L_f over time is directly related to the concentration of ***X*** present in ***n*** layers of the biofilm. It is calculated according to a discrete integration and is the product of the amount of solids and biomass accumulating gradually in layers of the biofilm by the maximum thickness of the biofilm $L_{f,max}$ thus regulating the evolution of the thickness. It is defined as the sum of the layer thickness of each horizontal section as:

$$L_f = \sum_n \frac{X \cdot L_{f,\max}}{\rho_w f_{DM} n}$$

Where n is the number of layers. L_f is more or less increase over time depending on the amount of biomass X present in the biofilm to reach a constant value more or less close to the maximum thickness $L_{f,max}$. From that time, the layers of the biofilm must release the X faster in order to control the thickness.

External mass transfer and transport between liquid and biofilm

The equation employed for the diffusion of substrates from the bulk liquid into the biofilm is given by:

$$\underbrace{A_a \delta_L \left(\frac{dC^L}{dt} \right)}_{\text{Accumulation in liquid film}} = \underbrace{Q_L \left(C_{n-1}^L - C_n^L \right)}_{\text{Liquid flow}} - \underbrace{K_m A_a \left(C_n^L - C_n^{BL} \right)}_{\text{Diffusion into biofilm}} + \underbrace{K_L A_a \left(C_0 - C_n^L \right)}_{\text{Air/liquid exchange}} \quad \text{(I-17)}$$

where:

Aa-Surface area of biofilm where transport occur (m^2);

δ_L-Liquid film thickness (m);

C_n^L-Substrate concentration in liquid film section *n* (mg/L);

t-Time (days);

C_n^{BL}-Substrate concentration at biofilm/liquid interface section *n* (mg/L);

C_0-Saturated liquid film substrate concentration (mg/L);

Q_L-Volumetric flowrate of attached liquid film (L/d);

Km-Mass transfer coefficient from liquid to biofilm (m/d);

K_L-Oxygen transfer coefficient from air to liquid film (m/d);

A-Surface area of attached microorganisms (m^2);

D_Z-Substrate diffusion coefficient (m^2/d) ;

C-Substrate concentration in layer (mg/L);

Z-Thickness of biofilm layer (m);

Internal mass transfer and transport between layers

The diffusion through the biofilm is described by Fick's second law and supplemented by biological reactions as shown in Eq. I-18.

$$\underbrace{\frac{\partial C}{\partial t}}_{\text{Accumulation in biofilm}} = \underbrace{-D_Z \frac{d^2 C}{dZ^2}}_{\text{Diffusion into biofilm}} + \underbrace{\left(C_{n-1}^B - C_n^B \right) \left(\frac{Q_B}{A L_f} \right)}_{\text{Advection between biofilm layers}} - \underbrace{R_S}_{\text{Reduction}} \quad \text{(I-18)}$$

where:

Aa-Surface area of biofilm where transport occur (m^2);

δ_L-Liquid film thickness (m);

C_n^L-Substrate concentration in liquid film section *n* (mg/L);

t-Time (days);

C_n^{BL}-Substrate concentration at biofilm/liquid interface section *n* (mg/L);

C_0-Saturated liquid film substrate concentration (mg/L);

Q_L-Volumetric flowrate of attached liquid film (L/d);

Km-Mass transfer coefficient from liquid to biofilm (m/d);

K_L-Oxygen transfer coefficient from air to liquid film (m/d);

A-Surface area of attached microorganisms (m^2);

D_Z-Substrate diffusion coefficient (m^2/d) ;

C-Substrate concentration in layer (mg/L);

Z-Thickness of biofilm layer (m);

C_n^B-Substrate concentration in attached biofilm layer *n* (mg/L);

Q_B-Volumetric flowrate of attached biofilm layer (L/d);

L_f-Biofilm thickness (m);

R_S-Substrate utilization rate (mg/L·d)

From the Petersen matrices for substrate biodegradation (Appendix 2) and substrate diffusion in the liquid (Eq. I-17) and in biofilm (Eq. I-18), the resolution of the model requires knowledge of:

- 16 state variables: Si, Ss, Xi, Xs, Xbh, Xba, Xu, Xsto, Sno, Snh, Snd, Xnd, Snn, So, Salk, Xii;
- 2 physical parameters: filter depth L, specific surface area SSA;
- 3 hydraulic parameters: flowrate Q, liquid residence time LRT, liquid film thickness δ_L;
- 5 parameters related to the intrinsic kinetics of biofilm (heterotrophic/ autotrophic): μ, Ks, K_{O2};b, Y
- 2 parameters for biofilm expansion and sloughing: r_{attach}, r_{detach}
- 2 parameters of biofilm properties: L_f;ρ_f
- 2 parameters related to the substrate and oxygen diffusion in the biofilm: D_S and D_{O2};
- 2 environmental parameters: temperature and pressure.

2. Partial conclusion

1. The software BIOWIN can be applied for our MSB treatment performance simulation, because of its complexity and flexibility for wastewater treatment;

2. The sensitivities of different kinetic parameters should be examined before calibration of simulation;

3. Parameters including the operating parameters, physical parameters, influent components fractionation, and kinetic parameters should be calibrated. 3 hydraulic parameters are required, Chapter 3 will be dedicated to their determination.

4. Simulation results after calibration should be compared with experimental results to adjust main affective parameters to improve the simulation performances and to instruct the real pilot application.

Part 6: Rural wastewater characteristics

The objective of this part is to underline the specificities of the wastewaters from decentralized or rural treatment systems. Special attention is paid to variations of concentrations, of flows and fluxes because it will greatly affect the removal capacity of a TF.

1. Introduction

For designing a bioreactor to treat the rural wastewater, the hydraulic flow and the mass loading of the wastewater sources should first be estimated. The reliability of data from both daily and long term hydraulic flow and its variation will influence the design, hydrodynamic characteristics of the system, optimization and operation. The mass loading of wastewater constituents is necessary for an appropriate technology option, and for designing a system to fulfill the effluent requirements. The hydraulic flow and mass loading variation of rural wastewater were thus characterized.

2. Characteristics of rural wastewater

2.1 Rural wastewater quality

Generally, rural and decentralized wastewater characteristics depend on activities in the community. They contain lower concentrations of pollutants comparing to the municipal and industrial sewage. A comparison was made between a typical rural wastewater and a municipal sewage from Central Waste Water Treatment Plant (CWWTP) in their composition concentrations and shown in Table I-1.

Table I - 1: Pollutants composition of a typical rural wastewater comparing with wastewater from a CWWTP in China (Yu et al, 2006; Ma et al, 2010)

Wastewater Source	pH	COD_{Cr} (mg/L)	BOD_5 (mg/L)	NH_4^+-N (mg/L)	TKN (mg/L)	TP (mg/L)	SS (mg/L)
Rural community	6.5~7.5	150~350	80~180	10~50	20~80	2~9	180~500
Mean value		250	120	30	50	6	350
CWWTP	7.5~8.5	300~1000	150~500	20~80	30~100	10~25	350~1200
Mean value		600	300	50	60	20	700

However, with only these lumped data, it is not possible to estimate precisely the potential of a biological treatment system (Kujawa-Roeleveld, 2000). Roeleveld and van Loosdrecht, (2002) reported a physical-chemical method to characterize the soluble and particulate fractions, combined with a BOD-analysis for characterizing the biodegradable fraction of the influent COD. The development of different models, such as Activated Sludge Model (ASM) in recent decades, led to the requirement of a more intensive wastewater characterization of different components, as the fractionation of wastewater components. For example, wastewater COD fractions were divided according to solubility (soluble COD and particulate COD) and biodegradability (biodegradable fraction measured by ultimate BOD or BOD5, and non-biodegradable) (Roeleveld and van Loosdrecht 2002; Gillot and Choubert 2010).

The biodegradability or the treatability of rural wastewater was thus investigated based on the stoichiometric ratio of COD fractions and Nitrogen, concerning both the COD removal and nitrification.

2.2 Treatability of rural wastewater

Treatability of a wastewater depends on various aspects such as nature of the components (biodegradability/refractory character; soluble colloidal or particulate form), their absolute concentrations (inhibitory effects), the ratio between concentrations of some specific compounds (metabolism requirements), etc.

Roeleveld and van Loosdrecht, (2002) characterized the wastewater based on a physical-chemical method to estimate the soluble and particulate fractions of COD and BOD. To analyze if a type of wastewater is easily biodegradable, the stoichiometric ratios such as BOD5/COD or BODu/COD was applied in ancient method, as the measurement of ultimate BOD (BODu) or BOD5 could estimate the biodegradable fraction of wastewater (Metcalf and Eddy, 1991; Henze et al., 1995; Makinia and Wells, 2000). The remaining part is non-biodegradable COD.

Non biodegradable COD versus total COD and corresponding BOD5/COD ratio is shown in Table I-9, as reported by Henze et al., (1995).

Table I- 9: Relation between non-biodegradable COD fractions and BOD_5/COD ratio

*COD_{nb}/COD	0.1	0.2	0.3	0.4	0.5	0.6	0.7	0.8
BOD_5/COD	0.52	0.46	0.41	0.35	0.29	0.23	0.17	0.12

*COD_{nb} denotes the non-biodegradable COD.

From the data of Table I-9, the BOD5/COD can be estimated to be 0.4-0.5 for rural and decentralized WW, which indicates the non-biodegradable fraction is less than 30% of total COD.

Figure I-15 shows the comparison of the stoichiometric ratios of several types of decentralized wastewater, the data of rural wastewater from a village of 400 persons was summarized from an investigation during 4 years in China.

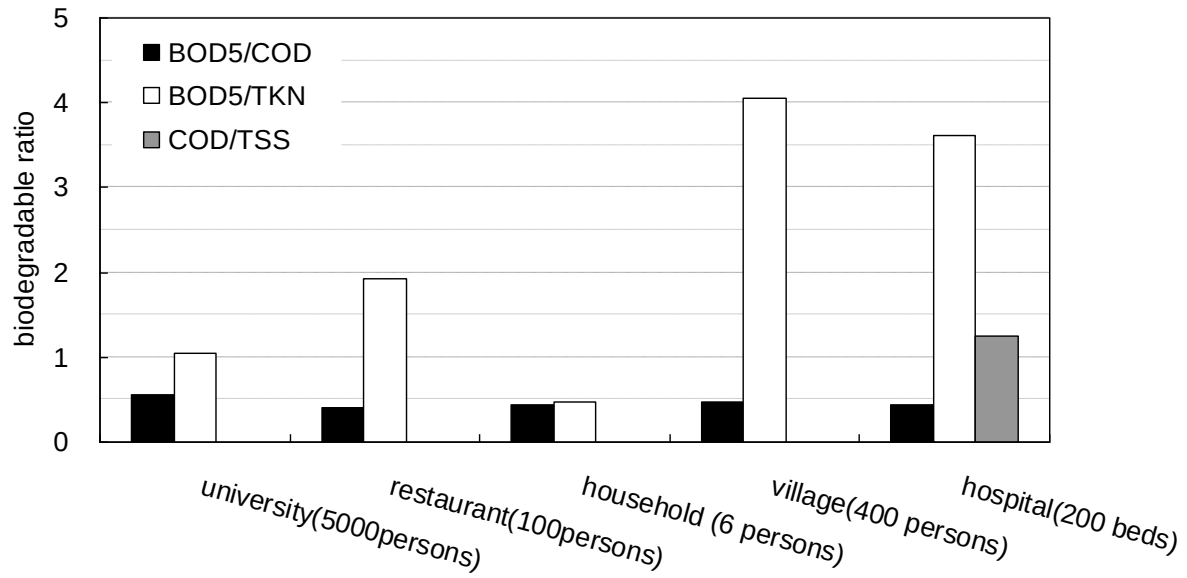

Figure I- 15: Comparison of biodegradability of several decentralized wastewater (Shi et al, 2005;Yu et al, 2006; ZHANG et al, 2008; MOREL, 2006)

From Figure I-15, the ratio BOD_5/COD≈0.4-0.5 of rural wastewater, the non-biodegradable COD was less than 30% (from Table I-2) of total COD which implies good biodegradability of COD. The BOD_5/TKN ratio was generally less than 4, indicating the particulate fraction is lower, which implies that nitrification will occur together with the heterotrophic growth.

3. Rural Wastewater Flow

3.1 Daily discharge of rural wastewater

The discharge flow of rural wastewater is generally less than that of the municipal sewage and that is true in various countries. A summary of worldwide rural wastewater discharge is shown in Table I -10.

Table I- 10: Household water consumption and accordingly wastewater discharge (per capita) in rural areas in different countries/areas

Country/Area	household consumption* (L/per capita/d)	rural wastewater discharge (L/per capita/d)
China	70-110	25-70
France	150-200	180
United States	>400	190
Japan	200	180
Algeria, Morocco, Turkey	20-65	50
Africa	15-35	20
Southeast Africa	30-70	60
Western Pacific	30-90	80
Eastern Mediterranean	40-85	55
Latin America and Caribbean	70-190	110
Europe	180-250	200

*Data adapted from (Salvato, 1992); (GUO, 2010); (AWWARF, 1999); (EEA 2005); (Siegrist, 1976.); (Samie, 2009)

Table I-10 shows that the daily discharge of rural wastewater in Asian and African countries (i.e. China<100 L/per capita/d) is distinctly less than for European countries (i.e. France<200 L/per capita/d).

When the population (per capita) in a rural community or a village is taken into account, discharge of individual resident (per capita) can help to determine the average, minimum and maximum daily flow. For example, if a plant is required treating the wastewater for a village of 2000 *per capita* in a village, taken the mean daily flow of 180 L/per capita/d in France into account, the max flow of rural wastewater can be calculated as 360m³/d for the plant.

However, the time discharge is not constant in rural areas; it varies hourly due to the routine of habitants. To design a plant cannot only consider the mean daily flow, the variation should also be considered. The daily flow variation was thus introduced.

3.2 Hourly flow and components' concentrations variation

Hourly flow and pollutants concentrations of a typical rural wastewater are shown in Figure I -16.

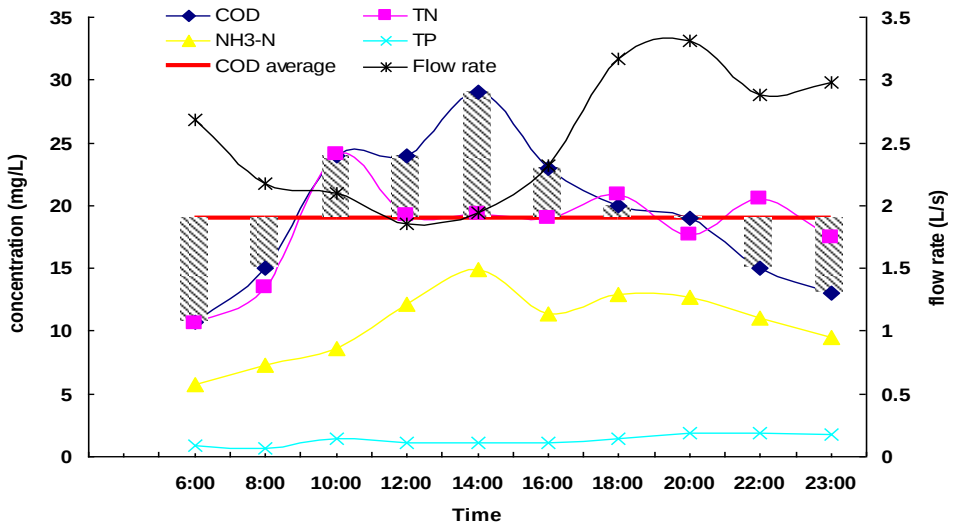

Figure I- 16: Rural wastewater diurnal flow and components concentrations variation
*Data from a village of China (Nengwang 2004)

In Figure I-16, the Total nitrogen (TN) concentration achieved the peak after 4 h from the sampling time; for COD concentration after 8 h. For flowrate (discharge flow) after 14 hrs; ammonia-nitrogen (NH_3-N) concentration fluctuated similar to that of COD, which was after 8 hrs. The Total Phosphorus (TP) concentration varied little.

Generally, after about 8 hrs, the pollution attains the maximum, as also observed by some French researchers (Cornier et al., 1994). They found that, in France, 90% of the pollution is produced during 8 hours/day.

Due to the high variations, the flow variation coefficient is thus introduced. The daily variation coefficient K_d, hourly variation coefficient K_h and total variation coefficient K_t (shown in Eq. I-19 to Eq. I-21) were used to calculate flow rate variations.

$$K_d = \frac{Q_{d\ max}}{\overline{Q}} \qquad \text{(I - 19)}$$

$$K_h = \frac{Q_{h\ max}}{\overline{Q}} \qquad \text{(I - 20)}$$

$$K_t = K_d \times K_h \qquad \text{(I - 21)}$$

where:

$Q_{d\ max}$- The maximum daily flow;

$Q_{h\ max}$- The maximum hourly flow during the day with maximum daily discharge.

The total variation coefficient K_t is plotted in Figure I-17 against the mean daily flow rate (data from a WWTP in Shanghai of China).

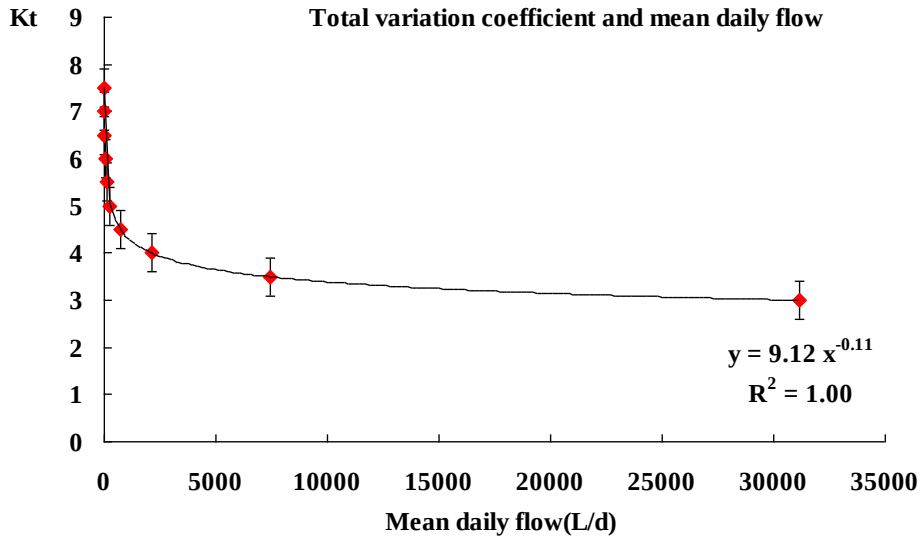

Figure I- 17: Total variation coefficient with respect to the daily flowrate (modified from (State-Planning-Commission, 1987)

In Figure I-17, the variation coefficient of rural wastewater is in the range of 3-6; on contrary, when mean daily flow is higher than 35m³/d (equivalent 200 PE in France, 500 PE in China from TableI-10), it approaches a constant value of 3. When daily flowrate was lower, the variation was greater. From this curve, the variation of rural wastewater discharge flow can be greater than that of municipal wastewater due to its lower discharge. Taking the average daily flow of 2.5 L/s (from Figure I-16) e.g.; the value of K_t is approximated 2.4 from the curve of Figure I-17. The classic value of K_d of rural wastewater in China is usually around 3-5 (Guo et al., 2010), we can estimate the K_h by 2.4/5=0.48 via substituting K_d=5 owing to the local climate variation; daily flow variation was calculated by 2.5(L/s)×0.48=1.2 L/s. The max and min daily flow is hence of 2.5±1.2 L/s (200±104 m³/d), which agrees with the data from

Figure I-16 of the range 1.9-3.3 L/s (150-300 m³/d). It represented about 90% of the max and min calculated values.

In general, typical daily flow of rural wastewater is in the range of 100-300 m³/d. In fact, the daily flow rate could vary from one location to another depending on the amount of inhabitants and their daily activities. However, only the daily flow provides not enough information for a treatment system design and operation, long term hydraulic flow and mass loading with variation were also involved and then introduced.

4. Partial conclusion

In general, rural wastewater is distinguished from municipal and industrial wastewater and other types of wastewater, in terms of its non-point sources and dispersed discharge, lower flow rate, relatively lower components' concentrations, flow and organic loads variation, good treatability because of containing more biodegradable fractions. The typical municipal and rural wastewater in relation with their flow, COD loads and Total Ammonia Nitrogen (TAN) loads, also shows daily variation as shown in Table I-11.

Table I- 11: Comparison between the typical municipal and rural wastewater in terms of their daily flow, COD loads, TAN loads and variation of daily flow

	Range of flow m^3/d	Range of COD loads kg/d	Range of TAN loads kg/d	Range of variation
Typical municipal wastewater	>300	>300	>30	<3
Typical rural wastewater	<200	<24	<2	3-5

From Table I-11, rural wastewater is more diluted than the municipal wastewater and the daily flow has higher variation. It is not easy to analyze the shock conditions for our pilot and the dynamic of daily flow is not easy to realize. Due to the duration of our experiments, we cannot test all situations with various conditions. Hence we did not consider the high variation of daily flow, and we used more loaded wastewater with lower constant flow rate.

From what we discussed about the typical rural wastewater, the typical stoichiometry ratio $BOD_5/COD \approx 0.4\text{-}0.5$ implies good biodegradability of organic matter. The ratio of

BOD_5/TKN<4, indicated the nitrification may occur effectively together with the heterotrophic growth. However, the potential of nitrification inhabited by heterotrophic growth should be refer to specific fractionation of rural wastewater at different locations. The hydraulic flow (less than 200 m^3/d) and mass loading (COD loading less than 24 kg/d and TAN loading less than 2 kg/d) should be taken into account in further design, simulation and modeling.

Moreover, considering the characteristics of rural wastewater, several important factors of fixed-film technologies for wastewater treatment should be discussed:

- The Hydraulic Residence Time (HRT), this is associated with hourly and daily flow. It will affect mass transfer and oxygen transfer influencing the nitrification. The hydrodynamic behaviors of treatment system are to be investigated.
- Fraction of particulate matter. The fraction of particulate matter/total matter is considered; because it influences the biodegradable substrate removal and consequently affects the nitrification.

Objectives of this thesis:

The main objective of this research project focuses on the study of the Chemical Oxygen Demand (COD) removal and nitrification in a newly designed Multi-Section Bioreactor (MSB) especially for rural wastewater treatment, and validation of a model for dynamic conditions in the BIOWIN software but never previously tested. To limit the influence of mechanisms and competition of autotrophic and heterotrophic biomasses, the model is tested in treatment of COD removal and nitrification. To do this, a methodology was developed and setting implementation through an experimental protocol carried out in parallel on a semi-industrial pilot. The experiment should really be selected according to the properties of the model as it is not realistic to be able to identify the model parameters from a set of data prior to any discussion of modeling. That is why, in addition to a set of data collected in the field continuously for a long period, a protocol is established based on specific experimental tests to feed the TF model.

Finally, the acquisition of this experimental basis is addressed by two types of research defining two specific objectives in this PhD thesis:

Experimental part

Although one can find in the literature numerous studies on the overall efficiency of TF process, no research has been done on the MSB. This is what defines the uniqueness of this part (Chapter III and IV) that will enable:

- The physical characteristics such as specific surface area, bulk density, porosity of the packing should be determined both before the installation of bioreactor and during the running period to confirm the hydrodynamics of the packing and the filter.
- In order to verify the treatment efficiency under the rural wastewater conditions, the limiting processes should be well determined.
- Furthermore, how to realize more reliable nitrification process together with COD elimination? In view of the open structure of the biofilter, what is the effect of

structure on the oxygen transfer process and is there an oxygen limitation?

- How will the packing and biofilter hydrodynamics affect the treatment performance and mass transfer, such as liquid retention time and liquid film thickness?
- How do the hydrodynamics affect the biofilm attachment and detachment such as shear stress, and further influence the biofilm local retention time?
- Which parameters determine the limitation of nitrification? Both along the biofilter and inside the biofilm?
- How are oxygen transfer and mass transfer into the biofilm distributed along the filter?

Simulation part

Following a thorough study of TF model to apply in both COD removal and nitrification for a pilot similar to our MSB, the originality of this part (Chapter V) is that of:

- Simulation was carried out by the simulator-BIOWIN under the rural wastewater conditions to predict the treatment performance and the main parameters that affect the organic substrate removal and nitrification processes;
- Check the validity of an existing TF model but never tested with actual field data. Try to improve the fitness between simulation and experiments.
- Try to find hydrodynamic parameters that could affect the oxygen transfer, and which could further affect the biological treatment.

Chapter 2

Material and methods

PART 1: Medium and bioreactor characterization and hydrodynamic behavior investigation

1. Objectives

With the ultimate aim of optimizing Trickling Filter (TF) design and operation, the main objective of this study was to characterize the hydrodynamic behavior of two types of TFs filled with the same porous medium in order to assess the impact of the properties of the medium on the overall hydrodynamics. Such impact was measured in terms of liquid holdup fractions, liquid film thickness under the regimes with and without biofilm along the column after cultivated at two organic loading rates. By using Residence Time Distribution (RTD) experiments and modeling, our further objective was to investigate the changes in liquid flow pattern and residence time due to the presence of biofilm in the Multi-Section Bioreactor (MSB). Additionally, the study attempted to verify whether the configuration of the bioreactor, a conventional Trickling Filter Column (TFC) and a new designed Multi-Section Bioreactor (MSB), would affect its hydrodynamic characteristics. The collected data will be used to proceed to accurate BIOWIN simulation in Chapter 5.

1.1 Experimental System

The experimental system was set up with two types of Trickling Filter, a TFC in Figure II-1(a) and a MSB in Figure II-1(b), linked with a balance or a conductometer connected with a data acquisition system.

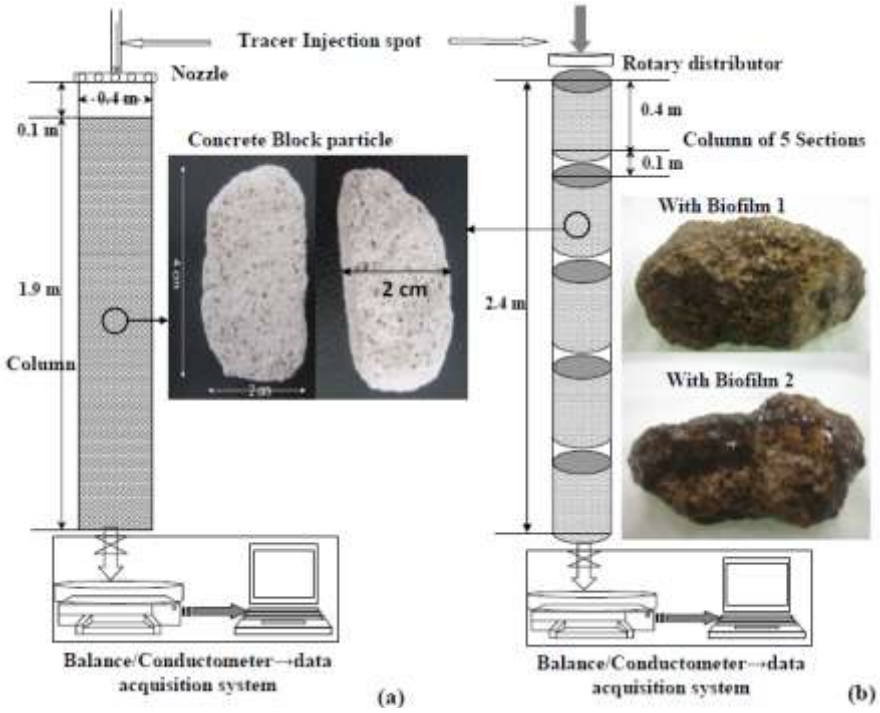

Figure II- 1: Diagram of TFC (a) and MSB (b)

The TFC had a diameter of 0.4 m and a height of 2 m and was enclosed in a structure made of PVC. It was packed with Concrete Block medium to a height of 1.9 m. The MSB was composed of 5 uniform open-structured frames (like baskets) stacked vertically, whose individual height and diameter were 0.4 m and 0.2 m, respectively. The total pilot height was 2.4 m while the packing bed was 2 m high with an interval of 0.1 m between consecutive sections. The geometric characteristics of the two bioreactors are shown in Table II-1.

Table II- 1: Geometrical characteristics of the TFC and the MSB

Bioreactor	Column Height (m)	Column Diameter (m)	Packed bed Depth (m)	Distributor Height (m)	Single Section height (m)	Injection spot height (m)
TFC	4	0.4	1.9	2	-	2.5
MSB	2.4	0.2	2	2.5	0.4	2.5

Porous Concrete Block media were used for the solid phase. They were made up of fly ash, gypsum, and cement. A typical Concrete Block particle without biofilm is shown in the middle of Figure II-1; two colonised particles obtained from two organic regimes are shown on the right of Figure II-1.

The MSB, filled with particles of the Concrete Block medium, was fed with the primary sludge from a French WWTP-GINETOUS, after sifting through a 1 mm-mesh sieve and mixing with tap water of 1 and 3 L, respectively, to fulfil the influent requirements for two organic loads. The compositions of these two feed wastewaters are shown in Table II-2.

Table II- 2: Composition of feed wastewater for two cultivated organic loads

Composition	Concentrations			Units
	Low OLR	High OLR		
	by Primary sludge	by Primary sludge	by Viandox	
TSS	318±95 (18)*	1096±225 (11)	0	g/m³
VSS	175±64 (18)	603±77 (11)	0	g/m³
CODt	298±71 (46)	1026±164 (35)	1001±8 (20)	gCOD/m³
CODs /CODt	0.18±0.08 (46)	0.16±0.08 (35)	1	-
CODp/VSS (icv)	1.4±0.22 (18)	1.43±0.05 (11)	-	-
BODu/CODt	0.6±0.2(3)	0.6±0.1(3)	-	-
TKN	46±5 (44)	161±14 (35)	162±5 (20)	gN/m³
Ammonia	30±3 (44)	100±11 (35)	104±5 (20)	gN/m³
N-NH_4/TKN	0.65±0.06 (44)	0.63±0.08 (35)	0.64±0.02 (20)	-
COD_{bio}/TKN	5.1±1.1[a]	5.2±0.9[b]	-	-
Nitrite & Nitrate	0	0	0	gN/m³
Organic load (OLR)	0.38	1.27	1.27	kgCOD/ m³d
Surface organic loads	0.76	2.55	2.55	kgCOD/ m²d
TKN loads	0.06	0.20	0.20	kgN/ m³d
Surface TKN loads	0.12	0.41	0.40	kgN/m²d
Hydraulic load (HLR)	2.55	2.55	2.55	m³/m²d

()* is the number of sampling. [a b] are calculated based on the mean fraction of CODbio/CODt of 0.6, 0.7 respectively. Due to the heterogeneity of both medium packing bed and biofilm, the surface organic loads are not usually applied in TF process operation. The volumetric organic loading rate (OLR) is calculated by dividing by the filter volume.

where CODt is total COD; CODp is particulate COD; CODs is soluble COD; BODu is ultimate BOD; COD_{bio} is biodegradable COD;

The concentrations of pollutants were ascertained from the mean measured values. The pilot-scale MSB was fed with two organic loads for 120 days each, at the same flow rate of 0.08 m³/d. (In the following sections, the regimes with biofilm 1 and biofilm 2 represent the regime with lower and high cultivated organic loads , respectively).

1.2 Methods

1.2.1 Particle Diameter and Density

The particle diameter is detailed estimated in Appendix 3, by cumulative and differential distribution sampling methods.

Volumetric methods were used to determine the material density, particle apparent density, and porosity as follows: A beaker was partially filled with tap water and the corresponding volume was measured and fix equal to V_0 liter. 20 pieces original particles were immersed into the water until there were no air-bubbles released from the material pores, and then the volume was read as V_1. Use PVC glue to cover the surface of completely coated these 20 particles. Immerse these particles with PVC glue into the water and then read the volume as

V_2. The difference between V_2 and V_1 is the volume of water that was trapped inside the pores of media particle. The relation to calculate the material density, particle density and particle porosity are shown in Eq. II-1-Eq. II-3.

$$Material\ density = \frac{Particle\ \ weight}{V_1 - V_0} \quad \text{(II-1)}$$

$$Particle\ density = \frac{Particles\ weight}{V_2 - V_0} \quad \text{(II-2)}$$

$$Solid\ porosity = \frac{V_2 - V_1}{V_2 - V_0} \quad \text{(II-3)}$$

1.2.2 Static hold-up measurements

Operation without biofilm

Liquid static holdup without biofilm was measured by a weighing method as reported in other study (Brunazzi and Viva 2006). The procedures were: Weigh the dry packing mass; Immerse the dry packing into a container filled with tap water and shake it at least 5 min in order to remove trapped air bubbles; Remove the packing particles from the container, then hold the wet packing just above the container for about 30 min to let the free water drain back into the container. Weigh the moist packing after the complete drainage. The mass difference between the mass of the moist packing after drainage and the mass of dry packing is the static holdup mass, which represents the liquid captured in the particles.

During the static holdup experiments without biofilm, a definite quantity of particles was picked for the purpose of analyzing the liquid static holdup weight versus dry packing weight, making the assumption that liquid static holdup weight was correlated with the total packing weight. Then, nine groups (10, 20, 40, 60, 100, 300, 500, 700 and 1000 particles) of experiments were carried out and each group was repeated 5 times to assess the reliability.

Operation with biofilm

The method for the regimes with biofilm in the MSB differ from the previous method for regimes without biofilm; In order to avoid the destruction of biofilm, the particles coated with biofilm cannot be removed from their initial locations. The mass of each section packed with particles coating by moist biofilm at steady-state (no free water drained but moist) were first weighed; then fed to the pilot with tap water at a lower flowrate of 0.0046m^3/h for 1 h; stopped after 1 h and the pilot was left draining until no free draining water appeared; the mass of each section was weighed. Then the pilot was fed at a higher flowrate (0.0091, 0.0182, 0.0137 and 0.0228 m^3/h, respectively) for 1 h; the same protocol was repeated as that under

low flowrate.

The mass difference between the section with particles & moist biofilm for lower flowrate feeding and that for higher flowrate was taken to represent the mass of the liquid static holdup captured in the particles and biofilm.

The liquid static holdup volume V_{LS}, solid volume V_{solid}, total packing volume $V_{packing}$, the porosity of particle ε', the total void fraction of packing bed ε and the volume of column V_{column} were then taken into account to calculate the liquid static retention β_S:

$$\beta_S = \frac{V_{LS}}{V_{solid}} = \frac{V_{LS}}{V_{packing}(1-\varepsilon')} = \frac{V_{LS}}{V_{column}(1-\varepsilon)} \qquad \text{(II-4)}$$

The water adsorption fraction of the media F_{ad} can then be calculated as the liquid static holdup weight m_{LS} divided by the dry packing weight m_{DP}:

$$F_{ad} = \frac{m_{LS}}{m_{DP}} = \frac{\rho_L}{\rho_{particle}} \cdot \frac{V_{LS}}{V_{packing}} = \frac{\rho_L(1-\varepsilon')}{\rho_{particle}} \cdot \beta_S \qquad \text{(II-5)}$$

1.2.3 Static hold-up model

In experimental studies no particular care is usually taken to clearly determine the residual holdup, which is even left undefined in some cases involving non-spherical particles (Kundu et al., 2003). In this paragraph, we try to evaluate the residual holdup in our column using the model proposed by Behrens et al., (2007).

The static hold-up is comprised of two parts: external capillary hold-up $hl_{externalcap}$ and internal capillary hold-up $hl_{internalcap}$. The total static hold-up can be presented:

$$hl_{cap} = hl_{externalcap} + hl_{internalcap} \qquad \text{(II-6)}$$

In the study of Viva and Brunazzi, (2009), for the capillary hold-up correlation in single packing unit, they took into account the sphere diameter d_p, liquid surface tension σ, liquid density ρ_L, packing porosity ε and also the contact angle between the liquid and solid sphere θ with no external pressures imposed on the vertical capillary. With their assumptions, the capillary rise height is given by:

$$h_{cap} = \frac{6(1-\varepsilon)\sigma}{d_p \varepsilon \rho_L g}\cos\theta \qquad \text{(II-7)}$$

Furthermore, they gave the correlation of capillary rise hold-up for the whole volume of the packing, with h_{cb} as the height of the packing and φ_{cb} as the fraction of packing element occupied by the material particle:

$$hl_{cap} = \frac{h_{cap}\varepsilon}{h_{cb}}\varphi_{cb} \qquad \text{(II-8)}$$

The methods proposed by Ortiz-Arroyo et al., (2003) that applied the height of capillary holdup h_{cap} to determine the cosθ was employed; then the total capillary holdup hl_{cap} was calculated in this manner for both reactors.

1.2.4 Dynamic hold-up measurements

The drainage method reported by Brunazzi and Viva, (2006) was modified to measure the liquid dynamic holdup. Our method was as follows: the column was firstly stabilized by feeding at greater hydraulic flow of 0.0228 m^3/h for at least 1 h; after stabilization at the constant flow measured at the outlet, the flow was cut off. The liquid held by packing began to drain into the collector lying on the balance. The drained mass of liquid collected was measured and recorded by the acquisition system. When the steady state of drainage was achieved (constant outlet values observed), the measurements were stopped.

The dynamic retention β_d was calculated from:

$$\beta_d = \frac{V_{Ld}}{V_{column}(1-\varepsilon)} \qquad \text{(II-9)}$$

The total liquid retention β_t was derived from:

$$\beta_t = \beta_s + \beta_d = \frac{V_{LS} + V_{Ld}}{V_{solid}} = \frac{V_{Lt}}{V_{solid}} \qquad \text{(II-10)}$$

where V_{Ld} denotes the liquid dynamic holdup volume; V_{Lt} denotes total liquid holdup volume and V_{solid} is the pure solid volume.

Three stages of the liquid draining curve were monitored during the drainage experiments: a linear stage of the curve from the initial point is the fast dynamic holdup and a curvilineal stage is the slow dynamic holdup, until the parallel stage which showed the end of drainage. The liquid mass difference from the point when the influent was cut off until the last point on the linear stage was the fast dynamic holdup mass; nevertheless, the mass difference from the last point on linear stage until the parallel stage was calculated as the slow dynamic holdup mass.

The total liquid holdup was then calculated from the hypothesized liquid fractions given in Eq. II-11. The corresponding liquid fractions are depicted in Figure II-2(c), and compared with other definitions proposed in the literature by Vogelpohl et al., (1975) in Figure II-2(a) and Behrens, (2006) in Figure II-2(b):

$$h_{Lt} = hl_{fast\ dynamic} + hl_{slow\ dynamic} + hl_{internal\ capillary} + hl_{external\ capillary} \qquad \text{(II-11)}$$

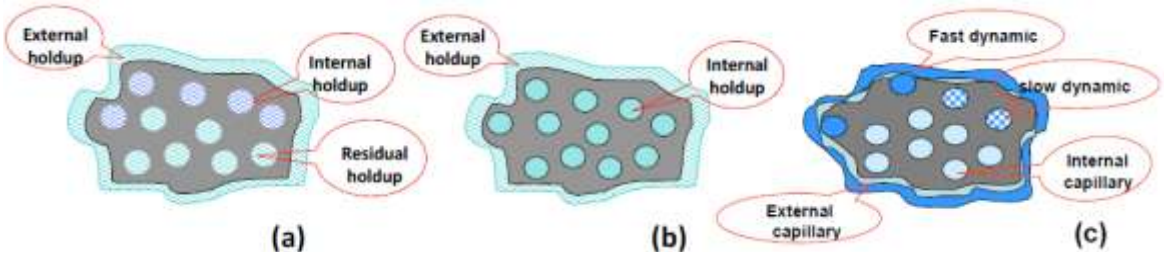

Figure II- 2: Liquid holdup fractions in literatures (a) (b) and in this study (c)

Numerous investigations (Davidson et al., 1959; Buchanan et al., 1967; Bemer and Kalis, 1978) have been made into dynamic holdup in packed columns. Most investigators agreed that for G=0 (i.e. no gas flow rate), the relation between liquid flow rate and dynamic holdup is given by:

$$\beta_d = a \cdot U_L^{f_w} \qquad \text{(II-12)}$$

where U_L is the liquid superficial velocity, a depends on the media and liquid properties and fw is the wetting fraction.

1.2.5 Residence Time Distribution (RTD)

Residence time distribution experiments were realized by the tracer method reported by Viva and Brunazzi, (2009). After stabilization of flow in the column, an impulse of salt tracer (30 ml×300 g/L aqueous solution of sodium chloride) was injected via a syringe from the injection point. The conductivity of the liquid with tracer leaving the column was measured by a flow-through probe (XE100, RADIOMETER ANALYTICAL S.A.) connected to a conductometer (CDM210 Conductivity Meter, RADIOMETER ANALYTICAL) and the conductivities were monitored as a function of time by the data acquisition system in the computer. After each experiment, a rinse was performed to remove the residual salt absorbed by the particles.

Analyzing the real RTD curves allows one to identify the flow regimes in the column and the liquid fraction involved in the tracing. Furthermore, the shapes of RTD curves, and the distribution of liquid in the packed bed, are related to the configuration and geometry of the packing.

The liquid holdup obtained from the RTD curve should generally correspond to the dynamic holdup (Sharvelle et al., 2008). However, Viva and Brunazzi, (2007) reported that the liquid holdup in the RTD curves of catalytic structured packing agrees with the total liquid holdup, including the dynamic holdup and the static holdup determined by the drainage method. The dimensionless Residence Time Distribution E(θ) as a function of the dimensionless time θ is given by Eq. II-13 and the dimensionless time θ in Eq. II-14. The mean Liquid Residence Time (LRT) μ is given by Eq. II-15.

$$E(\theta) = \frac{C(t)}{C_0} \quad \text{(II-13)}$$

$$\theta = \frac{t}{\tau_H} \quad \text{(II-14)}$$

$$\mu = \frac{\sum tC(t)}{\sum C(t)} \quad \text{(II-15)}$$

where $C_0=m_{tracer}/V_{effective}$ (g/L) is the tracer mass held by the total liquid volume; C(t) is the tracer mass held by liquid at measuring time t; μ is the mean liquid residence time (s); τ_H denotes the theoretical Hydraulic Retention Time (HRT), is assumed equal to mean residence time in this chapter, $\tau_H=\mu$; *Q* is the flow rate of liquid (m^3/h); the effective liquid volume involved in RTD tracing $V_{effective}=\mu\times Q$.

1.2.6 RTD models

The tracer injected into a reactor undergoes dispersion in the fluid flow, which in the case of ideal reactors may range from zero (plug flow reactor) to a completely mixed reactor. The dispersion of the tracer may be due to the configuration of the velocity profiles as well as molecular diffusion.

Axially dispersed Plug Flow

One of the most frequently used models is Plug Flow (PF), superimposed on a mechanism of dispersion. This model is sometimes called dispersive piston (Wen and Fan, 1975). Considering the concentration C of a reagent, the general mathematical expression for this model is:

$$\frac{\partial c}{\partial t} = \nabla \cdot (D\nabla c) - \bar{u} \cdot \nabla c + \phi(c)$$

where D denotes the dispersion coefficient, $\bar{u}$ is mean velocity of liquid flow (in our case of flow in porous media, it is the average interstitial velocity) and ϕ(c) is the rate of substrate production or consumption by reaction.

Solving the differential equation with various boundary conditions lead to introduce the dimensionless Peclet number *Pe*, defined as:

$$Pe = \frac{\bar{u}L}{D_Z} \quad \text{(II-16)}$$

where $\bar{u}$ is the liquid interstitial velocity, L is the filter height; Dz is the axial dispersion coefficient.

When $Pe \to 0$, $D_Z \to \infty$; it means the liquid circulation is close to complete mixed;
When $Pe \to \infty$, $D_Z \to 0$; it means the liquid circulation is close to plug flow.

For limited dispersion, the distribution of residence time may be well approximated by a Gaussian distribution regardless of the boundary conditions (Levenspiel et al., 1972):

$$E(t) \approx \frac{1}{2t_o}\sqrt{\frac{Pe}{\pi}}\exp\left[-\frac{Pe(1-t/t_0)^2}{4}\right] \qquad \text{(II-17)}$$

When E(t) is converted to the dimensionless E (θ) taken θ=t/τ, this equation can be rearranged to give:

$$E(\theta) \approx \frac{1}{2}\sqrt{\frac{Pe}{\pi\theta}}\exp\left[-\frac{Pe(1-\theta)^2}{4\theta}\right] \qquad \text{(II-18)}$$

CSTR and CSTR with dead zone model

The model of *n* identical *Continuous Stirred Tank Reactors (CSTR) in series* with stagnant/dead zone reported by Levich et al., (1967) and Sant'Anna et al., (1982) was also employed to investigate the liquid profile in a trickling filter. ***Plug Flow*** can be approximated by a large number of *CSTR in series.* The model of ***n CSTRs with stagnant zone in series*** in the form of Eq. II-19 was applied to investigate the RTD with its variance given by Eq. II-20.

$$E(\theta) = \frac{1}{m^n}\frac{n^n}{(n-1)!}\theta^{n-1}e^{\frac{-n\theta}{m}} \qquad \text{(II-19)}$$

$$\sigma^2 = \frac{\sum t^2 C(t)}{\mu^2 \sum C(t)} - 1 \qquad \text{(II-20)}$$

Here ***m*** is the fraction of active zone, ***m=μ/τ***, ***n*** is the number of CSTRs; for ***m*=1**, no stagnant/dead zone is present in the packing bed. Eq. II-21 can then be rearranged into the model for ***n CSTRs in series***:

$$E(\theta) = \frac{n^n}{(n-1)!}\theta^{n-1}e^{-n\theta} \qquad \text{(II-21)}$$

When the variance ***σ²*** approaches 0, the liquid profile in the column is close to plug flow; whereas, when ***σ²*** approaches 1, the liquid profile is close to perfect mixing.

When ***n*** is greater than 25, the RTD calculated from the model of n reactors in series with RTD calculated from the dispersive piston model, as proposed by Villermaux, (1993):

$$Pe = 2(n-1)$$

where ***n*** is the estimated number of identical reactors in series.

1.2.7 Liquid film thickness estimation

Liquid flow is represented according to a laminar liquid film model. Liquid flows over the surface of particles and is partially adsorbed by particles when biofilm is absent; whereas it flows over the biofilm surface and is adsorbed by biofilm. The thickness of this liquid layer can be calculated from the volume of dynamic liquid against the contact area. A schematic of this assumption is depicted in Figure II-3.

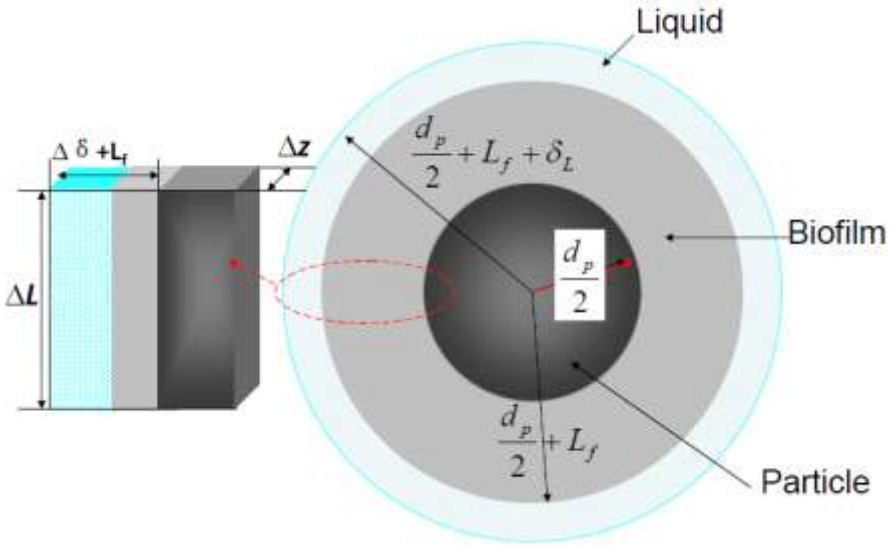

Figure II- 3: Schematic of liquid layer and contact surface

For a single particle, the volume of liquid $V_{p,L}$ is estimated from Eq. II-22.

$$V_{p,L}=\int_0^{\delta_L} d\delta \int_{\pi(d_p+2L_f)}^{\pi(d_p+2L_f+2\delta_L)} dL \int_0^{\pi d_p} dz \approx 4\pi(d_p/2+L_f)^2\delta_L \qquad \text{(II-22)}$$

where δ_L denotes the liquid film thickness; L_f is the mean biofilm thickness when with biofilm, or L_f=0 when without biofilm, L_f is the mean biofilm thickness assuming a homogeneity of biofilm in the packed bed and uniformly-coated particles.

For the packed bed, the volume of dynamic liquid corresponds to Eq. II-23 with the wetting fraction f_w taken into account.

$$V_{Ld}=N_{particles}V_{p,L}\cdot f_w \qquad \text{(II-23)}$$

where $N_{particles}$ is the estimate number of particles in the packing bed; $V_{p,L}$ represents average liquid volume in one particle;

The liquid film thickness is then calculated from:

$$\delta_L=\frac{V_{Ld}}{N_{particles}a_p\cdot f_w}=\frac{V_{Ld}}{N_{particles}4\pi(d_p/2+L_f)^2 f_w} \qquad \text{(II-24)}$$

where ap is the surface area of each particle.

1.2.8 Volumetric oxygen transfer coefficient kLa estimation

In a trickling filter, when oxygen is transferred through the liquid film to reach the biofilm surface, substrates are utilized by bacteria also consuming oxygen on the liquid-biofilm interface.

A schematic diagram of oxygen transfer is shown in Figure II-4.

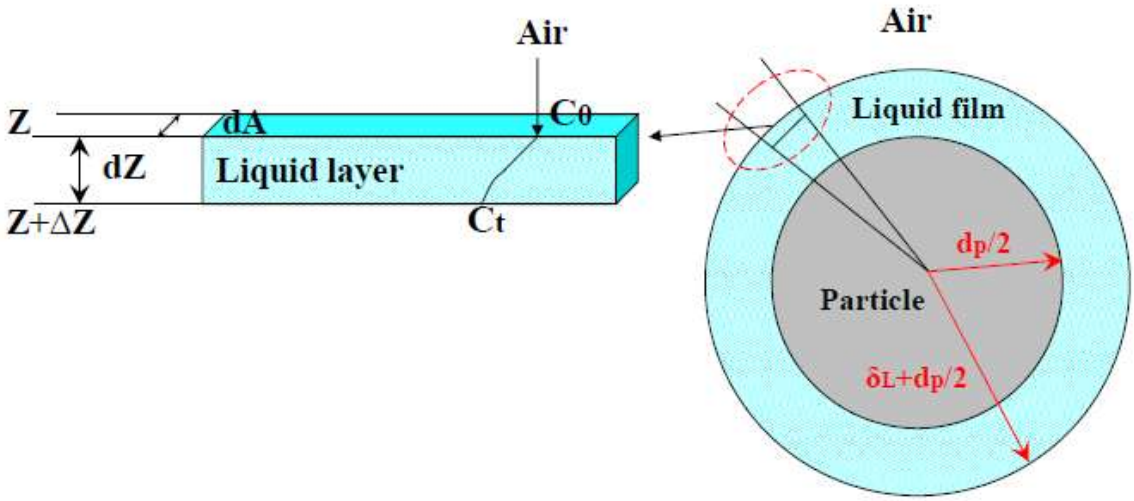

Figure II- 4: Schematic of oxygen transfer

Higbie, (1935) proposed the penetration model of oxygen transfer; where the surfacial oxygen transfer rate from the air to the liquid is estimated by:

$$r_{O_2} = 2\left(\frac{D_{O2}}{\pi \times t_c}\right)^{\frac{1}{2}}(C_S - C_t) \qquad \text{(II-29)}$$

where r_{O2} is the oxygen transfer rate; D_{O2} is oxygen diffusion coefficient; C_S is oxygen concentration in liquid bulk phase; C_t is oxygen concentration in bulk liquid at time t; t_C is the contact time related to the liquid film renewal.

For a single particle, the volumetric oxygen transfer coefficient k_La is calculated from Higbie's theory (Higbie, 1935):

$$r_{O_2} = K_L a(C_s - C_t) = K_L \frac{A}{V}(C_s - C_t) = 2\sqrt{\frac{D_{O_2}}{\pi \cdot t_c}}\frac{A}{V}(C_s - C_t) \qquad \text{(II-30)}$$

$$K_L a = 2\sqrt{\frac{D_{O_2}}{\pi \cdot t_c}}\frac{A}{V}$$

V and A was given by the equations as follows:

$$V = V_{p+l} - V_p = \frac{4\pi}{3}(r_p + \delta_L)^3 - \frac{4\pi}{3} r_p{}^3$$

$$A = 4\pi(r_p + \delta_L)^2$$

When the biofilm is present, the thickness of biofilm was taken into account in calculating V and A.

The initial and boundary conditions corresponding to this assumption are:

At Z=0, t=0; $C=C_0$

At Z =z, C=Ct

At $Z=\delta_L$, $C= C_\delta$

With the two definitions of V and A, the volumetric oxygen transfer coefficient in this study derives from Eq.II-31:

$$K_L a = 6\sqrt{\frac{D_{O_2}}{\pi t_c}} \frac{(d_p/2 + L_f + \delta_L)^2}{(d_p/2 + L_f + \delta_L)^3 - (d_p/2)^3} \qquad \text{(II-31)}$$

The Eq.II-32 was then employed to estimate the local contact time $\boldsymbol{t_c}$, assuming that the liquid volume at the particle surface is renewed when it covers the particles' surface areas and will be ready to transfer again with a free zone where the air is in contact.

$$t_c = \frac{d_p}{U_L} = \frac{d_p}{U_0/\varepsilon_{Ld}} = \frac{\varepsilon_{Ld} d_p}{U_0} \qquad \text{(II-32)}$$

where U_0 is the liquid superficial velocity; U_L is liquid interstitial velocity; ε_{Ld} is the fraction of dynamic liquid holdup.

$$\frac{Log(C_S - C_0)}{Log(C_S - C\ )} = k_L a \cdot t_c \qquad \text{(II-33)}$$

where C_S is the saturation concentration of oxygen in the liquid film; C_o and C are the local concentrations at the bottom of the filter and top of the biofilm.

PART 2: Biological experiments

1. Introduction

The aim in this part was to investigate the performances of both COD removal and nitrification on a pilot scale. Special attention is devoted to the competition between nitrification and heterotrophic growth. The capacity of MSB was also evaluated regarding the clogging. Two experimental approaches were thus analyzed in order to address these phenomena:

1. Competition between nitrification and heterotrophic elimination of COD were considered at two OLR for different locations in the MSB. The increase of Organic Loading Rate (OLR) was thus used in order to increase the competition factors such as the oxygen demand, the biofilm thickness, the competition for space, detachment frequency and amplitude.
2. The capacity of clogging in the TF was studied. In this case, we significantly increased the OLR to favour solid retention inside the pores and thus clogging. To know the effect of particulate COD of the influent in clogging processes, a shift from a real WW containing a large amount of particulate COD to the Viandox substrate that contained only soluble and colloidal COD was performed; the COD concentration and OLR were maintained constant in the feed stream.

2. Material and methods

2.1 Feeding conditions

Based on the evaluation of the flowrate and the Organic Loading Rate (OLR) for rural wastewater characteristics presented in Chapter 1, the constituents (mean values unless otherwise stated) and ratio of constituents of the feeding wastewater, the hydraulic loading rate (HLR) and the organic loading rate (OLR) for the different phases are shown in Table II-3. A detailed description of the composition of the primary sludge from the WWTP-Ginetous (Toulouse, France) used throughout this study and the composition of Viandox are presented in the Appendix 4.

Table II- 3: Composition of wastewater fed for two regimes of organic loads cultivation

Composition	Concentration Values			Unit
	Low OLR	High OLR		
	by Primary sludge	by Primary sludge	by Viandox	
TSS	318±95 (18)*	1096±225 (11)	0	g/m³
VSS	175±64 (18)	603±77 (11)	0	g/m³
CODt	298±71 (46)	1026±164 (35)	1001±8 (20)	gCOD/m³

CODs /CODt	0.18±0.08 (46)	0.16±0.08 (35)	1	-
XCOD/VSS (icv)	1.4±0.22 (18)	1.43±0.05 (11)	-	-
BODu/CODt	0.6±0.2(3)	0.6±0.1(3)	-	-
TKN	46±5 (44)	161±14 (35)	162±5 (20)	gN/m³
Ammonia	30±3 (44)	100±11 (35)	104±5 (20)	gN/m³
N-NH_4/TKN	0.65±0.06 (44)	0.63±0.08 (35)	0.64±0.02 (20)	-
CODbio/TKN	5.1±1.1[a]	5.2±0.9[b]	-	-
Nitrite & Nitrate	0	0	0	gN/m³
Organic load (OLR)	0.38	1.27	1.27	kgCOD/ m³d
Surface organic loads	0.76	2.55	2.55	kgCOD/ m²d
TKN loads	0.06	0.20	0.20	kgN/ m³d
Surface TKN loads	0.12	0.41	0.40	kgN/m²d
Hydraulic load(HLR)	2.55	2.55	2.55	m³/m²d

()* is the number of sampling. [a b] calculated based on the mean fraction of COD_{bio}/COD_t as 0.6 and 0.7 respectively. Due to the heterogeneousness distribution of both medium packing bed and biofilm, the surface organic loading are not usually applied in Trickling Filter, the volumetric organic loading rate (OLR) is estimated by dividing by the filter volume.

Wastewater was composed of diluted primary sludge after sifting of the diluted broth by a 1 mm sieve. The concentration of Total Ammonia Nitrogen (TAN) was artificially controlled to give a ratio COD/NH_4-N=10. The concentration of influent ammonia-nitrogen was thereafter set-up as 30 mg/L and 100 mg/L by $(NH_4)_2SO_4$ solution of 40 mgN/L. During the phase fed by Viandox, because the ammonia-nitrogen and nitrate concentration from initial Viandox solution can be ignored after dilution, the concentration of nitrogen was also fulfilled by $(NH_4)_2SO_4$ solution.

From Table II-3, it can be observed that, the wastewater had a high particulate COD, and Total Kjeldahl Nitrogen (TKN) content as well as a high inert COD fraction. It can be underlined that the increase in OLR was performed by an increase in concentrations, the flow rate being maintained constant of 0.08 m³/d. The increase in concentrations between period 2 (low OLR feeding for 80 days) and period 3 (high OLR for 80 days) is by a factor of more than 3. However, flow rate was still kept the same as during the inoculation phase.

2.2 Methods

2.2.1 Sifting method for primary sludge

Two sifting methods were applied to sift and dilute the primary sludge for influent wastewater:

1. Take 0.64 L of Primary Sludge (CODt of 70 g/L) + mix it with tap water into a plastic barrel of 30 L and agitate the mixture → sift the mixture on a 1 mm sieve → transfer the filtrate into the feeding tank, dilute it to 150 L; (applied during the inoculation period to acquire 300 mgCOD/L of influent)

2. Take 1 L (for period 2) or 3 L (for period 3, calculated required volume equals 2.14 L) of primary sludge + mix with tap water into a plastic barrel of volume 30 L and agitate the mixture → sift the mixture on a 1 mm sieve → measure the COD concentration of filtrated turbid liquor → choose the volume to mix with tap water that fulfills the feeding requirements (300 and 1000 mgCOD/L).(applied during phase 2 and phase3)

2.2.2 Main component analysis methods and apparatus

The methods and apparatus employed to measure the components of chemical carbon, nitrogen and suspended solids are shown in Table II-4.

Table II- 4: Analysis methods and apparatus employed in the study

Components	Methods	Apparatus
CODt, CODs, CODp	Centrifugation, Digestion, Dosage	COD Digester
$N\text{-}NH_4$,$N\text{-}NO_2$, $N\text{-}NO_3$	Filtration	Dionex ion analyzer
TKN	Mineralization, distillation, titration	TKN analyzer
TSS, VSS	Centrifugation, dehydration, ignition	Muffle furnace
Ultimate BOD	Centrifugation	Sapromat

2.2.3 Treatment performance evaluation

The performance of the system was represented in terms of the removal efficiency of total COD, ammonia and TKN, nitrification efficiency and nitrification rate, both for the entire pilot and for each basket. The effluent sample was collected into a plate from the 5^{th} section for the entire pilot performance analysis; the diameter of this collector was larger than the diameter of the basket. Similarly, the effluent of each section was collected under the bottom of each section from the interval between the sections.

The removal COD and nitrification efficiencies were thus calculated from the following relations:

$$\eta_{COD} = \frac{(C_{CODt,in} - C_{CODs,out})}{C_{CODt,in}} \times 100\% \quad \text{(II-34)}$$

$$E_{COD} = \frac{(C_{CODt,in} - C_{CODt,out})}{C_{CODt,in}} \times 100\% \quad \text{(II-35)}$$

where CODt is the total COD, CODs is soluble COD.

For nitrification, we have considered the total TKN for evaluating the nitrification efficiency. The removal efficiency of TKN is calculated.

$$\eta_{TKN} = \frac{(C_{TKNt,in} - C_{TKNs,out})}{C_{TKNt,in}} \times 100\% \quad \text{(II-36)}$$

$$E_{TKN} = \frac{(C_{TKNt,in} - C_{TKNt,out})}{C_{TKNt,in}} \times 100\% \quad \text{(II-37)}$$

where TKNt is Total Kjeldahl Nitrogen, TKNs is soluble Kjeldahl Nitrogen.

In our case, it was difficult to collect the released gas to verify whether denitrification occurred. We can assume no oxygen limitation existed due to the open structure of our pilot. Hence we assumed that the final nitrite and nitrate concentration can represent the nitrified nitrogen by nitrification. The nitrification efficiency was then calculated as follows:

$$E_{nitrification} = \frac{C_{N-NO_x outlet}}{C_{TKN_{inlet}}} \times 100\% \quad \text{(II-38)}$$

where N-NOx is nitrite and nitrate nitrogen

2.2.4 Sludge production and SRT estimation

The quantity of sludge production in a Trickling Filter is important in the design of sludge management facilities. Sludge released can be estimated by measuring the amount of particulate COD in the outlet of the reactor. Usually from Metcalf and Eddy, (1991), the sludge production from autotrophic growth can be ignored compared to that from heterotrophic growth. The total sludge production in a TF derives hypothetically from the biomass of heterotrophic growth, mineral material in the wasted sludge and also the inert non-biodegradable organic substrate:

$$P_{X,total} = P_{X,growth} + P_{X,\text{mineral}} + P_{X,refractive\ organic} \quad \text{(II-39)}$$

where P_{xtotal} is total VSS production, kg/d; $P_{x\ growth}$ is sludge production from cell growth; $P_{x\ mineral}$ is mineral material in the wasted sludge; $P_{xrefractive\ organic}$ represents the inert non-biodegradable organic substrate (some use the P_{xi})

Accurate evaluation of the true amount of sludge production inside the reactor is complicated, because a high particulate COD (COD_P) heterogeneity is spatially distributed along the column, and sampling is not feasible.

Moreover, the observed yield coefficient Yg,obs is calculated from the Heterotrophic yield coefficient Y_H, decay rate k_d and sludge retention time θ_d.

$$Y_{g,obs} = \frac{Y_H}{1 + k_d \theta_d} \quad \text{(II-40)}$$

When the Sludge Residence Time (SRT) is short, the cellular debris can be ignored in the sludge production, whereas when the SRT is long, this part should be involved in the sludge production.

In this study, we first estimate the value of Yg,obs, based on the outlet CODp over consumed COD of period 4. Without particulate COD input, the CODp at the outlet can be assumed from the direct sludge production. With this estimated Yg,obs, we can further to estimate the sludge production in other periods, multiplied by consumed COD, then adding the inert particulate COD at the outlet. In addition, we can use classic value Y_H of 0.44 gCOD/gCOD, k_d of 0.07 gCOD/gCOD to calculate the SRT of our pilot.

2.2.5 Accumulated biomass estimation

The net accumulated biomass was estimated based on some assumptions. The total wet mass of each basket were weighed every 7 days to evaluate the increment or decrement of net biomass accumulation. The contribution of this measured mass difference $\Delta \boldsymbol{MS}$ is given by the equation.

$$\Delta MS = MS_{biofilm} + MS_{LS} + MS_{Xi\ intercepted} \quad \text{(II-41)}$$

where $MS_{biofilm}$ is the mass of biofilm, including both the dry biomass from cell synthesis and the cellular water content; MS_{LS} is the static holdup water adsorbed by biofilm; $MS_{Xi\ intercepted}$ is the mass of non-biodegradable particulate substrate intercepted by the packing bed. The detailed estimation of accumulated biomass was shown in Appendix 8.

Furthermore, we attempt to investigate the ratio between assimilated nitrogen and consumed COD. This could underline the fraction of particulate nitrogen biomass in the sludge production. Assimilated nitrogen comes from two parts: the accumulated particulate TKN and particulate TKN at the outlet. Since the accumulated particulate TKN is hard to measure, the assimilated nitrogen is calculated by the total inlet TKN minus the soluble TKN at the outlet. Consumed COD is calculated by the inlet CODt minus the outlet CODs.

2.2.6 Biofilm density and thickness estimation

At the end of phases 2 and 3, the biofilm properties were measured. The biofilm measurements included estimations of biofilm density, biofilm thickness and biofilm porosity.

The protocol to estimate the biofilm density was as follows:

3-5 pieces of particles with biofilm attached were taken from different horizontal strata of each section (sampling depth of 10 cm for each section); then the mass of particles was weighed with wet biofilm on it as M1. Put the particles with wet biofilm into the oven at 100℃ for 24 h. Weigh the mass of dry particles with dehydrated biofilm as M2. Wash out completely all the biofilm, both from the surface and from inside of the particles with 75 ml physiologic solution.

The COD concentrations in the intermixture liquor of biofilm and physiologic solution were then measured to obtain the yield biomass.

The wet particles without biofilm were put into the oven at 100℃ during 24h. Weigh the dry particles mass as M3.

Wet biofilm mass $\boldsymbol{m_{WM}}$ =M1-M3 Dry biofilm mass $\boldsymbol{m_{DM}}$ =M2-M3;

The mean biofilm density $\boldsymbol{\rho_F}$ (g DM/m^3) and the biofilm volume $\boldsymbol{V_f}$ (m^3) was calculated from:

$$\rho_f = \frac{m_{DM}}{m_{WM} / \rho_W} \qquad \text{(II-42)}$$

$$V_f = \frac{m_{DM}}{\rho_f} \qquad \text{(II-43)}$$

Assuming an average wet biofilm density ρ_w of 1.02 g/cm^3, then with the obtained biofilm density, the biofilm thickness $\boldsymbol{L_f}$ was estimated from the biofilm volume $\boldsymbol{V_f}$ divided by the effective surface area $\boldsymbol{a_v}$ of particles, i.e.

$$L_f = \frac{V_f}{a_v} \qquad \text{(II-44)}$$

where a_v was calculated by assuming each particle to be a sphere, then it equals the surface area of a single particle πd_p^2. d_p is the mean equivalent diameter for the media particles, detailed results are shown in Appendix 3.

2.2.7 Packing bed porosity/voidage

The method to estimate the packing bed porosity was based on the theory proposed by Robin et al., (2010). A schematic diagram of this assumption is shown in Figure II-5.

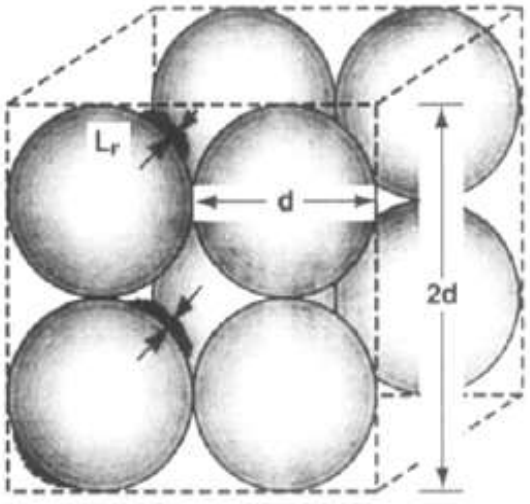

Figure II- 5: Schematic diagram of packing bed porosity estimation

Assuming the pores of medium particles were completely filled with biofilm, the relation to calculate the bed porosity $\varepsilon_{\text{theo. particle with biofilm}}$ is as follows:

$$\varepsilon_{theo.\ particle\ with biofilm} = \frac{V_{pores}}{V_{total}} = 1 - \frac{(\pi/6)(d_p + 2L_f)^3}{(d_p)^3} \quad \text{(II-45)}$$

where Vpores is the volume of all the pores inside medium particle, Vtotal is the total volume of particles, d_p is the estimated diameters of medium particle, L_f is the estimated biofilm thickness.

When no biofilm is present, L_f=0; ε=0.476 (packing bed voidage=77.4%)

$$\frac{\varepsilon_{particle\ with biofilm}}{\varepsilon_{particle}} = \frac{\varepsilon_{theo.\ particle\ with biofilm}}{0.476} \quad \text{(II-46)}$$

where $\varepsilon_{\text{particle with biofilm}}$ is the packing bed voidage when biofilm is present, $\varepsilon_{\text{particle}}$ is the voidage of particles.

2.2.8 Minimum oxygen demand estimation

The oxygen demand for the entire system contains the oxygen demand for oxidizing the biodegradable organic matter, also that for oxidizing the ammonia in nitrification, the endogenous respiration of biomass and the intake reconveyed by denitrification. The oxygen demand was therefore estimated as:

$$DO(kgO_2/d) = DO_{bio} + DO_{nitr} + DO_{res} - DO_{denit} \quad \text{(II-47)}$$

where DO_{bio} is the oxygen demand for carbon biodegradation, DO_{nitr} is the oxygen demand for nitrification, DOres is the oxygen demand for endogenous respiration, DOdenit is the oxygen demand for denitrification.

In our pilot, this demand of oxygen supply was estimated by mass balance estimation both of COD and TKN. When denitrification occurred, the equivalent oxygen consumption for denitrification was subtracted.

PART 3: Simulation and modeling by BIOWIN

1. General Approach

Work setting and validation TF model generates any discussion about the strategy to be developed to achieve this goal. To do this, we use the acquisition of robust experimental data from the pilot MSB in carbon and nitrification treatment, and different operating modes as described in Part 2. Thus, long-term monitoring will firstly help to calibrate the model with the comparison of measured and simulated input and output data to and for the system including the total COD, soluble COD, particulate COD, and nitrogen compounds such as TKN and $N\text{-}NH_4^+$ and $N\text{-}NO_3^-$. The continuous acquisition of these parameters, accompanied by specific tests, resulted in samples of effluent material, input / output / waste water, and samples along the column.

The third sub-section of this part describes specific experimental measurements carried out in parallel with the ongoing monitoring of the solver and that can directly determine some key parameters of the model and ultimately reduce the number of degrees of freedom of the system of equations.

In this chapter, software Biowin (version 4.0) was employed in the Trickling Filter (TF) simulation works. This simulator allows examination of the complex interactions between various unit processes interactively and dynamically, such as COD removal and nitrification. Understanding these relationships is critical for effective design, operation and control of the Multi-Section Bioreactor system.

Simulations under various environmental and physical parameters settings were carried out in order to simulate the COD removal and nitrification in a conventional TF, as well as in the lab-scale MSB investigated in our study. The simulations can also help to understand the main processes and kinetic models involved in those processes, such as substrate and oxygen transport at air/liquid interface, and diffusion of substrate and oxygen from liquid to the biofilm.

To start a simulation, the fraction of influent components should first be estimated to fit the experimental operating conditions. Then to apply a TF model in the BIOWIN simulator, a sensitivity analysis should be carried out before the simulation. This helps to find the main impact parameters for the whole process which affect the treatment performance. After the sensitivity analysis, the simulation of a single-stage TF system and a MSB system simulation were carried out. Both simulations were with respect to the experimental operating conditions, (such as influent components and their fractions, except for those which cannot be estimated

experimentally, where we used default values), the estimated physical properties of packed bed and of the media. All the simulations were carried out for steady-state conditions.

2. Fraction estimation of influent components

The objective of the model is to gain knowledge of the effluent compatible with model inputs beyond traditional measurements (COD, N-NH_4^+, TKN, N-NO_3^-). In particular, a breakdown of the Biological Organic Matter (BOM) is sought for different classes of biodegradability according to the definitions of the model biological conversion (ASM1).

Among the protocols for characterization of input waste found in the literature, the protocol of Roeleveld and van Loosdrecht (2002) has been chosen for this study. It is applicable to all wastewater input STEP Dutch and serves as a support for ASM models. This protocol is based on a physicochemical method of coagulation-flocculation characterizing the sum of the fraction soluble COD, combined with biodegradable (BOD monitoring over time) to determine the biodegradable fraction of gross COD. Both methods are described in Appendix 7. The proposal for splitting the nitrogenous material is also found in Appendix 7. The latter is purely computational and experimental measurement without implementation. It is derived from the continuous monitoring of conventional effluent parameters (COD, TKN and N-NH_4^+). These biodegradable fractions are derived from the equation of Henze et al. (1987) assuming that the ASM1 biodegradable fractions of nitrogen and Soluble Biodegradable Organic Nitrogen (Snd), Particulate Biodegradable Organic Nitrogen (Xnd) are in the same proportions as for carbon Readily Biodegradable Substrate (Ss) and Slowly Biodegradable Substrate (Xs).

The diagram of total COD, BOD_5 and ultimate BOD (BODu) measurement is shown in Figure II-6.

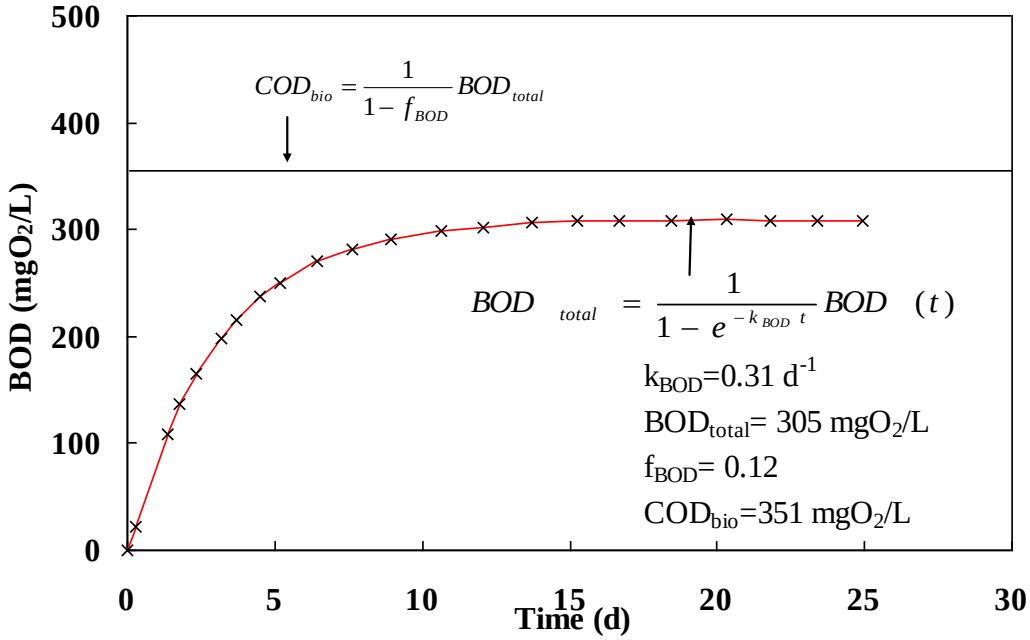

Figure II- 6: Diagram of biodegradable COD fractions in the laboratory analyses modified from Makinia et al., (2000) Corominas et al., (2010)

The estimated fractions of total COD are shown in Figure II-7.

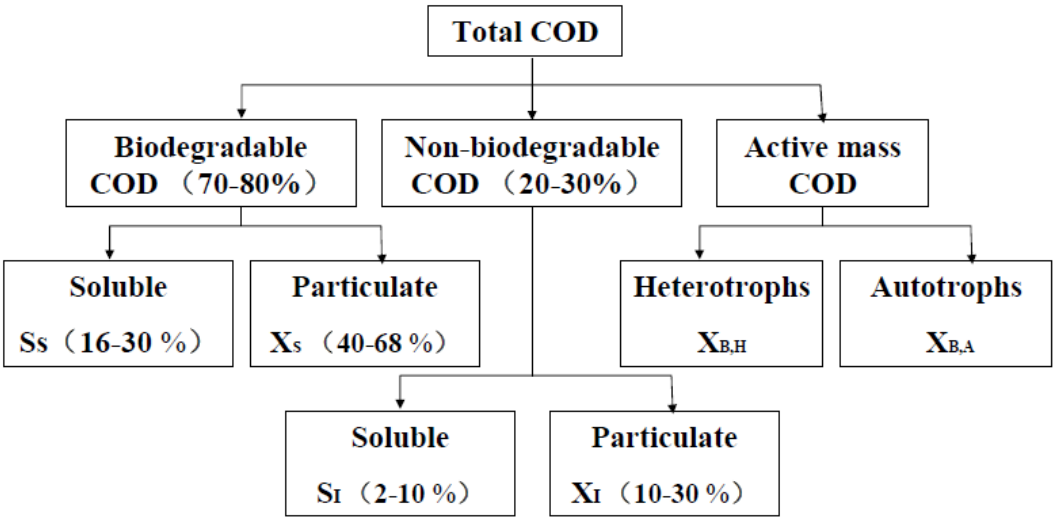

Figure II- 7: Fractions of total COD

Similarly, organic nitrogen fraction was easily determined by TKN minus the Free and ionized ammonia (S_{NH}). Furthermore, soluble biodegradable organic nitrogen (S_{ND}) was estimated by soluble TKN (TKNs) minus S_{NH}. The Inert Organic Nitrogen (X_{NI}) is usually estimated as 0.1-0.15 of the particulate inert organic material (Xi) (Metcalf and Eddy, 1991). The evaluated fractions of total nitrogen are shown in Figure II-8.

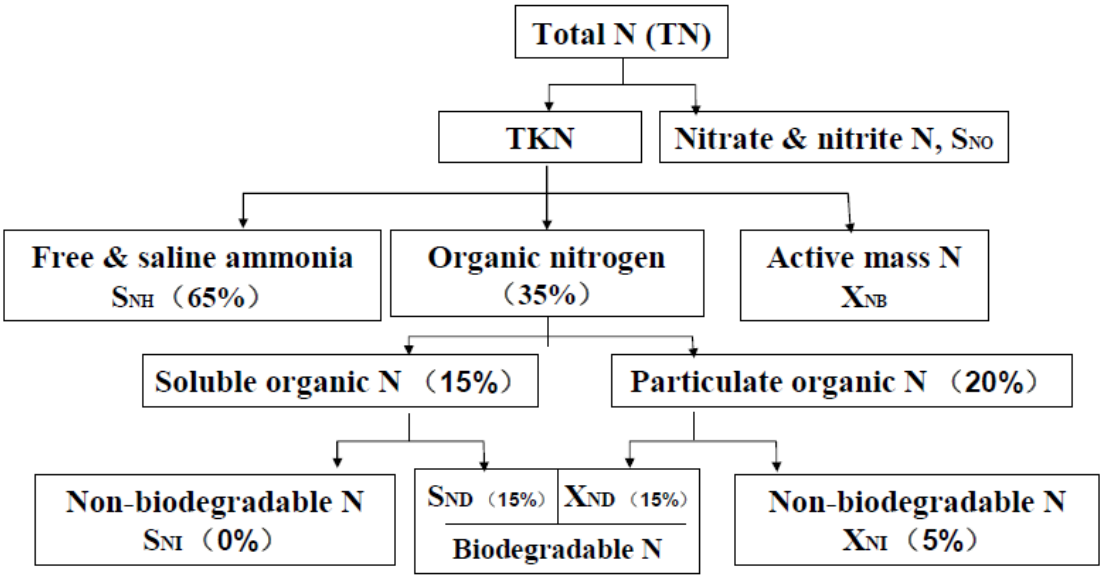

Figure II- 8: Fractions of total nitrogen

The fractions of the carbon and nitrogen material from Figure II-7 and II-8 are integrated into the model by applying the appropriate percentage to conventional parameters of urban wastewater.

3. Start the simulations of TFC and MSB

With any model, one of the first exercises to carry out is a sensitivity analysis of model parameters. A sensitivity analysis was performed using a one-variable-at-a-time approach. However, with BIOWIN, the software can work on the sensitivity analysis automatically.

3.1 Set the diagram of simulation system

To simulate an integrated process of a single-stage TF (called TFC in this thesis) and a Multi-Section Bioreactor (called MSB in this thesis), a diagram of the system was prepared as shown in Figure II-9. 5 single-stage TFs in series were used to represent a MSB pilot.

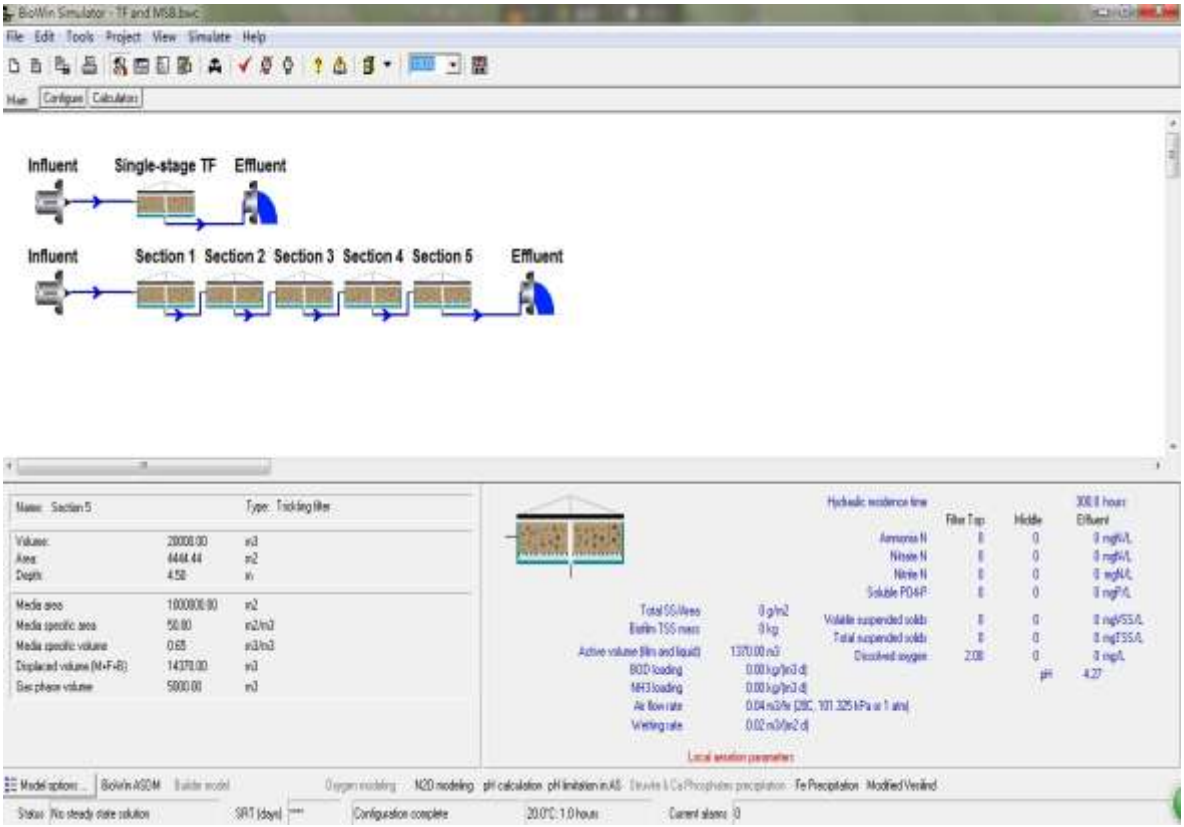

Figure II- 9: Schematic diagram of the TF and MSB system

Figure II-9 diagrammatically shows the experimental setup and describes the path of the hydraulic installation according to three modules (influent, bioreactor system, effluent) connected by piping. For each unit, the user must first select a model from those available in BIOWIN. Subsequently, one defines the physical characteristics and operating conditions obtained through field data and specific quantities such as the concentrations of S and X of the effluent, input feed rates, and flows of water and air, temperature, porosity of the medium, and bead diameter.

3.2 Initial operating conditions and influent components setting

The operating conditions, physical properties of the TF and influent components with their default kinetic parameters are shown in the following Tables II-5 to II-8. To start the simulation work, we applied the low organic loading rate which was the same influent conditions as applied in the Period 2 of Biological experiments for both bioreactors.

3.2.1 Operating conditions

The operating conditions applied for both mono-stage TF and MSB simulations are shown in Table II-5. Only the flow rates, inlet total COD concentrations, and the inlet TKN concentrations were adjusted, the rest were kept as default values.

Table II- 5: Input operating conditions

	Same OLR and NLR simulations		Oxygen effect simulations	Confront the biological experiment simulations		
	Simul_1000	Simul_300	All cases	Simul_300	Simul_1000	Simul_Viandox
Flow (m^3/d)	0.08	0.267	0.08	0.08	0.08	0.08
Total COD (mgCOD/L)	1000	300	1000	300	1000	1000
TKN (mgN/L)	151.51	46	151.51	47	161	144
Total P (mgP/L)	10	10	10	10	10	10
Nitrate N (mgN/L)	0	0	0	0	0	0
pH	7.3	7.3	7.3	7.3	7.3	7.3
Alkalinity (mmol/L)	6	6	6	6	6	6
ISS Influent (mgISS/L)	45	45	45	45	45	0
Calcium (mg/L)	80	80	80	80	80	80
Magnesium (mg/L)	15	15	15	15	15	15
D.O. (mg/L)	0	0	0	0	0	0

For the simulations at same OLR and NLR, we first fixed the conditions of Simul_1000; then to obtain the same organic and nitrogen loads for Simul_300, we adjusted the influent flow rate and TKN concentration.

For the oxygen effect simulations, two manners were applied, one is by changing the constant oxygen input concentration for oxygen modeling, the other one is by changing the air input flowrate. This will be detailed described in “aeration parameters”. We kept the same influent conditions to that of Simul_1000 for all the simulations rounds, only changing the oxygen input concentrations or the air input flowrate without changing the influent conditions.

For these simulations that confront the biological experiments of 3 periods, we first changed the influent CODt, TKN conditions which is the same value as the mean compounds concentration obtained in Chapter 4.

Though in the “operation conditions” we can only adjust the flowrate, CODt and TKN concentrations, the influent components concentrations were then adjusted by changing the fractions ratios.

3.2.2 Physical properties of mono-stage TF and MSB

The physical properties of the TFC and MSB are shown in Table II-6. These parameters were adjusted to correspond to the physical characteristics determined in part 1of this Chapter.

Table II- 6: Physical properties of TFC and MSB

Bioreactor	Volume [m^3]	Area [m^2]	Depth [m]	Media area [m^2]	Specific area [m^2/ m^3]	Specific volume [m^3/ m^3]
Single-stage TF	0.0628	0.0314	2.000	6.5940	400	0.08
MSB each section	0.0126	0.0314	0.4	1.32	400	0.08

Due to the types of media, selection was limited in this software. The software only includes ROCK, CROSSFLOW plastic media, Horizontal Media, Random media and Custom media.

We chose the Random Media as the media applied in the TF which was similar of the media type to our Concreted-Brick media (SSA=350±70 m^2/m^3) applied in the biological experiments; however, it had lower specific surface area (105 m^2/m^3). It will lead to lower total specific surface area of the packing bed and the treatment performance predicted by the simulation would be consequently weaker than obtained in the biological experiments. Then we adjusted the default SSA of media to the same SSA as our media.

3.2.3 Influent components

After the fractionation of influent wastewater by the biological experiments, we obtained the fractions of soluble and particulate substrate. The COD influent components were set to be the same for the TFC and MSB under different organic loads simulations, by changing the fraction ratios as shown in Table II-7.

Table II- 7: Fractions ratio adjustments to fit the biological influent components

Fractions ratio	Default	Simul_300	Simul_1000	Simul_Viandox
Fbs - Readily biodegradable [gCOD/g of total COD]	0.16	0.12	0.12	0.95
Fac - Acetate [gCOD/g of readily biodegradable COD]	0.15	0	0	0
Fxsp - Non-colloidal slowly biodegradable [gCOD/g of slowly degradable COD]	0.75	1	1	0
Fus - Unbiodegradable soluble [gCOD/g of total COD]	0.05	0.05	0.03	0.05
Fup - Unbiodegradable particulate [gCOD/g of total COD]	0.13	0.13	0.03	0
Fna - Ammonia [gNH3-N/gTKN]	0.66	0.66	0.66	0.7
Fnox - Particulate organic nitrogen [gN/g Organic N]	0.5	0.5	0.5	0
Fnus - Soluble unbiodegradable TKN [gN/gTKN]	0.02	0.02	0.02	0.03
FupN - N:COD ratio for unbiodegradable part. COD [gN/gCOD]	0.035	0.035	0.035	0
Fpo4 - Phosphate [gPO4-P/gTP]	0.5	0.5	0.5	0.75
FupP - P:COD ratio for unbiodegradable part. COD [gP/gCOD]	0.011	0.011	0.011	0
FZbh - OHO COD fraction [gCOD/g of total COD]	0.02	0.02	0.02	0
FZbm - Methylotroph COD fraction [gCOD/g of total COD]	1.00E-04	1.00E-04	1.00E-04	0
FZaob - AOB COD fraction [gCOD/g of total COD]	1.00E-04	1.00E-04	1.00E-04	0
FZnob - NOB COD fraction [gCOD/g of total COD]	1.00E-04	1.00E-04	1.00E-04	0
FZamob - ANAMMOX COD fraction [gCOD/g of total COD]	1.00E-04	1.00E-04	1.00E-04	0
FZbp - PAO COD fraction [gCOD/g of total COD]	1.00E-04	1.00E-04	1.00E-04	0
FZbpa - Propionic acetogens COD fraction [gCOD/g of total COD]	1.00E-04	1.00E-04	1.00E-04	0
FZbam - Acetoclastic methanogens COD fraction [gCOD/g of total COD]	1.00E-04	1.00E-04	1.00E-04	0
FZbhm - H2-utilizing methanogens COD fraction [gCOD/g of total COD]	1.00E-04	1.00E-04	1.00E-04	0
FZe - Endogenous products COD fraction [gCOD/g of total COD]	0	0	0	0

With respect to the fraction ratios adjustments shown in Table II-7, the reset influent components concentrations are shown in Table II-8.

Table II- 8: Components in the influent

Parameters	Default of 300	Simul_300	Default of 1000	Simul_1000	Simul_Viandox
Volatile suspended solids	118.66	156.12	395.52	532.9	0
Total suspended solids	164.05	201.51	441.83	579.2	0
Particulate COD	189.06	249	630.2	850	0
Filtered COD	110.94	51	369.8	150	1000
Total COD	300.00	300	1000	1000	1000
Soluble PO4-P	5.00	5	5	5	7.5
Total P	10.00	10	10	10	10
Filtered TKN	37.74	37.74	124.27	126.02	144
Particulate TKN	8.26	8.26	27.24	25.49	0
Total Kjeldahl Nitrogen	46.00	46	151.51	151.51	144
Filtered Carbonaceous BOD	67.97	25.43	226.58	84.76	671.01
Total Carbonaceous BOD	147.48	136.62	491.6	518.82	671.01
Nitrite + Nitrate	0	0	0	0	0
Total N	46.00	46	151.51	151.51	144
Total inorganic N	30.36	30.36	100	100	100.8
Alkalinity	6.00	6	6	6	6
pH	7.30	7	7	7	7
Volatile fatty acids	7.20	0	24	0	0
ISS precipitate	0	0	0	0	0
ISS cellular	0.39	0.39	1.3	1.3	0
ISS Total	45.39	45.39	46.3	46.3	0
Ammonia N	30.36	30.36	100	100	100.8
Nitrate N	0	0	0	0	0

In Table II-8, the components concentrations in the case default of 300 and 1000 were applied to these simulations at same OLR and NLR, then the oxygen effect simulations.

Simul_300, Simul_1000 and Simul_Viandox were applied in the simulations to fit the biological experiments.

3.2.4 Global Kinetic Parameters

Global kinetic parameters of Ordinary heterotrophic organisms (OHO), Ammonia oxidizing biomass (AOB), Nitrite oxidizing biomass (NOB), Nitrite oxidizing biomass (NOB) are shown in Table II-9.

Table II- 9: Default and current values of kinetic parameters

AOB	Default	Value	
Max. spec. growth rate [1/d]	0.9000	0.9000	1.0720
Substrate (NH4) half sat. [mgN/L]	0.7000	0.7000	1.0000
Byproduct NH4 logistic slope [-]	50.0000	50.0000	1.0000
Byproduct NH4 inflection point [mgN/L]	1.4000	1.4000	1.0000
AOB denite DO half sat. [mg/L]	0.1000	0.1000	1.0000
AOB denite HNO2 half sat. [mgN/L]	5.000E-6	5.000E-6	1.0000
Aerobic decay rate [1/d]	0.1700	0.1700	1.0290
Anoxic/anaerobic decay rate [1/d]	0.0800	0.0800	1.0290
KiHNO2 [mmol/L]	0.0050	0.0050	1.0000
NOB	Default	Value	
Max. spec. growth rate [1/d]	0.7000	0.7000	1.0600
Substrate (NO2) half sat. [mgN/L]	0.1000	0.1000	1.0000

Aerobic decay rate [1/d]	0.1700	0.1700	1.0290
Anoxic/anaerobic decay rate [1/d]	0.0800	0.0800	1.0290
KiNH3 [mmol/L]	0.0750	0.0750	1.0000
ANAMMOX			
Max. spec. growth rate [1/d]	0.1000	0.1000	1.1000
Substrate (NH4) half sat. [mgN/L]	2.0000	2.0000	1.0000
Substrate (NO2) half sat. [mgN/L]	1.0000	1.0000	1.0000
Aerobic decay rate [1/d]	0.0190	0.0190	1.0290
Anoxic/anaerobic decay rate [1/d]	0.0095	0.0095	1.0290
Ki Nitrite [mgN/L]	1000.0000	1000.0000	1.0000
Nitrite sensitivity constant [L / (d mgN)]	0.0160	0.0160	1.0000
OHO			
Max. spec. growth rate [1/d]	3.2000	3.2000	1.0290
Substrate half sat. [mgCOD/L]	5.0000	5.0000	1.0000
Anoxic growth factor [-]	0.5000	0.5000	1.0000
Denite N2 producers (NO3 or NO2) [-]	0.5000	0.5000	1.0000
Aerobic decay rate [1/d]	0.6200	0.6200	1.0290
Anoxic decay rate [1/d]	0.2330	0.2330	1.0290
Anaerobic decay rate [1/d]	0.1310	0.1310	1.0290
Hydrolysis rate [1/d]	2.1000	2.1000	1.0290
Hydrolysis half sat. [-]	0.0600	0.0600	1.0000
Anoxic hydrolysis factor [-]	0.2800	0.2800	1.0000
Anaerobic hydrolysis factor (AS) [-]	0.0400	0.0400	1.0000
Anaerobic hydrolysis factor (AD) [-]	0.2000	0.2000	1.0000
Adsorption rate of colloids [L/(mgCOD d)]	0.1500	0.1500	1.0290
Ammonification rate [L/(mgN d)]	0.0400	0.0400	1.0290
Assimilative nitrate/nitrite reduction rate [1/d]	0.5000	0.5000	1.0000
Fermentation rate [1/d]	1.6000	1.6000	1.0290
Fermentation half sat. [mgCOD/L]	5.0000	5.0000	1.0000
Fermentation growth factor (AS) [-]	0.2500	0.2500	1.0000
Endogenous products decay rate[1/d]	0	0	1.0000
Free nitrous acid inhibition [mmol/L]	1.000E-7	1.000E-7	1.0000

Due to lack of information of experimental estimation of kinetic parameters, all of the bio-kinetic parameters were maintained the same as default values.

3.2.5 Aeration equipment parameters

Although no forced-aeration equipment was applied in biological experiments, in the simulation of MSB pilot, we adjusted the value of off-gas O_2 volume percentage was set equal to that of supply gas O_2 as shown in Table II-10 to avoid the oxygen decline potential from the bottom to the top. Due to the open structure of MSB, we assumed that the driving force of oxygen from the bottom to the top of each section did not change, because the saturation concentration and bulk concentration were the same.

Table II- 10: Aeration equipment parameters

Element name	Supply gas CO_2 content [vol. %]	Supply gas O_2 [vol. %]	Off-gas CO_2 [vol. %]	Off-gas O_2 [vol. %]	Off-gas H_2 [vol. %]	Off-gas NH_3 [vol. %]	Off-gas CH_4 [vol. %]	Surface turbulence factor [-]
TF	0.0350	20.9500	2.0000	20.9500	0	0	0	2.0000
MSB								
Section 1	0.0350	20.9500	2.0000	20.9500	0	0	0	2.0000
Section 2	0.0350	20.9500	2.0000	20.9500	0	0	0	2.0000
Section 3	0.0350	20.9500	2.0000	20.9500	0	0	0	2.0000
Section 4	0.0350	20.9500	2.0000	20.9500	0	0	0	2.0000
Section 5	0.0350	20.9500	2.0000	20.9500	0	0	0	2.0000

3.2.6 Oxygen modeling setting

In order to investigate the oxygen effect on the MSB performance by Biowin, two manners of oxygen modeling were applied. This adjustment of oxygen modeling is shown in Figure II-10. One is to specify the dissolved oxygen concentration for each section of MSB or for mono-stage TF; the other is to specify a constant air flow rate. Attention should be drawn as show in the figure; oxygen modeling in this software can only input the oxygen from the top section towards the bottom section in a TF module, no reverse pathway of oxygen flux can be made, i.e. oxygen cannot go through TF module from the bottom to the top section.

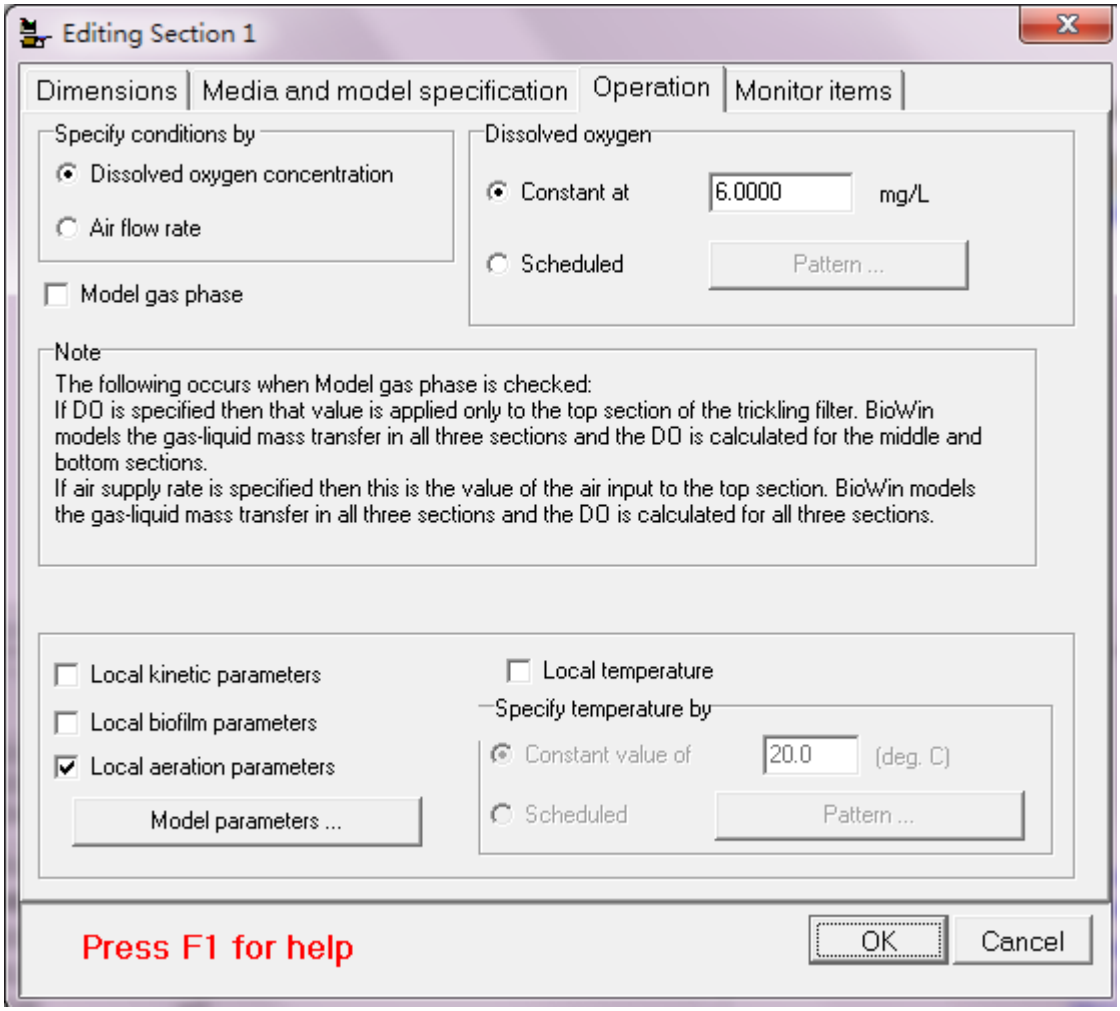

Figure II- 10: Oxygen modeling operations

3.2.7 Set output variables

After setting up the diagram of the simulation system and the influent conditions, the operating conditions, kinetic parameters; one right-click on the bioreactor configures and choose “add to album”. Choose the “element info (summary)” for general effluent biomass

concentrations output; “element info (state variables)” for effluent components concentrations output; “details” for local biomass and components concentrations outputs, displaying the concentrations in each layer and each section. Once the data are entered, the interface provides the ability to view any number of output variables of the system ("DISPLAY OUTPUTS") as the concentrations of S and X of the effluent output but also within the range. An example of a MSB simulation is shown in Figure II-11.

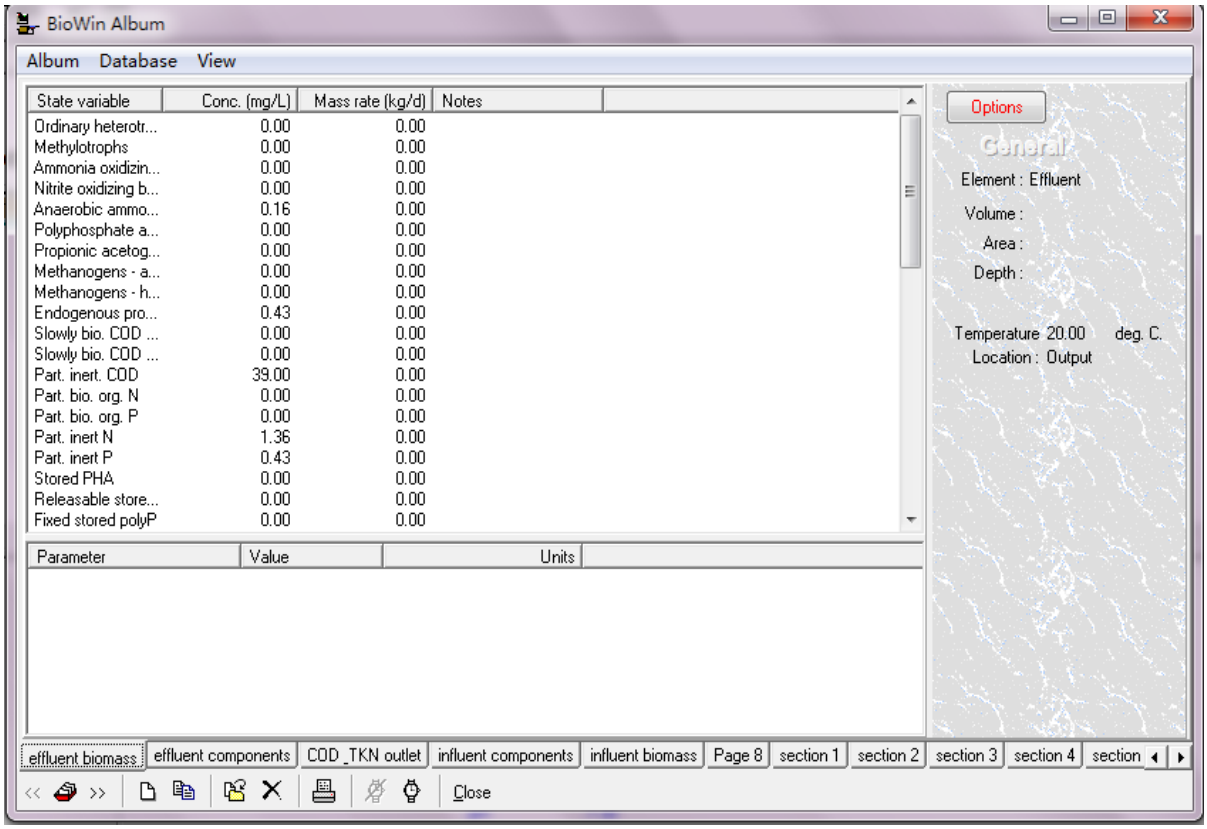

Figure II- 11: Biowin album for data output.

3.2.8 Start the simulation

Once the output variables were already set, click the “check data” bar to analyze whether or not the simulation system was well installed and the kinetic parameters are good to start simulating. It is shown in Figure II-12 in the red circle. Then click the “steady-state simulation” bar to start a simulation under steady-state as shown in Figure II-12 in the green circle.

Figure II- 12: Start to simulate considering the data check and simulate under steady-state

4. Finish the simulation and export data

Once the steady-state simulation is finished, a notification shows on the board saying "Steady-state solution found". It means that the simulation is finished and the simulation results and data can be exported by generating a simulation report as shown in Figure II-13.

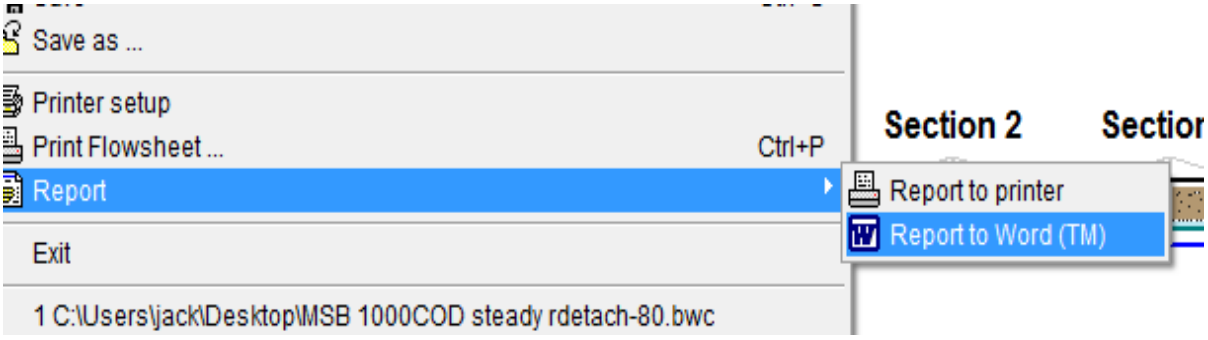

Figure II- 13: Generate a simulation report to Word

After generating the simulation report, we can obtain all the simulation related parameters and effluent data. With various tables and figures, the simulation results can be compared to the results of our biological experiments. If deviations occur, we can restart simulation by changing a critical parameter, such as biofilm detachment rate, or oxygen mass transfer coefficient, k_L.

Chapter 3

Hydrodynamic characterization of the TFC and MSB with and without biofilm

1. Introduction

As mentioned in Chapter 1, in a Trickling Filter (TF), complex mechanisms are taking place which depend strongly on hydraulic conditions. To improve and control the TF technology, it is essential to understand which physical parameters affect the hydraulic behaviour in order to accurately investigate these effects through software simulation and modelling.

Generally with conventional TF, the design and reliable scale-up are highly dependent on hydrodynamic performance and on the transport phenomena imposed by the internal packing and its geometry (Viva and Brunazzi 2007). The hydrodynamic behaviour of certain types of medium has been widely investigated (Suess and Spiegel, 1992; Darakchiev and Kolev, 1996; Samb et al., 1996; Seguret et al., 2000; Brunazzi et al., 2002; Urrutia, 1996). However, a number of natural and man-made non-spherical porous medium with biofilm are too complicated to be well investigated, even where appropriate boundary conditions have been provided in some studies (Tuller, 2003). The effect of biofilm on hydrodynamics in a TF has seldom been reported (Seguret et al., 2000; Mounir, 1991); most reports have assumed the biofilm to be homogeneous along the packed bed, but even so, they have not quantified the biofilm.

The hydraulic characteristics such as liquid dynamic retention, liquid superficial velocity, shear stress, liquid residence time and liquid film thickness normally affect the mass transfer of oxygen and nutrients; they further affect the biological processes in the biofilm. The total liquid holdup can be divided into: static and dynamic (Johann et al.,1998)(Behrens, 2006). Static holdup, the fraction of liquid retained within and around the particles by capillary forces after complete drainage depends on the type of media. Dynamic holdup is formed by the flowing liquid and is highly dependent on the liquid load. For some types of medium, e.g. structured and non-porous medium (Viva and Brunazzi, 2007), dynamic holdup can be considered to be the predominant part of the total liquid holdup (Suess and Spiegel, 1992; Nakov et al., 2000). However, due to the physical characteristics of the porous packing employed in our study, the static holdup fraction contributes more to the total liquid holdup than the dynamic.

With the ultimate aim of optimizing TF design and operation, the main objective of the work of Chapter 3 was to characterize the hydrodynamic behavior of two types of TF (TFC and MSB) filled with the same porous medium but differing in its spatial organization (The TFC is a close structure without interval spaces, whereas the MSB has an open structure with interval spaces). It was our objective to determine the impact of the properties of the medium

and its organization in the reactor on the overall hydrodynamics. The impact was measured in term of liquid holdup fractions, liquid film thickness with and without biofilm (two organic loading rates were applied) along the column. A further objective was to use RTD experiments and modeling to investigate changes in liquid flow pattern and liquid residence time due to the presence of biofilm in the MSB. Additionally, the study attempted to verify whether the configuration of the bioreactor (TFC or MSB, mainly focused on the close/open structure and presence of the interval spaces) affects its hydrodynamic characteristics.

2. Results and Discussion

The physical properties of Concrete block media were firstly determined by conventional methods, such as volumetric method and weighing method. Static, dynamic and RTD experiments were then carried out to investigate the dynamic behaviors of the media in the MSB and compare with the TFC. Further modeling of liquid residence time distribution was associated with the static and dynamic holdup and fractions. Based on those, the liquid film thickness can be estimated and the oxygen transfer coefficient can be determined based on the liquid film thickness.

2.1 Media and packed bed properties

Based on the volumetric and weighing methods, the physical properties of the media and packed bed were determined, with details provided in Chapter 2 M&M and Appendix 3. The physical properties of media particle and packed bed are summarized in Table III-1:

Table III-1: Physical properties of Concrete block media and packed bed

Particle porosity	Material Density	Specific Surface Area	Particle Density	Particle Equivalent Diameter	Particle sphericity	Total packed bed void fraction	Apparent packed bed void fraction
(%)	(kg/m^3)	(m^2/m^3)	(kg/m^3)	(cm)			(%)
ε'	ρ_{powder}	a_p	$\rho_{particle}$	d_p	Φ	ε	φ_{cb}
61	1337	350±70	586.4	2.17±0.4	0.74±0.07	79.1 / 72.7*	46.4/42

* For the MSB packed bed void fraction calculation, the interval spaces between two adjacent sections were not taken into account.
Total packed bed void fraction contains the external voidage space in the column excluding the packed bed and the internal voidage of particles. Apparent packed bed void fraction only contains the external voidage space.

2.2 Static holdup

2.2.1 without biofilm

Figure III-1 plots the water adsorption fraction (static holdup liquid mass/dry packing's mass) versus the number of particles.

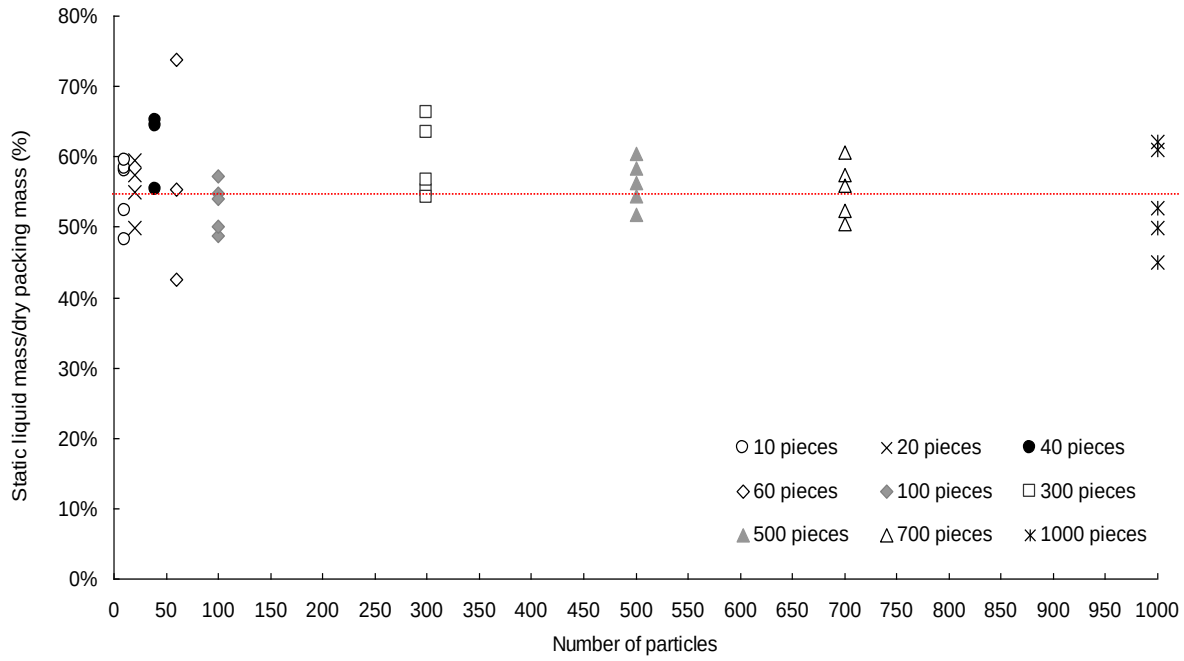

Figure III- 1: Relation between number of particles and liquid static hold-up fraction.

From Figure III-1, it can be observed that the hold-up fraction values were more reliable when a sufficient number of particles, more than 300 were employed in experiments. Moreover, a constant water adsorption fraction F_{ad} of approximately 56% ± 6% was found. This constant value was applied to both reactors to calculate their corresponding liquid static retention (liquid volume per pure solid volume).

Since the total packing weight of the TFC was 75 kg, the total static weight, calculated as 75kg×56% was 42 ± 0.45 kg. The total packing weight in the Multi-Section Bioreactor (MSB) was 25.63 kg; correspondingly, the total static hold-up weight was 14.35 ± 0.15 kg.

Furthermore, the total packed bed void fraction and the column volume were taken into account to calculate the liquid static retention of the TFC:

$$\beta_S = \frac{V_S}{V(1-\varepsilon)} = 84\%$$

where V_s , the static liquid volume for the TFC, =0.042 m^3; ε the total packed bed void fraction, was 79.1% (see Table III-1) and V the column volume, equals 0.238 m^3.

With a similar approach, the static retention of the MSB was calculated:

$$\beta_S = \frac{V_S}{V(1-\varepsilon)} = 84\%$$

where V_s the static liquid volume in the multi-section bioreactor, equals 0.01435 m^3; ε the total packed bed void fraction, equals 72.7% (see Table III-1), and V, the volume of the multi-section bioreactor, is 0.0628 m^3.

Assuming that the number of particles might be an indicator to predict the static hold-up mass or volume, the experimental static hold-up volume is plotted versus number of particles in Figure III-2.

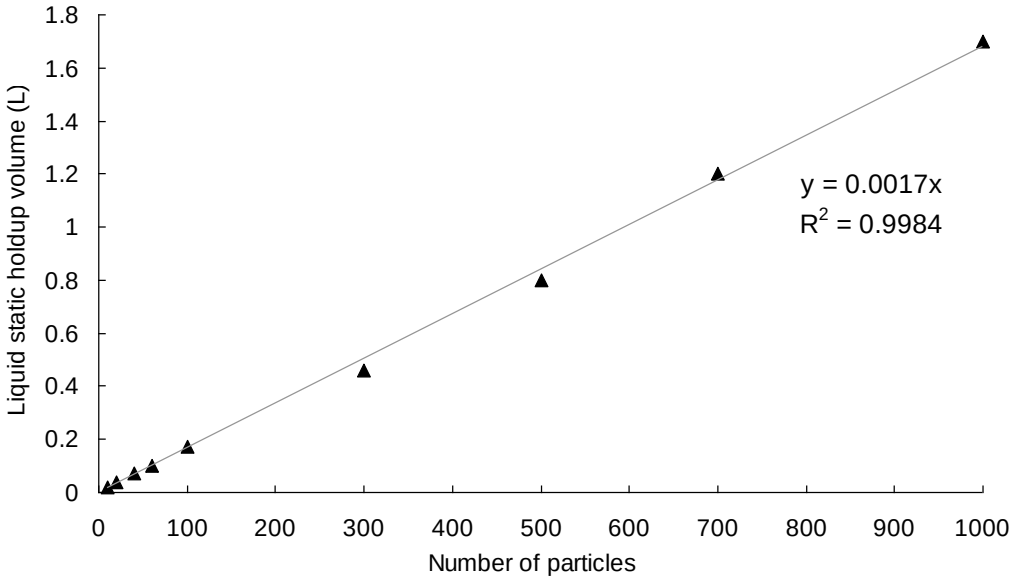

Figure III- 2: Static hold-up volume versus number of particles.

Figure III-2 indicates that the static hold-up volume increased linearly as the number of particles increased. The curve shows good linearity which implies good correspondence between the number of particles $N_{particles}$ and the static liquid hold-up volume V_{LS}.

$$V_{LS} = 0.0017 \times N_{particles} \qquad \text{(III-1)}$$

For a definite number of particles, Eq. III-1 relating the static hold-up volume to the number of particles holds, implying a stable adsorption capacity of each particle for liquid. Based on this relation, the number of particles packed in one column can be estimated. For example, the static hold-up volume was calculated as 42 L based on the liquid static hold-up fraction in the TFC, the number of particles inside the column was hence estimated as 24700.

2.2.2 Static holdup models without biofilm

The static holdup models correspond to the approach proposed by Viva and Brunazzi (2007) to predict the static holdup related to one structured packing module in a trickling filter, adapted to our porous packing media. The general principal is based on the relation between the liquid capillary rise height and liquid surface tension, to estimate the external and internal capillary force imposed on the media. Detailed calculation of static holdup according to Viva and Brunazzi's model is shown in Appendix 5.

The capillary rise height of a single particle/pore and the mass of liquid external/internal capillary holdup $hl_{ex.cap}$/ $hl_{in.cap}$ of entire packed bed were calculated for both reactors and are presented in Table III-2.

Table III-2: Internal and external capillary rise height, capillary holdup and mass

Reactor	α	$h_{ex.\ cap}$	$h_{in.\ cap}$	$m_{ex.\ cap}$	$m_{in.\ cap}$	m_{LS}	β_S
	(°)	(m)	(m)	(kg)	(kg)	(kg)	(%)
TFC	62	0.00029	0.013	0.9	41.2	42.1	84.4
MSB	56	0.00035	0.016	0.31	14.03	14.34	84.1

From Table III-2, the calculated total static holdup weights of both bioreactors (42.1 kg and 14.34 kg, respectively) are in excellent agreement with the experimental results from the water adsorption fraction (42kg and 14.35kg, respectively). This indicates that the static holdup models proposed by Viva and Brunazzi (2007) can be applied to our static holdup estimation.

Generally, the residual holdup cannot be disregarded due to the porous structure of medium, also investigated by Kundu et al., (2003). However, the main fraction of the liquid held by our medium was mainly due to internal capillary forces, which act specifically inside the particle. The fitted solid-liquid contact angles (62° and 56°) that match our static experimental holdup generate reasonable values for static liquid holdup; they are also in accord with contact angles generally encountered for water with cements (Ortiz et al., 2003). According to these contact angles, the model can predict the static holdup mass in the TFC and MSB. The liquid static retention fractions calculated by the model were very similar in the both reactors, 84% in both the TFC and in the MSB, in close agreement with the previous experimental result for static retention (again 84%).

2.2.3 Calculation of the static holdup with biofilm

Only the MSB pilot was used for biological experiments. Liquid static retention fractions of the entire MSB pilot and of each section after two regimes of organic loads feeding were calculated by the modified weighing method (Chapter 2), which measures the mass difference of a section with biofilm for feeding at a higher flowrate after stabilizing the same section at a lower flowrate. In reality, during the biofilm accumulation in the MSB, it was observed that the biofilm thickness varied with the packed bed depth and in each section; even at the same horizontal level, the distribution of biofilm thickness was not homogeneous. Owing to the lack of enough accurate information regarding biofilm thickness $\boldsymbol{L_f}$ distribution, for simplicity, the values of mean biofilm thickness $\boldsymbol{L_f}$ adopted in our study were calculated by means of a drying method which determined the volume of total dry biomass per particle surface area. The assumption was adopted that the distribution of biofilm thickness was homogeneous along each section at the same horizontal level. In addition, particles were assumed to be completely coated by biofilm. The liquid static retention fractions in each section and in the entire pilot are plotted against the surface hydraulic loads under two organic loads cultivation in Figures III-3 a and b.

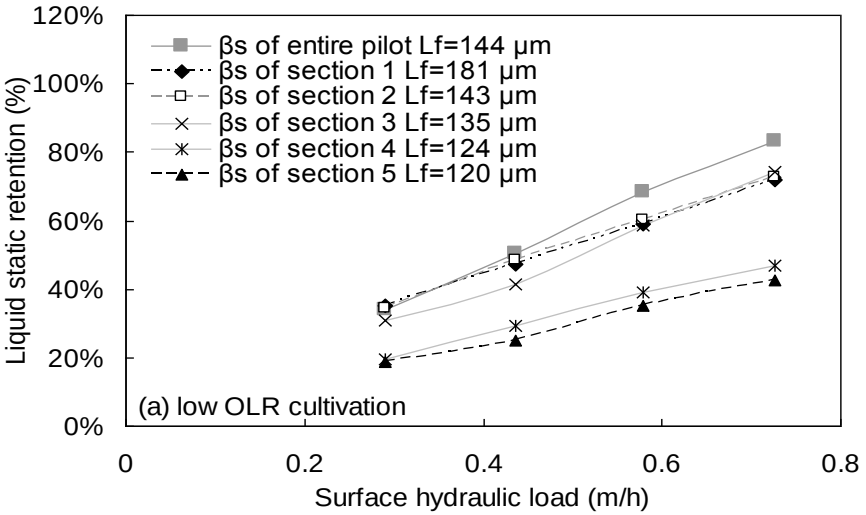

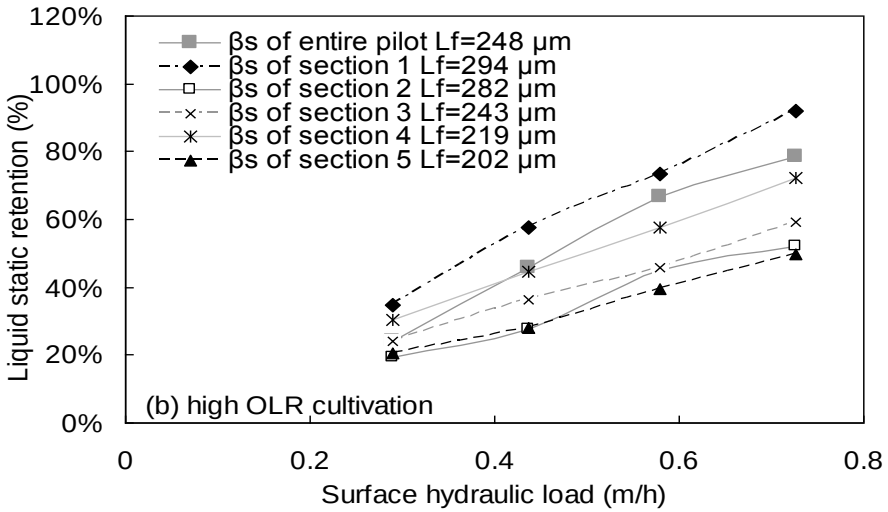

Figure III- 3: Liquid static retention of each section (section 1 is located at the top) and the entire pilot under different hydraulic conditions

From Figure III-3, the liquid static retention fraction increases when the hydraulic loads rises in each section and in the entire pilot. At large hydraulic loads, high static retention is observed (80%), close to those obtained without biofilm. The liquid static retention generally increases when the biofilm thickness increases which could result from larger absorption capacity due to the presence of the biofilm. Along the pilot depth from the top section to lower sections, the biofilm thickness gradually decreased. However, static retention did not strictly decrease along the depth with the decline in thickness, implying that the biofilm porosity and density should also be taken into account. Biofilm absorption capacity depends on its porosity and on its density.

2.4 Dynamic holdup

According to the observation of the real-time liquid drainage mass curve shown by the data-acquisition system in the dynamic experiments without and with biofilm, two portions of dynamic holdup were distinguished; the linear segment is the fast dynamic fraction, whereas the curve segment is the slow dynamic fraction. Dynamic holdup experiments in two bioreactors without biomass under different hydraulic loads were firstly carried out.

2.4.1 Dynamic holdup without biofilm

Interpretation of a typical draining curve

A typical curve showing draining liquid mass curve against the drainage time in the TFC at a flowrate of 0.3m³/h is plotted in Figure III-4.

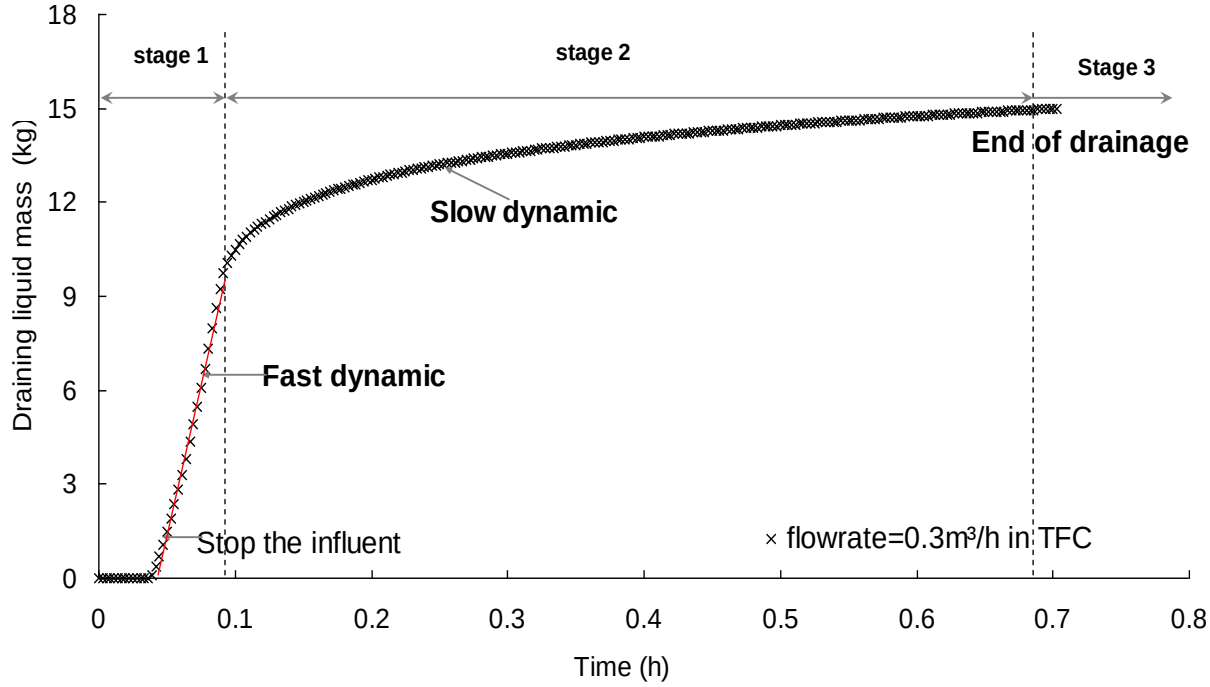

Figure III- 4: Dynamic holdup release process curve for a flowrate of 0.3 m3/h in TFC

From Figure III-4, three stages can be observed: Stage 1 characterizes the dynamic holdup release; this step appears on the curve with a strong slope, it corresponds to the fast removal of water volume around the particles. It may be represented by a capillary surface volume plus free water volume in the bed; Stage 2 corresponds to the internal and external capillary holdup release or pore water release. This step appears on the curve like a smooth slope. It represents a slow phenomenon which describes the removal of water from inside the particles' pores; Stage 3 corresponds to a plateau of the curve obtained when the output is stopped characterizing the residual holdup. The residual holdup corresponding to the capillary holdup, gives the water fraction remaining inside and outside the particles' pores, and it should be in good agreement with static experiments presented previously. However the capillary holdup cannot be calculated from the method, because this static fraction cannot leave the solids and be measured.

Two types of dynamic holdup can be calculated from the curve reported in Figure III-4, firstly the external dynamic holdup, and secondly the internal dynamic holdup.

Example of dynamic holdup calculated from typical drainage curve

As an example, from Figure III-4 the different dynamic holdup masses were calculated according to the method developed in chapter 2. (See paragraph of dynamic holdup measurements):

Fast dynamic holdup weight =10.07-1.91=8.16 kg (from the straight line reported in Figure III-4), this corresponds to the external layer and to the internal large pores where capillary forces are weak compared to gravity forces.

Slow dynamic holdup weight =15-10.07=4.93 kg (from the initial point of stage 2 and end point of stage 3), this corresponds to the external layer and internal pore volume in opposition with the capillary forces. The embedded mass in the column can then be estimated from the static holdup and the slow dynamic holdup:

Embedded mass = 42-4.93=37.07 kg, this corresponds to the water weight definitely locked into the solid.

Due to the small pore size of the solid, the main part of the fast dynamic holdup is due to external layer volume. The fast dynamic holdup mass is estimated to be 8.16 kg, a large value compared to the external static capillary weight 0.9 kg calculated from the previous model (refer to Appendix 5).

Similar calculations of fast and slow dynamic holdup mass were carried out for the MSB at regimes without biofilm.

The results of both reactors (TFC and MSB) are presented in Table III-3:

Table III- 3: Results of Holdup mass from two bioreactors' experiments

TF	m_p	HL	m_{LS}	m_{Ld}	m_{Lfd}	m_{Lsd}	m_{Lt}	f_{ab}	V_{embed}	β_d	β_S
	kg	m/h	kg	kg	kg	kg	kg	%	L	%	%
TFC	75	2.4	42	13.1	8.2	4.9	55.1	56	37.1	26	84
MSB	26	0.3	13.9	3.4	1.8	1.6	17.3	54	12.3	20	82
	26	0.4	13.8	3.4	1.6	1.8	17.2	54	12.0	19	81
	26	0.6	12.3	3.7	2.7	1.0	16.0	48	11.3	22	72
	26	0.7	14.0	2.8	1.0	1.8	16.8	55	12.2	16	82

TFC: Trickle Fix-bed Column; MSB: Multi-section Bioreactor; m_p: Total packing mass; H.L.: Hydraulic Loads; m_{LS}: Static holdup mass; m_{Ld}: Dynamic holdup mass; m_{Lt}: Total liquid holdup mass; βd: Dynamic retention; βs: Static retention; m_{Lfd}: Fast dynamic holdup mass; m_{Lsd}: Slow dynamic holdup mass;

Both the static and dynamic experiments in the case without biofilm and modeling indicate that our media have a constant liquid adsorption capacity when the biofilm is absent. The static retention was thus almost not dependent of the hydraulic loads applied. The static volume was greater than the dynamic volume due to this significant adsorption capacity, especially from the internal capillary forces, based on the static holdup model. Whatever the type of reactor, the fast dynamic holdup fractions, $\boldsymbol{m_{Lfd}}$, are mostly higher than for the slow dynamic fractions, $\boldsymbol{m_{Lsd}}$.

2.4.2 Comparison of TFC and MSB

The results of dynamic and static retention in the two bioreactors are reported in Figure III-5.

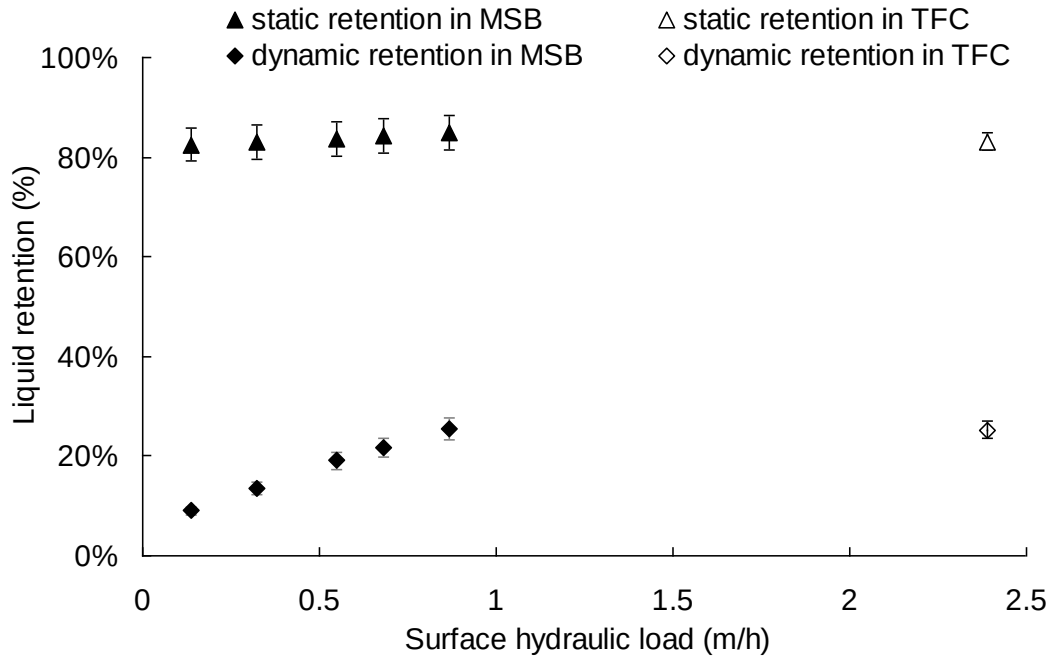

Figure III-5: Liquid retention versus surface hydraulic loads in two bioreactors without biofilm

This shows that the static retention values for both bioreactors without biofilm were close together, with a value of approximately 84%, even though the hydraulic loads used for the TFC were higher. This implies that this type of medium has constant adsorptive capacity of liquid when no biofilm was present. In contrast, in the case of MSB the dynamic retention increased (from 9% to 25 %) when the hydraulic loads rose (from 0.14 to 0.87 m/h), indicating that the dynamic holdup increases when increasing the flow rate. Even if the experiments in the TFC were carried out at greater hydraulic load (2.39 m/h), its dynamic retention (25.6%) was not much higher than the best value recorded for the MSB (25 %). This resulted from the different mass of packing applied into the column; however, the net volume of liquid dynamic holdup was higher than for the MSB.

Whatever the type of reactor, a large static retention (84%) and a smaller dynamic retention (25%) are obtained. This indicates that a large absorption capacity is available when porous media are used in the TF.

2.4.3 Effect of biofilm on the dynamic holdup

In the MSB, the liquid retention experiments were carried out after biofilm development on the media at the same flow rates as applied when no biofilm was present. The liquid retention at regimes with biofilm in each section and in the entire pilot set-up is presented in Figures III-6 a and b with respect to the surface hydraulic loads.

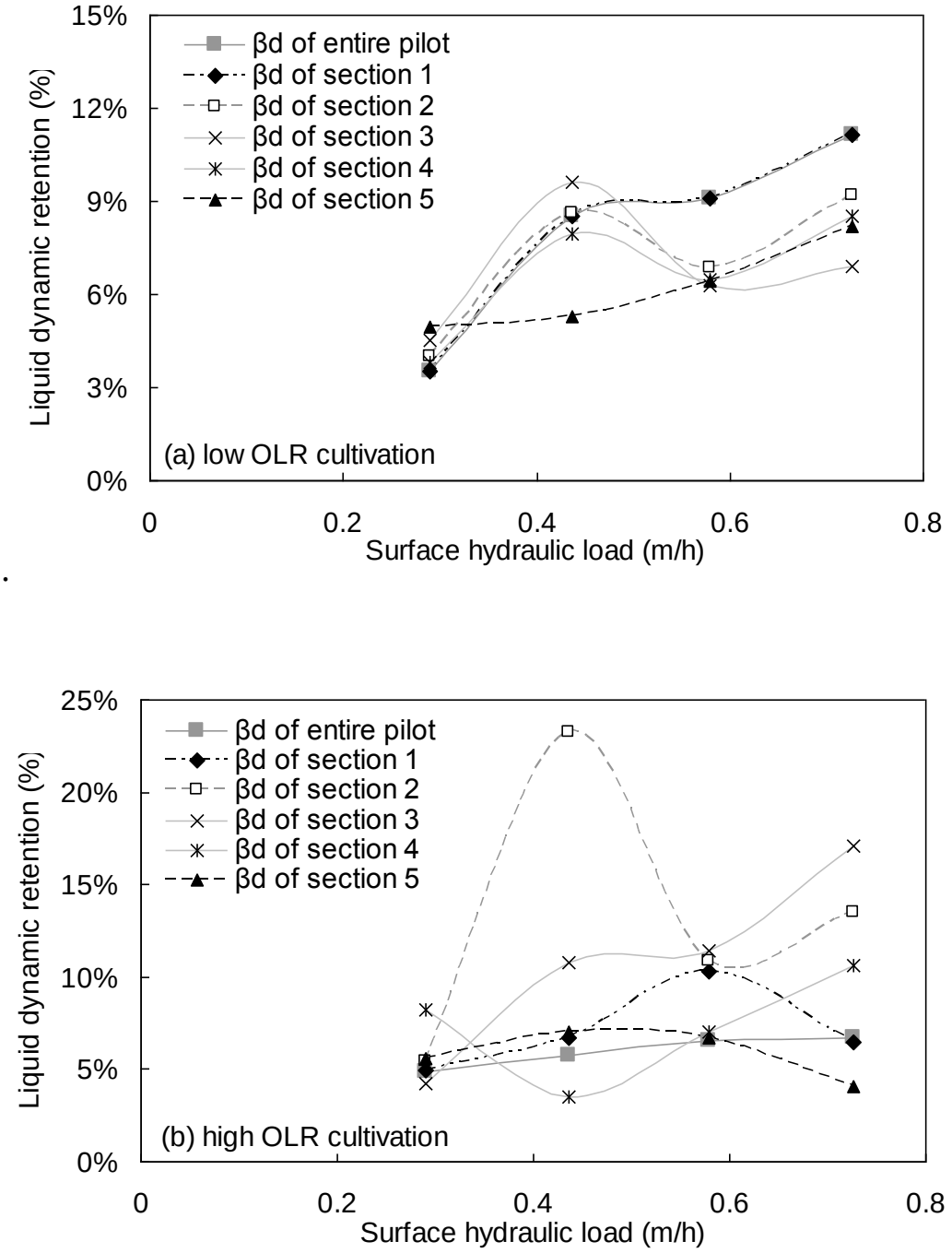

Figure III-6: Liquid dynamic retention versus surface hydraulic load for the MSB reactor in presence of biofilm.

From Figure III-6, it can be seen that with biofilm, the dynamic retention varied little (from 5% to 10% for the entire pilot set-up) when the flow rates rose compared to the static retention (see Figure III-3) which significantly increased (from 24% to 83%) with higher hydraulic loads. Those results imply that most of the liquid was held by the particles coated by biofilm. It was also observed that under various operating conditions in each section; the liquid dynamic retention was lower, ranging between 5% and 15%. The maximum liquid dynamic retention observable in Figure III-6(b) at hydraulic loads slightly higher than 0.40 m/h is difficult to explain by an error measurement as mass balance and timer accuracies were very good. So we believe that it could be due to an accumulation of water in the 2nd section, due to a thicker biofilm that could clog the packed-bed, compared to other sections. This accumulation could account for the large dynamic liquid volume collected on the balance after the stop time.

We also observed biofilm detachments that occurred in the 1st and 2nd section at higher than 0.40 m/h and is consistent with this assumption.

In the regimes without biofilm, in contrast (see Figure III-5), the dynamic retention increased slightly (from 9% to 25%) when the flow rate rose, while the static retention remained a constant at about 84%.

2.4.4 Dynamic holdup relation

Numerous investigations (Davidson et al., 1959; Buchanan et al., 1967; Bemer and Kalis, 1978) found that the dynamic holdup was correlated with the characteristics of the media, liquid superficial velocity and wetting fraction of media. The calculated values of the factor (a) and the wetting fraction ***fw***, from the literature and our results, with respect to different range of liquid interstitial velocity ***U***, based on Eq. II-12 (see Chapter 2) are summarized in Table III-4.

Table III- 4: Dynamic model results from literatures and in this study

Reference	Nominal d_P mm	Biomass	a	f_w	U_{min} m/h	U_{max} m/h
(Van Swaaij et al., 1969,)	22	Without biofilm	1.85	0.69	2.3	21.5
	10.3	Without biofilm	3.12	0.68	2.3	17.5
	6.4	Without biofilm	4.8	0.67	2.3	17.5
(Mounir, 1991)	-	Without biofilm	0.65	0.65	0.96	2.5
	-	With biofilm	1.19	0.65	0.93	2.77
Our study	22	Without biofilm	0.27	0.6	0.37	0.94
	22	With thin biofilm	0.63	0.61		
	22	Section1	1.26	0.8		
	22	Section2	1.03	0.79		
	22	Section3	0.99	0.77		

22	Section4	0.84	0.75		
22	Section5	0.22	0.76		
22	With thick biofilm	0.53	0.64	0.83	2.1
22	Section1	0.86	0.9		
22	Section2	0.52	0.7		
22	Section3	0.65	0.66		
22	Section4	0.43	0.9		
22	Section5	0.84	0.99		

From Table III-4, compared to the results from the literature, our results for ***fw*** are higher and it varies in different sections. Generally, with the biofilm development (from thin biofilm to thick one), the biofilm thickness increases and leads to lower values of ***a,*** while the wetted fraction ***fw*** increases, implying that the biofilm surface could be better wetted by liquid. Due to Eq. II-12 (refer to Chapter 2) having two variables, it is difficult to compare accurately the average values for ***a*** and ***fw***. However, according to the values obtained for each section, we can be sure that a better wettability is obtained when biofilm is present on the media (***fw*** = 0.6 without biofilm; ***fw*** = 0.8 with biofilm).

2.5 Discussion and conclusion

It was found that the majority of liquid is held inside the pores of the medium's particles coated by biofilm. The observed static retention in cases with biofilm could be close to those obtained in the cases without biofilm, when large loading is imposed. The dynamic retention with biofilm was less than without biofilm. The high water absorption efficiency shown by our porous packing was reduced by the biofilm layer that retarded water movement from the inner to the outer parts of the particles. However, at steady state, the external liquid volume (dynamic holdup) would be sufficient to ensure the requisite nutriment mass transport from the waste liquid to the biofilm.

Whatever the type of reactor and operating conditions (with or without biofilm), a large static retention is obtained (80%) and a smaller dynamic retention is obtained (20%), this means that a large absorption capacity is available when porous media are used in TF.

2.6 Residence Time Distribution (RTD)

Analyzing the real RTD curves allows identification of the variation of flow regimes in the column and the liquid fraction involve. Furthermore, the shape of RTD curves and the distribution of liquid in the packing are related to the configuration and geometry of the packing. The RTD curves and modeling can help to understand the biological processes related to the liquid hydrodynamic characteristics. With such knowledge, it is useful to

optimize the design and operation of bioreactors, and to work further with BIOWIN.

2.6.1 Experimental results

In order to acquire the dimensionless residence time distribution function E(θ), the trends of the conductivity was first measured versus time. The experimental real-time conductivities versus measuring time in the MSB without biofilm at 4 different flow rates are plotted in Figure III-7.

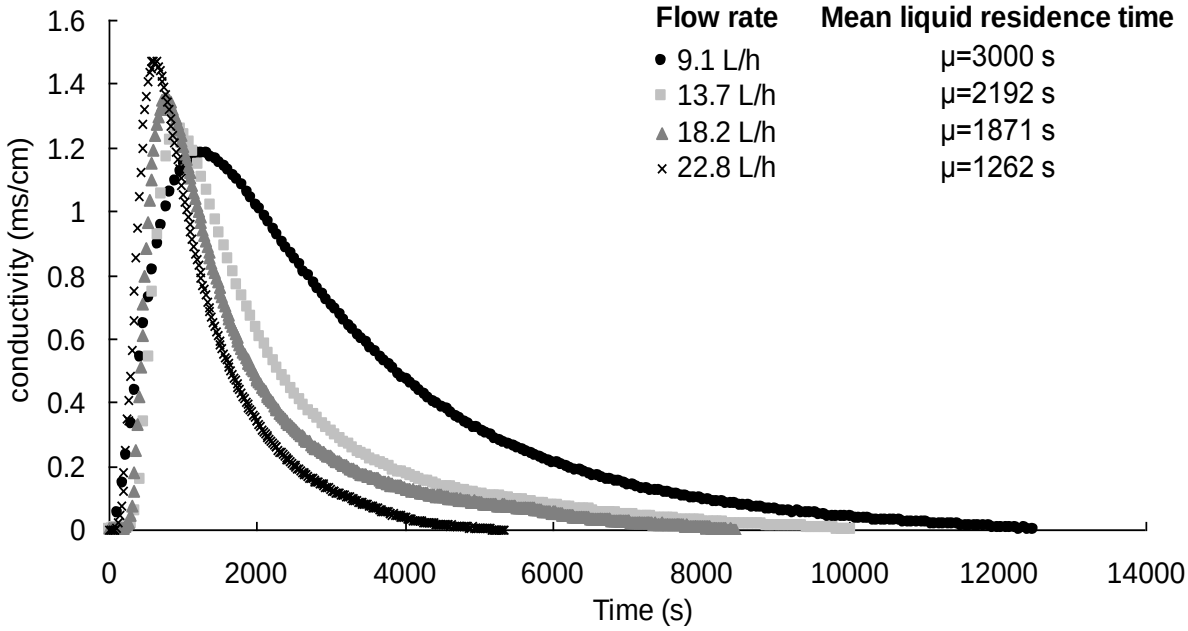

Figure III- 7: Conductivity versus time at different flow rates in MSB.

From Figure III-7, increasing the flow rate leads to taller and thinner curves and thus less spread in the liquid residence time distribution, with higher peaks implying less tracer adsorption by solid. However, the asymmetric behavior, in particular the "tail" in the curves may be due to stagnant zones.

If the mean liquid residence time $\boldsymbol{\mu}$ is considered to be the theoretical liquid residence time $\boldsymbol{\tau_H}$; the effective liquid volumes $V_{effective}$ can be calculated as the $\boldsymbol{\mu}$ multiplied by the flowrate, Q. The liquid holdup represented in the RTD curve should generally correspond to the dynamic holdup (Sharvelle et al., 2008), V_{Ld}. However, Viva and Brunazzi, (2007) reported that the liquid holdup in the RTD curves of catalytic structured packing agrees with the total liquid holdup V_{Lt}, including the dynamic holdup V_{Ld} and the static holdup V_{Ls} determined by drainage. Therefore, it was decided that the estimated $V_{effective}$ can be compared with the experimental dynamic holdup volume V_{Ld} and the total holdup volume V_{Lt} estimated from the drainage method, in order to determine which volume represents the liquid holdup volume in the RTD curves.

Figure III-8 compares the dynamic holdup and calculated effective liquid volume involved in the RTD curve.

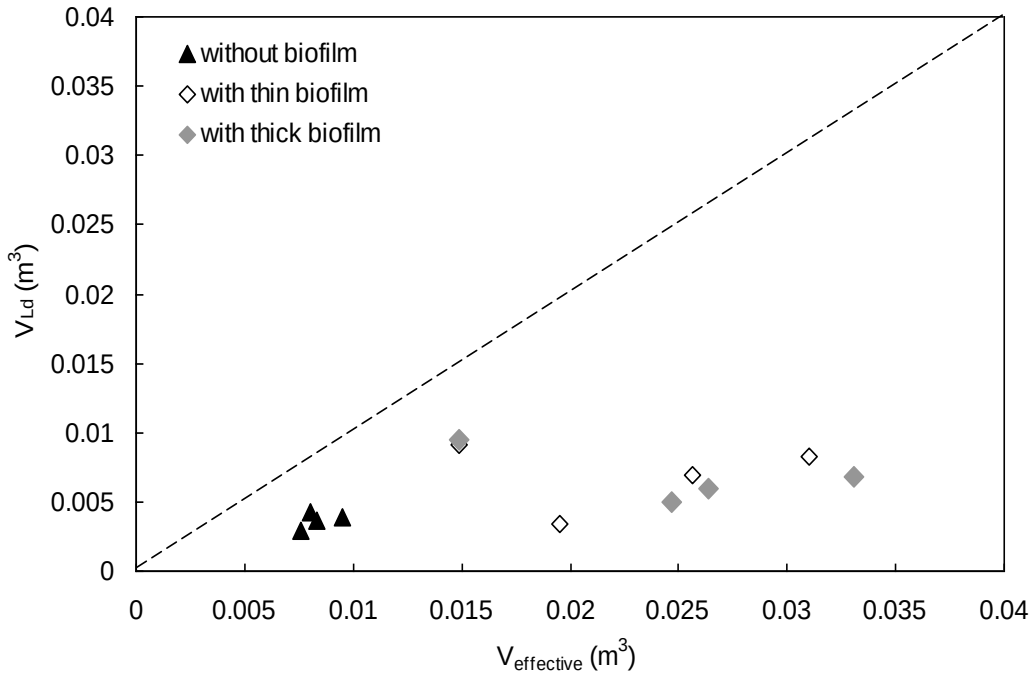

Figure III- 8: Volume of liquid represented in RTD determination

In Figure III-8, it appears that without and with biofilm, the dynamic volume is always less than the effective liquid volume obtained from the RTD curves. With biofilm in particular, the liquid dynamic holdup volume are much lower than the liquid volumes determined from the RTD curves.

The calculated liquid volume involved in the RTD curve, V_{liquid}, the measured dynamic volume, and the $V_{effetive}$/ V_{Ld} ratio are given in Table III-5.

Table III- 5: Effective liquid volume $V_{effective}$ calculated based on mean liquid residence time μ and flowrate Q, compared to the dynamic liquid volume V_{Ld} by drainage

Types	Q (m^3/h)	μ (s)	$V_{effective}$ (m^3)	V_{Ld} (m^3)	$V_{effective}$/ V_{Ld} -
TFC without biofilm	1.1500	46	0.0146	0.00697	2.1
MSB without biofilm	0.0091	2998	0.0076	0.00290	2.6
	0.0137	2192	0.0083	0.00370	2.3
	0.0182	1871	0.0095	0.00390	2.4
	0.0228	1262	0.0080	0.00430	2.9
MSB with thin biofilm	0.0091	7699	0.0195	0.00343	5.7
	0.0137	6728	0.0256	0.00693	3.7
	0.0182	6128	0.0310	0.00829	3.7
	0.0228	2258	0.0149	0.00909	1.6
MSB with thick biofilm	0.0091	9760	0.0247	0.00501	4.9
	0.0137	6940	0.0264	0.00595	4.4
	0.0182	6550	0.0331	0.00684	4.8
	0.0228	2350	0.0149	0.00943	1.6

From Table III-5, for the cases without and with biofilm, the estimated effective liquid volume involve in the RTD curve $V_{effective}$ are all greater than the dynamic volume V_{Ld} measured by the drainage. This implies that besides the dynamic volume, the static volume is also involved in the RTD curve, leading to more effective tracing volume than only the dynamic volume.

Furthermore, with biofilm presence, increasing the flowrate, Q, caused $V_{effective}/ V_{Ld}$ to decrease (e.g. from 5.7 to 1.6 for the thin biofilm case). This decrease implies that increasing the hydraulic loads reduces the diffusion of tracer between the static liquid phase and the dynamic liquid phase. These changes may result from the reduction of contact time between the liquid and solid phase when increasing the flowrate. Since when the flow rate is higher, dynamic liquid leaves the column more quickly; liquid residence time is shorter, resulting in smaller mass exchange through diffusion between the liquid and biofilm.

However, these ratios were higher for the thicker biofilm than for the thinner one. For example, it increased from 3.7 to 4.8 at the flowrate of 0.0182 m^3/h; this indicates that diffusion of tracer increased during biofilm development for the same hydraulic condition, possibly resulting from more static volume involved in the RTD curves. This implies that with a thicker biofilm, the biofilm acts like a "sponge" which retarded the release of liquid and caused better tracer diffusion.

2.6.2 Dimensionless residence time distribution function E(θ)

The curves of dimensionless E(θ) as a function of the dimensionless time θ at different hydraulic loads for both bioreactors without and with biofilm are plotted in Figures III-9(a) and (b). The dimensionless time θ was calculated as the ratio of the time $\boldsymbol{t}$ on mean residence time $\boldsymbol{\mu}$ from Table III-5. The effective liquid holdup volume $V_{effective}$ was used to calculate C_0.

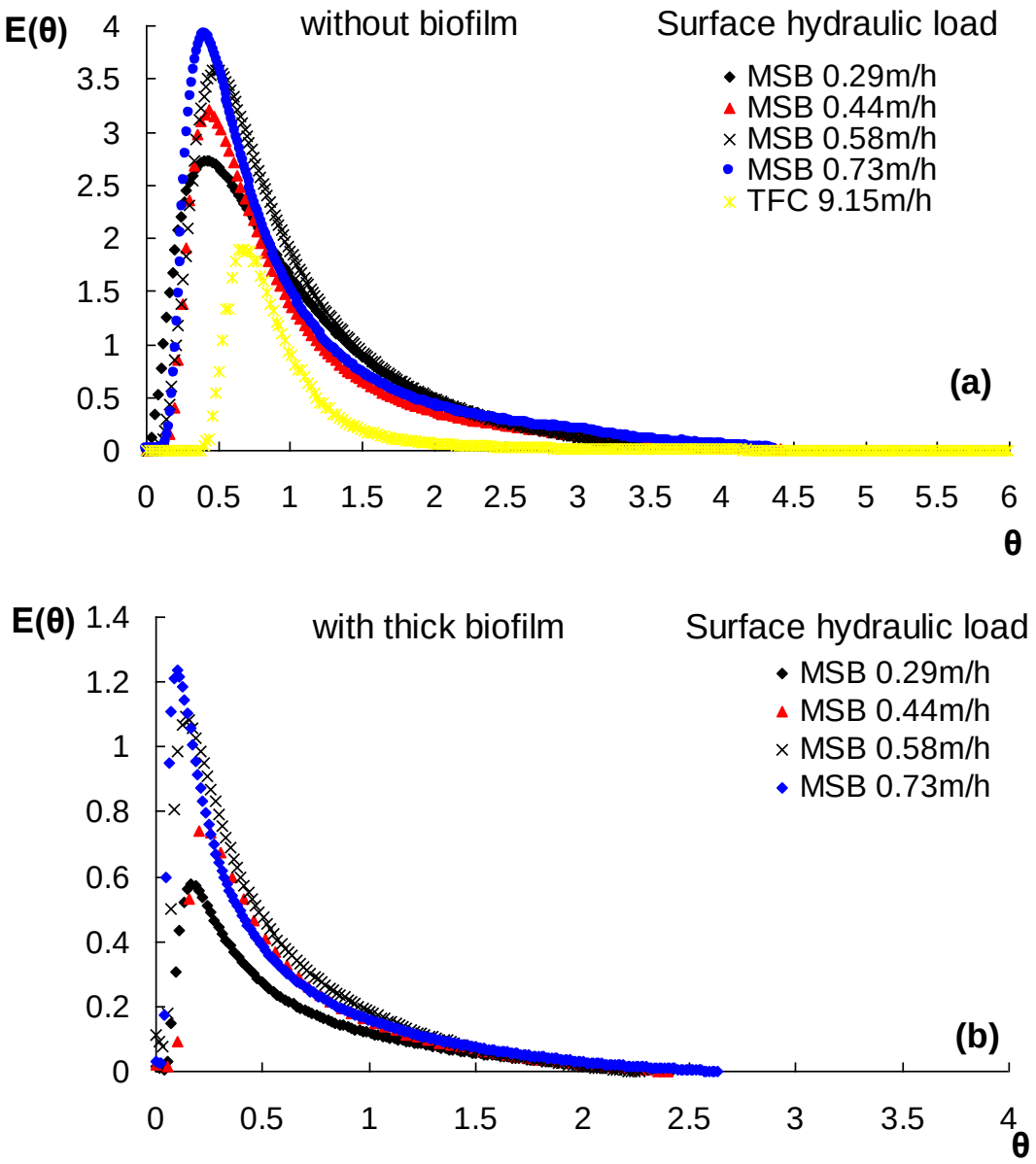

Figure III- 9: Dimensionless RTD curves with thick biofilm and without biofilm at different surface hydraulic load in two reactors

Comparison of the RTD curve at greater flowrate in the TFC with those reported on Figure III-9 (a) and obtained without biofilm at lower flowrates in the MSB, show different behavior. We assumed that this difference was almost solely due to the liquid flow rate. In fact, in the TFC a large flow rate involves a short liquid residence time that cannot strengthen the diffusion phenomena to provide a long tail. On the contrary, when very small flow rate was imposed in MSB, a long liquid residence time can enhance the diffusion phenomena in porous media, decreasing the peak curve and delaying the salt release (long tail). According to Figure III-9 (b) for the MSB reactor with biofilm, we observe a similar effect of flow rate. When the

flow rate increased, the peak decreased and the tail decreased. Whatever the biofilm capacity to retain a certain liquid volume, a large decrease of residence time involves a reduction of diffusion phenomena leading to less deviation from plug flow.

The regimes with and without biofilm can also be compared at each volumetric flow rate (from Figure III-9). A comparison of the case without biofilm to the case with thick biofilm is plotted in Figure III-10 for a small flow rate of 0.0091 m³/h.

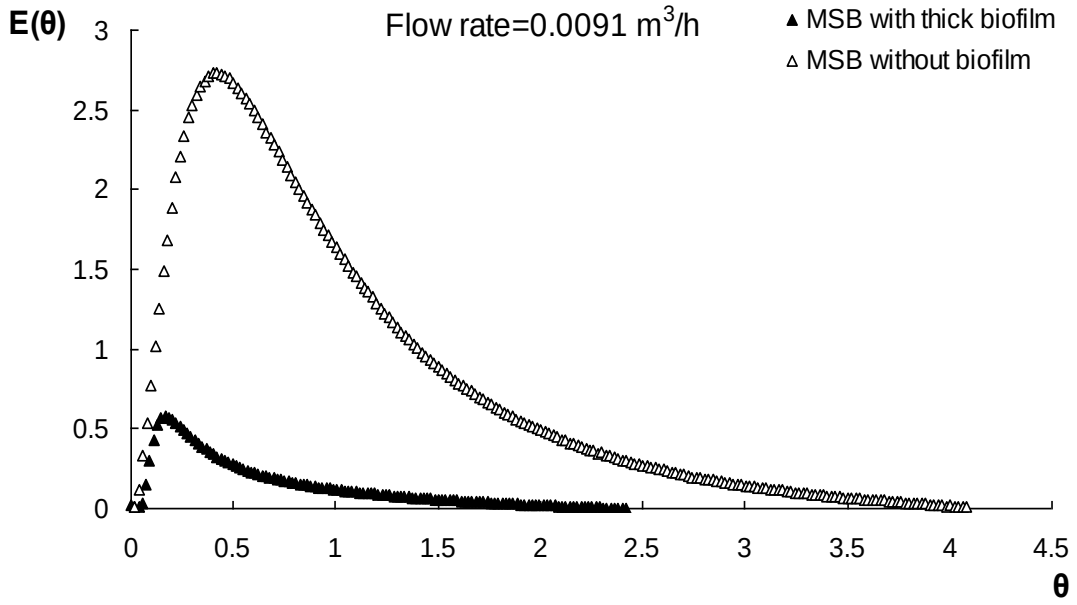

Figure III- 10: RTD curve with/without biofilm at flow rate of 0.0091 m^3/h in MSB

Based on Eq. II-14 in Chapter 2, when the liquid residence time τ_H increases, θ correspondingly decreases. From Figure III-10, it is clear that the presence of biofilm lengthened the liquid residence time in the filter ($\theta \rightarrow 2.5$) compared to times without biofilm ($\theta \rightarrow 4.0$). This could imply two time scales: one related to the dynamic flow, and the other related to the diffusive process that was promoted by the presence of biofilm which decreased the packed bed porosity and increased the contact time between liquid and biofilm. In addition, the lower peak when biofilm was present implies more tracer dispersion and diffusion into the biofilm compared to when biofilm was absent. Based on Eq. II-13 in Chapter 2, this lower peak implies more effective liquid volume was involved in the RTD curves. Similar behavior was observed at other flow rates. In a bioreactor with biomass, the tracer can be transported within the biofilm by diffusion. The biofilm slowly exchanges tracer with the flow-through zones; this can significantly increase the tailing and lead to a sustained release process, as was also observed and investigated by Riemer et al., (1980) who proposed a "biodiffusion model" to fit the liquid residence time distribution in their study.

2.6.3 Discussion - conclusion

Based on the RTD experiments, both in the cases without and with biofilm, the liquid volume involved in the RTD curves represented both the dynamic volume and partial static volume. When the biofilm developed, i.e. as the biofilm thickness increased, the fraction of static volume involved in the RTD curves was greater than for the cases of thinner biofilm. It indicates the biofilm acts like a "sponge" that sustained and released partial static holdup liquid. The presence of biofilm can effectively improve the mass diffusion between the bulk liquid and flow-through zones. In the cases of the packed bed without biofilm, liquid residence time (LRT) was shorter than in the cases with biofilm. This implies that the presence of biofilm lengthened the liquid residence time, enhanced the mass diffusion from the dynamic volume to the biofilm, improving consequently performance in pollutants treatment.

2.7 RTD models

Calculated RTD curves based on n CSTRs in series, n CSTRs in series with dead zones and axially dispersed plug flow were plotted for all cases at different hydraulic conditions. Simulated curves are compared to the experimental results in Figures III- 11 (a) and (b) as two examples without biofilm and with a thick biofilm, respectively. Other comparisons between models and experiments for different flow rates, with and without biofilm, are provided in Appendix 6.

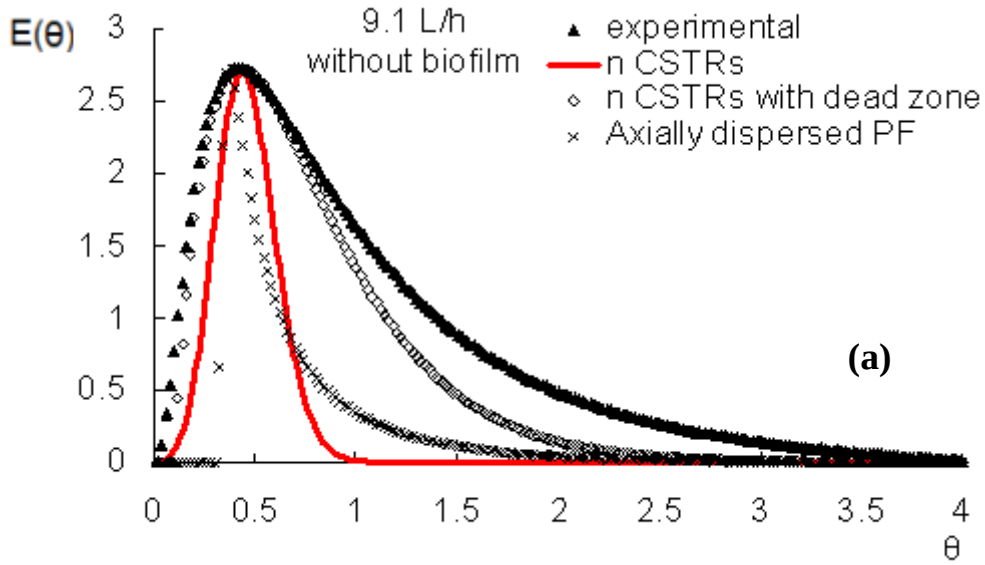

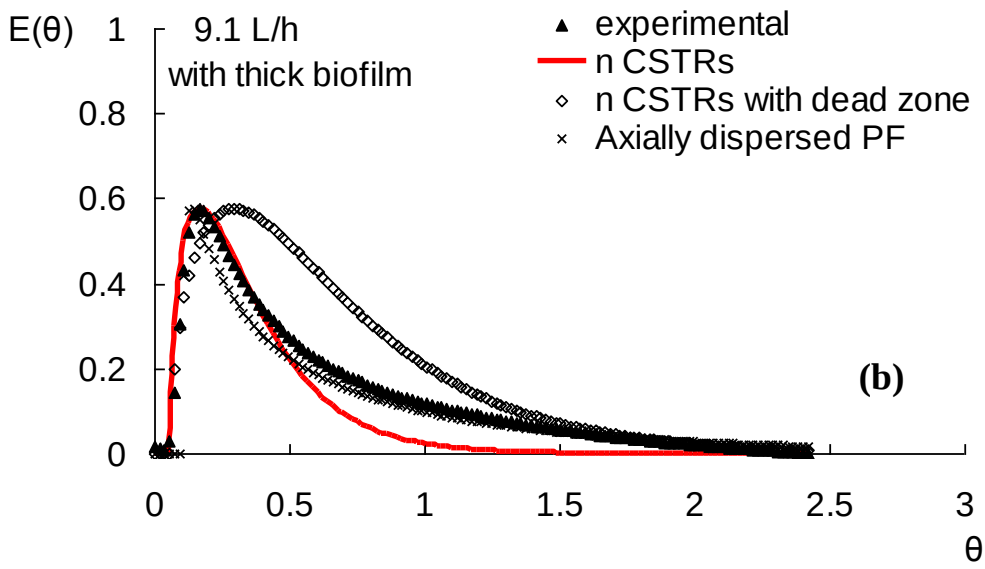

Figure III- 11: Calculated RTD curves based on three models and experimental RTD for the cases without and with biofilm at a flow rate of 9.1 L/h

From Figure III-11, when without biofilm, at a lower flow rate conditions, n CSTRs with dead zone fits well the experimental RTD curve. The axially dispersed plug flow model fits well with the experimental RTD curve when biofilm was present at the same hydraulic condition. The other two models, the CSTRs and CSTRs with dead zone do not fit with the experimental RTD curves very well, mainly the tail differ. The Root Mean Square (RMS, denote as σ^2) calculated for each model and reported in Table III-6 confirm that the axially dispersed plug flow model is best able to describe the TF hydrodynamic behavior when biofilm is present. Square deviation σ^2 and modeling parameters such as active fraction ***m***, number of CSTRs ***n,*** Peclet number ***Pe*** are also reported in Table III-6 for a general comparison among the 3 models tested.

Table III- 6: General results comparison of 3 different models

Cases	Q	n CSTRs with dead zone			N CSTRs in series		Axially dispersed Plug Flow		
	(m^3/h)	***m***	***n***	σ^2	***n***	σ^2	***Pe***	***n***	σ^2
TFC without biofilm	1.15	0.88	6	0.39	5.2	0.16	8	5	0.14
MSB without biofilm	0.0091	0.44	8	0.75	3.5	0.47	6	4	0.54
	0.0137	0.47	13	0.52	6.1	0.46	10	6	0.44
	0.0182	0.52	17	0.50	7.3	0.52	12	7	0.4
	0.0228	0.43	21	0.54	11.0	0.35	20	11	0.21
MSB with thick biofilm	0.0091	0.72	2	0.85	1.2	0.59	2	2	0.69
	0.0137	0.65	3	0.63	2.1	0.49	4	3	0.66
	0.0182	0.60	11	0.61	6.3	0.47	10	6	0.63
	0.0228	0.65	12	0.52	8.0	0.45	14	8	0.52

From Table III-6, the number of CSTRs in series increase when increase the flow rate. For TFC, the σ^2 estimated from three models (0.39, 0.16, 0.14) are close to 0, implying a plug flow in TFC at a higher flow rate. The σ^2 values estimated for MSB without and with biofilm decrease, when the flow rate increases. With thick biofilm at lower flow rates, σ^2 estimated approaches 1, implying better tracer dispersion and diffusion between liquid and biofilm. The fraction of the active zone increased (m=0.60 to m=0.72) when the biofilm was present comparing to without biofilm (m=0.43 to m=0.52). In addition, the number of CSTR decrease (n=2 to n=12) compared to the cases without biofilm (n=8 to n=21). This increase of active liquid fraction ***m*** corresponds well to the trend of the increased $V_{effective}/ V_{Ld}$ ratio, where the exchange between the dynamic and static phases increased. This indicates that the presence of biofilm resulted in enhanced mass dispersion and diffusion in the filter.

Also from Table III-6, the values of ***Pe*** increased when the flow rate increased and much greater than 10 for higher flow rates (both for the MSB without and with biofilm). This indicates that the liquid distribution was closer to plug flow when the flow rate increased. With thick biofilm at lower flow rate, calculated ***Pe*** of 2 suggests better mass diffusion. Actually, the presence of biofilm decreased ***Pe*** compared to the cases without biofilm at the same hydraulic condition. This decrease of ***Pe*** indicates the greater axial dispersion of tracer.

2.8 Liquid Residence Time (LRT)

Based on the experimental RTD data and RTD models, means Liquid Residence Time in the filter from the models and experiments differ. The Liquid Residence Time (LRT) reflects the possible time in which the liquid is exposed to the biofilm surface, but also the ability of the bioreactor to equalize or dilute shock loads due to the hydraulic flow and substrate flow. Indeed, when investigating the LRT with biofilm presence, may introduce errors, because the biofilm could attach and detach over time depending on the hydraulic conditions. The estimation of LRT may vary with the changes of biofilm properties. To minimize the inconvenience, we assumed that the distribution of biofilm along the packed bed was homogeneous and independent of time. Under this assumption, the calculated LRT for different interval distance of the pilot set-up and with biofilm of different thicknesses are plotted in Figure III-12 against the flowrate and corresponding surface hydraulic loads.

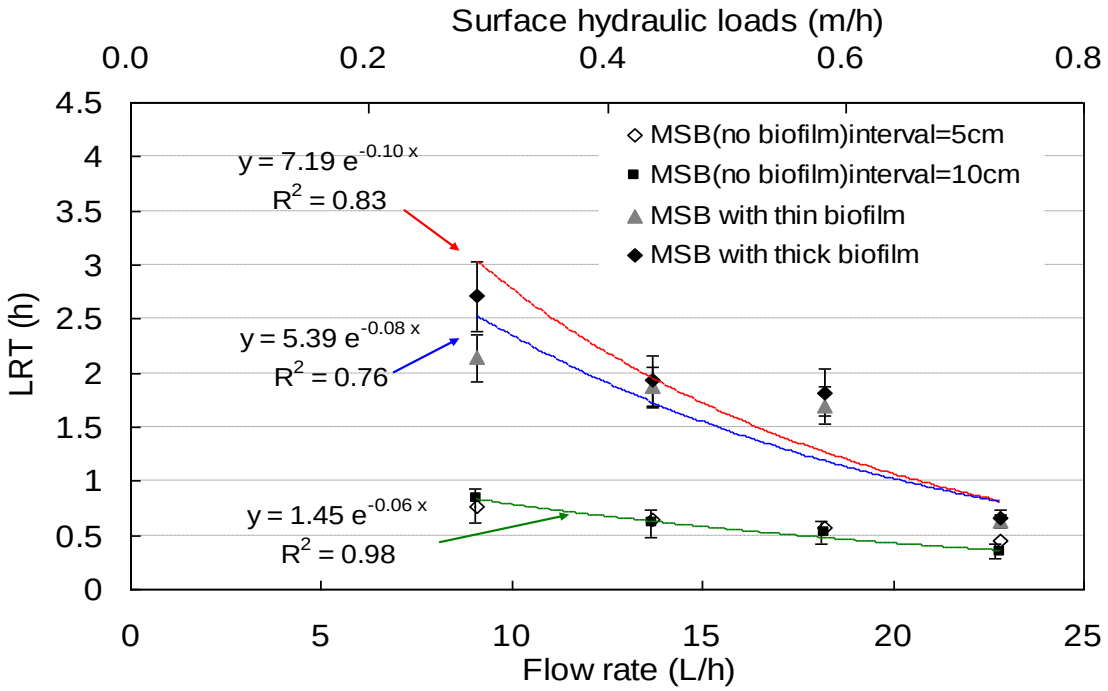

Figure III- 12: Calculated LRT based on RTD under different flow rates

From Figure III-12, whatever the operating conditions, we can observe that the flow rate decreases the LRT. When a biofilm is present we observed an increase of LRT related to an increase of the liquid volume embedded into the biofilm; we also observed that a thicker biofilm increase the LRT. With thick biofilm at lower hydraulic loads (0.37m/h), liquid residence time can rise by 200% compared to the regimes without biofilm and by 100% compared to thinner biofilm. About the interval influence without biofilm no strong effect is displayed, and the exponential behavior is observed with flow rate. Consequently in MSB reactor, increase the space interval will not significantly affect the liquid residence time, when the interval is limited less than 10 cm, leading to a better air circulation and renew.

2.9 Liquid film and mass transfer under biofilm conditions

In MSB, due to the open structure, mass transfer measurements were very difficult to perform with conventional methods applied in TFC. In fact, fresh air is everywhere in contact with the liquid, implying a constant oxygen concentration in the liquid and gas phase. From hydrodynamics experiments we calculated the liquid film thickness and estimated the volumetric mass transfer coefficient from a Higbie modeling approach.

2.9.1 Oxygen transfer in TF

Based on Eq.II-29 in Chapter 2, $r = k_L a(C^* - C)$, oxygen transfer in the TF system is proportional to the driving force of oxygen (C*-C), which results from the difference between the saturation concentration and local oxygen concentration. The driving force of oxygen (C*-C) in the MSB was considered to be uniform from the bottom to the top (i.e. $C_{in}=C_{out}$). Due to the open structure of MSB that everywhere puts in contact the liquid with fresh air, the local oxygen concentrations at different axial locations were almost the same. On the contrary, for the TFC, no extra oxygen from the exterior of column is supplied due to the close structure of the TFC. From the bottom to the top of the column, oxygen concentration gradually decreases in the liquid phase (i.e. $C_{in}>C_{out}$) after consumption by biodegradation and nitrification. But at the same time the oxygen concentration in the gas phase decreases due to the oxygen transfer without any fresh air in contact. Consequently the driving force of oxygen (C*-C) from the bottom to the top of column differed for the MSB and TFC and was generally greater for the MSB where liquid was always in contact with fresh air.

2.9.2 Liquid film thickness

The liquid film thicknesses for different cases were calculated from the dynamic holdup volume V_{Ld} over the surface area a_v. Dynamic holdup volume V_{Ld} measured by drainage method was substituted into Eq. II-24 (see Chapter 2). Additionally, during the hydrodynamic experiments, it was observed that even at the top of the column, liquid was not well distributed; particles that were not wetted at the beginning were finally wetted due to the diffusion among adjacent particles after a long enough time. It was hence assumed that the wetting factor f_w in Eq. II-12 (refer to Chapter 2) equals 1. Applying the equivalent particle diameter d_p of 0.0217 m, the total surface area of media was calculated by total number of particles $N_{particles}$ multiply the surface area of each particle when no biofilm was present (L_f=0). When biofilm was present, the biofilm thickness L_f was considered into Eq.II-31, to estimate the liquid film thickness. Under these assumptions, the liquid film thicknesses under different surface hydraulic loads of regimes without/with biofilm in both bioreactors are plotted in Figure III-13.

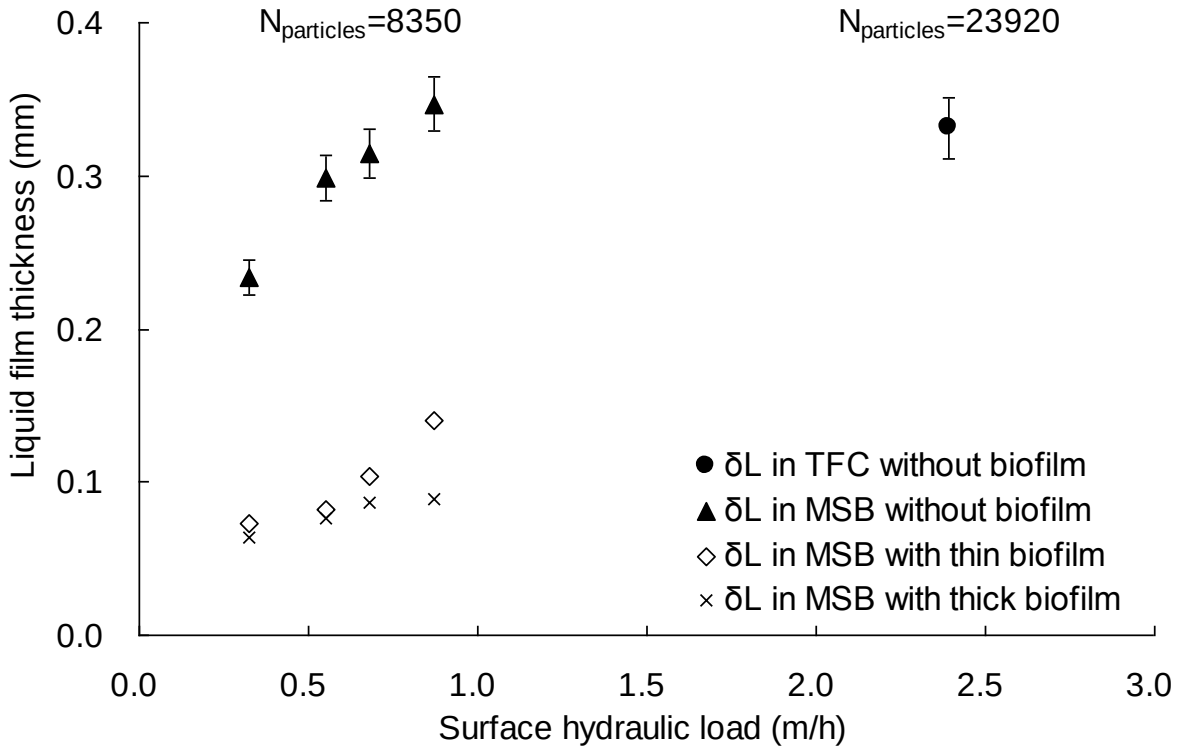

Figure III- 13: Liquid film thickness versus hydraulic loads of regimes with/without biofilm

As shown in Figure III-13, the liquid film thickness in the TFC without biofilm at a hydraulic load of 2.39 m/h was 0.33 mm. At lower hydraulic loads (0.29-0.73 m/h) in the MSB, the calculated liquid film thicknesses (0.23-0.35 mm when biofilm was absent; 0.07-0.14 mm for biofilm 1 regimes; 0.06-0.09 mm for biofilm 2 regimes) were less than those obtained in the TFC.

It was found that without biofilm, the thickness of the liquid layer was significantly greater than with biofilm, which may be due to the greater volume of dynamic holdup. However, in the same bioreactor, but at a lower flow rate, the smaller dynamic holdup volume resulted in a reduction of liquid film thickness.

The presence of biofilm led to a thinner liquid film compared to that obtained without biofilm, a result attributable to the increase of surface area with biofilm development and the decrease of dynamic drainage volume. Such behavior will promote the oxygen transfer rate by decreasing the limited liquid layer and lengthening the contact time between the liquid and biofilm. However, these behaviors hold true under our assumption that the packed-bed was fully wetted.

2.9.3 Volumetric mass transfer coefficient estimation

Based on our assumption of the oxygen penetration model (Higbie, 1935) and the estimation of contact time between liquid and air (see Chapter 2, Eq. II-32), the volumetric oxygen transfer coefficients without biomass and with biomass are calculated from equation II-31 and are plotted against the flowrates in Figure III-14.

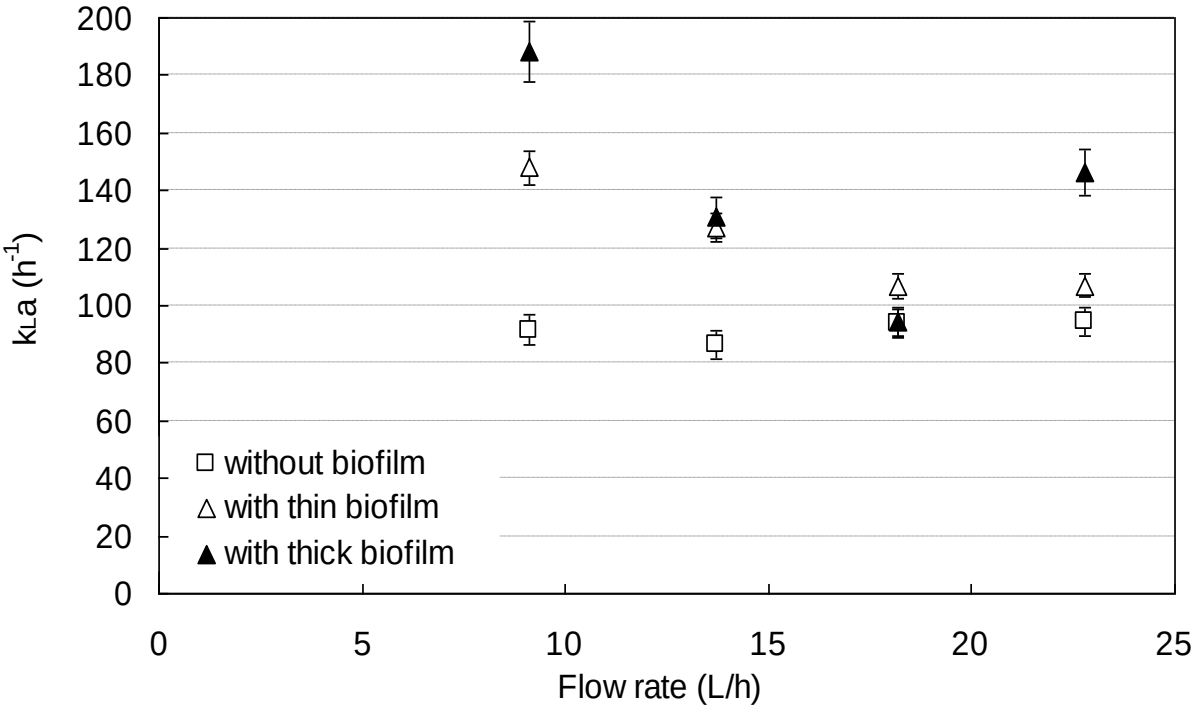

Figure III- 14: Volumetric oxygen transfer coefficient under different flowrates in cases without and with biofilm

From Figure III-14, the estimated values of k_La with biofilm were generally higher than without biofilm. The k_La slight increase from 86 to 94 h^{-1} without biofilm, as the flowrate increased from 9.1 to 22.8 L/h. Compare to the case without biofilm, k_La was significantly greater with biofilm presence (higher about 130% with thin biofilm; and by 250% with thick biofilm) at a flowrate of 9.1 L/h. Increasing the inlet flowrate from 9.1 L/h to 18.2 L/h, k_La first decreased from 148 to 106 h^{-1} with thin biofilm. This trend could result from less contact time (t_c). Then the oxygen transfer slightly increased to 107 h^{-1} at high flow, resulting from the significant decrease of contact time, but an increment in liquid film thickness. With thick biofilm, the k_La significantly decreased from 188 to 94 h^{-1}, at the inlet flowrates from 9.1 L/h to 18.2 L/h; then it increased significantly up to 146 h^{-1} at the flow rate of 22.8 L/h. The observed drop in the k_La not only results from the liquid film thickness, but also from the contact time, assuming a constant driving force of oxygen.

Many authors have reported the k_La from different types of Trickling Filter with or without biomass. Some values are shown in Table III-7 compared with our calculated k_La results.

Table III- 7: k_La from literatures and estimated in this study

Ref.	HLR m/h	Reactor	Medium	Air flowrate kgO_2/m^3h	$\mathbf{k_La}$ h^{-1}
(Mezaoui, 1979)	2.76-6.92	TFC	Flocor, no biofilm	0.26-0.47	32-58
			Biopac, with biomass	0.44-1.15	54-120
(Sant'Anna,1980)	3.51-13.26	TFC	Flocor, no biofilm	-	-
(Nyadziehe,1980)	4.44-13.33	TFC	Flocor, no biofilm	-	83-180
(Grasmick et al., 1981)	20-35	Fluidized reactor	Biolite, no biofilm	-	17-55
(Amar et al., 1986)	2-3.6	UFBR	Biolite, no biofilm	0.12-0.36	-
(Mounir, 1991)	2-2.5	TFC	PLASdek, no biofilm	0.12-0.3	14-35
			with biofilm	0.45-0.47	54-47
Our study	0.29-0.73	MSB	Concrete brick, no biofilm	-	91-94
			With thin biofilm	-	105-172
			With thick biofilm	-	93-163

From Table III-7, our estimated k_La values are greater than the results of others, even though no forced-aeration was applied in our experiments. This implies that some deviations may occur due to the heterogeneous distribution of actual biofilm in the biological experiments or due to our special porous media that forms very thin liquid layer under our flow rate conditions. These differences of estimated k_La may result from the estimation of biofilm thickness, the total surface area of packed bed with biofilm and the estimation of contact time.

3. Conclusion of this chapter

Different hydraulic experiments were carried out, essentially on a new type of Trickling Filter made up of a Multi-Section Bioreactor, packed with concrete block medium particles. The purpose of this study was to investigate the hydrodynamic characteristics particularly in the light of the influence of biofilm on hydrodynamic behavior.

The static experiments with biofilm indicate that most of the liquid is retained by medium particles coated with biofilm, increasing static retention and, consequently, reducing dynamic retention. It was also found that the liquid static holdup makes a greater contribution than the dynamic holdup to total liquid holdup, on account of the high adsorption potential of the concrete block medium, resulting from its porous structure. Moreover, the static holdup does not correlate with the configuration of TF, but dependent on the type of medium.

The effective liquid volumes represent in the Residence Time Distribution (RTD) curves are not only the dynamic holdup, but also partial static holdup volume, resulting from the sustained release of partial static holdup in the biofilm. Increasing the flow rates, the effective liquid volume involved in RTD first increases. However, when the flow rate was too low or too high, the effective volume decreases, resulting from low flow and short liquid residence time, respectively. RTD experiments also show that at lower flow rates, the mass dispersion and diffusion between the liquid and biofilm was better than that at higher flow rates. Increasing the hydraulic load resulted in the flow approaching plug flow in the bioreactor, resulting in less mass dispersion and diffusion. The Liquid Residence Time (LRT) estimated from RTD models shows that the presence of biofilm will lead to a longer LRT in the filter, and thus promote the dispersion of mass in the bioreactor. Comparing the drainage and RTD methods allows us to show that dispersion and diffusion can occur in the biofilm, increasing the contact time between liquid and biofilm. Too low (less than 9 L/h) or too high (greater than 23 L/h) flow rates will not make advantages to the bioreactor performance, resulting from low effective liquid volume and short liquid residence time.

The presence of biofilm was also found to decrease the thickness of the liquid film compared to the cases without biofilm under the same hydraulic conditions, on account of the greater surface area and smaller dynamic holdup volume.

The estimation of oxygen transfer coefficient, based on the estimated liquid film thickness, shows that at lower flowrate, oxygen transfer is better than at higher flowrate. When biofilm was present, oxygen transfer was promoted compared to without biofilm, resulting from thinner liquid film. Increase the biofilm thickness under same hydraulic conditions, lead to better oxygen transfer.

Furthermore, the physical properties of MSB and medium, liquid film thickness, liquid residence time, and also the estimated oxygen transfer coefficient obtained in this chapter will be applied to Biowin simulator of Chapter 5.

Chapter 4

Biological experiments

1. Introduction

Objective of biological experiments:

The aim of biological experiments was to investigate only in the Multi-Section Bioreactor (MSB), the performances of both Chemical Oxygen Demand (COD) removal and nitrification, and also to investigate the competition between nitrification and heterotrophic growth. The first goal of our experiments was to provide data to help understand the various processes occurring in the biofilter, i.e. biological transformations, attachment, detachment, oxygen transfer, liquid repartition… The second goal was to provide information for a better design and operation of this type of Trickling Filter (TF).

Two main aspects are thus analyzed in this chapter:

1. The competition between nitrification and heterotrophic elimination of COD is considered at two Organic Loading Rates (OLR) for different locations in the MSB (period 2 and 3). The increase of OLR was thus used to increase the competition factors such as oxygen demand, biofilm thickness, competition for space, detachment frequency and amplitude.
2. The clogging tendency in the TF was studied. Hence, we significantly increased the OLR, a shift from a real WW containing a large part of COD as particulate COD-CODp (during period 3) to the Viandox substrate (during period 4) that contained only soluble-CODs and colloidal COD, was performed, while the COD concentration was maintained constant in the feed.

In this chapter, we divide the biological experiments' results into 3 parts, including COD removal, nitrogen removal and the combination of biological performance and hydrodynamic elements.

2. Experimental plan

2.1 Description of the pilot and its inoculation

The MSB reactor was used as described in the M&M section of Chapter 2. It was inoculated by 0.08m^3/d of domestic wastewater flowing through the filter during 40 days.

Figure IV-1 represents the time course of COD removal yield (based on soluble outlet CODs), nitrogen removal yield (based on outlet ammonia concentration) and nitrification yield (based on outlet nitrate divided by total TKN concentration), for this inoculation period.

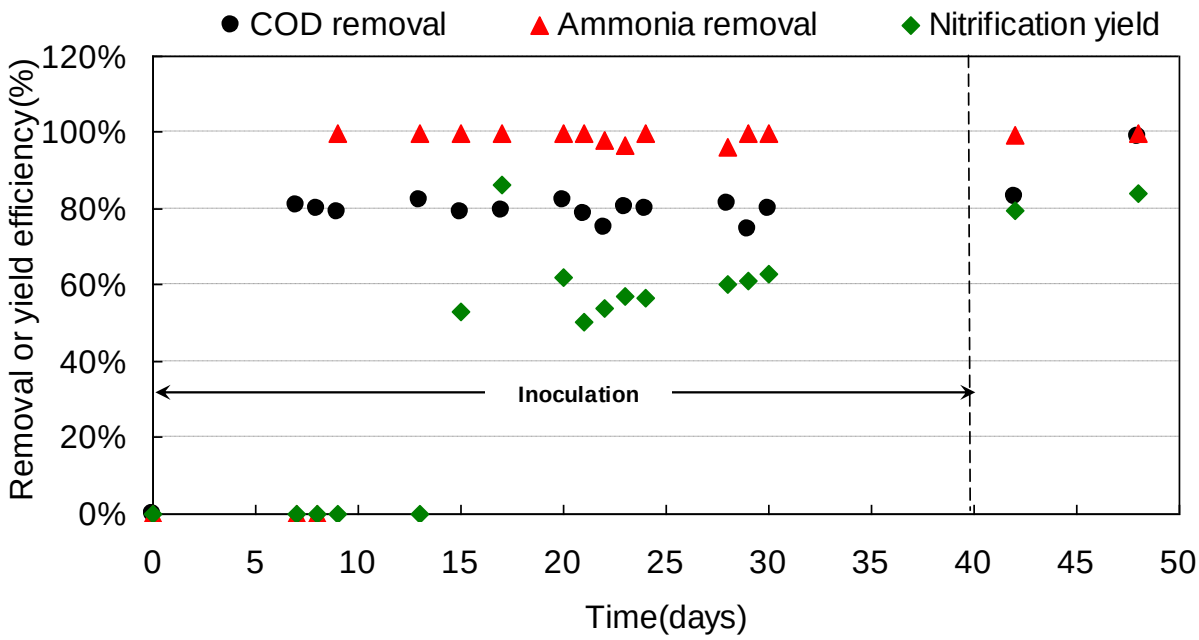

Figure IV- 1: COD removal, nitrogen removal and nitrification yield on time course

From Figure IV-1, it can be assumed that correct inoculation is achieved after 40 days because the removal yields reach roughly stable values. These criteria will be confirmed by the observations of the MSB performances during period 2 where the pilot was run under a similar loading rate.

2.2 Experimental plan

Once inoculated, the lab scale pilot plant was operated in order to assess its performances under various loading rates. Three periods of operations were then carried out under different organic loading rate as shown in Table IV-1.

Table IV- 1: Operating conditions during the three periods 2 - 4.

	Period 2	Period 3	Period 4	Unit
Flow rate	80	80	80	L/d
Surfacial organic loading rate	0.76	2.55	2.55	kgCOD/ m²d
Surfacial hydraulic loading rate	2.55	2.55	2.55	m³/ m²d
Hydraulic Retention Time (HRT)	2	3.5	3.2	h
Inlet CODt	298±71	1026±164	1001±8	mg/L
Inlet CODp	240±12	841±18	0	mg/L
Inlet CODp /CODt	0.82±0.17	0.84±0.11	0	-
Inlet TKNt	46±5	161±14	162±5	mg/L
Inlet Ammonia	30±3	100±11	104±5	mg/L

Note that the increase in loading rate was achieved by increasing the inlet concentration rather than the flow rate. COD concentrations were increased from around 300mg/L during period 2 to 1000 mg/L for periods 3 and 4.

This experimental plan still does not cover the real situation. Two aspects were not covered:
(1) Use of higher flow rates because increasing OLR by increasing the inlet concentration may have a different effect on the MSB performance than increasing the OLR by increasing the flow rate.
(2) Inclusion of the daily variations of the flow to study the capacity of the reactor to adapt to these variations. A lack of time explains why we did not study these operating conditions.
Our reactor is not connected to a settler. As a consequence, both particulate and soluble matter is recovered at the outlet. It was decided to differentiate two types of removal yields, one considering the total matter at the outlet (denoted E_{COD} for CODt removal) and the other considering only the soluble fraction of the compound at the outlet (denoted η_{COD} for CODs removal). Indeed, biological transformation during treatment produces new cells that should be counted as sludge production and not as released COD or nitrogen (thus decreasing the removal yield).
In our analysis of the removal performances of the MSB, the global removal yields were first considered and then, detailed analysis of the removal feature is presented section by section.

3. Results and discussion

3.1 COD removal

3.1.1 Analysis of COD removal efficiencies

As described previously, three periods were run on the pilot in order to test different OLR regimes and WW qualities. The COD removal efficiencies during periods 2, 3 and 4 are summarized in Table IV-2.

Table IV- 2: COD removal efficiency in period 2-4.

	Period 2	Period 3	Period 4	Unit
Inlet CODt	295±81	998±176	1001±9	mg/L
Final outlet CODs	24±21	34±29	53±4	mg/L
Removal efficiency (η_{COD})*	93±6	96±2	94±3	%
Final outlet CODp (sludge)	40±32	30±27	13±7	mg/L
Global Removal efficiency (E_{COD}) **	82±8	88±4	93±4	%

* The mean efficiency is calculated considering only CODs in the effluent
** The efficiency from CODt is calculated also considering CODt at the outlet

For the three periods, and thus whatever the OLR and type of WW, the mean η_{COD} is rather high and the obtained values allow compliance with the standard limits. Surprisingly, for high OLR, the η_{COD} was slightly, but significantly, higher than for low OLR. Similarly, for the same high OLR, η_{COD} was higher when the WW contained particulate COD compared to Viandox, period 4.

3.1.2 Spatial COD degradation

The MSB allows sampling at the outlet of 5 sections of each of 40 cm depth. The sampling operation is described in the M&M section (see Chapter 2). Hence, the study of the COD removal along the filter is easier than for a conventional TF. This allows reaching original behavior description in the bioreactor.

Apparently the first section played a greater role in term of COD removal than the other four sections. Consequently, for a clearer representation, the COD dynamic profiles measured for sections are presented in separate figures. The time-evolution of CODt and CODs concentrations in the first section are shown in Figure IV-2-4 for periods 2, 3 and 4. The reader must be aware that the scale of COD concentration changes from one figure to another because of the increase in the inlet COD concentration for periods 3 and 4.

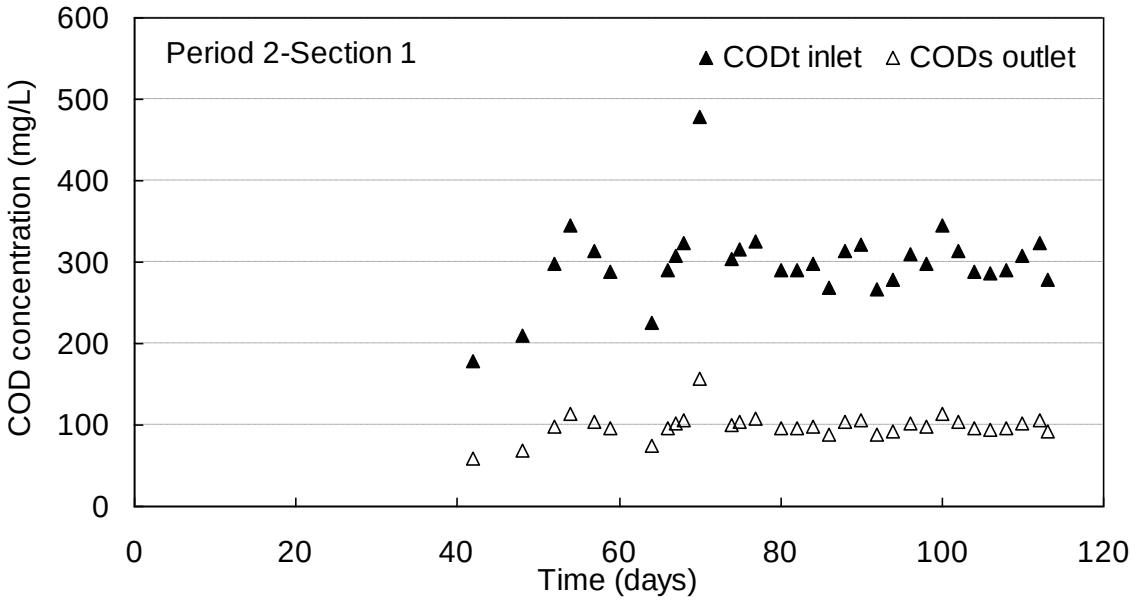

Figure IV- 2: CODt inlet and CODs outlet from the first section. Period 2 Low loading condition, water from diluted real WW

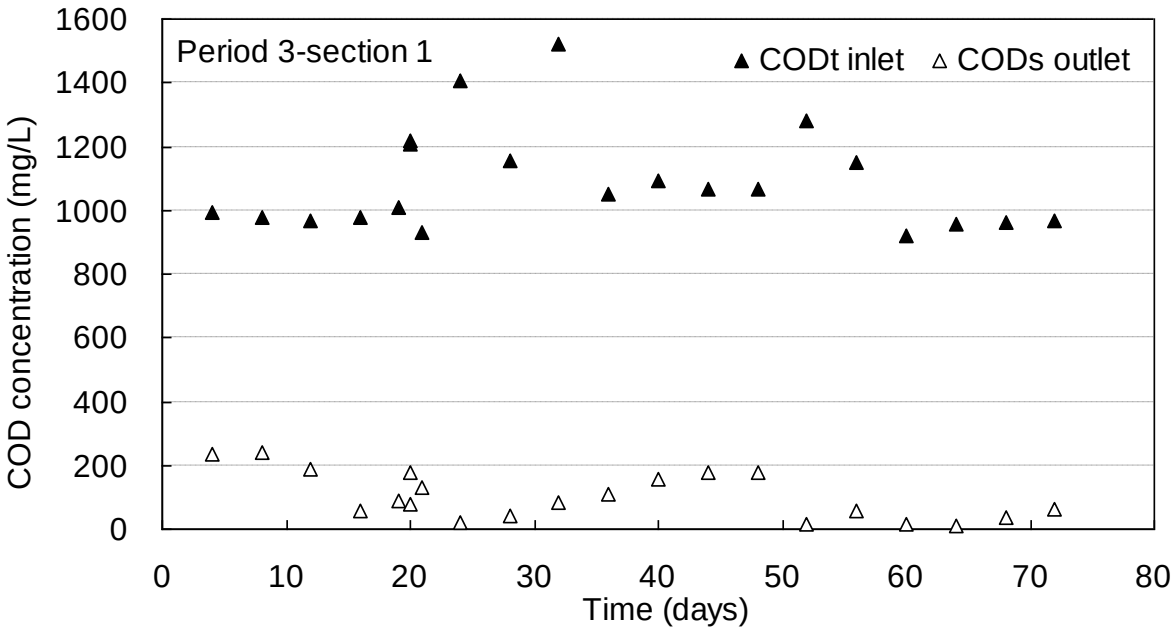

Figure IV- 3: CODt inlet and CODs outlet from the first section. Period 3 high loading condition, water from diluted real WW

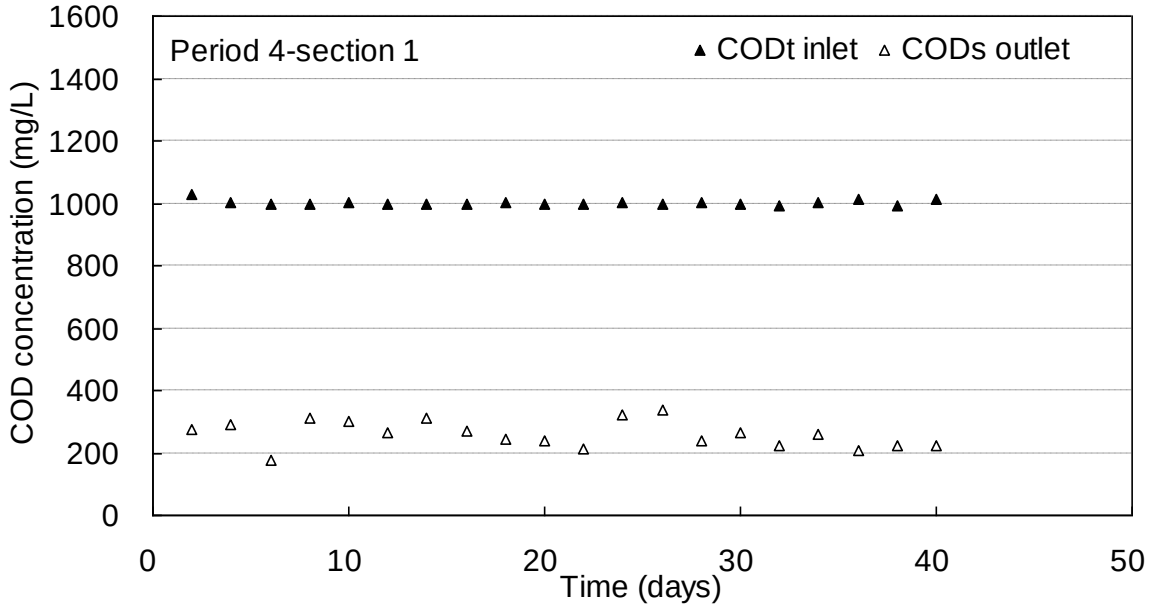

Figure IV- 4: CODt inlet and CODs outlet from the first section. Period 4, high loading condition, Viandox

From Figures IV-2 to 4, it is clear that high COD removal occurred in the first section of the MSB whatever the loading rate. It seems that higher OLR led to a substantial increase in the CODt removal capacity of the first section in particular.

Figure IV-5 to IV-7 show the time-evolution CODs concentration from section 1 to section 4 for low and high loading conditions during the three periods. To make the reading of the figures easier, results for section 5 are not plotted because in all cases the outlet CODs was very close to that from section 4.

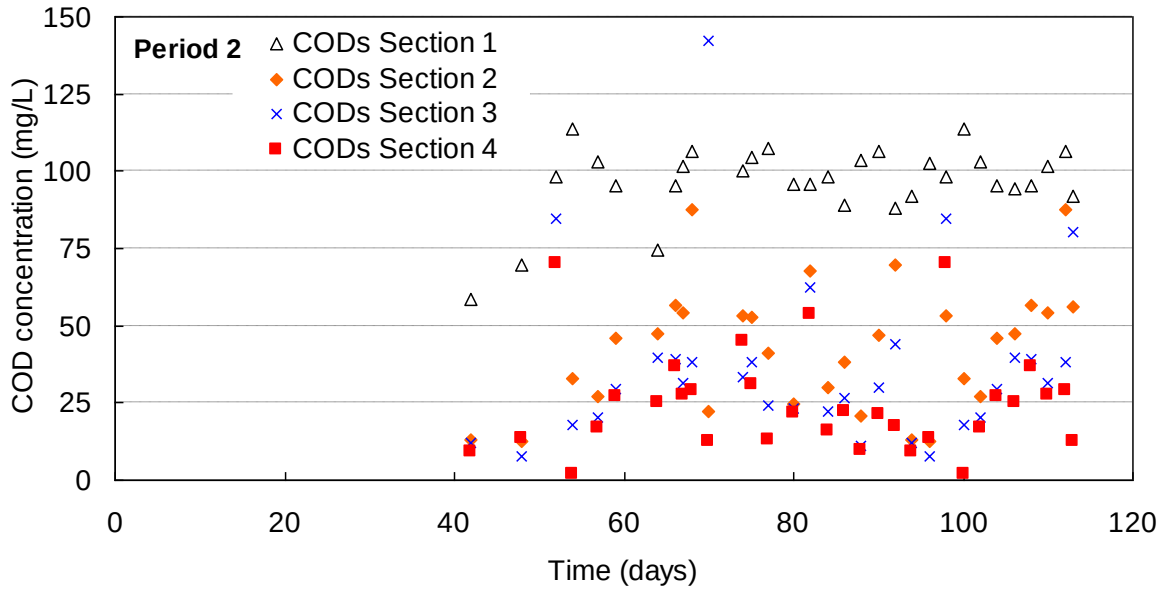

Figure IV- 5: Soluble COD time-evolution concentration variation in section 1 to section 4. Period 2 Low loading condition, water from diluted real WW

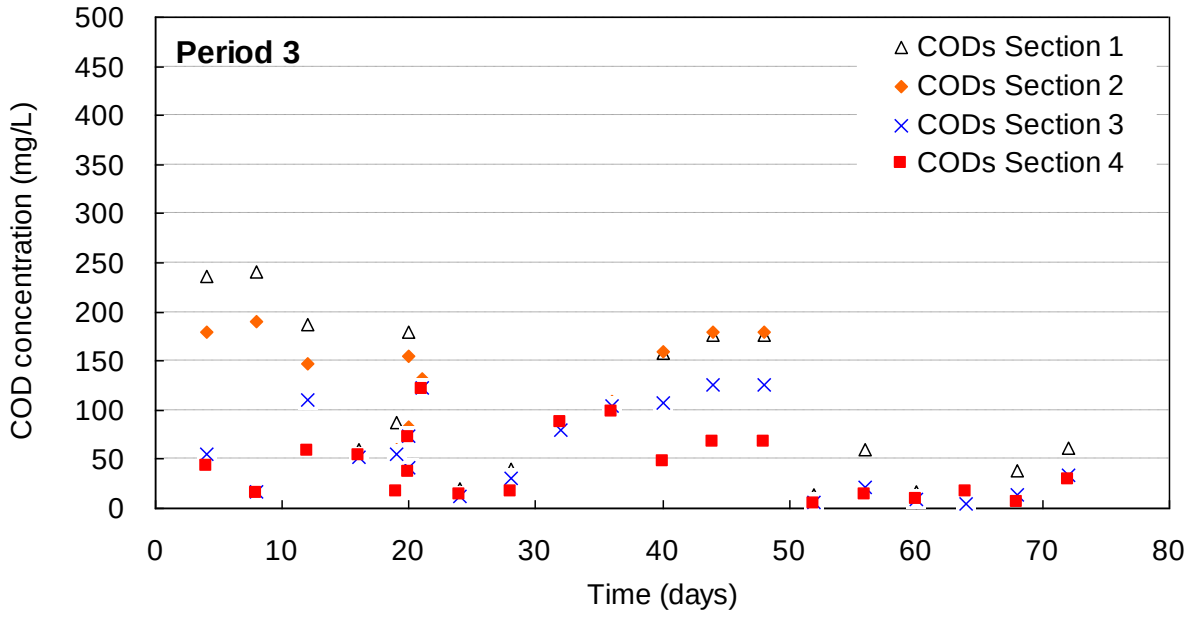

Figure IV- 6: Soluble COD time-evolution concentration variation in section 2 to section 4. Period 3 high loading condition, water from diluted real WW

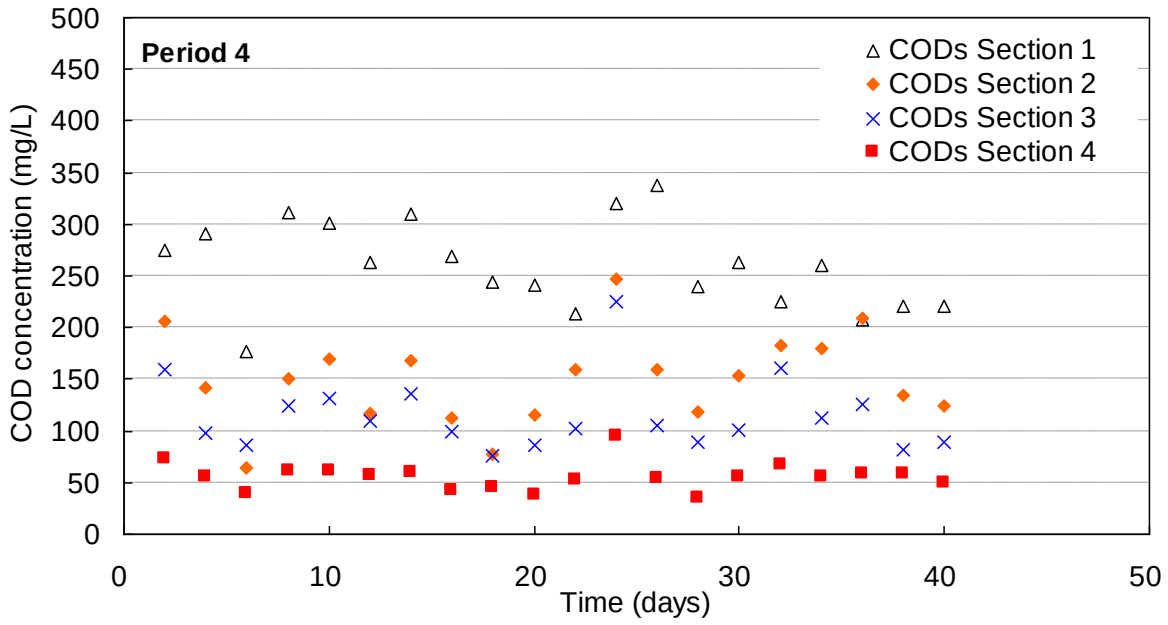

Figure IV- 7: Soluble COD time-evolution concentration variation in section 2 to section 4. Period 4, high loading condition, Viandox

As shown in Figures IV-5 to 7, during the three periods 2 to 4, CODs from influent, but also from CODp hydrolysis, still remain to be removed in the sections downstream of section 1. Hydrolysis appears to be significant in sections 2 and 3, a little less so in section 4 and very low in section 5. This result gives an idea about the retention profile of the CODp (both biomass and inlet CODp) along the filter.

CODs at the outlet of sections 2 and 3 for all operating conditions showed greater variability than for sections 4 and 5. This high variability can be explained by the effect of biomass detachment and hydrolysis of particulate substrate. However, owing to the observation of biomass in these sections, detachment of biofilm can be seen during our operation. To quantify the detachment, and the hydrolysis, it will be left to the simulation and modeling.

The final concentration of CODs at the outlet of the pilot is around 20 mg/l for Period 2 at low OLR, but 50 mg/l for Period 3 at High OLR. As the Readily biodegradable COD ($COD_{S,U}$) was the same in the influent for periods 2 and 3, the 3.3-times increase in CODt of the influent should have implied a 3.3-times increase of CODs,u in the outlet. Hence, we should have obtained 66 mgCODs, but only 50 mg/L of CODs was measured. We can conclude that a slight increase in COD removal capacity occurred when the OLR was increased by a factor of 3.3.

For Period 4, as shown in Figure IV-7, the final outlet CODs was around 50 mg/L, accounting for about 5% of total inlet COD (1000mg/L). This CODs may be an estimation of the inert soluble COD, i.e. $COD_{S,U} \approx 5\%$ of CODt.

The sludge production corresponding to the particulate COD released from section 1 was then analyzed. Furthermore, the time-evolution sludge production in other sections was then introduced to demonstrate the effect of history during the three periods. This will give a good indication of the sludge production and the detachment of biofilm.

3.1.3 Study of CODp against time

Time-evolution CODp concentrations in each section and during each period are plotted in Figures IV-8 to IV-13

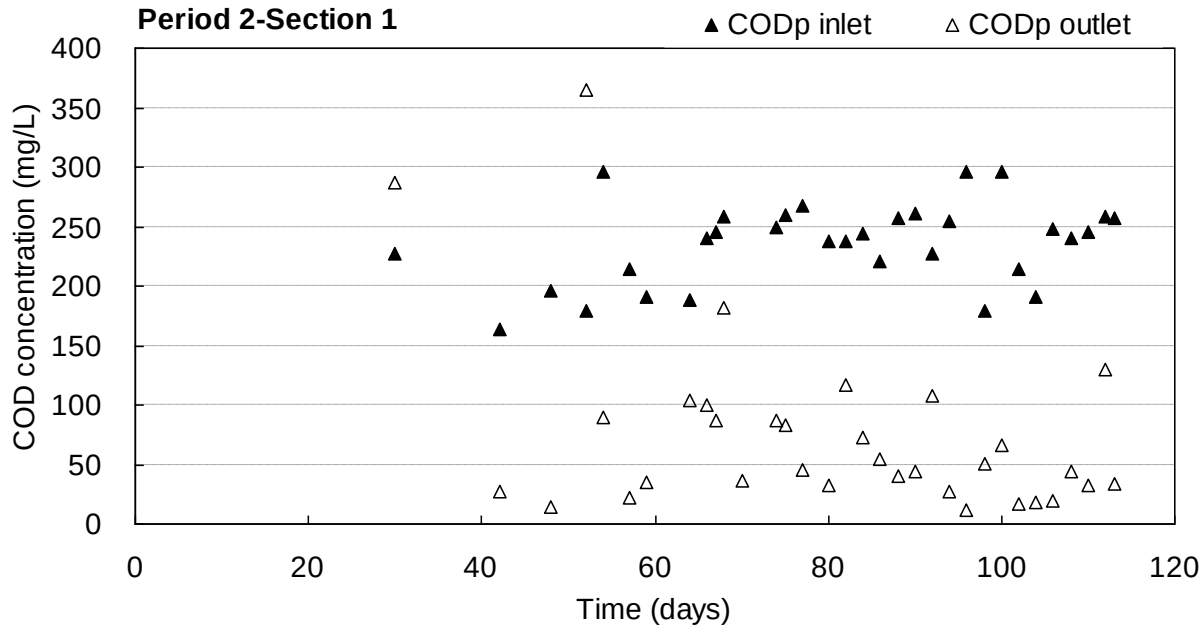

Figure IV- 8: Time-evolution of CODp at the outlet of section 1. Period 2, low loading condition, real WW

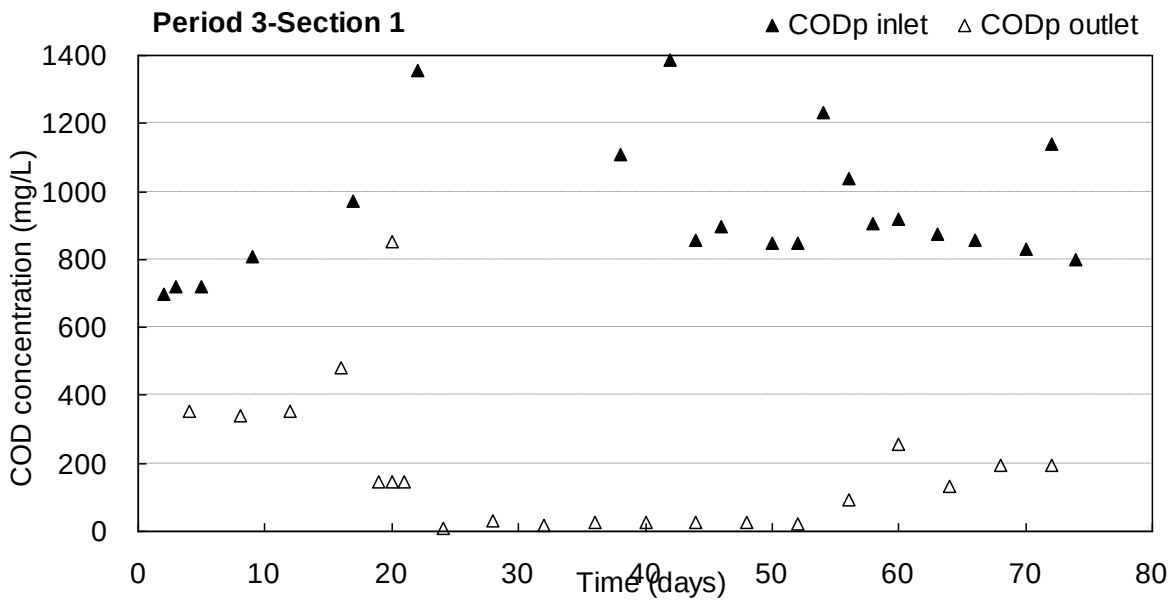

Figure IV- 9: Time-evolution of CODp at the outlet of section 1. Period 3, high loading condition, real WW

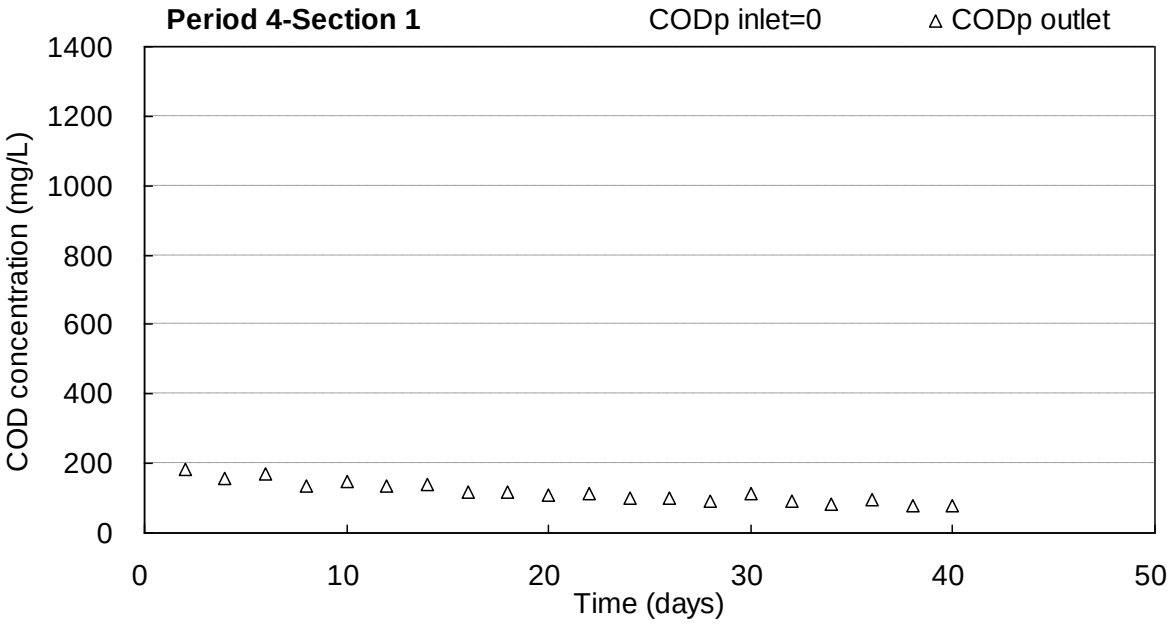

Figure IV- 10: Time-evolution of CODp at the outlet of section 1. Period 4, high loading condition, Viandox

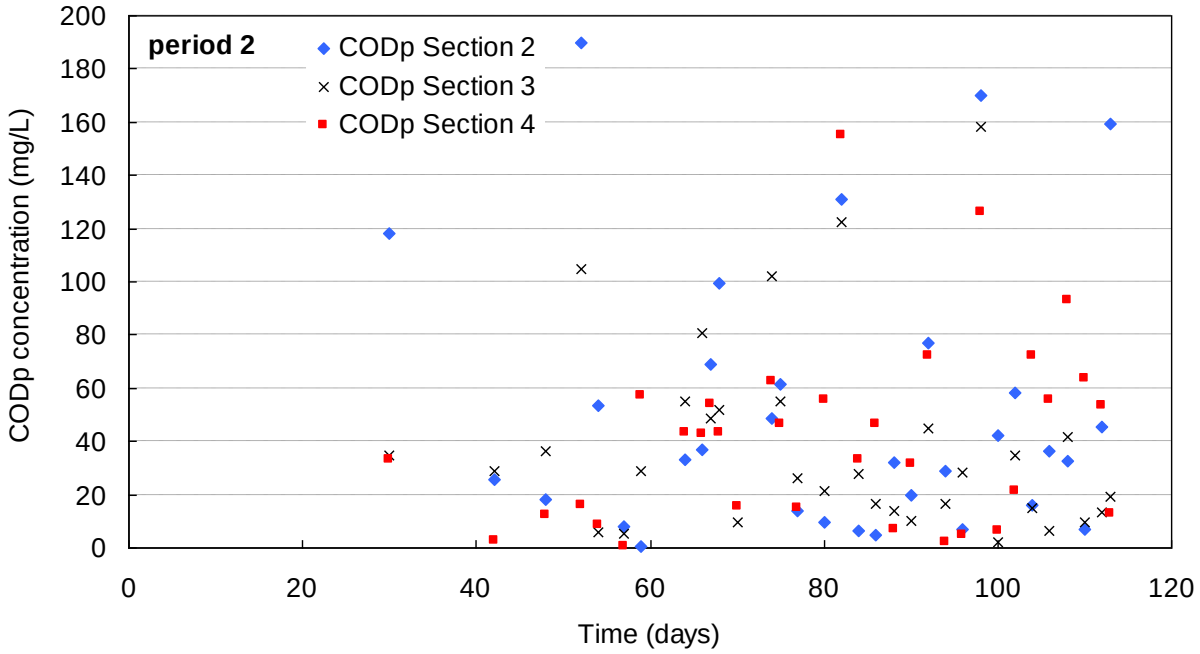

Figure IV- 11: Time-evolution of CODp concentration in section 2-section 4. Period 2, low loading condition, real WW

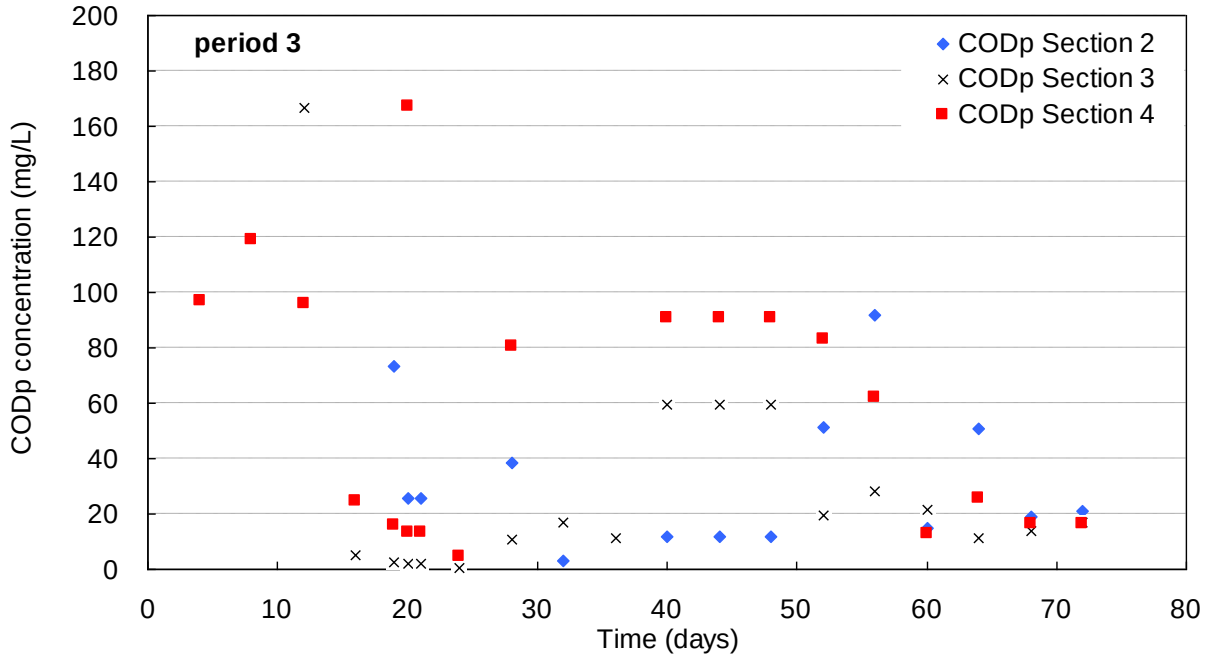

Figure IV- 12: Time-evolution of CODp concentration in section 2-section 4. Period 3, high loading condition, real WW

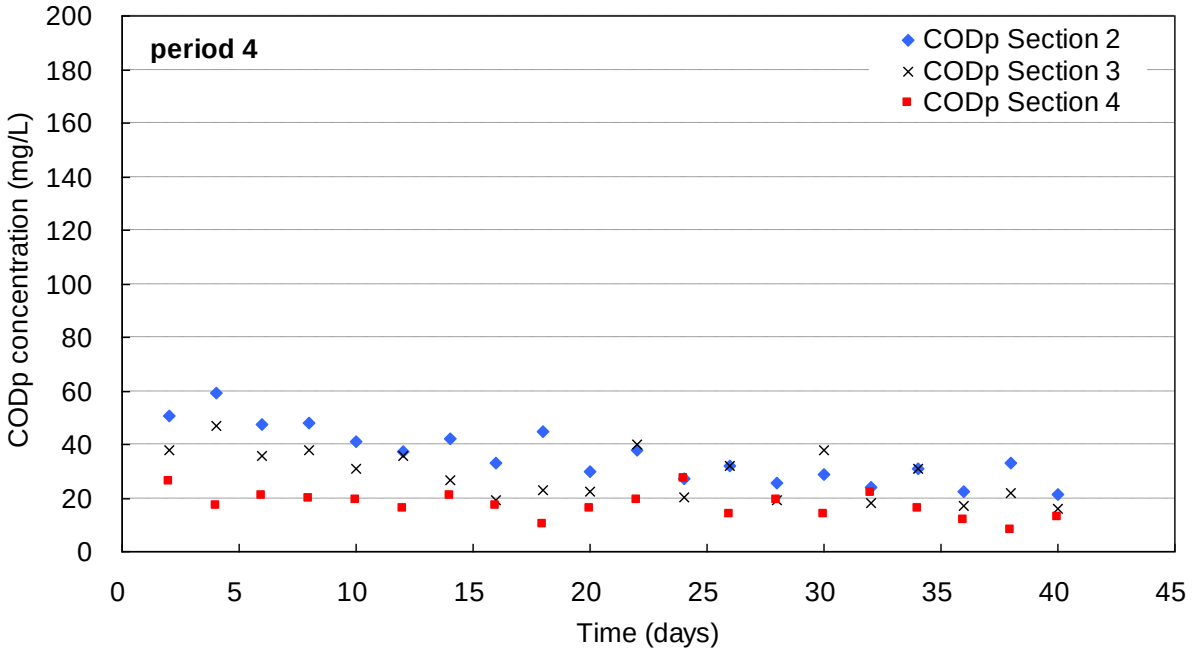

Figure IV- 13: Time-evolution of CODp concentration in section 2-section 4. Period 4, high loading condition, Viandox

From these figures, the following observations can be made:

Globally, the CODp released during periods 2 and 3 for all sections showed strong variability. This may result from detachment, a stochastic event whose frequency depends on many complex factors.

Changing the feed induced a dynamic evolution of CODp inside the biofilter. Some evidence of this phenomenon is as follows:

For example 1, see Figures IV-8, IV-9 and IV-10: When the inlet COD concentration was increased at the beginning of period 3, the CODp release first increased at the outlet of section 1, then strongly decreased, and increased again. This may be due to a succession of steps: first an increase of CODp due to the inlet concentration increase, then, as the biofilm thickness increased (resulting in a decrease of the packing bed porosity); a greater CODp entrapment was assumed, leading to the observed strong decrease of CODp at the outlet of section 1. Finally, the higher detachment observed may be due to the increasing of the liquid velocity, leading to a new increase of the section 1 outlet CODp

On the contrary, when CODp is eliminated from the feed (start of the period 4 with Viandox, Figure IV-9), the outlet CODp regularly decreased, showing dynamic detachment of the previously accumulated CODp. At the end of period 4, the particulate COD at the outlet of the pilot reactor should consist mainly of detached cells. Hence it may allow estimation of the

global apparent sludge production, apparent because it does not consider any biomass accumulation in the reactor.

For example 2, see Figures IV-11, IV-12 and IV-13: In the sections downstream of section 1, the released CODp is highly variable during period 2 and seems to slightly increase from sections 2 to 4 (given the assumption that growth=sludge production). In Figure IV-11, one can observe significantly higher CODp in section 4 compared to the previous sections as a result of an increase in sludge production between periods 2 and 3. Moreover, the variations of CODp at the outlet of the sections appear to show cyclic behavior. Detachment may increase when more biomass is accumulated inside the reactor. The amount of accumulated biomass in the sections may be regulated because of changes in the local hydrodynamic conditions. During period 4, the CODp released is observed to decrease for each section. At the end of period 4, mainly cells and cell debris are released from the sections.

Considering the mean values for released COD fractions at the outlet of each section, a COD removal profile can be drawn (Figures IV-14-16).

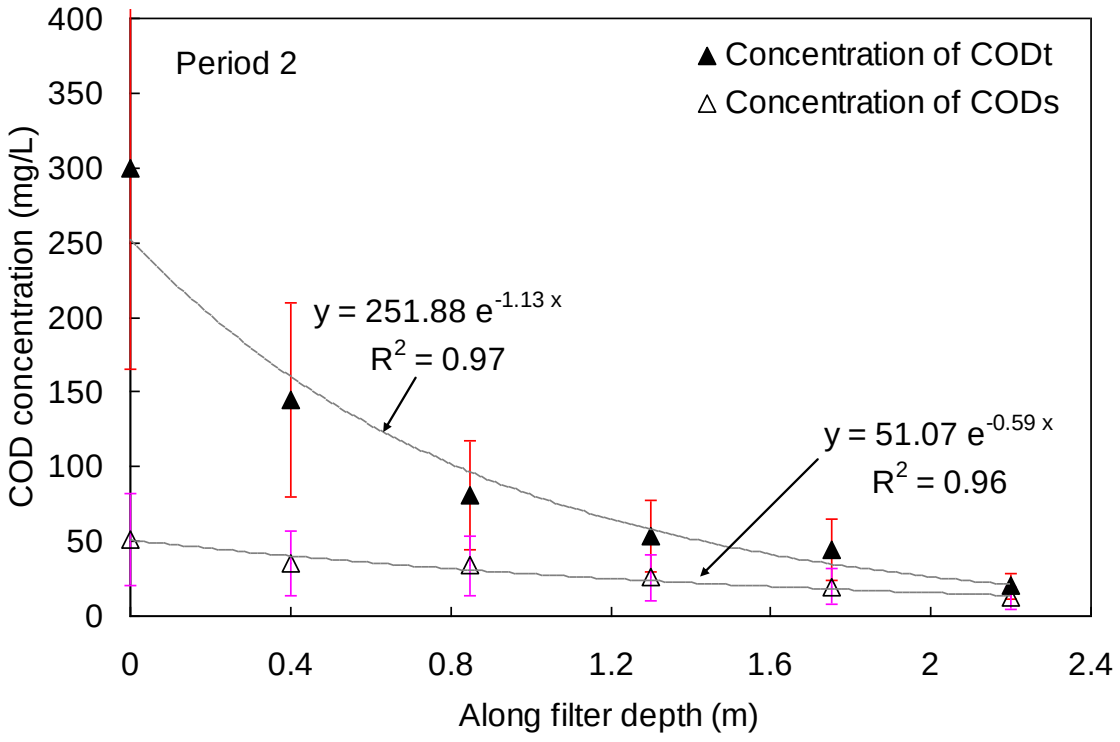

Figure IV- 14: CODt and CODs along the filter. Period 2, low loading condition, real WW

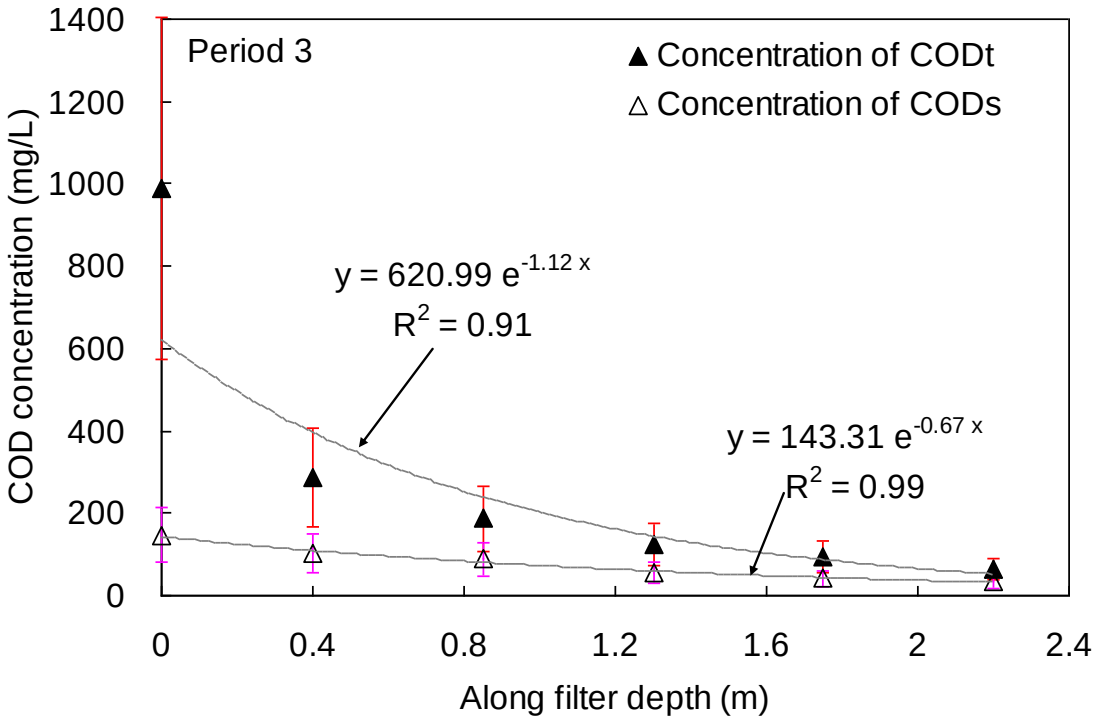

Figure IV- 15: CODt and CODs along the filter. Period 3, high loading condition, real WW

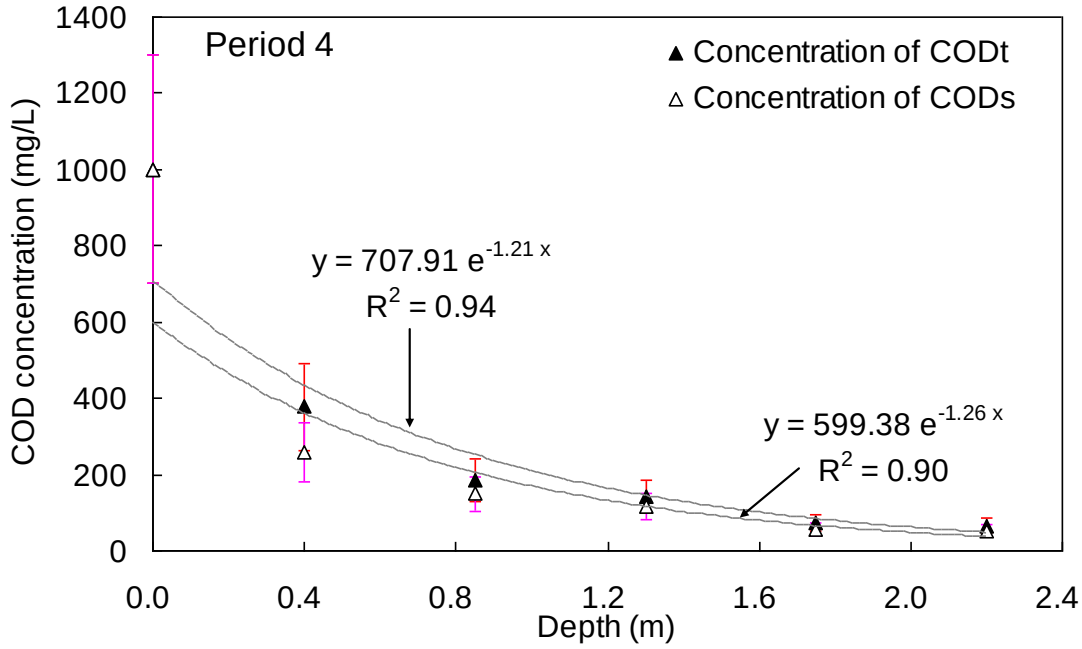

Figure IV- 16: CODt and CODs along the filter. Period 4, high loading condition, Viandox

The CODp profiles in Figure IV- 14 to 16 confirm the preponderant role of the first section in entrapping the particulate matter and converting the biodegradable COD into cell biomass. Note that along the filter depth, the CODs concentration only slightly decreased. Hydrolysis of particulate COD occurred in sections 1 and 2, providing CODs for the following sections. This is certainly dependent on the amount of sludge entrapped in each section.

3.1.4 Visual characterization of the MSB

Photos of section 1, taken at the end of each period, are shown in Figure IV-17.

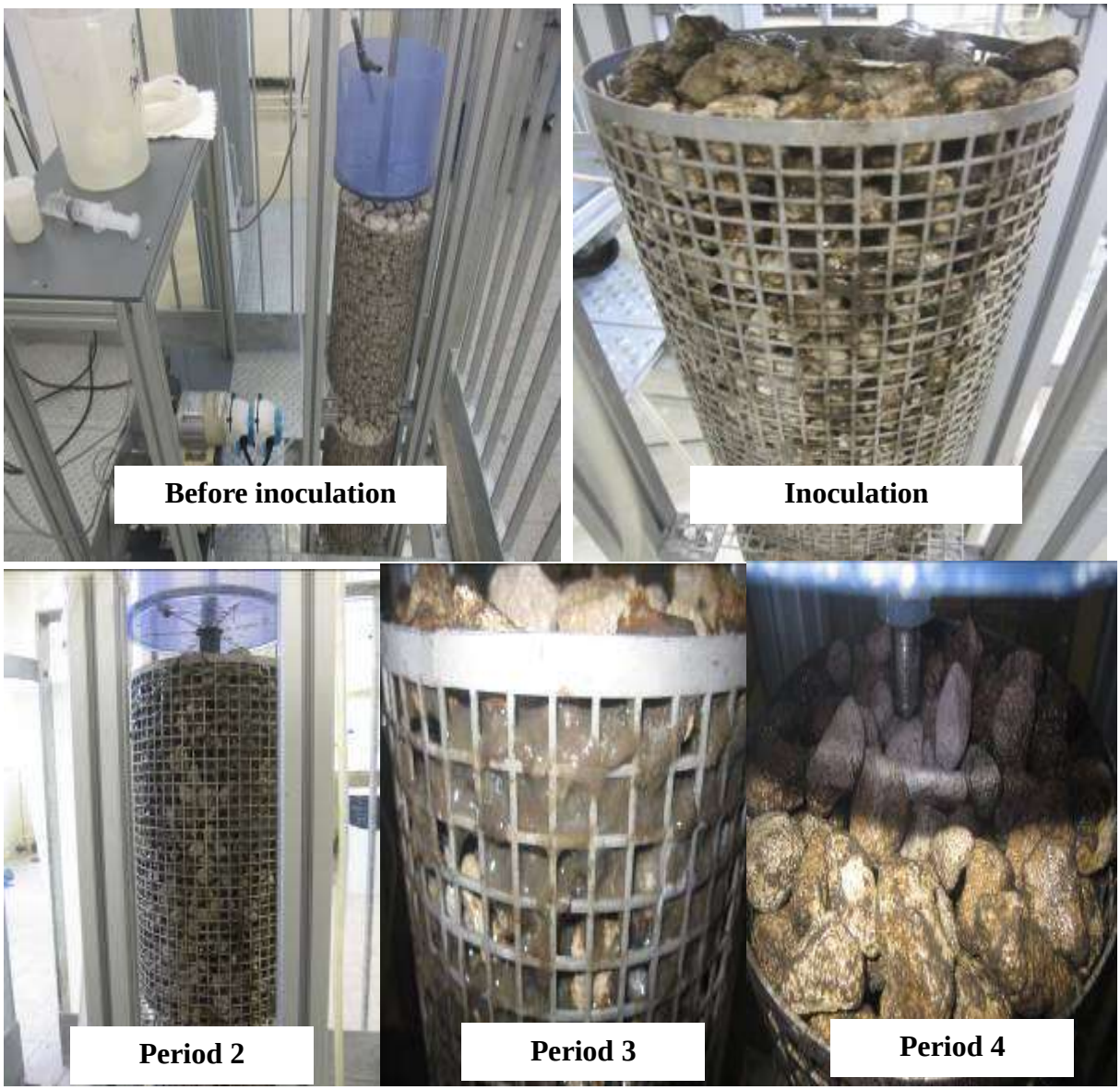

Figure IV- 17: Photos of section 1 at the end of each period

From Figure IV-17, the biomass in section 1 gradually increased; however, biomass in section 1 during period 4 after feeding Viandox appeared to be less than for of period 3 when it was fed by primary sludge. The “white spots” on the biofilm surface in Period 3 correspond to the worms and the biofilm was potentially clogging.

3.2 Comparison with other full-scale MSB COD removal performance

3.2.1 General comparison

Full-scale open structured MSB has already been applied in some rural area for wastewater treatment in Shanghai, China. Thanks to our cooperation with Shanghai Jiaotong University (SJTU), we have their collected data for some full-scale demonstration units to compare with our pilot-scale experimental results.

The COD removal by the full-scale MSB and another lab-scale MSB applied in China was compared and the operating conditions and removal efficiencies are shown in Table IV-3.

Table IV- 3: Removal efficiency of a full-scale unit in comparison with literature

	Full-scale MSB	Lab-scale MSB	MSB in literature
Reference	Li Xudong, 2008	This study	Ou wentao, 2009
Reactor volume (m^3)	45	0.0628	0.15
Cross-section area (m^2)	15	0.0314	0.07
Height (m)	0.5*6 sections	0.4*5	0.35*6
Media	Volcanic rock	Concrete brick	Volcanic rock/ Clay ceramisite/ Concrete brick
SSA of media (m^2/g)	7	6	6.5 /7 / 6
Flow rate (m^3/d)	60	0.08	0.14
Surface hydraulic loading rate ($m^3/ m^2 \cdot d$)	4	2.55	2
Inlet CODt (mg/L)	300	300	500
Organic load ($kg/ m^3 \cdot d$)	0.40	0.35	0.48
Surface organic loading rate ($kg/ m^2 \cdot d$)	1.2	0.8	1.0
Duration of operation (days)	600	260	60
Mean CODt Removal efficiency (E_{COD})	77%	82%	83% / 72% / 56%

From Table IV-3, even the organic loading rate applied for our pilot, and another lab-scale pilot were close to the full-scale reactor (lower in our case) unit, the total COD removal efficiencies were different. The difference in the total COD removal efficiency was due to the higher hydraulic load applied in the full-scale unit and the lab-scale pilot in China.

3.2.2 Comparison with full scale MSB with respect to COD removal

The full scale plant was designed to treat 1000 population equivalents of a domestic wastewater in China (suburb of Shanghai). The operating conditions were: a flow rate of 60 m^3/d giving a surface hydraulic loading rate of 4 m^3/m^2d, a mean OLR of 1.1 $kgCOD/m^2d$. The mean CODt in the influent was around 300 g/L. There is no settler after the MSB, and thus the outlet COD contained both CODs and CODp. The depth of the filter is 3 m, similar to the depth of the MSB pilot in this study. Figure IV-18 shows the inlet and outlet CODt concentrations measured over nearly 600 days of operation in a full-scale MSB unit.

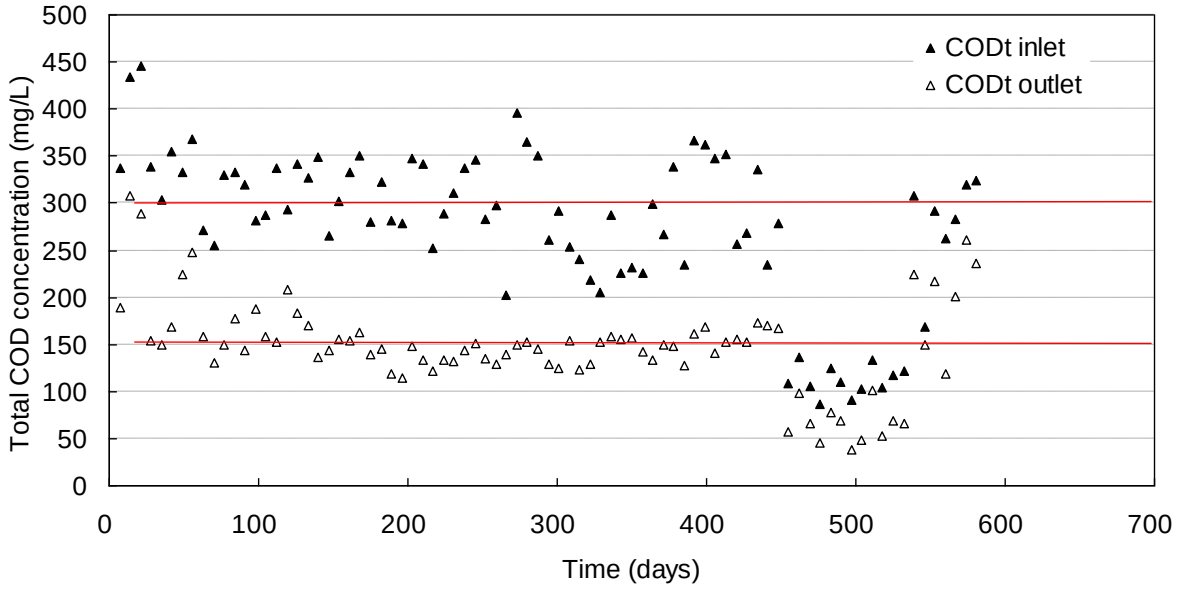

Figure IV- 18: Total COD removal in a full-scale demonstration unit in China

Figure IV-18 and Table IV-3 show that, over a year of operation, the full-scale demonstration unit only obtained about 50% CODt removal. Unfortunately, only CODt data are available and the specific features of CODs and CODp cannot be distinguished. This efficiency was much lower than that obtained in this study; even the same medium was applied. This implies that under high OLR and greater flowrate, the COD removal performance is worse than the cases under lower flowrate and lower organic loadings.

3.3 Pathways of COD

Mass balance on COD allows us determining the pathways of the COD from the wastewater in the MSB pilot. The Figures IV-19 represents the COD routes for the three periods. As it is difficult to evaluate the accumulated COD inside the biofilter, since oxidized COD (oxygen consumption) and accumulated COD in the MSB pilot are not distinguished.

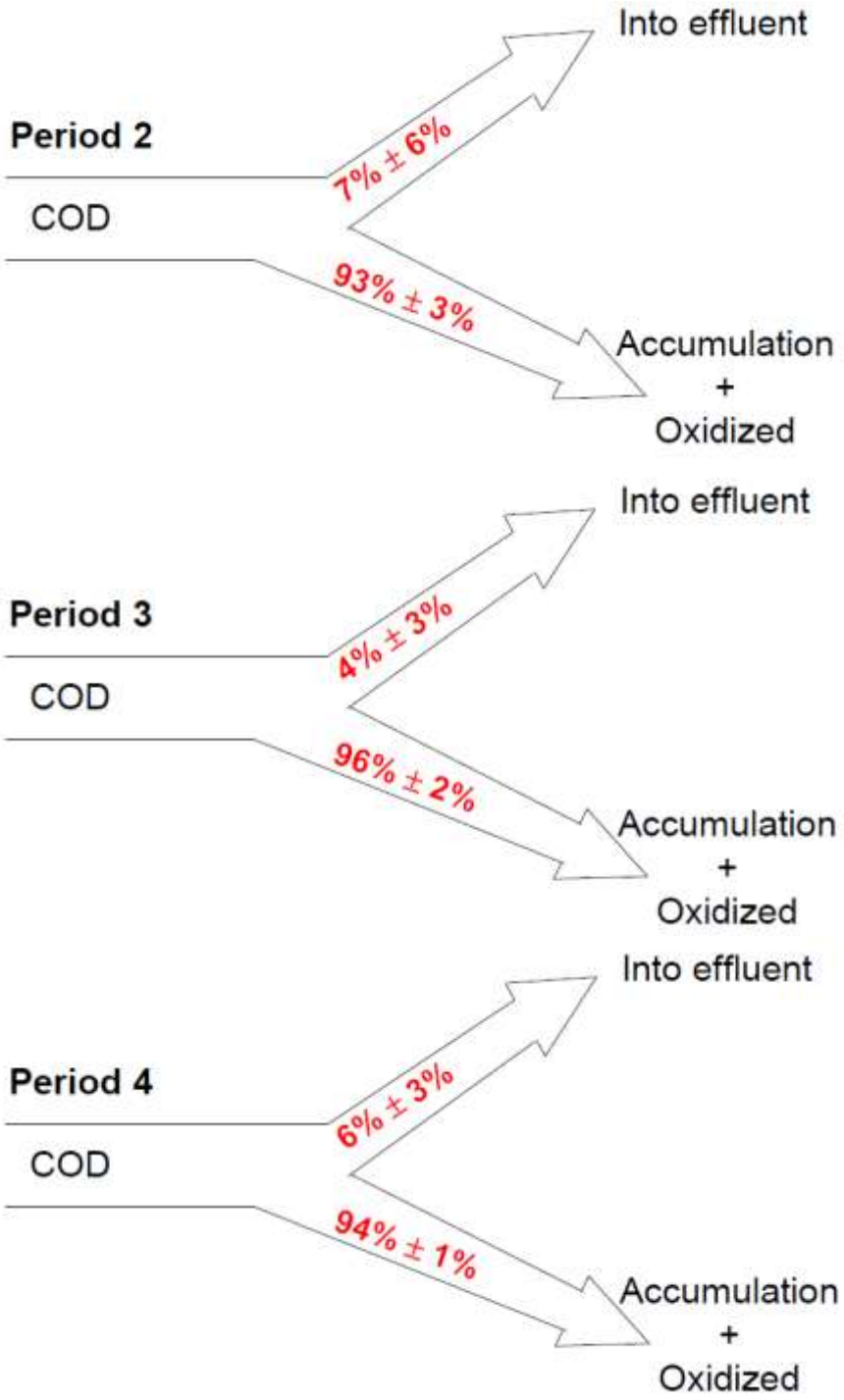

Figure IV- 19: Pathways of total COD

From Figures IV-19, most total COD accumulated and oxidized, with a small part left in the effluent leading to high removal efficiency.

3.4 Sludge production estimation

Estimation of sludge production is crucial both to the design works and to understand the processes occurring in the filter. It is, however, a hard task because the accumulation of CODp inside the filter must be taken into account (unless we assume steady state for particulate compounds), but the particulate compounds is very difficult to measure. An attempt is made here to assess the sludge production in our pilot.

The observed release of CODp can first be determined and the ratio of CODp in the outlet to COD removed can be calculated for the three periods (see Table IV-2). Secondly, the Viandox was employed as a feeding solution to analyze the performance of COD removal of the pilot, when no particulate COD (both Biodegradable COD and Ultimate COD) were present in the feed. It can be used thus to estimate the observed growth yield ($Y_{g,obs}$). This calculation has only been done for the 1st section in period 4. After 30 days, transformations in section 1 seemed to achieve a pseudo steady-state, with an outlet CODp of 80-112 mg/L. This range may correctly represent outlet COD from released cells for the Viandox substrate. Hence, considering the average outlet CODp of around 86 mg/L in the last 10 days of period 4, and the assumption that no biomass accumulates in the section at this stage, the observed cell production yield ($Y_{g,obs}$) from the Viandox substrate can be calculated. The removed COD was about 780 mg/L (see Figure IV-16). In addition, we consider the inert particulate COD in the sludge production. Thus $Y_{g,obs}$ =86 mgCOD/780 mgCOD=0.11 gCOD/gCOD. This value is lower than the data from other literature (Spérandio et al. 2012) in the case where a synthetic wastewater is also used.

With this $Y_{g,obs}$ value of 0.11 gCOD/gCOD, the SRT can be estimated from the Eq. II-40, by substitute the classic values of Y_H of 0.44 gCOD/gCOD and k_d of 0.07 gCOD/gCOD. The estimated SRT for period 4 is thus around 43 days.

In addition, the sludge production estimation of 3 periods during biological experiments is described in Appendix 8.

3.5 Assimilated nitrogen versus consumed COD

It is known that part of the ammonia is also assimilated for bacterial syntheses (refer to Chapter 1), consumed as the source of nutrient by heterotrophic growth. A relation between assimilated ammonia and the consumed COD can be established based on the nitrogen mass balance, which will be further estimated in following part of nitrogen removal. The total inlet TKN is directed to the nitrified nitrogen pool (nitrite plus nitrate), the assimilated nitrogen

and the accumulated or released nitrogen. Meanwhile, assuming the system achieves a pseudo steady-state in the last 10 days of the period, the accumulation can be assumed to be 0. The assimilated nitrogen in section 1 was calculated by the total inlet TKN minus the outlet soluble TKN, consumed COD was calculated by the total inlet COD minus the outlet CODs. The assimilated nitrogen is plotted in Figure IV-20 against the consumed COD.

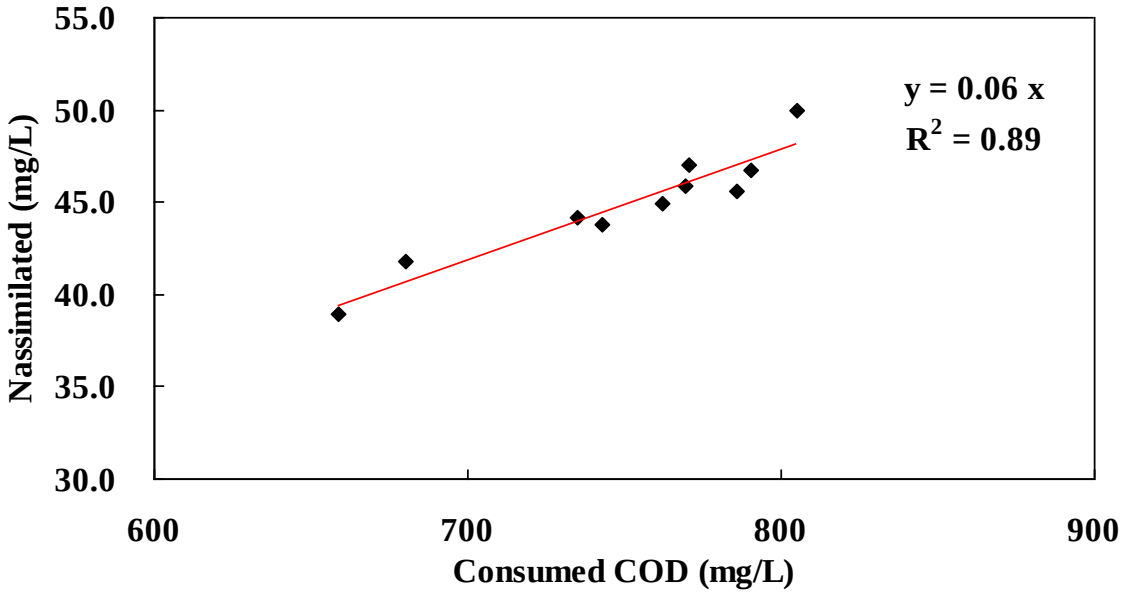

Figure IV- 20: Relation between consumed COD and nitrogen assimilation. Period 4, high loading condition, Viandox

Figure IV-20 indicates that assimilated nitrogen accounted for about 6% of the consumed COD for heterotrophic growth. Assuming that biomass from nitrogen should be around 12% of TKN, which is a conventional value formed in the performance. Accordingly, 50% of consumed COD is oxidized. Sludge production should thus be around 0.5 of the consumed COD, i.e. Yobs=0.5 g biomass/g $COD_{consumed}$. This value is too high comparing to conventional value of 0.4.

3.6 Discussion and conclusion on COD removal

3.6.1 Assessment of design parameters for COD removal

OLR range of operation:

Experiments performed in this work had the objective to help in designing a MSB. However, restrictions due to the too narrow experimental plan studied must be underlined. In the performed experiments, the increase in OLR was only achieved by increasing the COD

concentration in the feed instead of increasing the flow rate. Various processes may be affected when using a higher flow rate. In particular, the wet fraction of the carrier and the oxygen transfer rate.

What knowledge has been brought?

In the experiments, the increase of OLR was realized by increasing the COD concentration in the feeding wastewater, instead of increasing the flow rate. This has been the result of limitation of the storage tank capacity. That means that an increase in the concentration gradient should have occurred at the surface of the biofilm, leading to a higher substrate flux and hence to better utilization of the biofilm mass. This is true if COD is limiting the reaction rate (and not oxygen, e.g.). Oxygen transfer certainly remained high because the flow rate was not increased. These aspects are discussed in more detail at the end of this chapter.

Time-scale characteristics of some processes

One major question arises when operating the bioreactors when biofilm is present. Has the steady-state COD removal reached for each period? Though a rather stable influent was used for each period, dynamic variations were observed during inoculation and due to the change of influent COD concentration and nature for each period.

Dynamics were observed when varying the inlet COD concentration (periods 3 and 4). Rearrangements of CODp inside the biofilter sections were observed that affected the balance, on the one hand of the accumulation of produced cells and attachment and, on the other hand, the release of CODp through detachment and CODp hydrolysis. Increasing the OLR increased biomass retention that improved attachment (capture of CODp) and the global COD removal rate. Local hydrodynamic conditions varied because the porosity changed over time due to biomass accumulation that affected detachment rate. It is difficult to know whether stable operating conditions were achieved for each period because clogging could occur for longer operating duration. However, clogging was not observed during the operation in this work.

Viandox was employed as a feeding solution to analyze the performance of COD removal of the pilot when no particulate COD (both COD_B and COD_U) was present in the feed. In addition, using the Viandox, it should be easier to estimate specific parameters such as the observed sludge production yield.

Figure IV-8 to 13 showed that the CODp concentration dynamically decreased as a function of time for the last 30 days for 3 periods, which resulted from an effect of history. Indeed,

after the change in the feeding composition from an urban wastewater to Viandox, no more CODp from the influent was introduced to the system. Consequently, hydrolysis still continued in the reactor section, and the release of CODp from section 1 decreased.

Attachment and detachment are important processes that distribute the CODp along the filter. These processes are strongly dependent on the OLR and local hydrodynamic conditions. Surprisingly, for high OLR, the COD removal capacity was promoted. This is certainly due to a better entrapment of particulate substrate and biomass.

3.6.2 Discussion and conclusion on COD removal

It appears that a rather conventional feature for COD removal was observed for the MSB compared to a TF. High removal efficiency was found in the higher part of the reactor, decreasing gradually with depth. Therefore, sections 4 and 5 played only a "polishing" role for the COD removal. High COD removal capacities (>93%) were obtained for the pilot under all the operating conditions tested. A settler is of course required in order to recover the released CODp. That means the pilot is able to treat the highest loading rate applied in this study.

Hydrolysis, entrapment, attachment and detachment are key processes to describe the MSB COD removal performances. In this work, an idea of the capacity of the MSB to capture the CODp is given. No clogging was observed during the 260 days of operation. However, CODp accmulation is approved. Sludge production has been roughly estimated.

MSB reactor COD removal performances are better for a low flowrate and high OLR (high COD inlet concentration) than for a high flowrate and a low OLR (small COD inlet concentration). This is in good agreement with the conclusion of the hydrodynamic study done in Chapter 3.

The performances of other studies were compared to the full scale study. Under similar organic loading rate but much lower flow rate, better COD removal efficiencies were obtained in our pilot. Moreover, even if the same concrete-brick medium was applied, the MSB pilot showed better COD removal performance compared to the full scale MSB unit operated at higher flow rate. This implies that the Multi-Section Bioreactor (MSB) can sustain high organic loading, but to optimize the COD removal performance, a low flow rate is needed.

3.7 For nitrification

Similar analysis of the data is proposed, but focusing on nitrogen removal and particularly on nitrification because this transformation is required to limit the effect of effluent on the receiving water. In periods 3 and 4, the inlet TKN has been increased proportionally to the increase of the inlet COD. Similar fractions of nitrogen are, however, conserved for periods 2 and 3. An attempt was made to maintain also same nitrogen fractions in period 4.

3.7.1 Analysis of nitrogen removal efficiencies

The performances of the MSB in terms of TKN and ammonia removal yields are shown in Table IV-4. The way to calculate each yield is described in the Material & Methods of Chapter 2.

Table IV- 4: TKN removal and nitrification performance

	Period 2	Period 3	Period 4	Unit
Inlet TKN	47±5	161±14	144±2	mg/L
Inlet ammonia	30±4	100±11	104±5	mg/L
Final outlet TKNt	4±2	6±4	4±1	mg/L
Final outlet ammonia	0.2±0.3	0.6±0.6	0.2±0.2	mg/L
Final outlet nitrite & nitrate	31±8	101±18	97±3	mg/L
TKN removal efficiency (E_{TKN})	91±3	96±4	97±2	%
Removal efficiency (η_{TKN})	97±1	97±3	98±1	%
Final outlet CODp (sludge)	32±40	30±27	13±7	mg/L
Nitrification efficiency	65±18	64±11	67±2	%

All average values were obtained from the data collected during the last 20 days of each period, assuming a pseudo-steady state.

From Table IV-4, the following observations can be emphasized: Advanced soluble nitrogen removal was achieved for all the conditions tested. Nitrification occurred for all experimental OLRs.

3.7.2 Spatial removal of TKN

TKN is a global composite parameter whose evolution reflects various transformations occurring with nitrogen, Hydrolysis of organic nitrogen leading to ammonia, incorporation of ammonia in cells during growth and nitrification (adsorption of ammonia is considered negligible). The mass balance on TKN allows estimation of the nitrifiable nitrogen by calculating the difference between total inlet TKN minus the outlet soluble TKN. Hence, the time-evolution of spatial TKN concentrations for the tree periods is plotted in Figures IV-21 to 23.

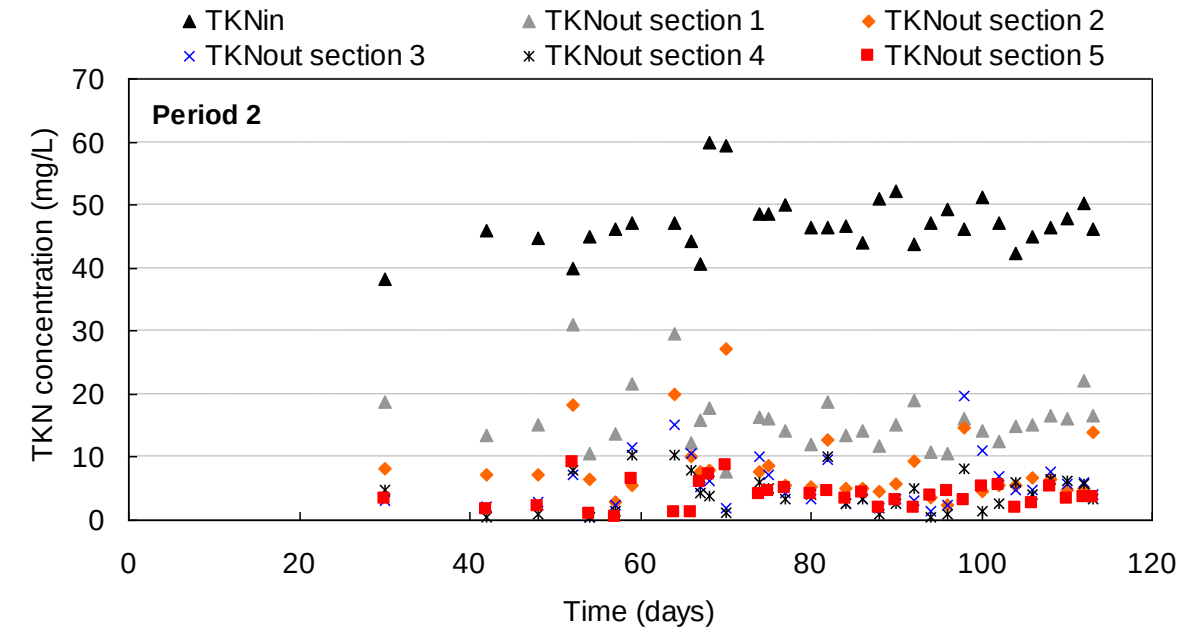

Figure IV- 21: TKN time-evolution concentration in each section. Period 2, low loading condition, real WW

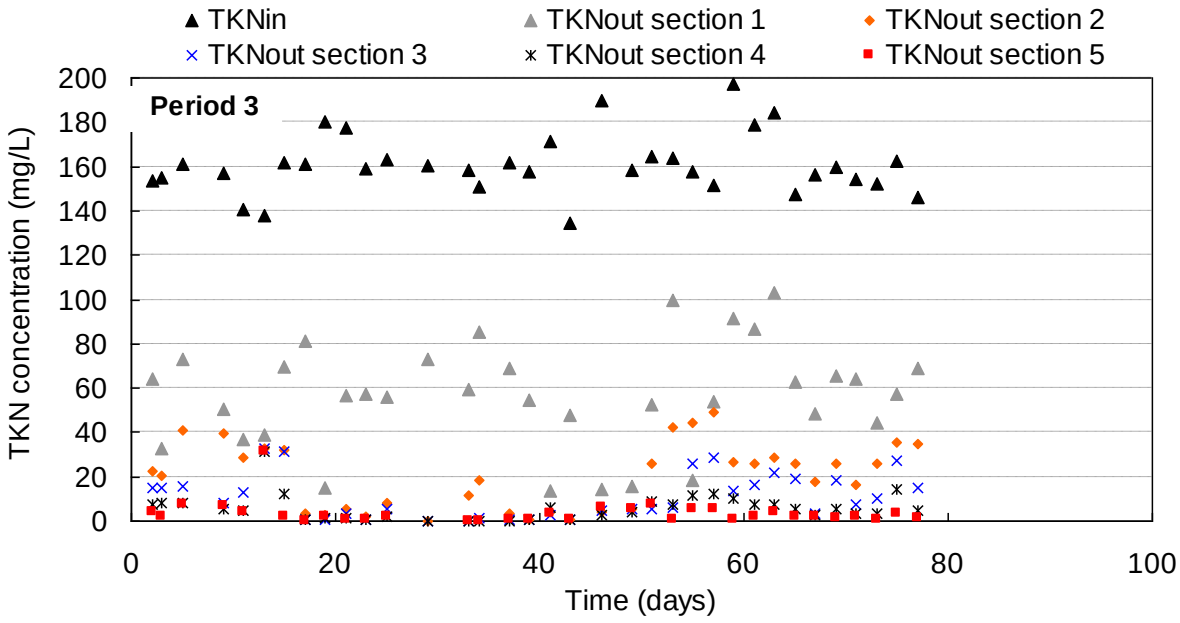

Figure IV- 22: TKN time-evolution concentration in each section. Period 3, high loading condition, real WW

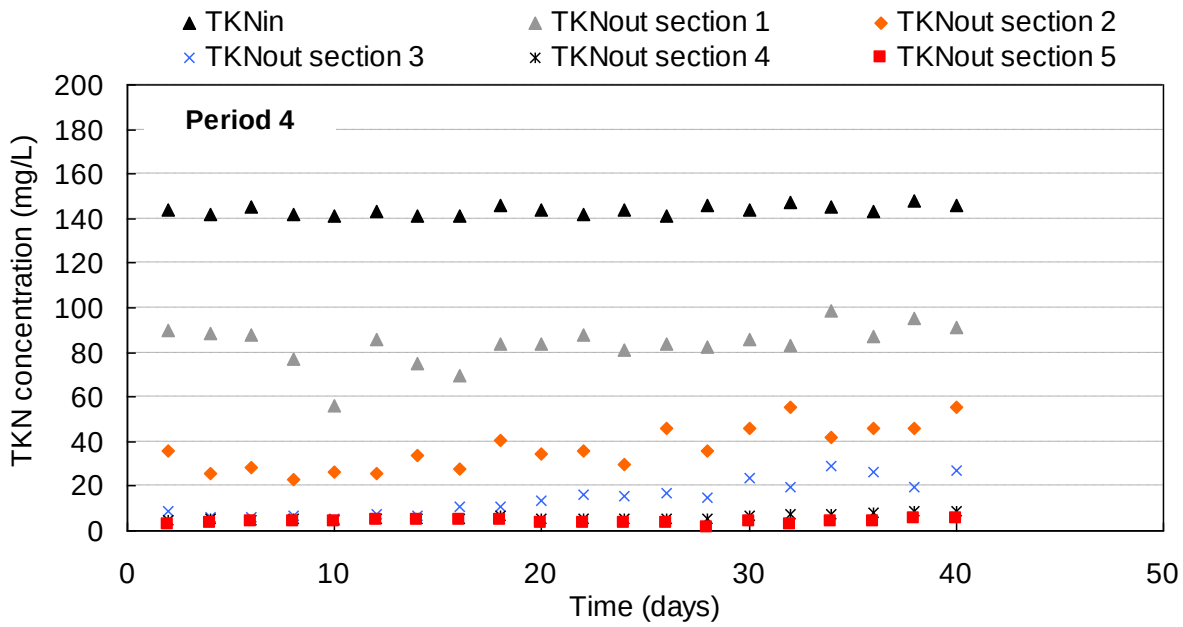

Figure IV- 23: TKN time-evolution concentration in each section. Period 4, high loading condition, Viandox

Globally from Figure IV-21 to 23, TKN is very efficiently removed in the MSB pilot since only around 1 mgTKNp/L was found at the outlet of the reactor (around 30 mg CODp/L was found at the same outlet). The removal is mainly achieved in section 1 and 2 (except for period 4 because TKN is mainly under soluble proteins), but the removal yield of these sections decreased with time. This may be due to a less efficient capture of TKNp or a higher hydrolysis rate.

Even under high OLR, about 40% of ammonia was removed in section 1.

To further analyze the nitrification in each section, the time-evolution concentration of nitrite and nitrate, collected at the outlet of each section are plotted in Figures IV-24 to 26. In the following figures, NOx-N represents the sum of nitrite and nitrate nitrogen (NOx-N=NO_2-N + NO_3-N).

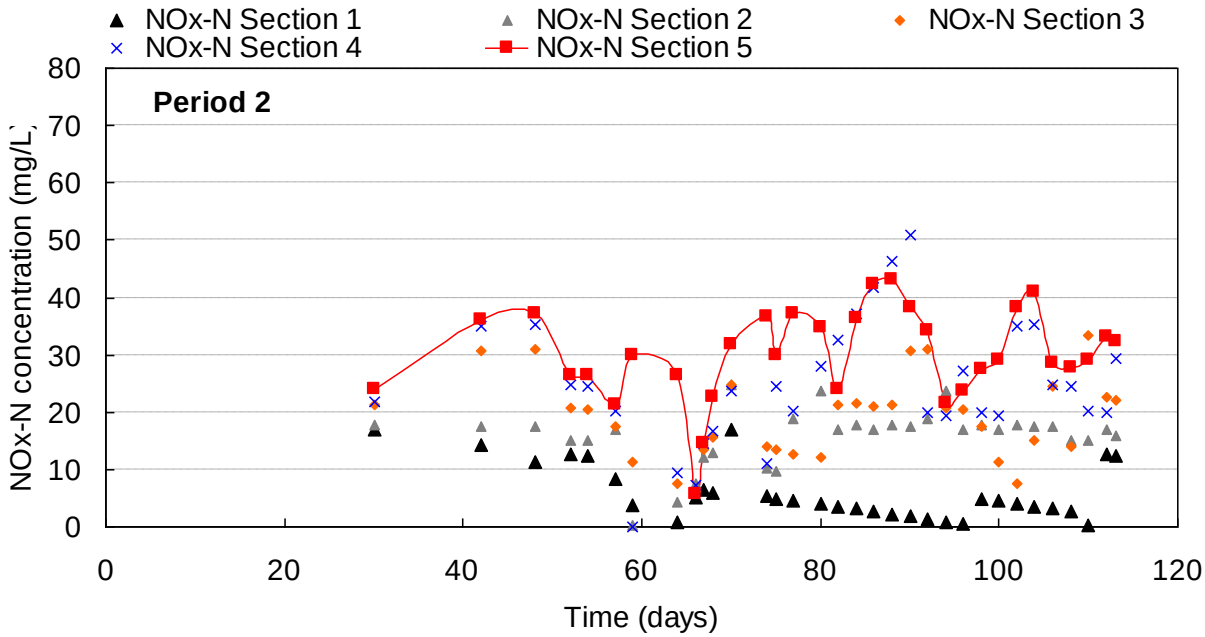

Figure IV- 24: Nitrate and nitrite time-evolution concentration in each section. Period 2, low loading condition, real WW

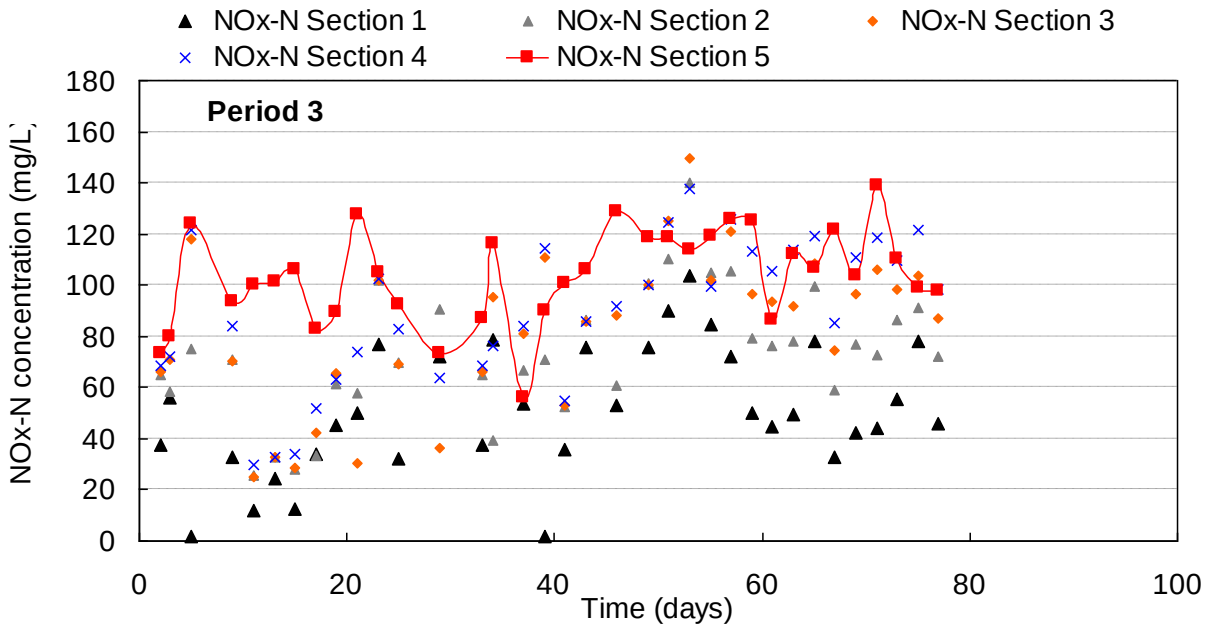

Figure IV- 25: Nitrate and nitrite time-evolution concentration in each section. Period 3, high loading condition, real WW

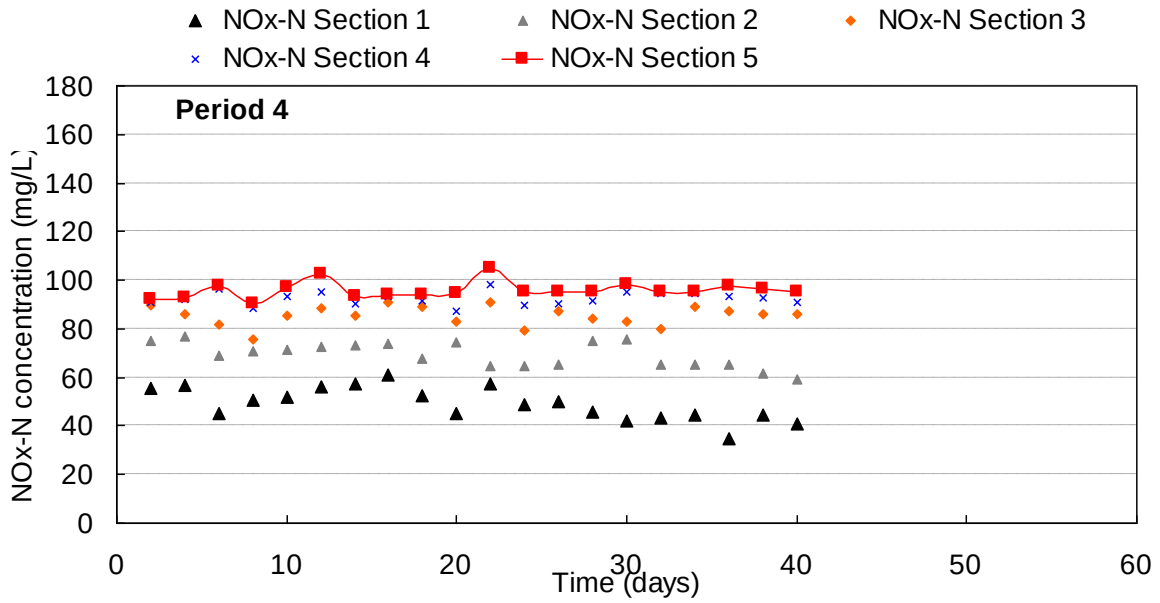

Figure IV- 26: Nitrate and nitrite time-evolution concentration in each section. Period 4, high loading condition, Viandox

For period 2 as shown in Figure IV-24, high variability of nitrate production against time was observed for this low loading condition. Moreover, nitrate production was rather low in the first section, but high in the second and third sections. In the first section, nitrate production decreased by a factor of 2 during period 2. From day 55 to day 60, there was a consecutive biomass detachment in section 1 which caused a sharp decrease of nitrate. Similarly, this occurred during day 89-90, biofilm fouling could have occurred.

In Figure IV-25, from the beginning of period 3, and despite a high OLR being applied, high nitrate production was observed in section 1 and to a less extent in section 2. That means that nitrification was able to very quickly adapt to the concentration increase and that the new OLR conditions allow a better performance of nitrification, even in the first section.
In period 4, as shown in Figure IV-26, nitrification took place in each section but with a high percentage in section 1. It is worth noting that nitrite was sometime detected for this high OLR condition, which accounted for 5% of nitrate in the first section. This indicates that the oxygen supply may not have been enough for nitrification in this section.

Nitrite was detected sometimes during our experiments. Both the nitrite and nitrate concentrations are plotted against time in the three periods in Figure IV-27.

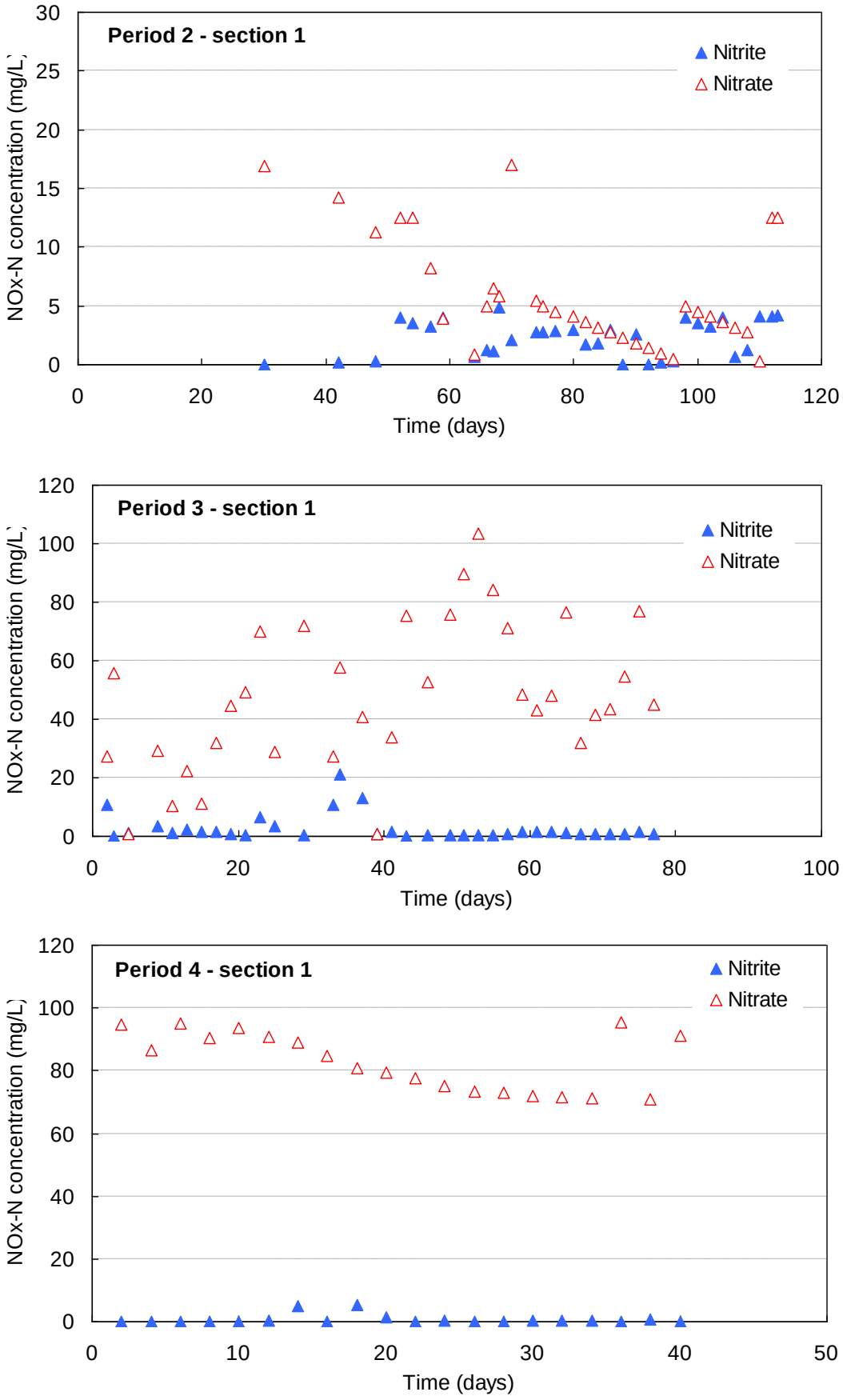

Figure IV- 27: Nitrate and nitrite time-evolution concentration in section 1. Period 2 to 4

In Figure IV-27 during period 2, the nitrite concentration of about 3 mg/L was higher than in periods 3 and 4 (which were close to 0). Considering that the oxygen was not limited, even under high organic loading conditions, this detection of nitrite may be due to the lower LRT in period 2 as found in Chapter 3, Figure III-13, providing less contact time for liquid and biofilm, and resulting in less time for complete nitrification.

Considering the mean values of the final 20 days of operation for the released TKN, nitrate and ammonia, removal profiles can be drawn of their mean concentrations. The TKN decrement and the increment of nitrate and nitrite as well as the decrement of ammonia in each section are plotted in Figures IV-28 to 30 for the periods 2 to 4.

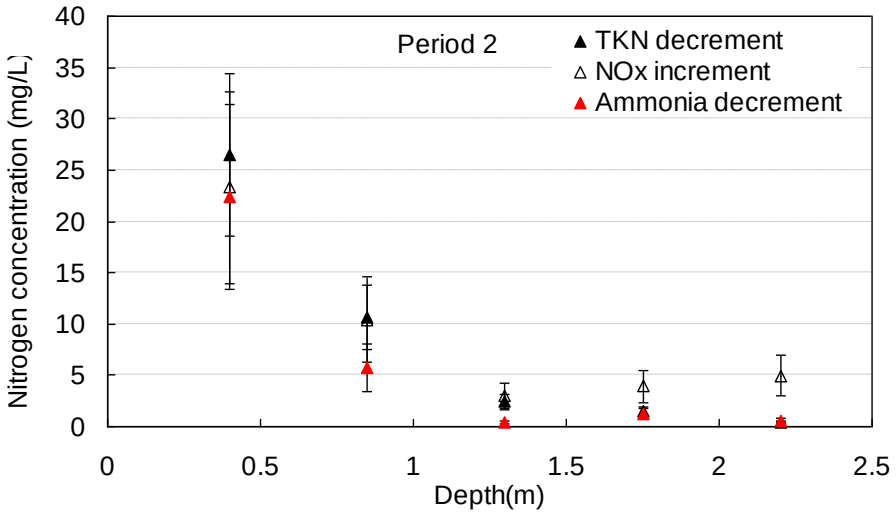

Figure IV- 28: Calculated TKN consumed, nitrate produced and ammonia consumed for each period of time. Period 2, low loading condition, real WW.

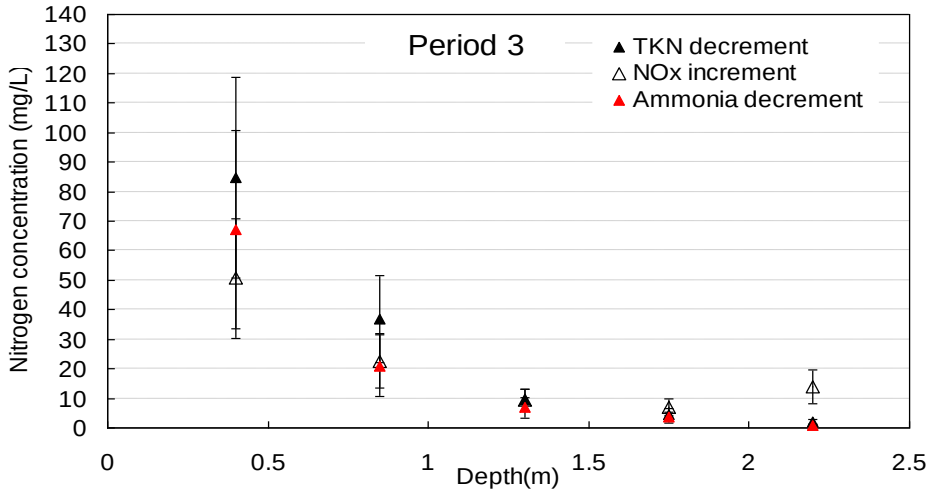

Figure IV- 29: Calculated TKN consumed, nitrate produced and ammonia consumed for each period of time. Period 3, high loading, real WW

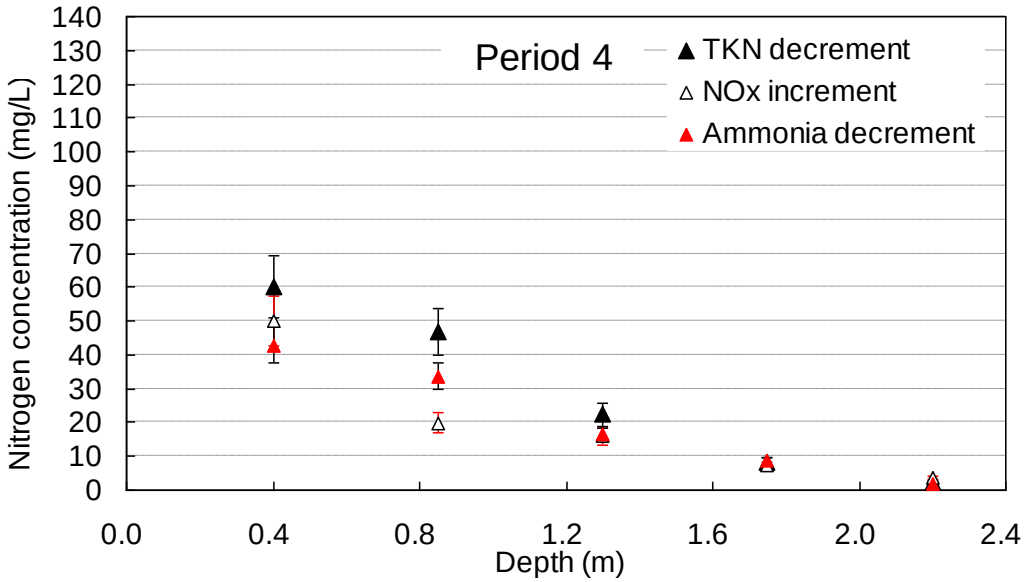

Figure IV- 30: Calculated TKN consumed, nitrate produced and ammonia consumed for each period of time. Period 4, high loading, Viandox

Nitrification mainly occurred in the first section. The nitrogen nitrified are always (except in Period 3 section 1) higher than the decrement of ammonia and increment of nitrite. This indicates that ammonium from organic nitrogen was consumed through nitrification. For high OLR, when nitrate production is lower than nitrified N, one can assume that denitrification occurred leading to loss of nitrogen. From section 3 to section 5, the increment of nitrite was higher than the consumption of nitrogen. That is explained by nitrate entering the section due to previous nitrate production in the upper sections.

Figure IV-26 shows that along the filter depth, ammonia was gradually removed and consequently the nitrate increased gradually.

3.8 Comparison with full scale MSB nitrogen removal performance

3.8.1 General comparison

The nitrogen removal by the full-scale MSB demonstration unit and another lab-scale MSB applied in China, are compared to our study in their operating conditions and removal efficiency. These are shown in Table IV-5.

Table IV- 5: Removal efficiency of a full-scale unit in comparison with literature

	Full-scale MSB	Lab-scale MSB	MSB in literature
Reference	Li Xudong, 2008	This study	Ou wentao, 2009
Reactor volume (m^3)	45	0.0628	0.15
Cross-section area (m^2)	15	0.0314	0.07
Height (m)	0.5*6 sections	0.4*5	0.35*6
Medium types	Volcanic rock	Concrete brick	Volcanic rock / Clay ceramisite / Concrete brick
SSA of media (m^2/g)	7	6	6.5 / 7 / 6
Flow rate (m^3/d)	60	0.08	0.14
Surface hydraulic loading rate (m^3/ m^2d)	4	2.55	2
Inlet TN (mg/L)	26±5	47±5	30±6
Surface nitrogen loading rate (kg/ m^2d)	0.10	0.12	0.06
Volumetric nitrogen loading rate (kg/ m^3d)	0.04	0.06	0.03
Inlet ammonia-N (mg/L)	20±4	30±4	20±4
Duration of operation (days)	600	260	60
Mean ammonia removal efficiency % ($E_{ammonia}$)	43±11	98±2	53 / 61 / 38
TKN removal % (η_{TKN})	32±11	97±1	50 / 63 / 26

From Table IV-5, in our study, we applied higher loading of nitrogen. The difference in the ammonia and total TKN removal efficiency was due to the lower hydraulic load applied in our case. Though, there is not enough information on nitrification efficiency in other papers to compare with this table, we believe that our pilot supplied enough oxygen for nitrification due to the porous structure, because our pilot was constructed with more external pores in baskets than the full-scale reactor applied in China; additionally, according to Chapter 3, the study of LRT indicates that our pilot could provide enough liquid residence time (more than 2 h during period 2, more than 3 h during periods 3 and 4) for hydrolysis of organic nitrogen, compared to the full-scale demonstration unit in China with their LRT less than 2 h as reported.

3.8.2 Comparison with a full scale MSB on nitrogen removal

The full-scale reactor operation, analyzed the total nitrogen and ammonia removal, which represented the nitrification performance in their system. The time-evolution concentration of Total Nitrogen (TN) and ammonia –nitrogen (NH_4-N) are shown in Figure IV-31.

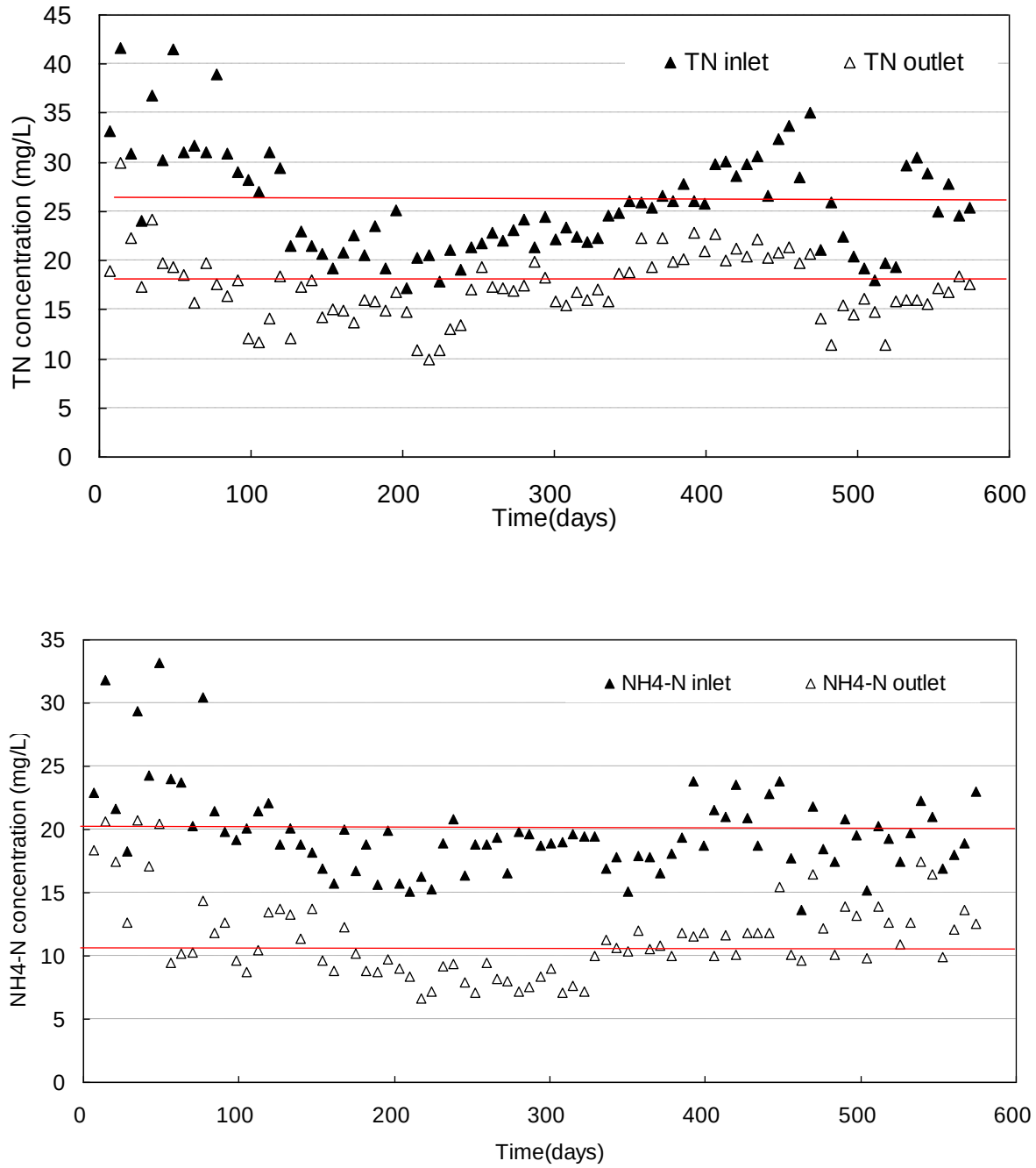

Figure IV- 31: TN and ammonia removal in full-scale reactor

Figure IV-31 indicates that the nitrification performance in the full-scale reactor operation was not ideal. The removal efficiencies of TN and ammonia were less than 50%. However, the nitrification efficiency in their system was not easy to analyze due to lack of information on nitrate production.

3.9 Pathways of nitrogen

Mass balance on nitrogen allows us determining the pathways of the TKN from the wastewater in the MSB pilot. The Figures IV-32 represents the total TKN routes for the three periods. The TKN in outlet was estimated by the soluble TKN in the effluent, and the nitrification route was based on the calculation from the yield of nitrate and nitrite; the rest is nitrogen that accumulated.

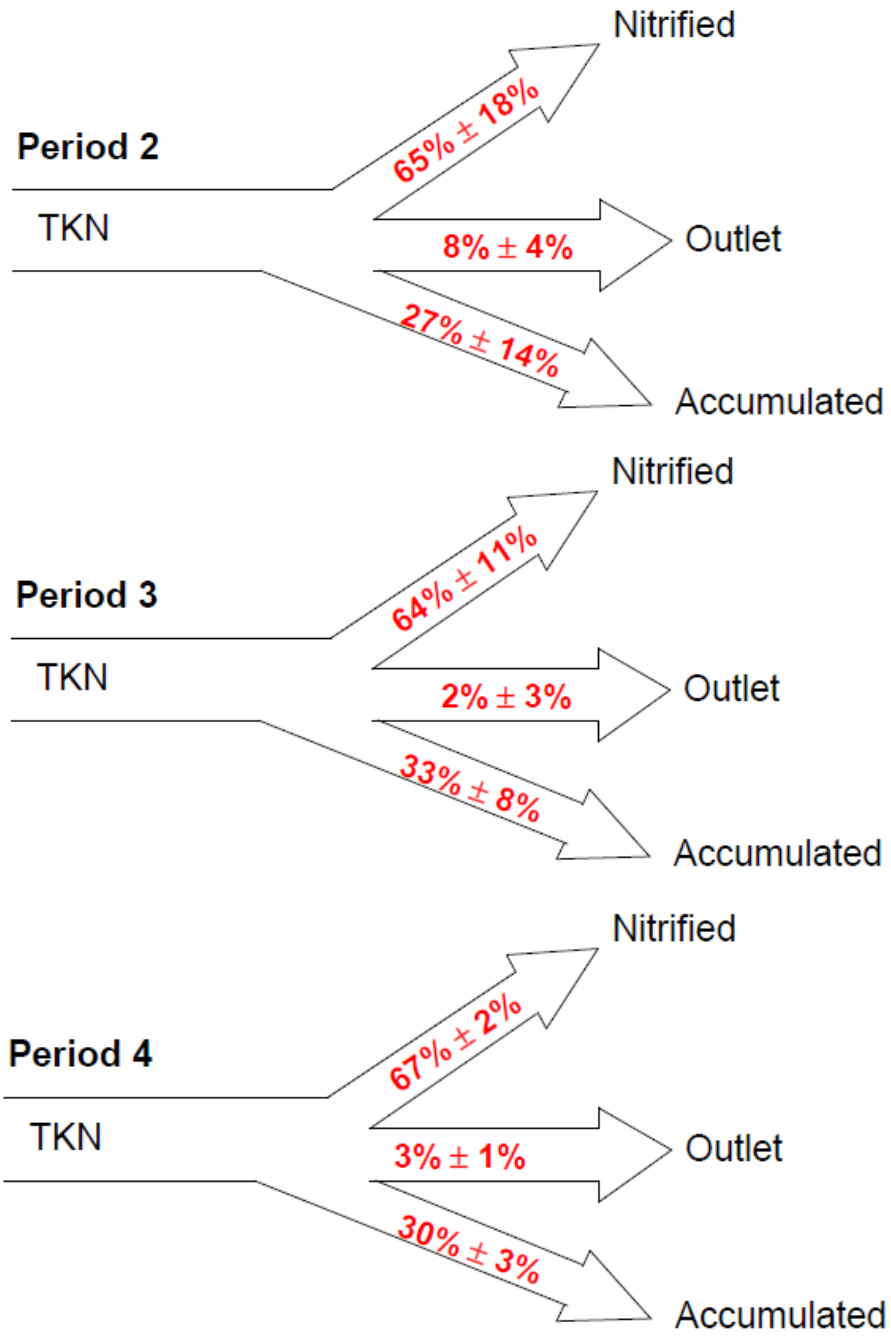

Figure IV- 32: Pathways of nitrogen

Figures IV-32 shows that most of nitrogen was nitrified during operations of 3 different periods. The nitrified nitrogen fraction of these 3 periods were close, the differences of other nitrogen fractions result from the accmulation of nitrogen into the biomass. Increase the organic loading, the fraction of nitrogen that accumulated in the packed bed slightly increased than under lower organic loading. This increase in the accumulated fraction may due to the effective entrapment of particulate nitrogen, caused by the thicker biofilm and lower packing bed voidage. This demonstrates that the CODp (biomass) is accumulating in the filter little by little. Clogging may occur after a long term of operation. The time-scale for studying clogging is greater than the duration of our experiments (<260 days). It is interesting to note that in China, with a higher OLR, clogging was observed after 2 years operation in a full-scale MSB unit.

3.10 Discussion and conclusion on nitrogen removal

Even under high OLR fed by Viandox, nitrification still occurred in each section, there was no obvious inhibition for nitrification in the first section, implying the good oxygen supply capacity of this pilot geometry.

Nitrification mainly occurred in sections 1 and 2, where more than 70% of inlet ammonia was removed. With no limitation of oxygen and mass transfer, nitrification should achieve a realistic efficiency, even under conditions where the COD removal was promoted.

Nitrite was detected in the first section, which indicates that under high OLR; too short LRT was applied for complete nitrification.

Even under high OLR, nitrification mainly occurred in the first section. From section 4 to section 5, less nitrification occurred due to lack of ammonia resource. The nitrite measured in section 4 and section 5 was from the accumulated nitrite release from the upper sections.

The nitrification performance in our study was better than in the full-scale reactor; even the inlet concentration of ammonia was much higher than that in full-scale reactor. Lower hydraulic flowrate applied in our study could lead to longer Liquid Residence Time (LRT) and thinner liquid film thickness, and accordingly better mass and oxygen transfer into the biofilm. Hence, though competition exists between heterotrophic bacteria and nitrifying bacteria, without great limitation of oxygen, the nitrification performance was better than the cases of full-scale unit.

3.11 Connection between biological and hydrodynamic experiments

Based on the results of hydrodynamic experiments in Chapter 3, along with COD and nitrogen removal discussed in this chapter, we attempt to explain the treatment performances for 3 different feeding conditions (periods 2 to 4) considering both hydrodynamic and biological elements, such as biofilm thickness, liquid residence time, and liquid film thickness.

We focus first on the estimation of biofilm thickness based on our biological experiments. Then we recall the LRT and liquid film thickness for three periods summarized in Chapter 3. Finally, combine hydrodynamic and biological elements to explain the biological performance for the three different conditions.

3.11.1 Estimation of biofilm thickness

As mentioned in Chapter 1, many processes occur in the biofilm and at the surface between biofilm and liquid, such as oxygen and soluble mass transfer and diffusion, particulate substrate attachment and detachment, and biofilm cell displacement. All these processes are influenced by the biofilm structure and its properties, especially the biofilm thickness and density, and also its porosity. Hence, estimating the biofilm thickness will help to analyze the different performances under different organic and hydraulic conditions.

Two methods were applied to evaluate the biofilm thickness along the filter depth. The detailed description of these two methods is presented in Chapter 2. Method 1 was used for period inoculation and period 2, which used the COD concentration measured in the biofilm to estimate the biofilm density; the biofilm thickness was estimated from the estimated biofilm volume dividing the surface area of particles. Method 2 was used in period 3 and 4, which first evaluate the wet and dry biofilm mass and then calculated the biofilm volume. Furthermore, Method 2 estimates the biofilm thickness by the volume divided by the surface area of particles. Biofilm thickness variation in section 1 and all along the filter depth are shown in Figure IV-33. These estimated values were only samples taken from the surface of particles taken for measurements; the bulk biofilm in the interspaces of particles could not be measured, though it was observed that the bulk biofilm thickness could be significantly greater than values calculated in this manner.

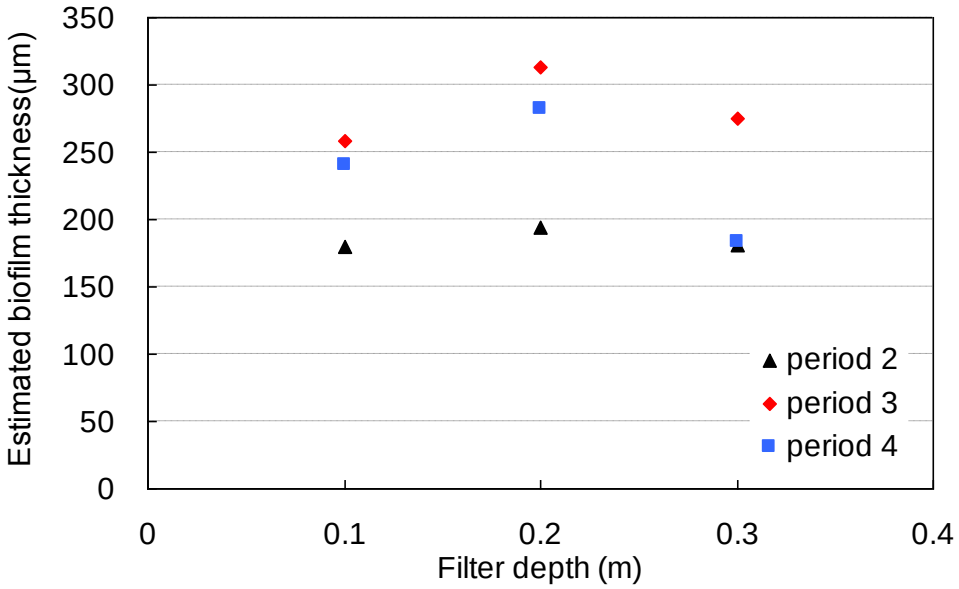

Figure IV- 33: Estimated biofilm thickness in section 1 during period 2 to period 4.

On the top of section 1, the biofilm thickness was lower than in the middle, possibly resulting from higher shear stress and greater biofilm detachment. The biofilm thickness for high loading conditions with feeding by primary sludge (period 3) was thicker than for feeding by Viandox (period 4). This indicates that the particulate substrate could be adsorbed to form the biofilm. These values should be much lower than the real mechanical biofilm thickness in this section, because the bulk biofilm thickness was hard to measure during period 3. The feeding conditions of period 2 introduced about 1/3 of the COD concentration of period 3 and 4. However, the biofilm thickness was not 1/3 of that in period 3 and 4, which means the biofilm density could increase and the biofilm porosity should decrease.

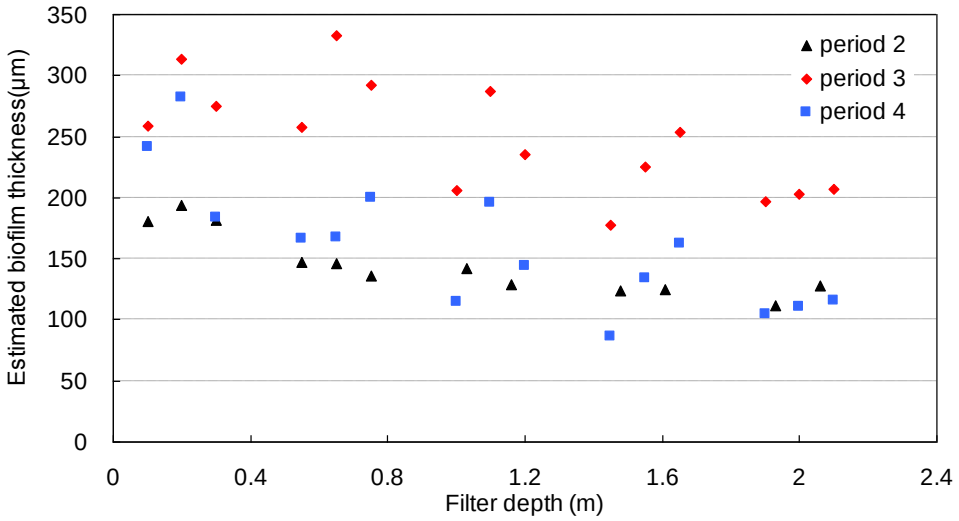

Figure IV- 34: Estimated biofilm thickness along filter during period 2 to period 4.

Along the filter depth, from section 1 to section 5, the estimated biofilm thickness decreased. From section 1 to section 3, in the middle of each section, the estimated biofilm thickness was thicker than at the top and bottom, indicating that most growth occurred in the middle of each section where there is enough substrate for biofilm growth. In sections 4 and 5, biofilm thickness gradually increased from top to bottom, implying that the biofilm formation in section 4 and 5 was mainly due to accumulation of particulate substrate released from the upper sections.

The optical method described in Appendix 10, was also deployed to compare with the mechanical method. Sample comparisons are shown in Table IV-6 and Figure IV- 35 of section 1 in particular.

Table IV- 6: Biofilm thickness estimation by optical method

Sample	Microscopic observation		Micrometer	Mean calculated physical thickness
	y_f (µm)	L_f (µm)	L_f (µm)	L_f (µm)
Glass slide	753.6	1002	1020	1000
	752.9	1001	1008	1000
Sample 1	323.3	430	-	180
Sample 2	857.2	1140	-	303

Figure IV- 35 represents the estimated biofilm thickness along section 1, by the optical method.

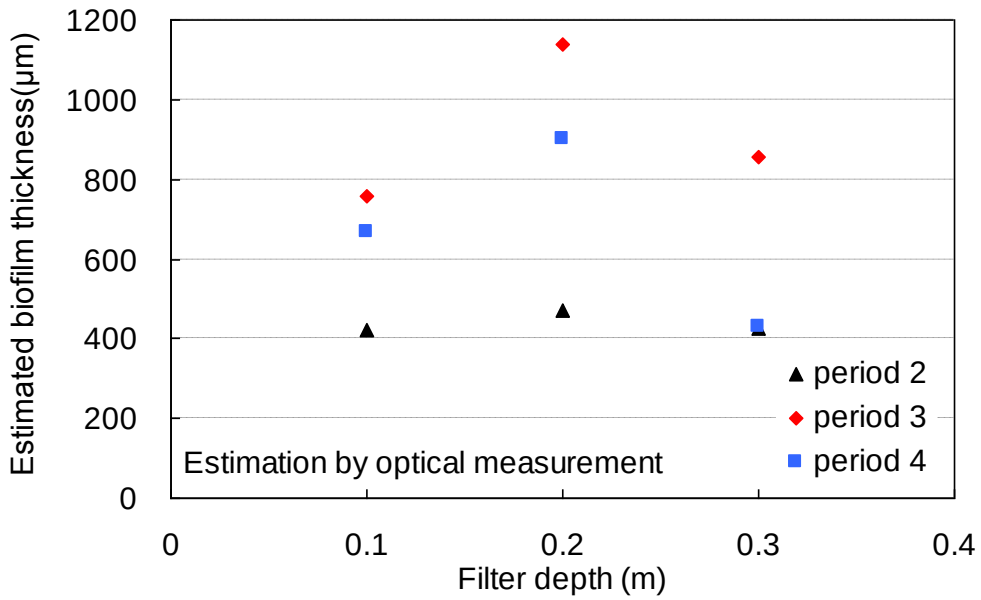

Figure IV- 35: Estimated biofilm thickness by optical measurement in section 1 during period 2 to period 4.

The measured biofilm thickness by optical methods was significantly greater (more than 400 μm) than the values obtained from mechanical methods (less than 350 μm). The differences result from the mechanical method not takes the biofilm porosity into account, because it assumes the biofilm as the whole volume without holes and assumes that the wet biofilm density is close to the density of water.

3.11.2 Recall the Liquid Residence Time and Liquid film thickness

To explain the COD removal performance and nitrification performance, the hydrodynamic elements, that affect the mass and oxygen transfer as discussed in Chapter 3, were analyzed in relation to the biological performance.

Figure IV-36 and 37 show the estimated LRT and liquid film thickness during different periods.

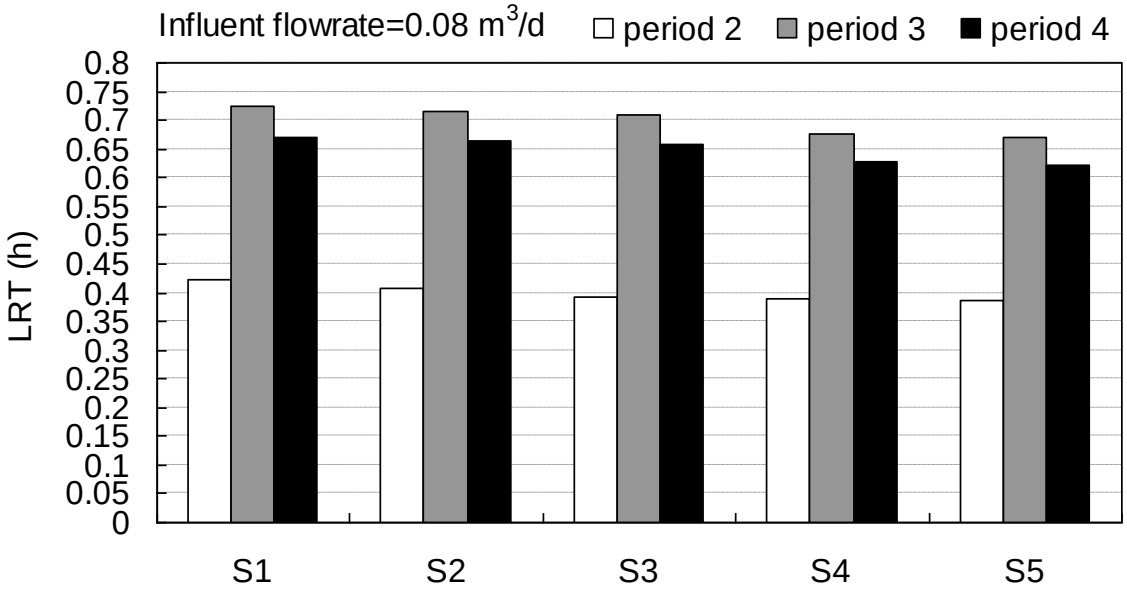

Figure IV- 36: LRT estimation during period 2-period 4.

In Figure IV-36, when the packed bed was attached by thin biofilm, the LRT was significantly lower than with a thicker biofilm. With a thicker biofilm, the entrapment of particulate substrate was more significant. The entrapment of particulate COD thus helped to increase the LRT.

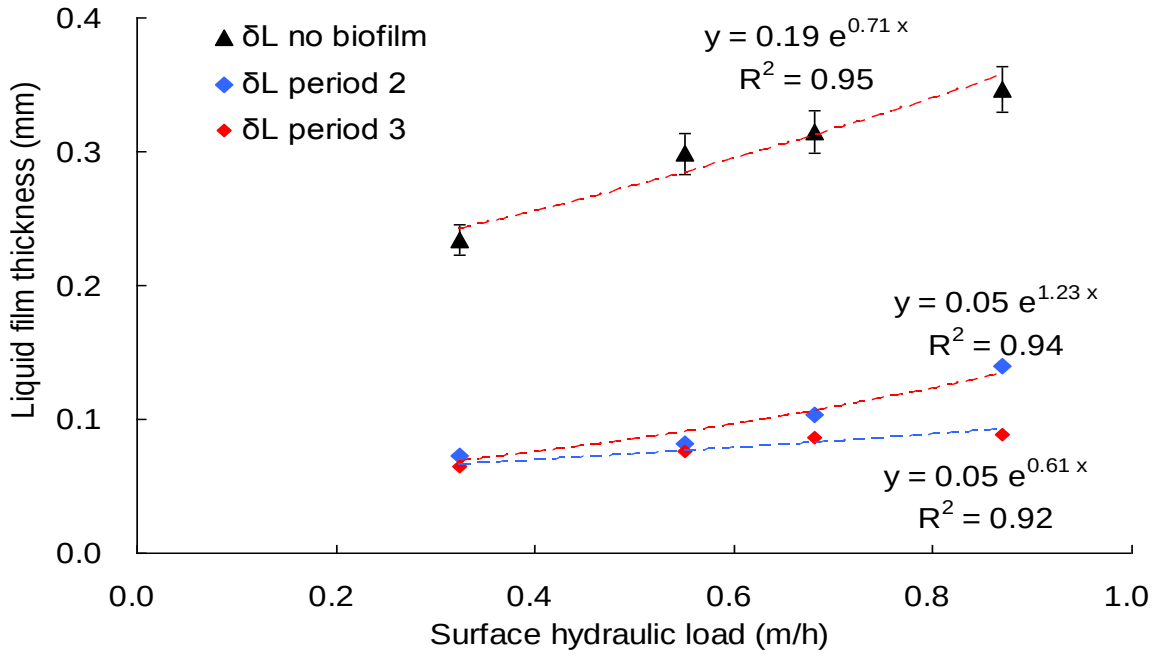

Figure IV- 37: Liquid film thickness estimation during period 2 to period 4.

In the case with a biofilm, the liquid film thickness was lower, leading to better oxygen and mass transport. At the same flow rate, the liquid film thickness in period 3 was less than in period 2. Hence the COD removal and nitrification may be promoted. As mentioned in the discussion of COD removal and nitrification, it could confirm that for a high OLR at the same flowrate, COD removal could be promoted, with or without particulate COD. Nitrification benefited from the better oxygen and mass transfer resulting from the decrease in liquid film thicknesses and longer LRT.

3.11.3 Schematic interpretation

In order to provide a visual explanation of the performance differences during different periods, a diagram for this proposal including the biofilm thickness, liquid film thickness, and feeding wastewater flowing along the surface of media, is shown in Figure IV-38.

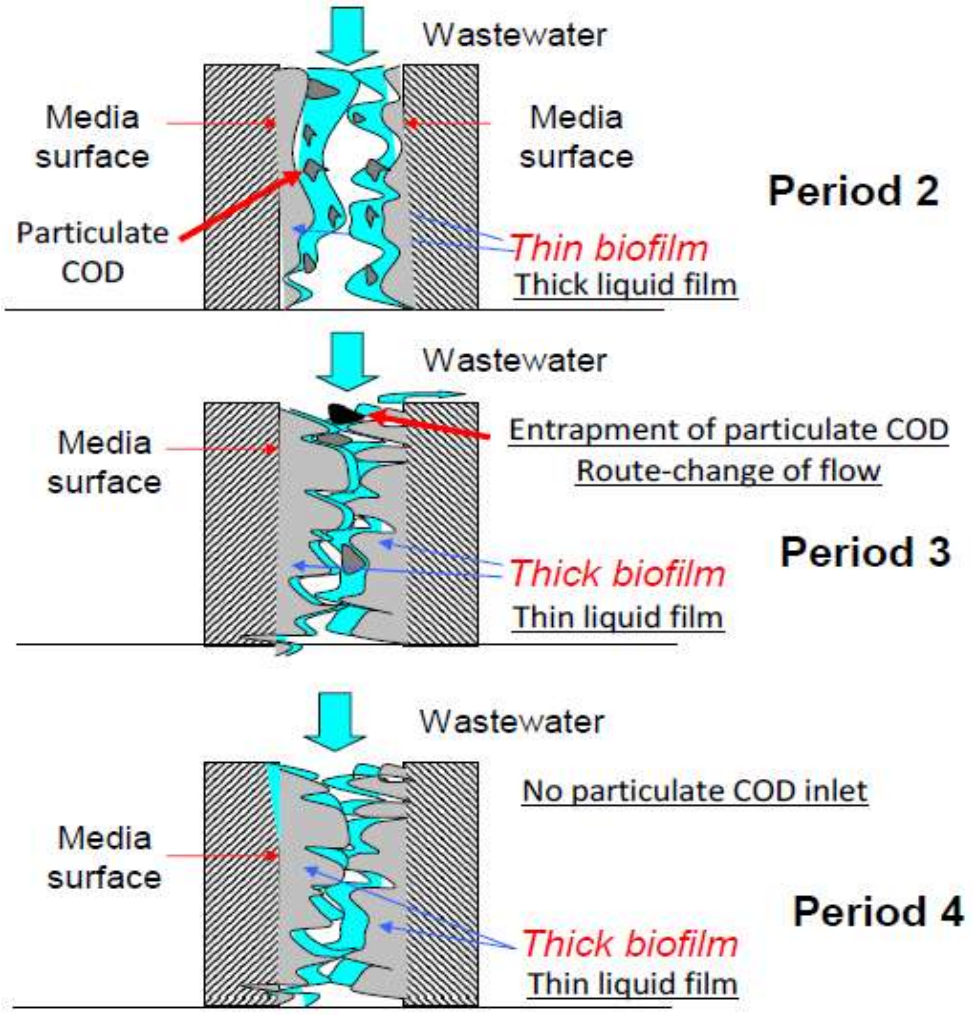

Figure IV- 38: Schematic diagram of biofilm and liquid film during period 2 to period 4.

During low loading conditions (period 2), the biofilm thickness was low, liquid film thickness was larger, the entrapment of particulate substrate was not efficient and Liquid Residence Time (LRT) was short. The removal of particulate COD was thus less efficient. The thick liquid film and short LRT led to less contact time for oxygen and mass transfer. It also led to less time for the hydrolysis of particulate substrate. Hence, the treatment efficiency of COD was not better than during period 3 and 4 (refer to Table IV-2), and the nitrification efficiency was not significantly higher than during period 3 when feeding with high OLR (refer to Table IV-4).

During period 3, with the development of biofilm, the biofilm thickness was much thicker than during period 2. This can reduce the free inter-space among the packing particles and help to retain the water and entrap the particulate substrate efficiently. Moreover, the increase of total packing surface area resulted from the increase of biofilm thickness, leading to thinner

liquid film thickness, as discussed in Chapter 3. However, when feeding the pilot with primary sludge, resulting in longer LRT, because feeding with particulate substrate led to some clogging spots for fluid through the medium particles (particularly where the real biofilm thickness was thick enough to block the inter-space and change the route of flow). The longer LRT and thin liquid film could offer more contact time for both mass transfer and hydrolysis process. Hence during period 3, even when feeding with highly concentrated COD influent, the removal efficiency of COD was greater than for period 2. Even the COD removal performance was significant. However, the nitrification efficiency was no less than in period 2, implying that oxygen supply and transfer were not limited for the nitrification process. The nitrification efficiency also benefited from longer LRT and a thin liquid film.

During period 4, feeding without particulate substrate, the liquid residence time was slightly shorter than during period 3. Even the biofilm thickness was similar to that of period 3. As a result, during period 4, the COD removal (η_{COD}) was less than during period 3, mainly due to less removal of particulate COD and less contact time for hydrolysis and mass transfer. However, the nitrification efficiency was higher than in period 3. This may be caused by the better oxygen supply (more free space) and less inhabitation impact by the particulate COD.

4. Discussion and Conclusion of Chapter

COD was mainly removed in section 1-3; biodegradation of COD mainly occurred in section 1 and hydrolysis mainly in sections 2 and 3. The removal performance decreased gradually along filter. Therefore, sections 4 and 5 play a “polishing” role for COD removal. More surprisingly, for a high OLR, the COD removal capacity is promoted. This promotion was accounted for by the entrapment of particulate COD and better oxygen transfer, as well as longer liquid residence time.

Nitrification occurred mainly in sections 1-3 under all OLR conditions; the role of sections 4 and 5 in nitrification was slight. For low OLR, nitrification mainly occurred in section 2, because in section 1 the heterotrophic growth counteracts nitrification. For high OLR, nitrification still occurred in each section, with no obvious inhibition of nitrification in the first section. This suggests good oxygen supply capacity for this pilot geometry.

Both COD removal and nitrification performance in our study were better than that in a full-scale reactor; even the inlet concentration of COD and ammonia was much higher than in full-scale reactor. The lower flowrate in our pilot could provide a longer LRT and thinner liquid film thickness. Even the competition between heterotrophic bacteria and nitrifying bacteria, nitrification performance was better in our pilot.

Chapter 5

Theoretical study of the Trickling filter using Bio-Win® software

1. Objectives

One objective of this chapter is to evaluate the possibility to describe the behaviour of a MSB by the Biowin® 4.0 software. Hence, the effect of hydraulics and mass transfer on the MSB performances will be briefly studied, looking COD removal and nitrification.

The use of Biowin® 4.0 software gives the possibility to study what could be the effect of a better oxygen mass transfer in the MSB compared to the mono-stage TF.

Finally, simulation results are compared to the biological experimental results obtained in our pilot plant run under various operating conditions.

2. Simulation of a TF and MSB using Biowin

Two operating conditions are simulated: Simul_1000 and Simul_300. These two conditions are characterized by a same OLR and NLR but with two different combinations of (concentration; flow rate):

- Simul_1000:(S_{in}=1000 gCOD/m³; Q_{in} = 0.08 m³/d) giving an OLR of 80 gCOD/m³.d.
- Simul_300:(S_{in}=300 gCOD/m³;Q_{in} =0.267 m³/d) giving a same OLR of 80 gCOD/m³.d

In Biowin software, **the TF reactor** is divided in three sections that are sub-divided in three parts (inlet, inside, outlet). With this spatial division, it is not possible to clearly represent the concentration profiles along the column. To get more insights in these profiles, it has been decided to build the **MSB configuration that consists in five TFs in series**. In that case an accurate concentration profile can be obtained and drawn. Of course the simulation time in this case considerably increases (various days). Hence, simulations had to be stopped before the steady-state can be obtained. It is the reason why the results that are presented in this chapter are often comparing results from TF and MSB model configurations (Figure V-1).

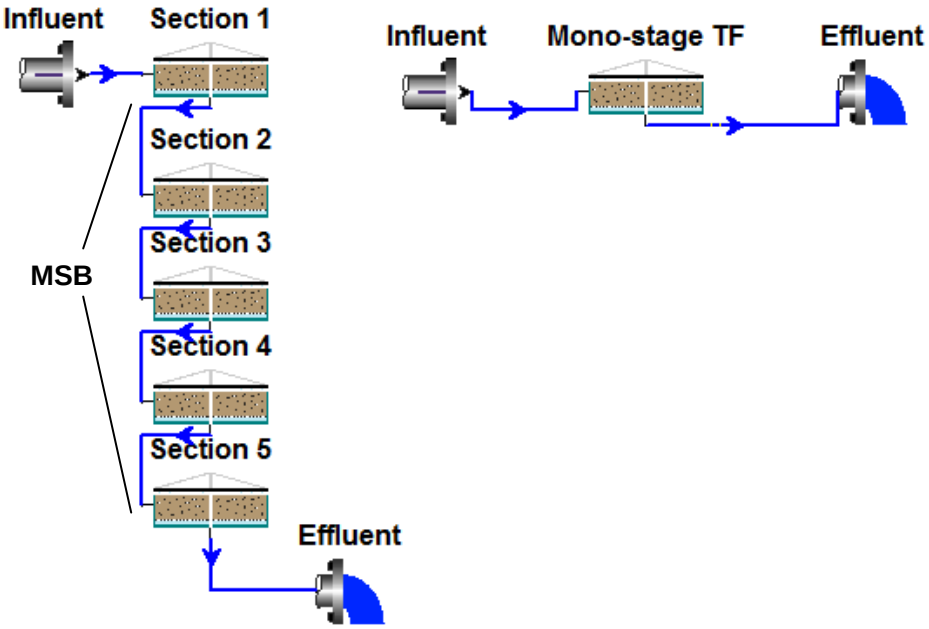

Figure V- 1: The MSB and TF configurations used for simulations

The model used is based on the TF model of Biowin® that is described in the Appendix 2. The default values proposed by Biowin® are in majority used, except for the following parameters: attachment and detachment rates, off-gas oxygen volume fraction, and physical parameters of bioreactor.

Firstly, physical parameters of the bioreactor were adjusted according to that obtained in Chapter 3, with respect to real pilot-scale MSB's physical characteristics. Hydrodynamic parameters such as liquid film thickness and Liquid Residence Time (LRT) were also reset with respect to that obtained in Chapter 3 by hydrodynamic experiments. Table V-1 shows the changes that have been performed on hydrodynamics.

Table V- 1: Adjustment of physical parameters according to hydrodynamic experiments

Parameter	Default value	Used value		remark
		Simul_1000	Simul_300	
Volume (m^3)	20000	0.0126	0.0126	Volume of each section
Area (m^2)	4444.4	0.0314	0.0314	Diameter of 0.2m
Depth (m)	4.5	0.4	0.4	Height of each section
Specific area (m^2/ m^3)	50	400	400	From estimated physical properties
Liquid thickness (mm)	1.25	0.07	0.08	Estimated from hydrodynamic experiments
Max. effective area factor	0.5	1	1	Carrier totally wetted
Liquid Residence Time (h)	300	0.6	0.2	

From table V-1, it can be seen that the only change due to hydrodynamic modification is the liquid thickness that was fixed according to the results in chapter III.

Secondly, the model for oxygen transfer capacity has been chosen. In the first simulations, the driving force of oxygen at different locations in the reactor has been kept constant; We performed the simulation with $6mgO_2/L$ in the liquid film. This leads to a condition where oxygen is not limiting the global biological transformation in the whole filter. Hence we decided to adjust the off-gas oxygen volume fraction equal to that of oxygen supply volume fraction (20.95% of air volume).

Thirdly parameters relative to transport and reactions of solids were changed. Table V-2 compares the default values and the changed values used in this study. The value of detachment rate was adjusted to equal that of attachment rate.

Table V- 2: Default and used values relate to mass transport and biomass reactions

Parameter	Default value	Used value	remark
Attachment rate (g/m^2 d)	80	80	
Detachment rate (g/m^3 d)	8×10^4	80	Too high default value
Hydrolysis (d^{-1})	2.1	2.1	
Biomass decay (d^{-1})	0.62	0.62	

Influent compositions are given in Table II-3 of the M&M section for the low and high organic loading conditions tested.

In this chapter, results of the simulation only give data from steady-state operating conditions (TF configuration) or results after a certain time of operation when simulations required too much time (MSB configuration).

Part 1. Simulations of MSB under same OLR and NLR

It is here recalled that two conditions of loading rates were applied to the reactor. The increase in OLR and NLR was achieved by increasing COD and TKN concentrations in the influent; while the flow rate was kept constant. This is an important point to consider because it is obvious that hydraulic and the liquid concentrations in contact with the biofilm may be key operating conditions that determine the MSB performances. In order to appreciate the impact of these two conditions, results of simulations are now presented that compare two MSB operating at the same OLR and NLR but with two different combinations of (concentration; flow rate). Simul_1000 and Simul_300 will refer to the two tested conditions:

Simul_1000: (S_{in}=1000 gCOD/m^3; Q_{in} = 0.08 m^3/d) giving an OLR of 80 gCOD/m^3.d.

Simul_300: (S_{in}=300 gCOD/m^3; Q_{in} =0.267 m^3/d) giving a same OLR of 80 gCOD/m^3.d

3.1.1 COD removal for two flow rates but under a same OLR

Figure V-2 represents the spatial evolution of COD fractions inside the TF in the case of simul_1000 (FigureV-2 a) and in the case of Simul_300 (Figure V-2 b).

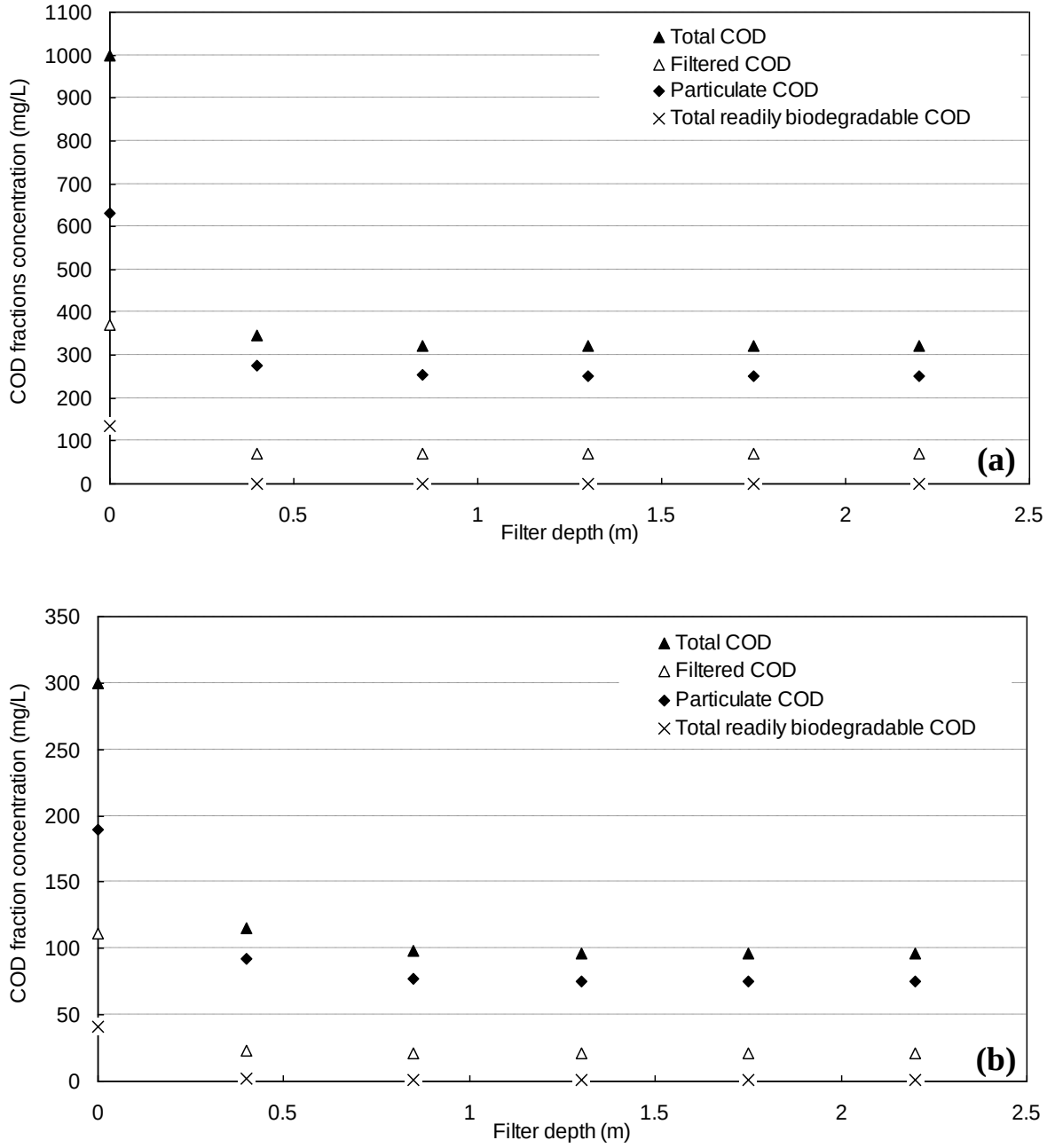

Figure V- 2: Spatial evolution of COD fractions inside the MSB both of simulation 1 (1000 gCOD/m³; 0.08 m³/d) and simulation 2(300 gCOD/m³; 0.267 m³/d).

From Figures V-2 a and b, the COD is mainly removed in section 1 (depth from 0 to 0.4m). For both flow regimes, nearly all the readily biodegradable COD (S_B) is quickly removed (value at the outlet close to 1 mg/L). In addition, the particulate COD is the major component of the total COD in the outlet that is logical because the produced biomass is note separated.

Table V-3 represents the concentrations at the outlet of the reactor of the main COD fractions (total COD, filtered COD, particulate COD, total unbiodegradable particulates from cell decay-Xu,e) and the corresponding fluxes for the two simulated cases.

Table V- 3: Concentrations of different COD fractions in the outlet of the MSB for Simul_1000 and Simul_300

Outlet concentrations (mg COD/L) and fluxes (gCOD/d)	Simul_1000 Concentrations (mg COD/L)	Simul_1000 Fluxes gCOD/d	Simul_300 Concentrations (mg COD/L)	Simul_300 Fluxes gCOD/d
Total COD	322	25.76	96	25.63
Soluble COD	69	5.52	21	5.61
Particulate COD	253	20.24	75	20.03
Total Xu,e	7.5	0.6	2.2	0.6

Xu,e is unbiodegradable particulates from cell decay

Similar outlet fluxes of around 26 g/d for total COD and an identical physical fraction of the COD are found for the two conditions.

COD removal efficiency, calculated only using the soluble COD in the outlet, gives η_{COD} = 93% for both conditions. Therefore, from the model simulations in the range of flow rates tested, COD degradation will be load-dependent but not affected by the concentration/flow rate distribution of the load.

The particulate COD concentrations are however strongly different (253 mg/l versus 75 mg/l) that may be a problem with respect to the regulations. Sludge production is equivalent for both conditions.

The particulate COD in the outlet comes from both biomass production and non-treated particulate COD; therefore, we have to consider and differentiate the fraction of unbiodegradable particulate COD that comes from the cell decay and from the influent the remaining biodegradable particulate COD and cell particulate COD.

It is interesting to compare the results on COD removal using the MSB model to that obtained using the TF model (Table V-4).

Table V- 4: Concentrations of different COD fractions in the outlet of the TF for Simul_1000 and Simul_300

Outlet concentrations (mg COD/L) and fluxes (gCOD/d)	Simul_1000 Concentrations (mg COD/L)	Simul_1000 Fluxes gCOD/d	Simul_300 Concentrations (mg COD/L)	Simul_300 Fluxes gCOD/d
Total COD	298	23.84	90	24.03
Soluble COD	51	4.08	16	4.27
Particulate COD	247	19.76	74	19.76
Total Xu,e	7.2	0.6	2.2	0.6

Xu,e is unbiodegradable particulates from cell decay

The outlet concentrations of the different COD fractions are much closed for the two model conditions. There are slightly lower for the TF model because the steady state condition is reached in that case.

3.1.2 General pathway of COD

COD mass balance is shown in Figure V-3 for the two simulated cases using the MSB configuration. For these calculations, steady state conditions are not reached, i.e. COD accumulation occurs. Using the results the following feature can be underlined: a net sludge production characterized by a yield coefficient Y_{obs} of 0.25 gCOD/gCOD that gives 0.176 gVSS/gCOD. This value is rather low and is explained by accumulation occurring in the media.

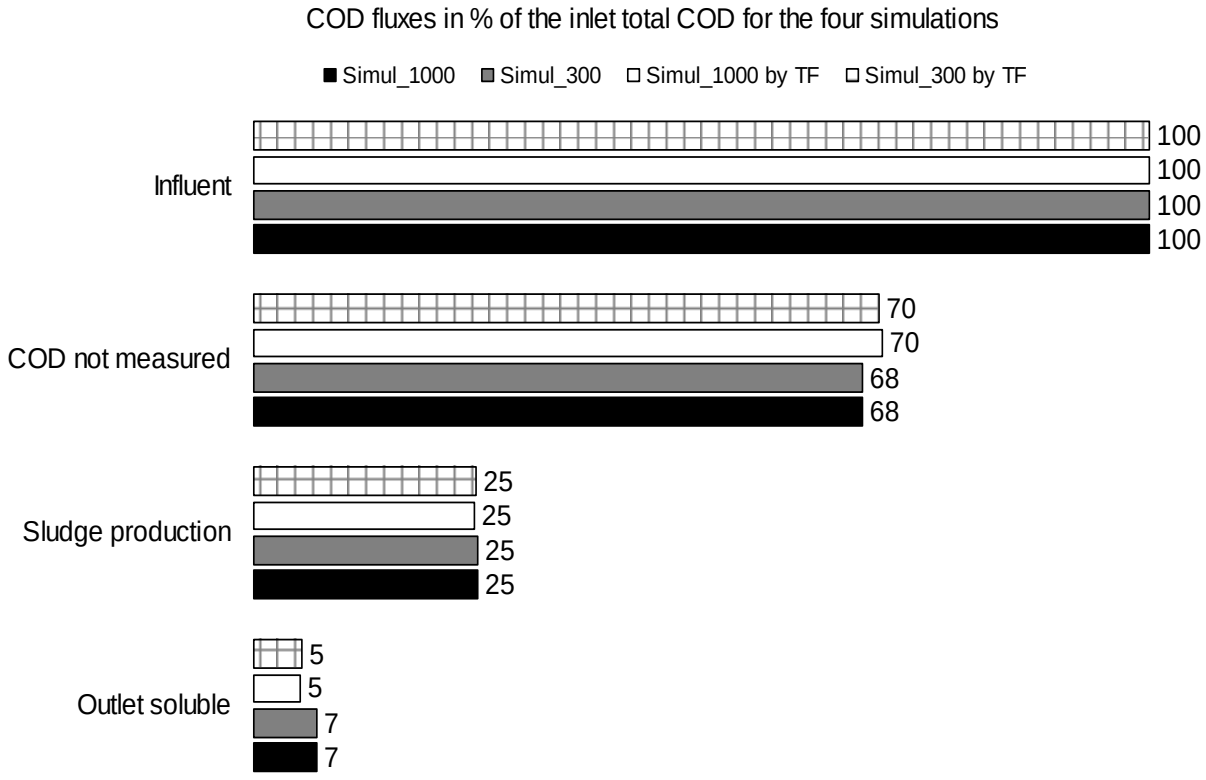

Figure V- 3: Pathways of COD becoming

Figure V-3 shows that with mono-stage TF simulations, lower soluble fractions at the outlet were obtained, however with MSB simulations, these fractions at the outlet are slight higher. This should due to the duration of MSB simulations, which have not attained the steady-state. However, no obvious differences were between Simul_1000 and Simul_300 for the same bioreactor simulations. This implies that no significant effect of OLR on the COD removal for Biowin simulations, even under different hydraulic conditions.

3.1.3 Local pathway of COD

With the inlet and outlet concentrations of different COD components for each section, it is possible to get more insights in the transformations of each fraction of the total COD, such as readily biodegradable COD (S_B), soluble unbiodegradable COD (S_U), slowly biodegradable COD (X_B), particulate unbiodegradable COD (X_U), colloidal biodegradable COD (Xcolloid.) and heterotrophic biomass (X_{OHO}).

An example of section 1 in the case of simulation Simul_1000 is plotted in Figure V-4 to represent the transformation of the COD components.

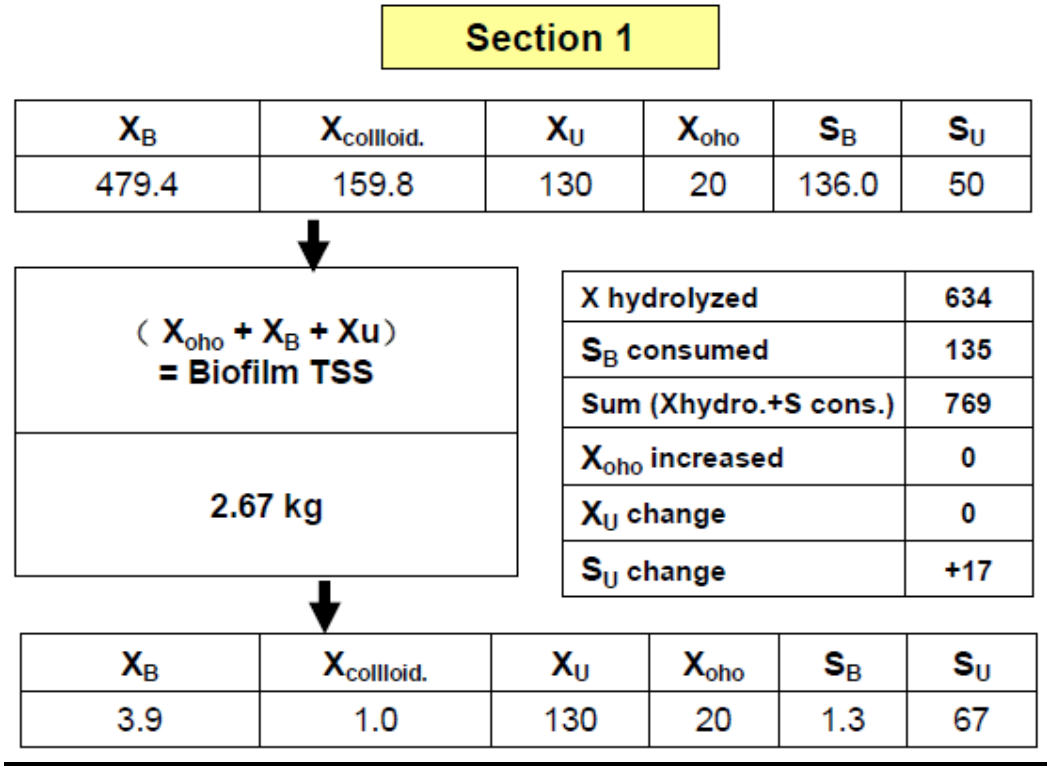

Figure V-4. Mass balances on the section 1 of the MSB configuration

Furthermore, the transformation pathways of COD components in each section under both flow rate conditions are shown in Table V-5.

Table V- 5: Local pathways of COD in the MSB for Simul_1000 and Simul_300

Simul_1000	**X_B**	**Xcollloid.**	**X_U**	**Xoho**	**S_B**	**S_U**	X hydrolyzed	S_B consumed	Sum (Xhydro.+S cons.)	Xoho net change	X_U change	S_U change
Influent	479	160	130	20	136	50						
Section 1	4	1	130	20	1	67	634	135	769	0	0	+17
Section 2	0	0	130	1	1	68	5	0	5	-19	0	+1
Section 3	0	0	130	0	1	68	0	0	0	-1	0	0
Section 4	0	0	130	0	1	68	0	0	0	0	0	0
Section 5	0	0	130	0	1	68	0	0	0	0	0	0
Simul_300	**X_B**	**Xcollloid.**	**X_U**	**Xoho**	**S_B**	**S_U**	X hydrolyzed	S_B consumed	Sum (Xhydro.+S cons.)	Xoho net change	X_U change	S_U change
Influent	144	48	39	6	41	15						
Section 1	5	1	39	12	2	20	185	39	224	+6	0	+5
Section 2	0	0	39	2	1	20	6	1	8	-10	0	0
Section 3	0	0	39	0	1	20	0	0	8	-2	0	0
Section 4	0	0	39	0	1	20	0	0	8	0	0	0
Section 5	0	0	39	0	1	20	0	0	8	0	0	0

The particulate biodegradable COD is quickly removed in the two first sections of the filter. Biomass released from section one to section two is significant but this biomass is caught by the following section. No X_{OHO} is released out of the filter. The CODp released at the outlet of the filter is mainly the unbiodegradable CODp.

3.2 Partial Conclusion on COD removal

Simulations have been performed using the Biowin® software to represent two hydraulic conditions (two flow rates) but keeping the OLR constant. During these simulations, the default parameters were mainly used. However a few parameters were adapted such as attachment and detachment coefficients, liquid film thickness to match with the considered experiments. Dissolved oxygen in the liquid film was fixed at 6 mg/l that means that the system is not limited by this compound.
The use of a MSB configuration for simulation help to study what is occurring inside the filter but is time consuming and steady state is not reached after several days of simulations.
Simulation with the TF configuration allows to reach the steady state and thus to get the real performances of the system.

For conditions (Simul_1000 and Simul_300), a very quick degradation or capture (attachment) of the CODB occurs in the first two sections of the filter. A good COD removal $\eta COD = 93\%$ is reached. Sludge production, similar for both conditions, is low and results mainly from the release of the unbiodegradable particulate COD. Accumulation of COD occurs inside the filter that certainly will lead to a reduction of the porosity and to clogging if no equilibrium is reached between accumulation and degradation. This process of clogging is not taken into account by the model and hence is not detected.

4. Nitrogen removal for two flow rates but under a same OLR

4.1 Objective

On the same simulation case-studies, i.e. Simul-1000 and Simul_300, using both the MSB and TF configurations, the feature of nitrogen removal is studied. Nitrogen can be removed mainly by growth and nitrification, denitrification being normally absent if sufficient aeration is provided (to be demonstrated). Accumulation of organic nitrogen inside the filter may also

occur. Hence, nitrogen removal must be characterized through the organic nitrogen becoming and the N-NO_X production. For the former, the ammonification rate, thus the hydrolysis and the lysis rates, and the growth rate are key processes to describe the becoming of TKN along the filter. For the later, nitrification, competition for space and oxygen certainly determines AOB and NOB activity distribution along the filter. The approach in this section is to describe these processes based on mass balances performed on the MSB configuration (steady state not completely achieved) and on the TF configuration (Steady state achieved).

4.2 Nitrogen removal in the MSB configuration

Figure V-4 represents the spatial evolution of ammonia and nitrate inside the MSB in the case of simul_1000 (Figure V-4 a) - NLR of 12.3 gN/d and in the case of simul_300 (Figure V-4 b) -NLR of 12.3 gN/d. The ratio CODt on ammonia was kept at 10 for the two simulations. It is remembered that oxygen concentration is kept at 6 mg/l in the liquid all along the filter depth. Nitrogen concentration in the influent is 151.51 mg/l. Table V-6 summarizes the concentrations and fluxes observed at the outlet of the filter.

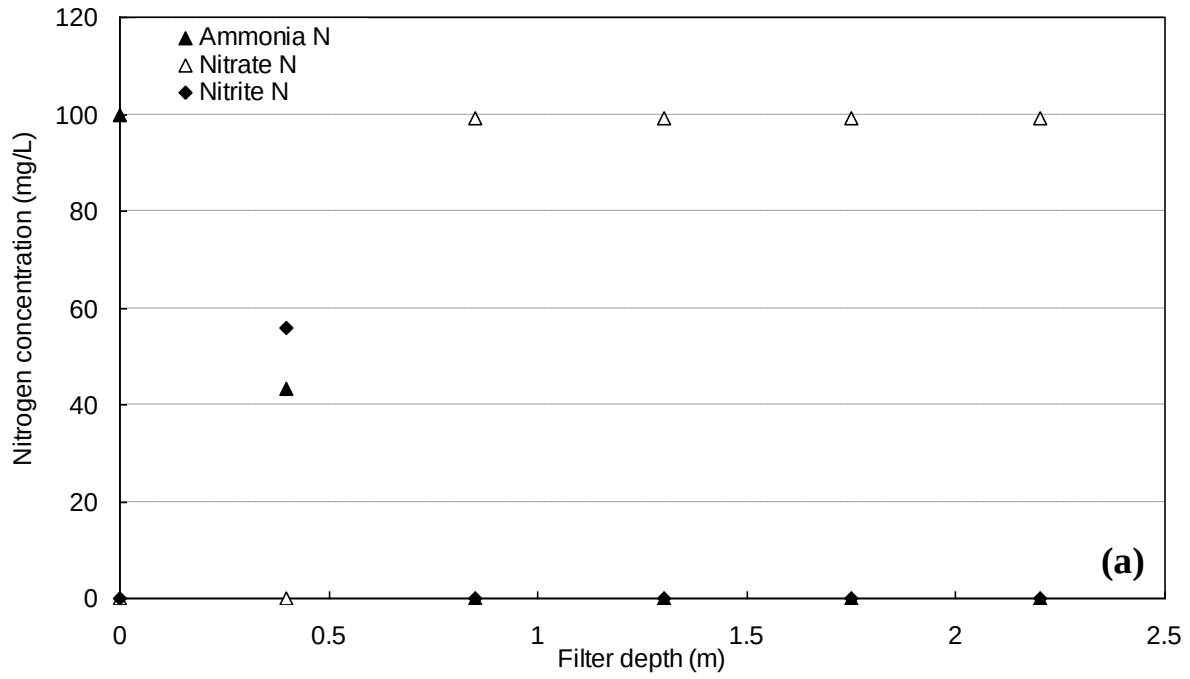

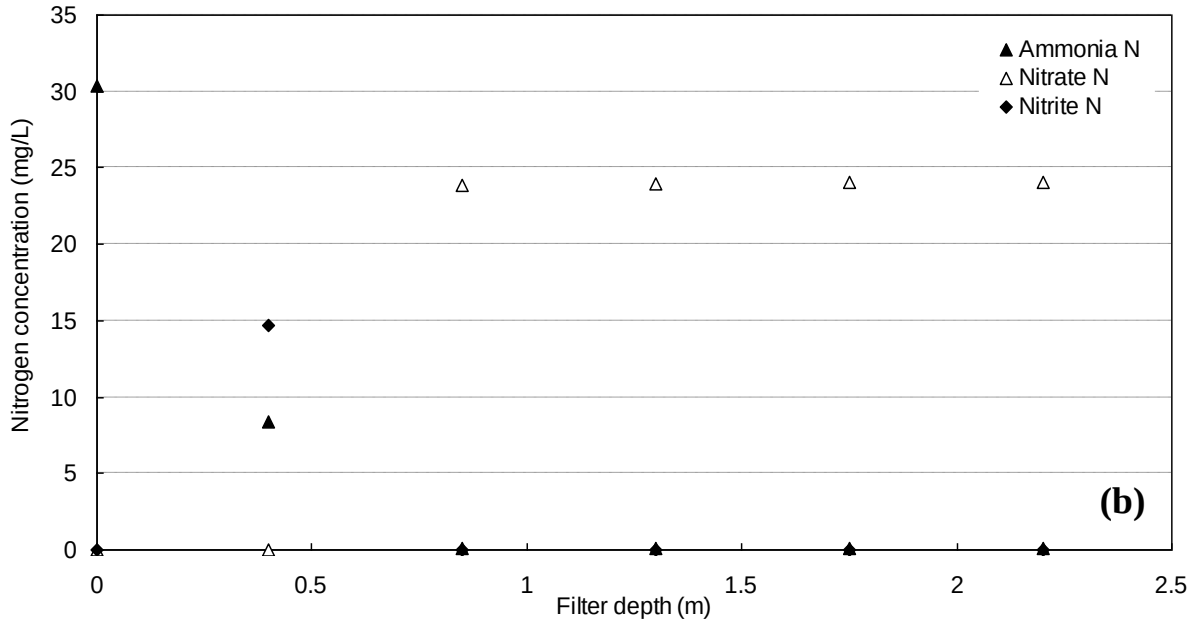

Figure V- 4: Spatial evolution of ammonia and nitrate inside MSB both simulation 1 and simulation 2

Table V- 6: Concentrations of different nitrogen fractions in the outlet of the MSB for Simul_1000 and Simul_300

Outlet concentrations (mg N/L) and fluxes (g N/d)	Simul_1000 Concentrations (mg N/L)	Simul_1000 Fluxes (g N/d)	Simul_300 Concentrations (mg N/L)	Simul_300 Fluxes (g N/d)
Total nitrogen	116.26	9.3	29.59	6.83
Soluble nitrogen	3.99	0.319	1.68	0.45
Particulate nitrogen	13.13	1.05	3.87	1.03
TKN	17.12	1.37	5.55	1.44
Nitrate	99.11	7.93	24.01	6.41
Accumulated TKN	-	2.82	-	4.38
Removal percentages				
% Outlet TKN		11		12
% Nitrified		65.4		52.3
% Accumulated		23.3		35.7

From Figure V-4 a and b, and Table V-6, a similar behavior is noted: ammonia concentration sharply decreased in the first two sections. Nitrite is first produced in the first sections and then nitrate is the only product that accumulates in the liquid. Though the features of NH_4^+ and N-NO_X are similar for the two simulations, significant differences in the amount of TKN nitrified is observed. As it will be seen in the next paragraph, it is because steady-state is not achieved in the simulations using the MSB configuration.

4.3 Comparison of Nitrogen removal in the TF and MSB configurations

Table V-7 summarizes the concentrations and fluxes observed at the outlet of the filter by mono-stage TF simulations.

Table V- 7: Concentrations of nitrogen fractions in the outlet of the mono-stage TF for Simul_1000 and Simul_300

Outlet concentrations (mg N/L) and fluxes (g N/d)	Simul_1000 Concentrations (mg N/L)	Simul_1000 Fluxes (g N/d)	Simul_300 Concentrations (mg N/L)	Simul_300 Fluxes (g N/d)
Total nitrogen	140.45	11.24	43.49	11.61
Soluble nitrogen	4.25	0.34	2.24	0.60
Particulate nitrogen	12.76	1.02	3.84	1.03
TKN	17.01	1.36	6.08	1.62
Nitrate	123.41	9.87	37.39	9.98
Accumulated TKN	-	0.88	-	0.67
Removal percentages				
% Outlet TKN		11		13
% Nitrified		81.5		81.3
% Accumulated		7.3		5.5

Based on the total TKN mass balance when the TF simulation configuration is used (steady-state reached), similar conversion yields are achieved for Simul_1000 and Simul_300 confirming that the difference in hydraulic is not influencing the N removal performances.

The difference between the MSB and the TF simulation configuration results from the ammonification processes that are further achieved when the duration of simulation is not limited (steady state reached). Hence, the majority of the biodegradable inlet nitrogen is converted to nitrate. These results point out the importance of the dynamic of ammonification processes in a trickling filter.

In the case where dissolved oxygen concentration in the liquid film is high, complete nitrification is achieved in the first sections of the filter. In the first section however, only nitritation occurs due to competition for oxygen and space inside the biofilm.

The Figure V-5 summarizes the becoming of nitrogen fractions for MSB and TF simulation configurations.

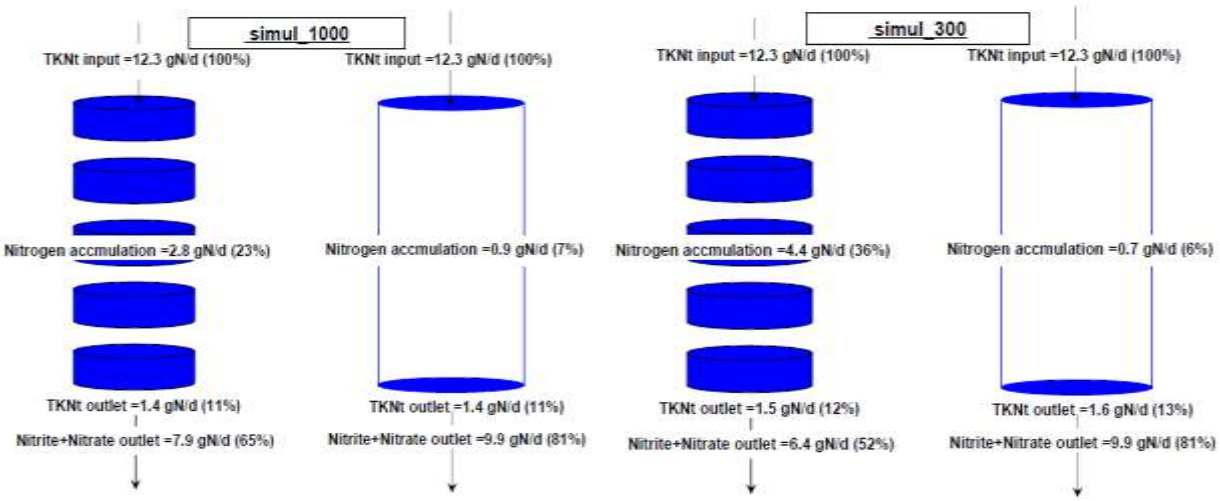

Figure V- 5: Comparison between MSB simulation and Mono-TF simulation with respect to the nitrogen removal

From Figure V-5, both in simul_1000 and simul_300, the mono-stage TF simulations represent higher nitrite & nitrate production at the final outlet of filter than MSB simulations. The nitrogen accmulation is thus lower than the MSB simulations. These differences is due to the simulation durations to achieve the steady-state, the simulations by MSB have not reach the final steady-state compared to the mono-stage TF simulations.

4.4 Local feature of nitrogen removal

With the inlet and outlet concentrations of different nitrogen components, we can investigate the transformation of each fraction in total TKN. Total nitrogen components include the ammonia-nitrogen, nitrite-nitrogen, nitrate-nitrogen, particulate biodegradable organic nitrogen (Xs,n), particulate inert organic nitrogen (Xi,n), soluble biodegradable organic nitrogen (Ss,n), soluble inert organic nitrogen (Si,n), nitrogen biomass (Noho) including Ammonia Oxidizing Biomass (AOB) and Nitrite Oxidizing Biomass (NOB) (where Noho=AOB+NOB).

An example of section 1 in the case of simulation 1 is plotted in Figure V-6 to represent the transformation of different COD components.

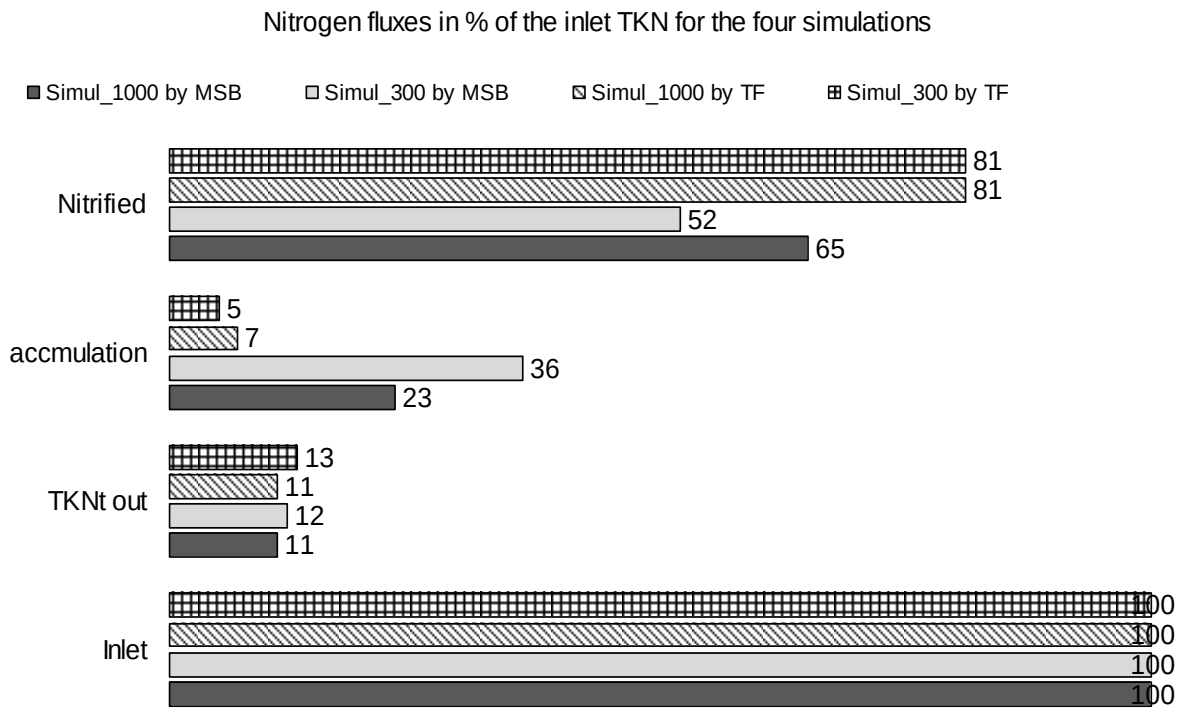

Figure V- 6: Pathways of nitrogen becoming

Similarly, the pathways of nitrogen transformation in each section under two flow conditions were shown in the Table V-8.

Table V- 8: Local pathways of nitrogen transformation

Simulation 1	Xs,n	Noho	Xi,n	ammonia	Ss,n	Si,n	Nitrite-N	Nitrate-N	N nitrified	Organic N hydrolyzed	Ammonia decrease	Noho assimilated	Xi,n change	Si,n change
Influent	21	0	5	100	21	3	0	0						
Section 1	1	2	5	64	1	3	30	0	30	41	36	40	0	0
Section 2	0	0	5	0	1	3	0	93	63	0	64	2	0	0
Section 3	0	0	5	0	1	3	0	93	1	0	0	1	0	0
Section 4	0	0	5	0	1	3	0	94	0	0	0	0	0	0
Section 5	0	0	5	0	1	3	0	94	0	0	0	0	0	0
Simulation 2	Xs,n	Noho	Xi,n	ammonia	Ss,n	Si,n	Nitrite-N	Nitrate-N	N nitrified	Organic N hydrolyzed	Ammonia decrease	Noho assimilated	Xi,n change	Si,n change
Influent	6	0	1	30	6	1	0	0						
Section 1	0	0	1	15	1	1	11	0	11	12	15	12	0	0
Section 2	0	0	1	0	1	1	0	26	14	0	15	1	0	0
Section 3	0	0	1	0	1	1	0	26	0	0	0	0	0	0
Section 4	0	0	1	0	0	1	0	26	0	0	0	0	0	0
Section 5	0	0	1	0	0	1	0	26	0	0	0	0	0	0

Moreover, according to the calculation of both COD and nitrogen mass balance, we can estimate the ratio between accumulated nitrogen and accumulated COD. With initial CODt and TKNt concentrations, we calculated the concentration of accumulated COD and accumulated nitrogen. The ratio between the two elements was found equal to 0.1 mgN/mg $_{BiomassCOD}$ under the two flow conditions.

4.5 Spatial distribution of heterotrophic and nitrifying bacteria inside the biofilter

In addition, spatial evolution of the Ordinary Heterotrophic Organisms (OHO) biomass and Ammonia Oxidizing Biomass (AOB) inside MSB in the case of simulation 1 & 2 are shown in Figure V-7 and Figure V-8, respectively.

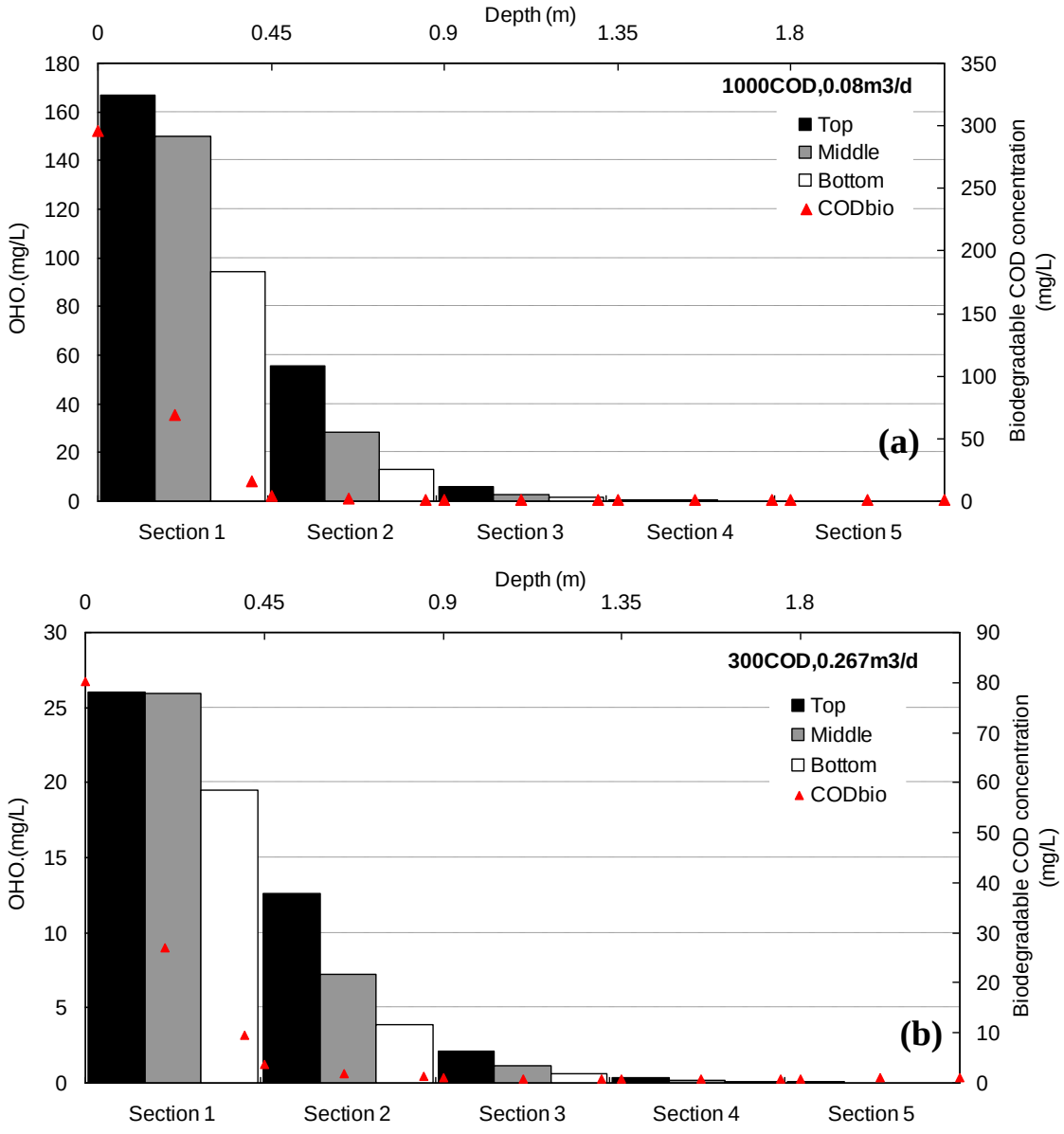

Figure V- 7: Spatial evolution of OHO in the case of simulation 1 and 2.

As shown in Figures V-7 (a) and (b) implementation of heterotrophic biomass follows the degradation of COD_B. A large part of the reactor is of low efficiency because of a low concentration of X_{OHO}.

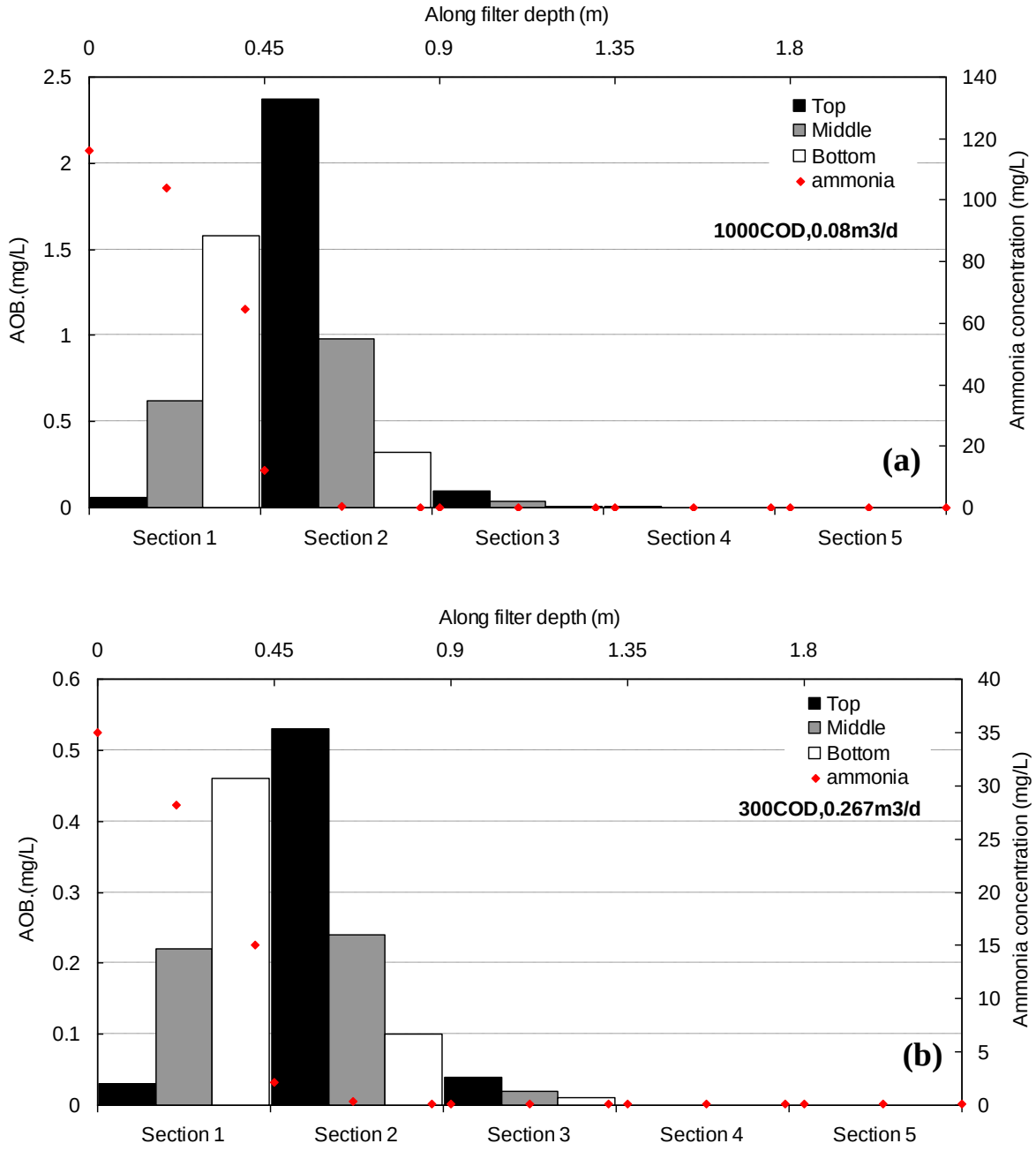

Figure V- 8: Spatial evolution of AOB in the case of simulation 1 and 2

Development of AOB mainly in section 2 is confirmed for both simulated situations (Figure V-8 (a) and (b)). No great difference on nitrification is observed depending on the used flow rate.

4.6 Discussion and Conclusion

By the use of two simulations at the same OLR and NLR but with two different combinations of COD inlet concentration and flow rate, a first evaluation of the TF and MSB models from Biowin 4 software has been done. For the tested conditions a quick degradation of the biodegradable COD (COD_B) occurs in the first two sections of the filter. Sludge production, similar for both conditions, is low and results mainly from the release of the unbiodegradable particulate COD (Xu). This is a rather idealistic feature. Confrontation to real data will help us to calibrate the model.

Based on the total TKN mass balance when the TF simulation configuration is used (steady-state reached), similar conversion yields are achieved for Simul_1000 and Simul_300 confirming that the difference in hydraulic is not influencing the N removal performances.

The difference between the MSB and the TF simulation configuration results from the ammonification processes that are further achieved when the duration of simulation is not limited (steady state reached). Hence, the majority of the biodegradable inlet nitrogen is converted to nitrate. These results point out the importance of the dynamic of the ammonification processes in a trickling filter.

In the case where dissolved oxygen concentration in the liquid film is high, complete nitrification is achieved in the first sections of the filter. In the first one however, only nitritation occurs due to competition for oxygen and space inside the biofilm

Part 2. Effect of oxygen mass transfer in the MSB compared to the TF

MSB differs from a conventional TF by the oxygen exchange potential. Indeed, due to the greater open space, the gas renewal could be higher in the MSB compared to that occurring in the TF. Moreover, in the MSB, as the height of each section is small, the oxygen concentration in bulk liquid could be the same from the bottom to the top of the filter and within a same section. Indeed, the driving force of oxygen transfer could be the same at all the locations in each section if the same Oxygen Uptake Rate (OUR) is achieved (same residual DO) (see Chapter 3, oxygen transfer coefficient estimation).

We used a simulation approach to study the effect of air flow rate on the competition between heterotrophic and nitrifier activities. MSB configuration has been used even if incomplete ammonification occurred due to the limitation of simulation time. The use of this configuration allows following the distribution of heterotrophic and autotrophic biomasses inside the global filter and also the evolution of chemical concentrations (COD, ammonia, nitrite and nitrate).

5.1 Effect of air flow rate on dissolved oxygen concentration

In the case of an Organic Loading Rate (OLR) of 80 gCOD/d and a Nitrogen Loading Rate (NLR) of 12.2 g TKN/d, different air flow rates were applied. Simulations were used in order to evaluate the resulting dissolved oxygen concentration that is found in the bulk liquid trickling on the media. The Figure V- 9 and 10 give the dissolved oxygen concentration in the outlet liquid of the 1st and 2nd sections for the applied air flow rates.

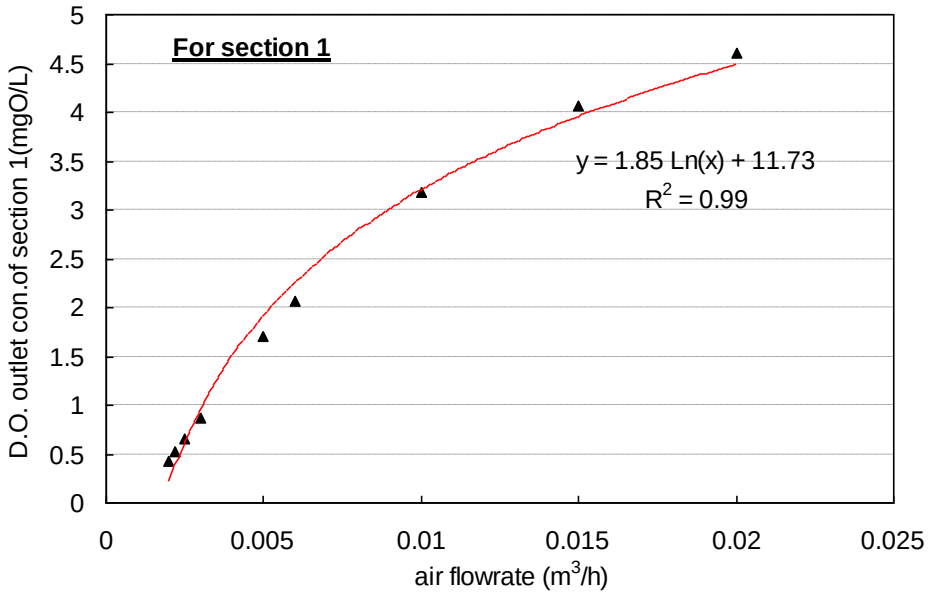

Figure V- 9: Residual dissolved Oxygen concentration at the outlet of section 1 under different air flow rate inputs

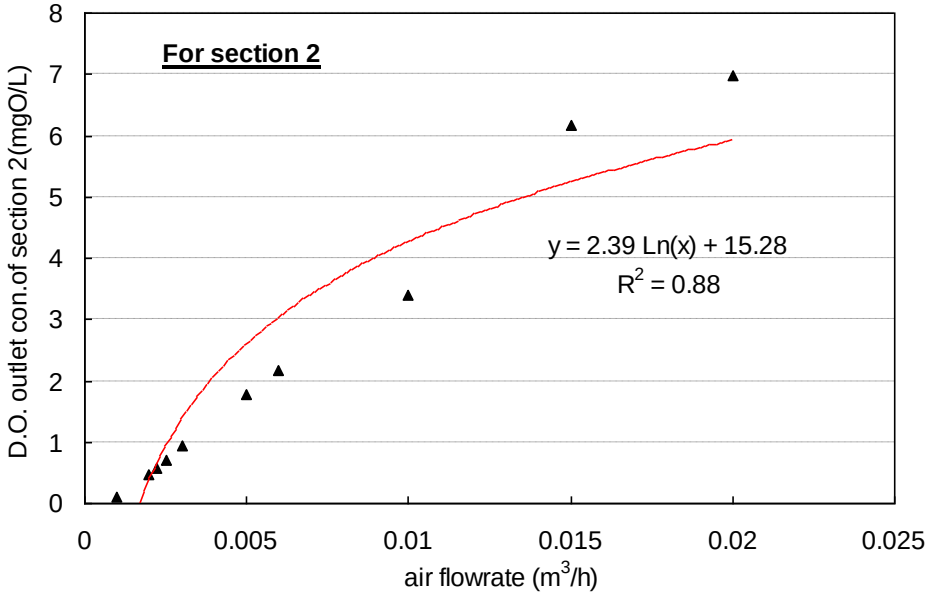

Figure V- 10: Residual dissolved oxygen concentration at the outlet of section 2 under different air flow rate inputs

Figure 9 and 10 show that increase air flow rate could certainly increase the residual dissolved oxygen concentration at the outlet. However, when the air flow rate is over 0.015 m^3/h, the trend of residual DO at the outlet will reach the saturation concentration of oxygen.

In the Figure V- 11 a,b,c, the distribution of COD_B and X_{OHO} along the filter for three air flow rates imposed at the top of each sections are represented. Figure V-12 a,b,c represent the distribution of ammonia concentration and X_{AOB} along the filter for three air flow rates imposed at the top of each sections.

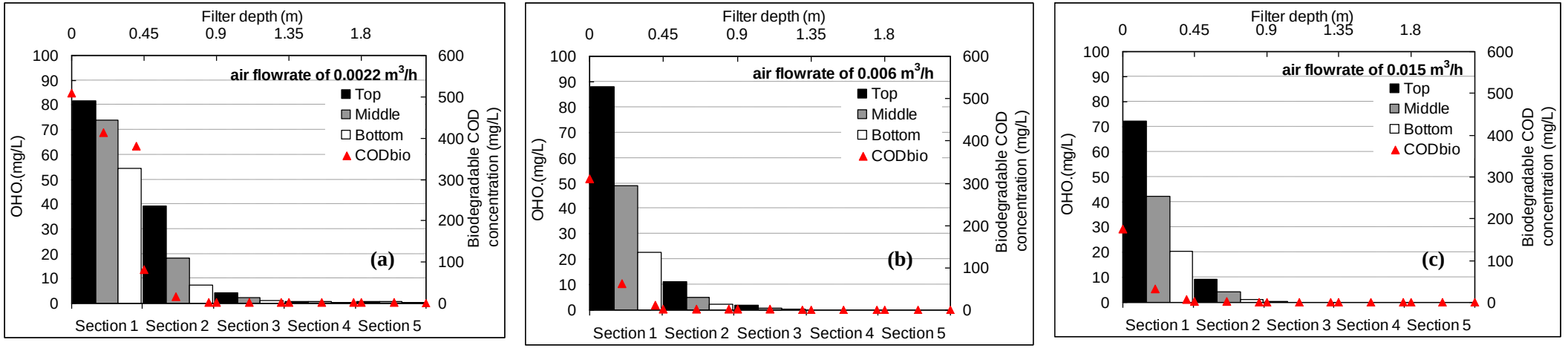

Figure V- 11: Distribution of biodegradable COD and OHO biomass

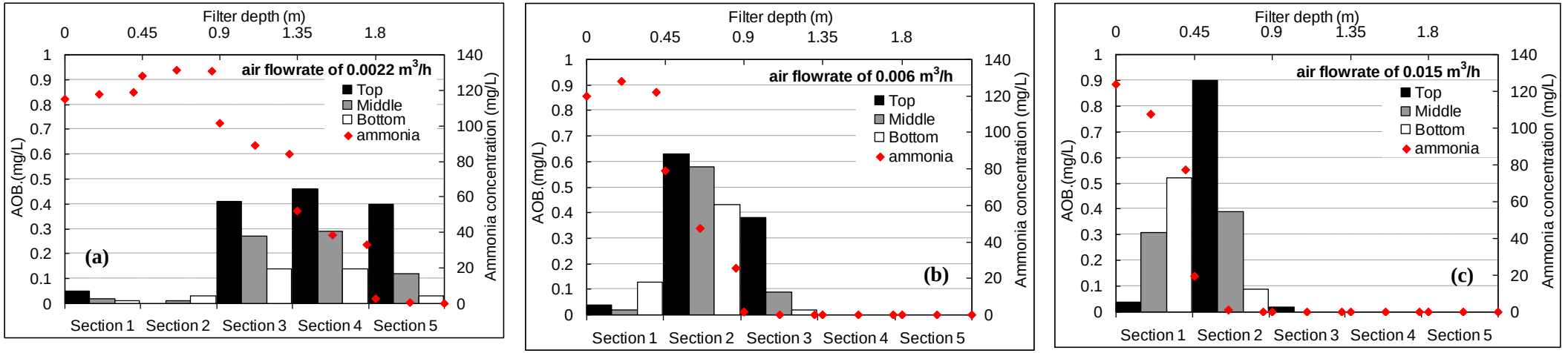

Figure V- 12: Distribution of ammonia and AOB biomass

Good correspondence between concentration profiles and cells distribution is noted. Over an air flow rate of 0.006 m^3/h, the COD removal feature inside the filter is not affected. On the contrary, at an air flow rate of 0.0022 m^3/h, oxygen limitation in the first two sections leads to a slower COD degradation that is displaced to the following sections. In the case of nitrification, the decrease in the air flow rate systematically leads to a spatial shift in ammonia removal.

In addition, simulations with various oxygen inputs concentrations for oxygen modeling were carried out to investigate the ammonia-nitrogen removal distribution inside the filter. The estimated height of filter, where 100% of ammonia was removed is plotted in Figure V-13 against the input oxygen concentrations.

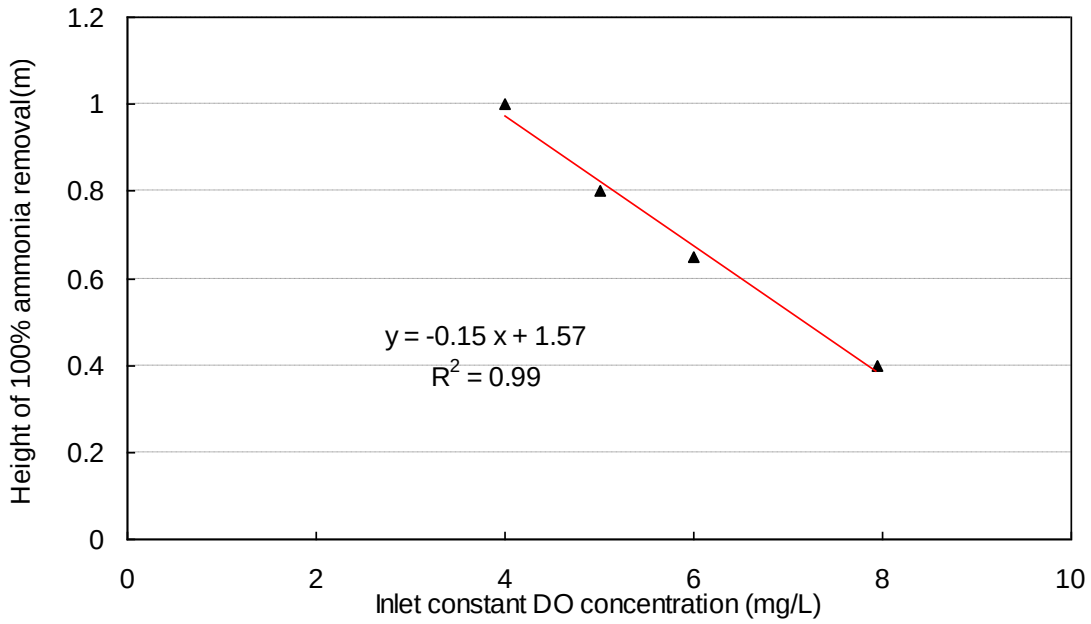

Figure V- 13: Estimated height in MSB, where 100% of ammonia removal under different constant input oxygen concentrations

Obviously, increase the input oxygen concentration decreases the height where ammonia is completely removed. The good linearity of trend can help to predict the oxygen demand at different depth.

5.2 Heterotrophic growth and nitrification limitation in the biofilm

The heterotrophic bacteria grow much faster than nitrifier. The dependence of nitrification on bulk phase COD concentrations is commonly explained with faster growing heterotrophic bacteria dominating towards the surface of biofilm. Nitrifiers tend to grow deeper in the

biofilm and they would be oxygen-limited if oxygen diffusing into the biofilm is consumed by heterotrophic growth (Wanner and Gujer 1985; Zhang et al. 1994). Consequently, in order to achieve high nitrification efficiency, the organic loads should be well monitored in order to limit the competition and maintained nitrification. In addition, both theoretical and experimental studies by (Stenquist et al., 1974) showed that because of the competition between heterotrophic bacteria and nitrifying bacteria, nitrification is not initiated until the $COD_{soluble}$ less than 27mg/L or soluble $CBOD_5$ less than 20 mg/L. This is a too rapid shortcut and it is necessary to better study the conditions where nitrifying activity is affected by heterotrophic growth.

A simple method to predict the potential for coexistence of heterotrophic and nitrifying bacteria is based on calculating the limiting substrate of heterotrophic bacteria (Gönenç and Harremoës, 1990). The key assumption is to consider the biofilm as the layered structure and the oxygen limitation can be predicted from the Equations as:

$$\gamma_{S,O_2} = \upsilon_{S,O_2} \bullet \frac{D_S}{D_{O_2}} \bullet \frac{S_{LF,S}}{S_{LF,O_2}} \quad \text{And} \quad \upsilon_{S.O_2} = \frac{r_S}{r_{O_2}} = \frac{1}{\left(1 - Y_{Het,O_2}\right)} \upsilon_{n,O_2} = \frac{r_{NH4}}{r_{O_2}} = \frac{1}{4.57 - Y_{Auto,O_2}}$$

where:

γ_{S,O_2} -heterotrophic growth convection coefficient

D_S and D_{O_2} - the diffusion coefficients for organic substrate and oxygen

$S_{LF,S}$ and S_{LF,O_2} - organic substrate and oxygen concentrations at the surface of the biofilm

$\upsilon_{S.O_2}$ -stoechiometric coefficient between organic substrate and oxygen consumption

r_S and r_{O_2} - the consumption rate of organic substrate and oxygen

Y_{Het,O_2} - The coefficient of heterotrophic bacteria conversion

3 cases of limitation with respect to γ_{S,O_2} :

1) When γ_{S,O_2} <1, the organic substrate is potentially limited inside the biofilm, heterotrophic growth is limited, so oxygen can penetrate all through the biofilm, which is considered as the substrate-limited regime;
2) When γ_{S,O_2} >1, the oxygen is potentially limited inside the biofilm, the organic substrate can diffuse through the interface; which indicates oxygen limitation for heterotrophic growth and counteract of the nitrifier bacteria. This is the oxygen-limited regime.

3) When $\gamma_{S,O_2} \approx 1$, both the oxygen and the organic substrate are both limited inside the biofilm.

In view of the 3 regimes above, there are mainly 3 types of biofilm that developed under different coefficient conditions: Heterotrophy Biofilm; Autotrophy Biofilm and Autotrophy & Heterotrophy Biofilm. Some researches on the coefficient γ_{S,O_2} and biofilm type are shown in Table V-9.

Table V- 9: Coefficient γ_{S,O_2} and the biofilm nature under this condition from literatures

Reference	γ_{S,O_2} coefficient	Nature of biofilm
(Zhang and Bishop, 1994)	5-21	Heterotrophy biofilm
	2-7	Autotrophy & Heterotrophy biofilm
	-	No biofilm
(Ohashi, et al. 1995)	Owing to the DO in liquid is not specified that coefficient cannot be calculated	Autotrophy & Heterotrophy biofilm
(Okabe et al. 1996)	Owing to the DO in liquid is not specified that coefficient cannot be calculated	Autotrophy & Heterotrophy biofilm
(Elenter et al. 2007)	0.05	Autotrophy & Heterotrophy biofilm
	0.3	Autotrophy & Heterotrophy biofilm
	1.1	Heterotrophy biofilm
(Gönenç and Harremoës, 1985)	1.0-2.0	Heterotrophy biofilm with non-precise COD
(Chen et al., 1989)	1.79	Heterotrophy biofilm with non-precise BOD
(Arvin et Harremoës, 1990)	1.67	
(Gönenç et Harremoës, 1985)	0.24	Autotrophy biofilm with ammonia
(Toettrup et al, 1994)	0.22-0.23	
(Chen et al., 1989)	0.23	
(Arvin et Harremoës, 1990)	0.25-0.29	

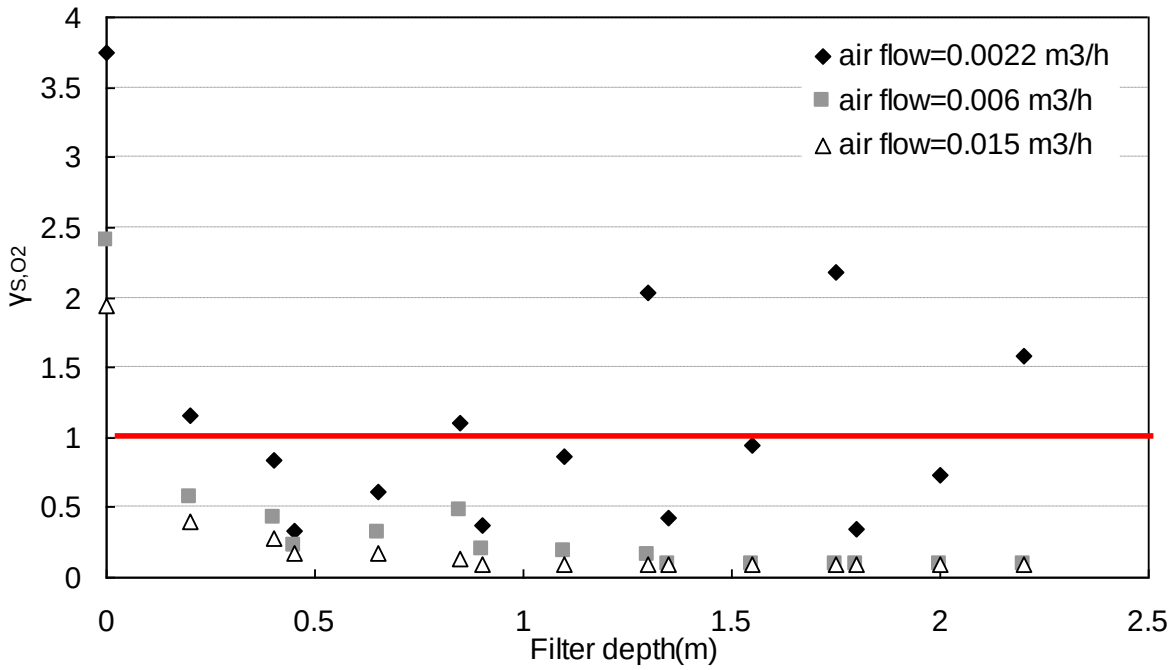

Figure V- 14: Heterotrophic growth convection coefficient along filter under 3 different air flow rate.

From Figure V-14, at very low air flow rate input, there is limitation of oxygen for heterotrophic growth on the top section of section 1. For other cases, oxygen was not limited for heterotrophic growth. Increase the air flow rate will reduce the limitation of oxygen along the filter.

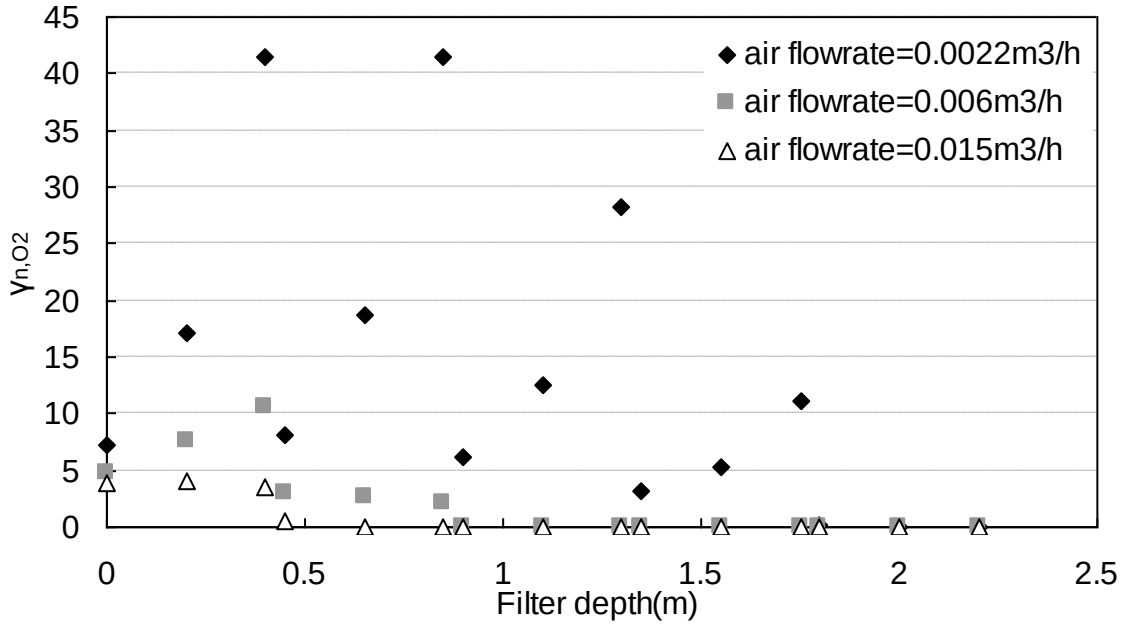

Figure V- 15: Autotrophic growth convection coefficient along the filter under 3 air flow rates input

From Figure V-15, oxygen was always limiting for nitrification along the filter at very low air flow rate of 0.0022 m³/h. Increase the air flow rate to 0.006 m³/h; oxygen was limited at the top sections of the pilot. Over a high oxygen input of 0.015 m³/h nitrification was limited by oxygen only for in the section 1.

Unfortunately we are not able to determine our experimental air flow rate, due to the open structure of MSB pilot. Only the oxygen concentrations can be estimated.

Another way to investigate the oxygen limitation conditions is the combination of heterotrophic growth and autotrophic growth demand for oxygen, comparing to the oxygen supply. The equation is given by (Gönenç and Harremoës, 1990):

$$\frac{\nu_n D_n S_n + \nu_s D_S S_S}{D_O S_O} = 1$$

This means that the demand of oxygen equal to the oxygen supply, no limitation of oxygen.

If $\nu_n D_n S_n + \nu_s D_S S_S > D_O S_O$, then oxygen will be limited.

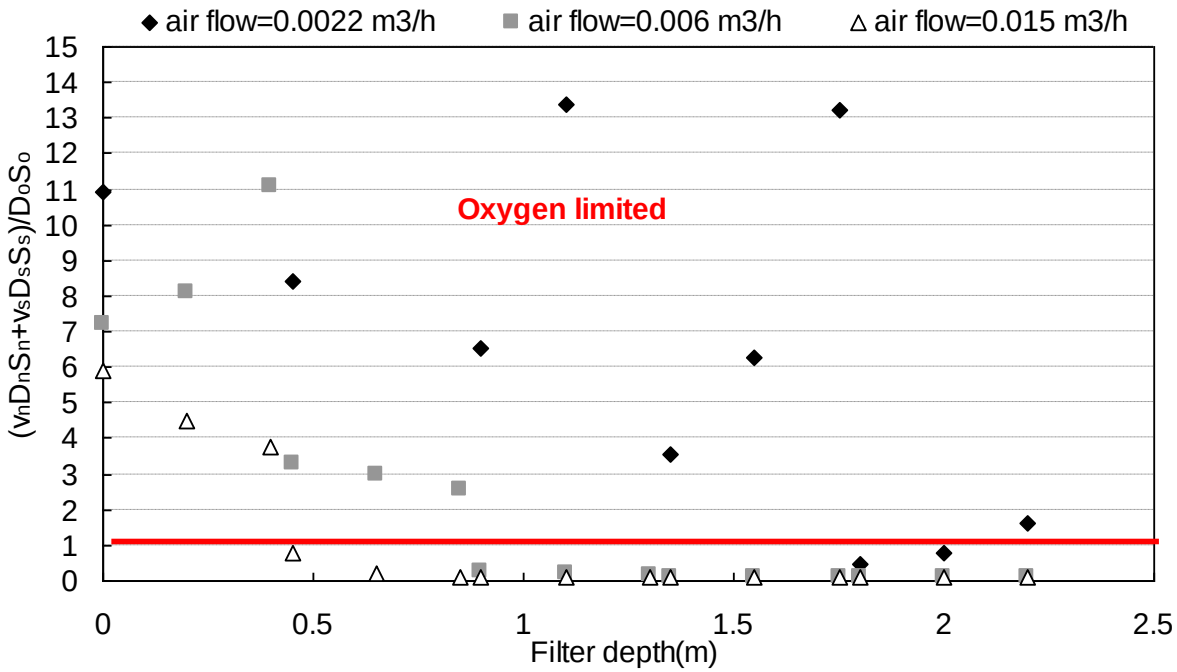

Figure V- 16: Oxygen limitation condition estimation along the filter under 3 different air flowrates, calculations were with respect to the study of Gönenç and Harremoës, (1990)

Figure V-16 indicates that increasing the air input flowrate leads to the shift of oxygen limitation inside the filter. At very low air flowrate of 0.0022 m³/h, oxygen is only not limited in section 5. In section 1, when air flowrate is lower than 0.015 m³/h, oxygen is always limited.

5.3 Partial Conclusion

By simulations with different air input flow rate, increasing the air flow rate will increase the residual oxygen concentration at the outlet until reaching the saturation oxygen concentration in the liquid.

Over an air flow rate of 0.006 m³/h, the COD removal feature inside the filter is not affected. On the contrary, at an air flow rate of 0.0022 m³/h, oxygen limitation in the first two sections leads to a slower COD degradation that is displaced to the following sections. In the case of nitrification, the decrease in the air flow rate systematically leads to a spatial shift in ammonia removal.

Based on simulation with different DO input concentrations, increasing the input oxygen concentration decreases the height where ammonia is completely removed. The good linearity of trend can help to predict the oxygen demand at different depth.

This work confirms the importance of oxygen transfer on the removal performances of a TF and gives quantitative values for optimal air flow rates depending on the OLR and NLR applied. These values should be compared to the air flow rate values of the industrial processes. However these latter values are not available. This is an aspect to be developed in future researches.

Part 3. Confrontation of simulations to experiments

Three experiments were performed that can be classified for simplification as a low OLR (and NLR) conditions (period 2), a high OLR condition (period 3) and a high OLR condition without particulate COD in the influent (period 4). Corresponding simulations were performed on Biowin software:

Simul_1: (300 gCOD/m³; 0.08 m³/d) giving an OLR of 24 gCOD/m³.d - Constant oxygen input concentration of 7.5 mgO2/L for oxygen modeling;

Simul_2: (1000 gCOD/m³; 0.08m³/d) giving an OLR of 80 gCOD/m³.d - Constant oxygen input concentration of 7.0 mgO2/L for oxygen modeling;

Simul_3: (1000 gCODs/m³; 0.08m³/d) giving an OLR of 80 gCOD/m³.d - Constant oxygen input concentration of 7.2 mgO2/L for oxygen modeling;

Moreover, the influent compounds & biomass concentration and stoichiometric ratio such as CODt, CODs and CODp, TKN, ammonia, nitrite & nitrate were reset as that in biological

experiments (refer to Chapter 2, Table II-3, page 21); physical properties of bioreactor and hydrodynamic variables were reset with respect to the experimental results in Chapter 3. These physical properties are the Liquid Residence Time (LRT), the Specific Surface Area (SSA) of media, the liquid film thickness, the off-gas O_2 volume fraction, and particularly the effective wetting fraction was reset as 1 (from 0 to 1). For the other parameters the default values were kept.

Measurements of COD and Nitrogen fractions for each segments of the MSB will greatly help us to get insights in the processes occurring inside the bioreactor and to compare with simulation of the MSB (five TFs in series). The use of the model will allow knowing the biomass distribution and thus interpreting the local and global capacities of the MSB.

Our approach for comparison between experimental and simulated results was based on the evaluation of the following processes:

- Distribution and performance of the degradation of soluble and particulate COD along the MSB. A special attention has been paid on the hydrolysis, attachment and detachment processes.

- Distribution and performance of the transformations of nitrogen species along the MSB. Competition between heterotrophs and nitrifiers will be analysed.

6.1 General simulation results compare to the biological experiments

Figure V-17 to 22 represent the general comparison between experimental and simulation results for COD degradation, ammonia removal and nitrite & nitrate production for the different operating conditions tested in this PhD work.

Additional figures are joined in order to make easier the comparison between experimental and simulated profiles of nitrate (Figures V-18 and 20) and to compare simulations obtained using the TF model (mono-stage) or the MSB model (5 stages) (Figures V-21 to 22).

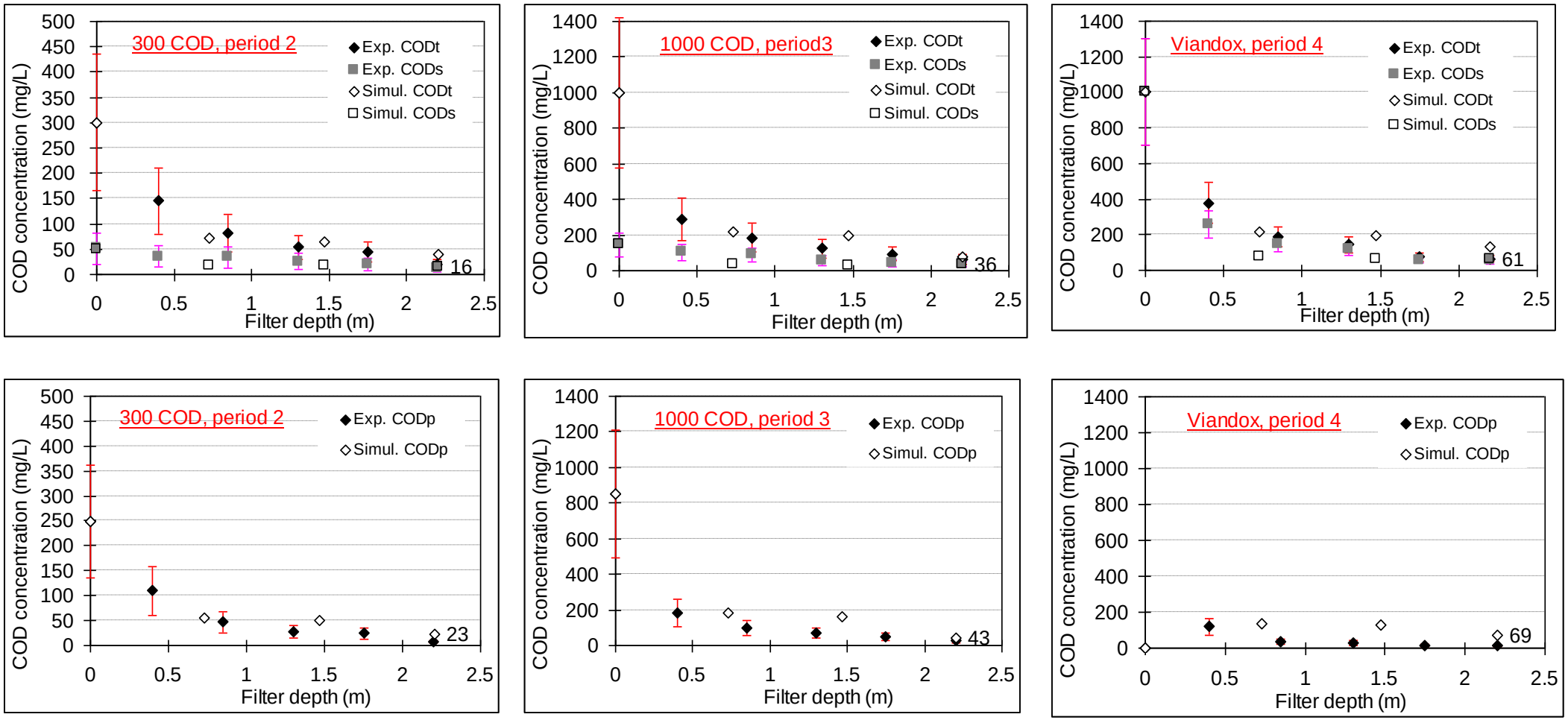

Figure V- 17: CODt, CODs and CODp profiles inside the filter, comparison between experiments and simulations by mono-TF

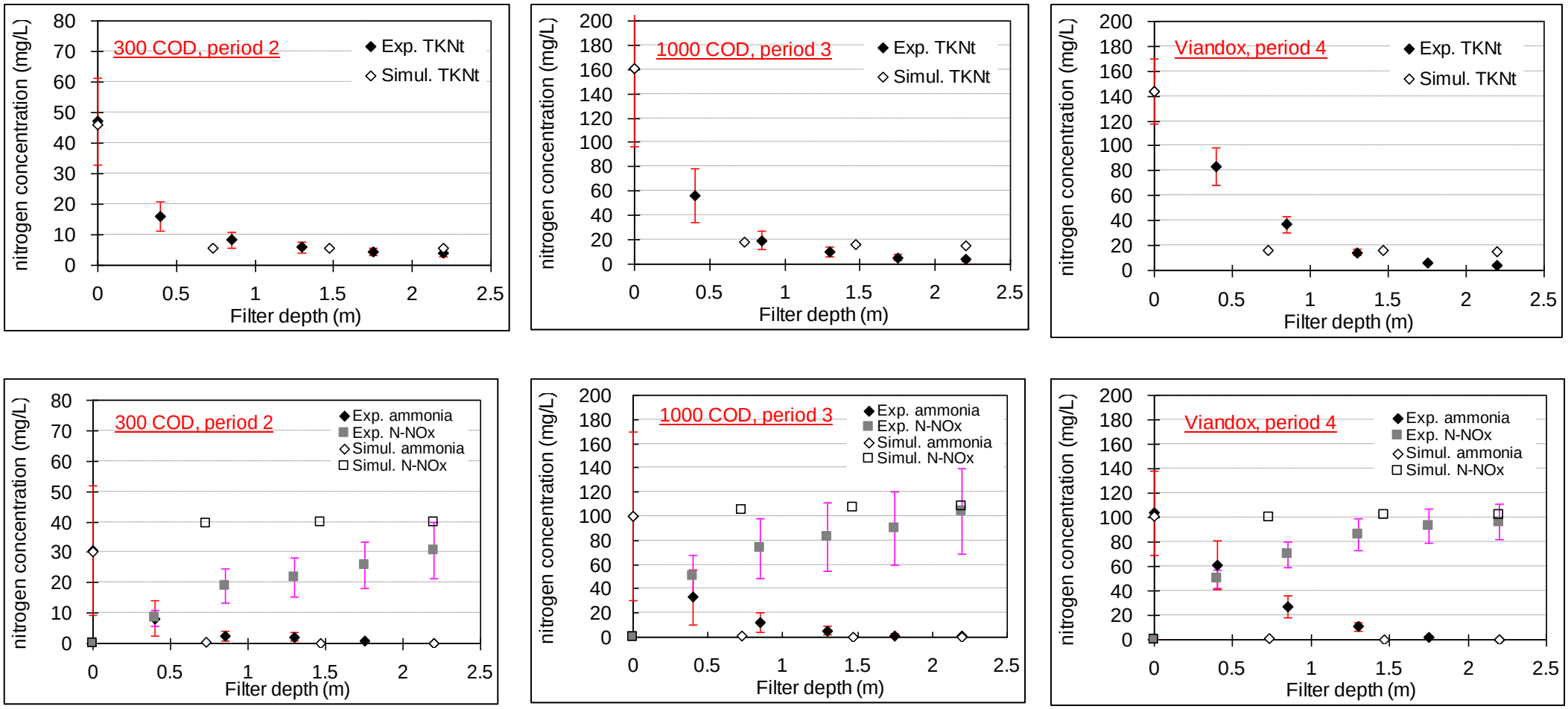

Figure V- 18: TKN and ammonia, nitrate profiles inside the filter, comparison between experiments and simulations by mono-TF

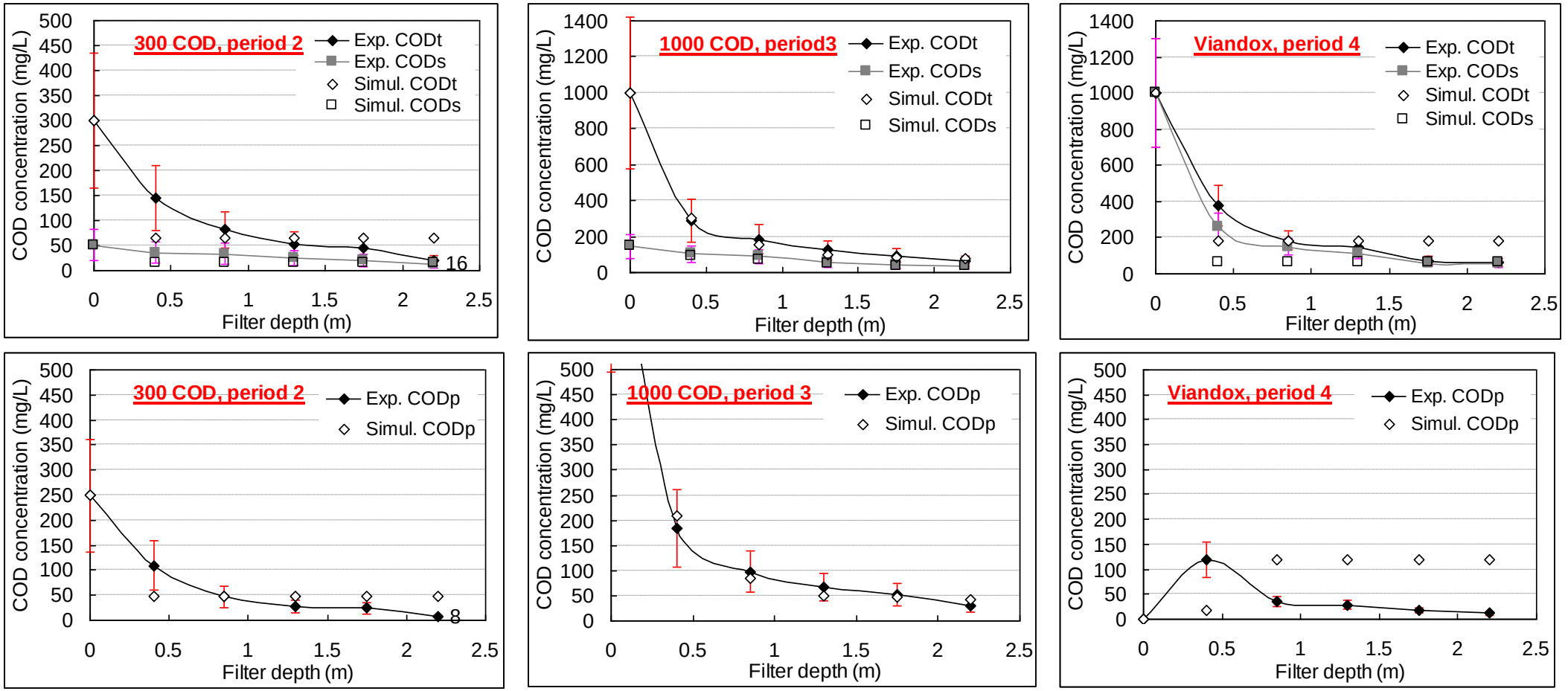

Figure V- 19: CODt, CODs and CODp profiles inside the filter, comparison between experiments and simulations by MSB

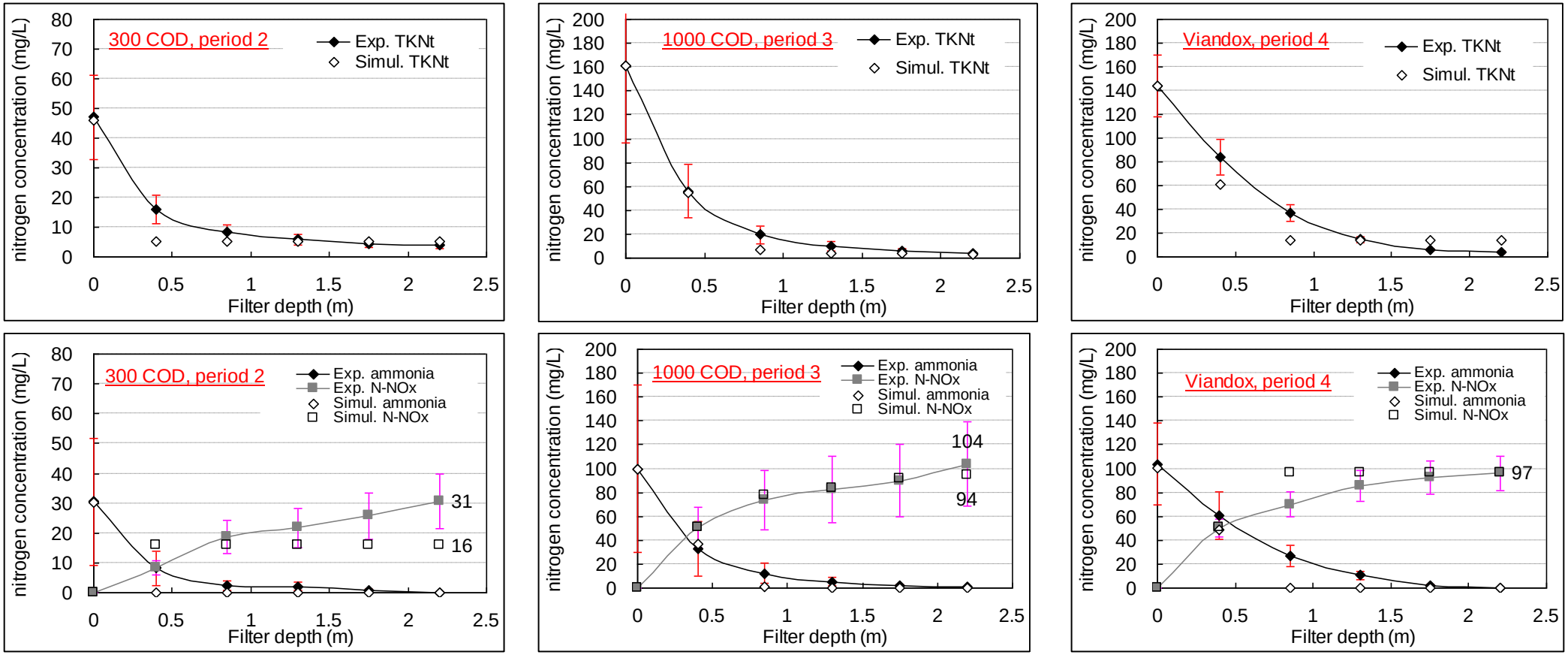

Figure V- 20: TKN and ammonia, nitrate profiles inside the filter, comparison between experiments and simulations by MSB

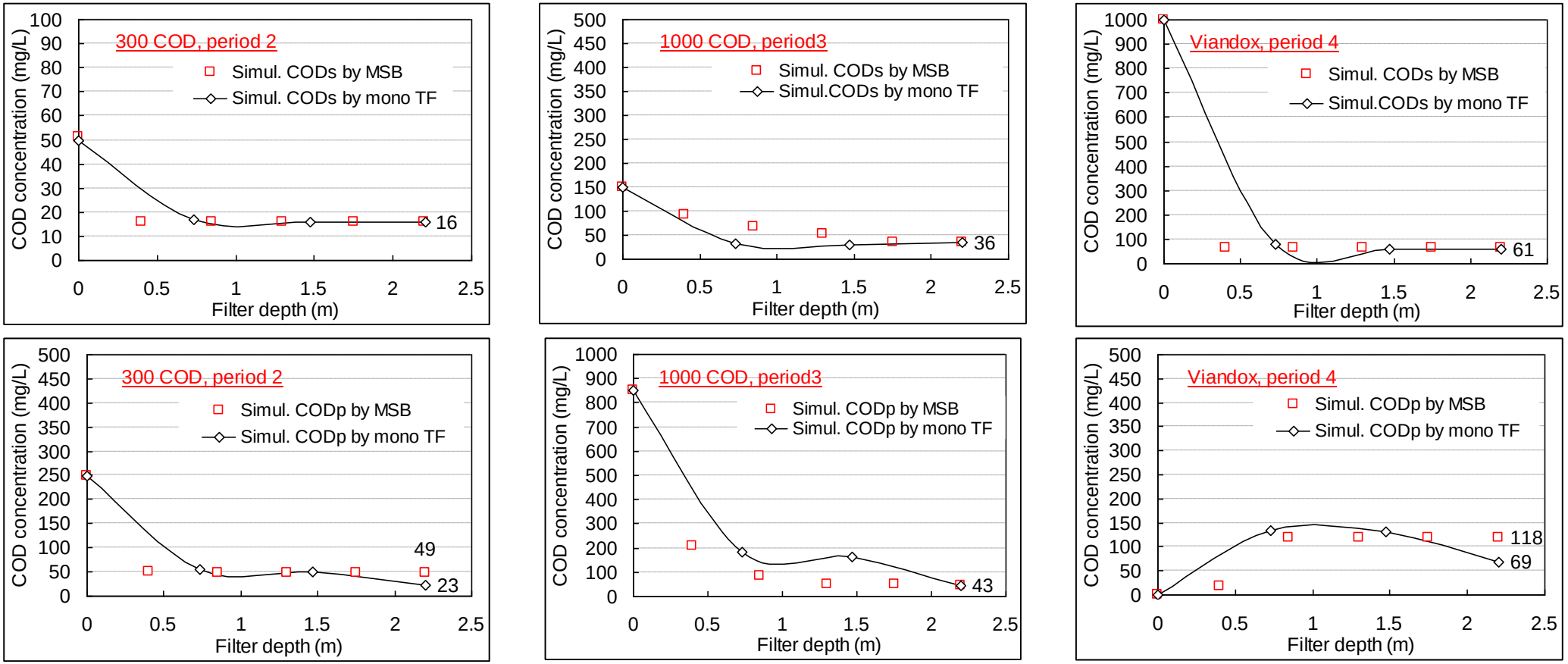

Figure V- 21: CODs and CODp profiles inside the filter, comparison between simulations by MSB and mono TF

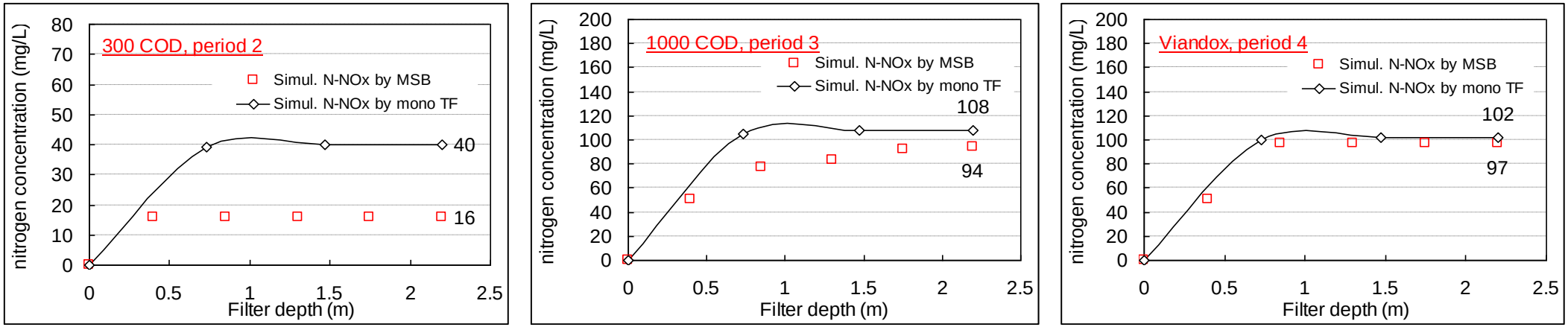

Figure V- 22: Nitrite & nitrate profiles inside the filter, comparison between simulations by MSB and mono TF

From the represented cases in Figures 21 and 22, it can be seen that the trickling filter model from Biowin 4.0 is able to capture all the tendencies of the dynamic transformations of COD and nitrogen along the filter. This result has been obtained with no calibration but taking into account the hydrodynamic specificities of our filter and considering that oxygen is delivered at a high rate.

A few aspects have to be underlined:

1 Comparison between experimental results and simulations using the TF model:

It is recalled that the use of the TF model allowed reaching the steady state because calculations are less complex than those in the MSB model. In addition, the positions of the simulated values are not very accurate because information given by the software is a mean value for the filter.

- The representations by the TF model of the CODt, the CODs and the CODp along the filter depth are acceptable. The removal efficiency is well predicted. That means that attachment and detachment are sufficiently well represented in the TF model.
- Evolution of CODp for Viandox is not well represented by the TF model.
- Nitrate production in section 2 and 3 is over estimated by the TF model
- Ammonia and TKN removal are on contrary well represented. That means that it is the ammonification process that is more pronounced in the case of the simulations by the TF model. It must be underlined that the study state has been reached for the model but not for the experiment.

2 Comparison between experimental results and simulations using the MSB model:

MSB model allows getting more accurate details on the concentrations for each section and on the biomass distribution. However, it has not been possible to reach steady states for the simulations because of the time required (various weeks).

- The order of magnitude for COD concentrations in the filter is correct. More CODp is found in the case of Viandox for the model compared to the experiments (figure V-24_viandox period 4). This is due to less capacity of capturing the CODp.
- Experimental nitrate profile is better represented in the case of the MSB model. This result may confirm the fact that the steady state conditions are not reached in the experimental conditions. In particular, nitrification is not completely implemented in the biofilm and especially in sections 2 and 3. The potential for nitrification should therefore be greater than that observed in the pilot.

3 Comparison between experimental results and simulations using the MSB model:

Comparison of the two simulations from the TF model and the MSB model confirms the good agreement of COD profiles and the difference in N-NOx profiles above all in sections 2 and 3 where hydrolysis and hence ammonification is very active. .

6.2 Does the distribution of AOB and NOB fits with the nitrite and nitrate profiles?

Table V-10 gives the concentrations of AOB and NOB and the Nitrite and nitrate concentrations along the depth for the three operating conditions and the two models. These concentrations values are reported in Figure V-23.

Table V- 10: AOB and NOB concentration profile along filter depth under 3 conditions by MSB and mono-stage TF simulations, plus nitrite & nitrate concentration profile inside MSB by experiments

	300 CODt		1000 CODt		Viandox		Unit
By MSB simulations							
Depth / m	AOB	NOB	AOB	NOB	AOB	NOB	mg/L
0	0.26	0.04	0.06	0.03	0.04	0.02	
0.2	0.05	0.01	0.62	0.01	0.49	0	
0.4	0.01	0	1.58	0	0.82	0	
0.45	0	0	0.23	0.06	0.61	0.15	
0.65	0	0	0.04	0.01	0.14	0.03	
0.85	0	0	0.01	0	0.03	0.01	
0.9	0	0	0	0	0.01	0	
1.1	0	0	0	0	0	0	
1.3	0	0	0	0	0	0	
1.35	0	0	0	0	0	0	
1.55	0	0	0	0	0	0	
1.75	0	0	0	0	0	0	
1.8	0	0	0	0	0	0	
2	0	0	0	0	0	0	
2.2	0	0	0	0	0	0	
By mono TF simulations							
Depth / m	AOB	NOB	AOB	NOB	AOB	NOB	mg/L
0	0.26	0.04	0.06	0.03	0.04	0.02	
0.73	0.01	0.00	0.21	0.04	0.08	0.02	
1.47	0.00	0.00	0.00	0.00	0.00	0.00	
2.2	0.00	0.00	0.00	0.00	0.00	0.00	
Experiments results							
Depth / m	NOx concen.	SD	NOx concen.	SD	NOx concen.	SD	mg/L
0	0	0	0	0	0	0	
0.4	8	5	51	25	50	7	
0.85	19	5	73	25	70	5	
1.3	22	8	83	30	86	4	
1.75	26	11	90	28	93	3	
2.2	31	8	104	18	96	3	

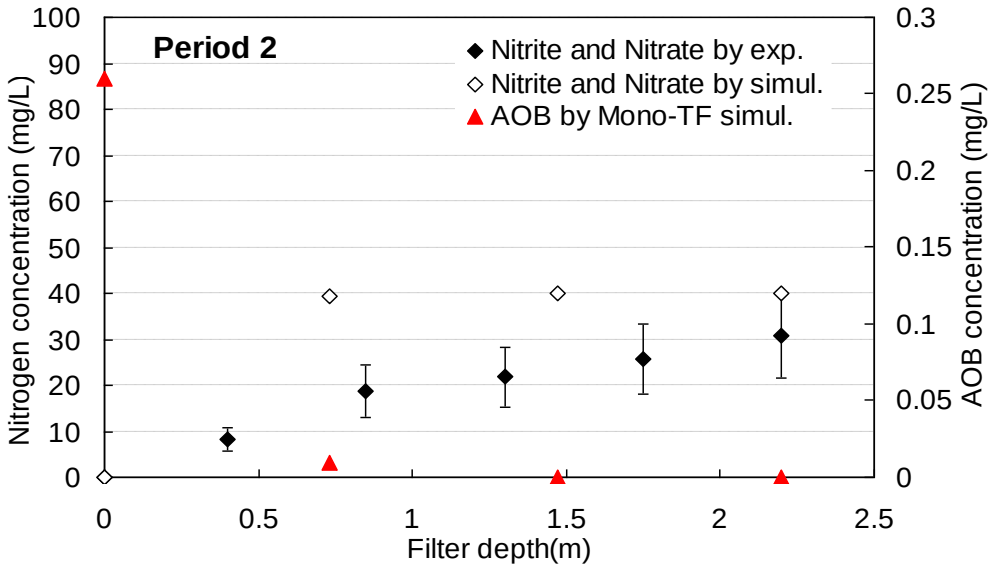
Period 2
Nitrite and Nitrate by exp.
Nitrite and Nitrate by simul.
AOB by Mono-TF simul.
Nitrogen concentration (mg/L)
AOB concentration (mg/L)
Filter depth(m)

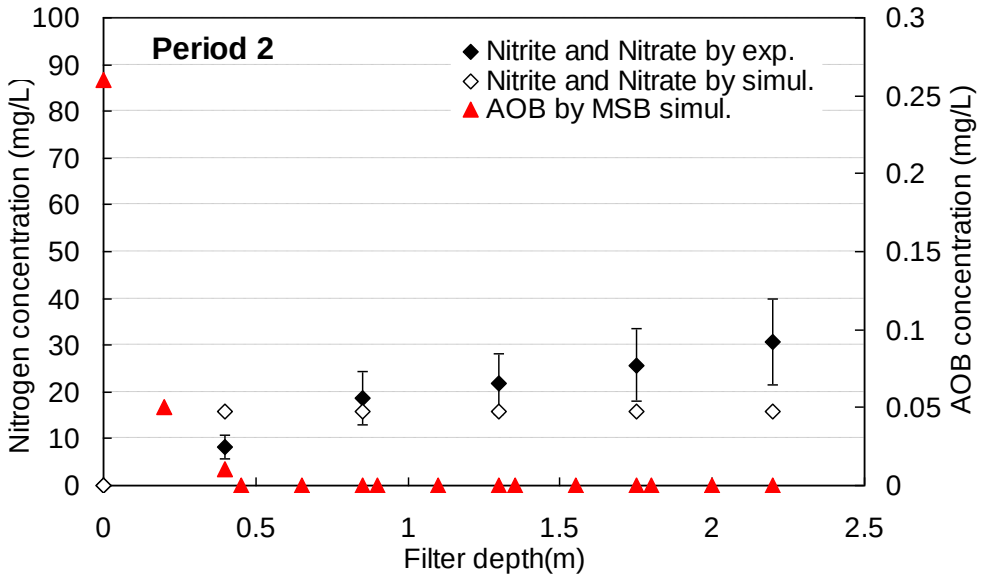
Period 2
Nitrite and Nitrate by exp.
Nitrite and Nitrate by simul.
AOB by MSB simul.
Nitrogen concentration (mg/L)
AOB concentration (mg/L)
Filter depth(m)

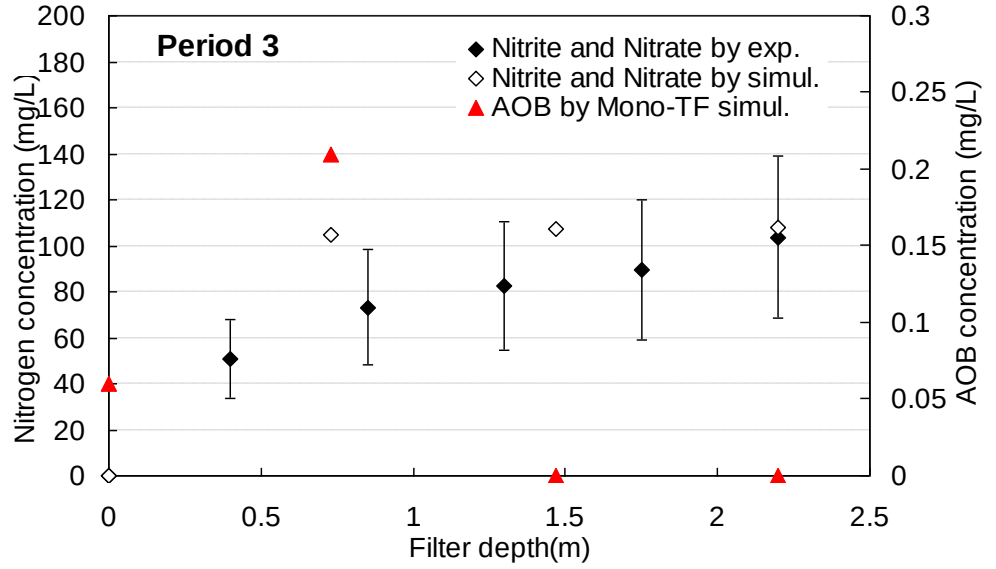
Period 3
Nitrite and Nitrate by exp.
Nitrite and Nitrate by simul.
AOB by Mono-TF simul.
Nitrogen concentration (mg/L)
AOB concentration (mg/L)
Filter depth(m)

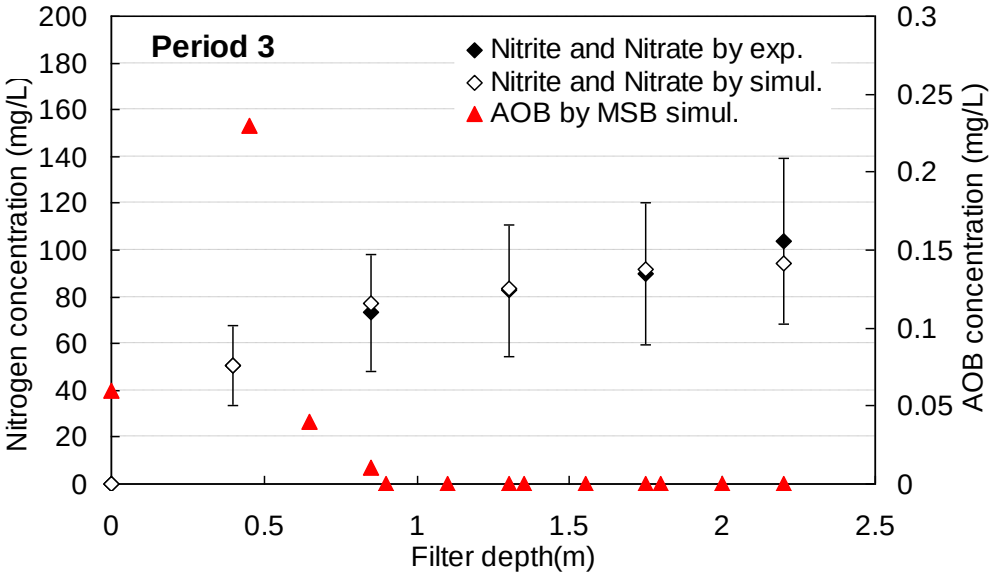
Period 3
Nitrite and Nitrate by exp.
Nitrite and Nitrate by simul.
AOB by MSB simul.
Nitrogen concentration (mg/L)
AOB concentration (mg/L)
Filter depth(m)

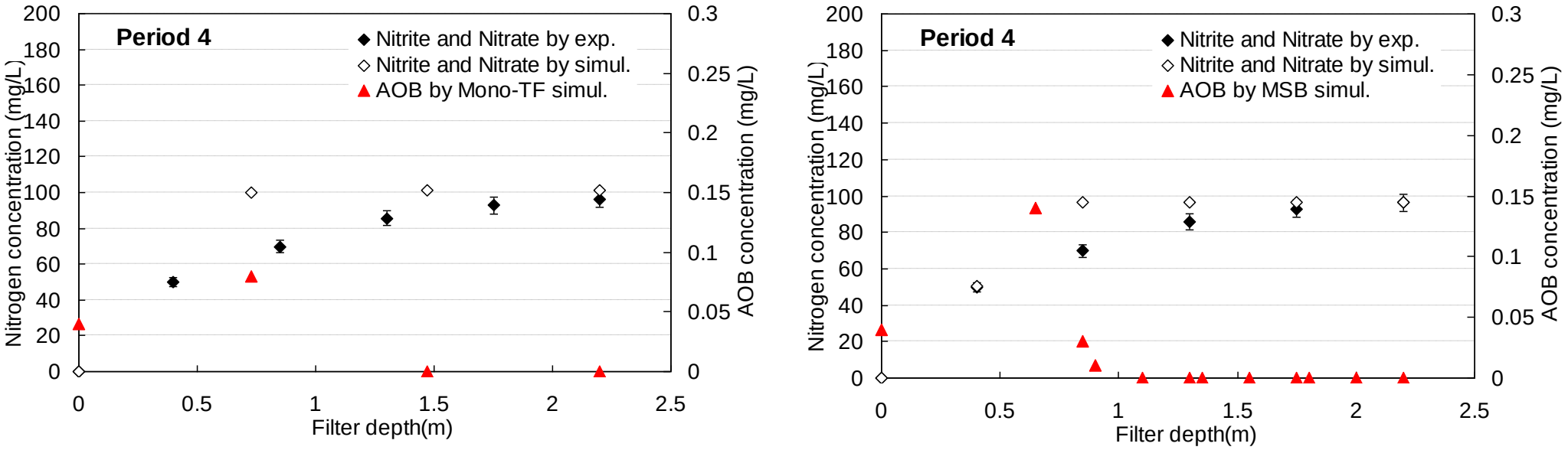

Figure V- 23: AOB, nitrite and nitrate profile inside filter by experiments and simulations with two models.

6.3 General balance of COD and nitrogen for experiments and simulations

Figure V-24 and 25 represent the general comparison between experimental and simulation results for COD and ammonia removal, and nitrite & nitrate production for the operating conditions tested.

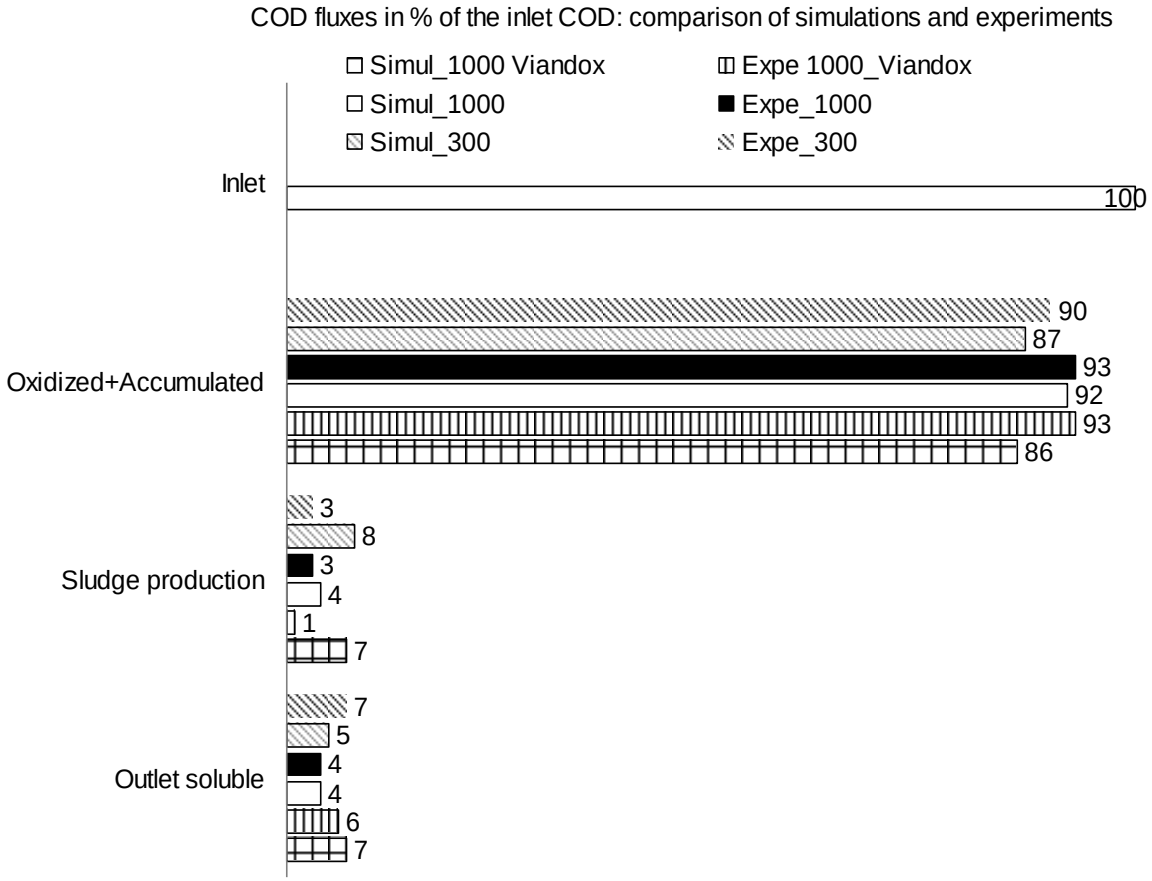

Figure V- 24: General simulation results comparison of COD removal under various conditions, both simulation and biological experiments

These mass balances confirm the observations on the Figure V-17 and19. Indeed, accumulation of biomass in the reactor is certainly significant and thus sludge production is not well predicted taking into account the outlet particulate solids only. The pilot is not in steady state and clogging should occur one day.

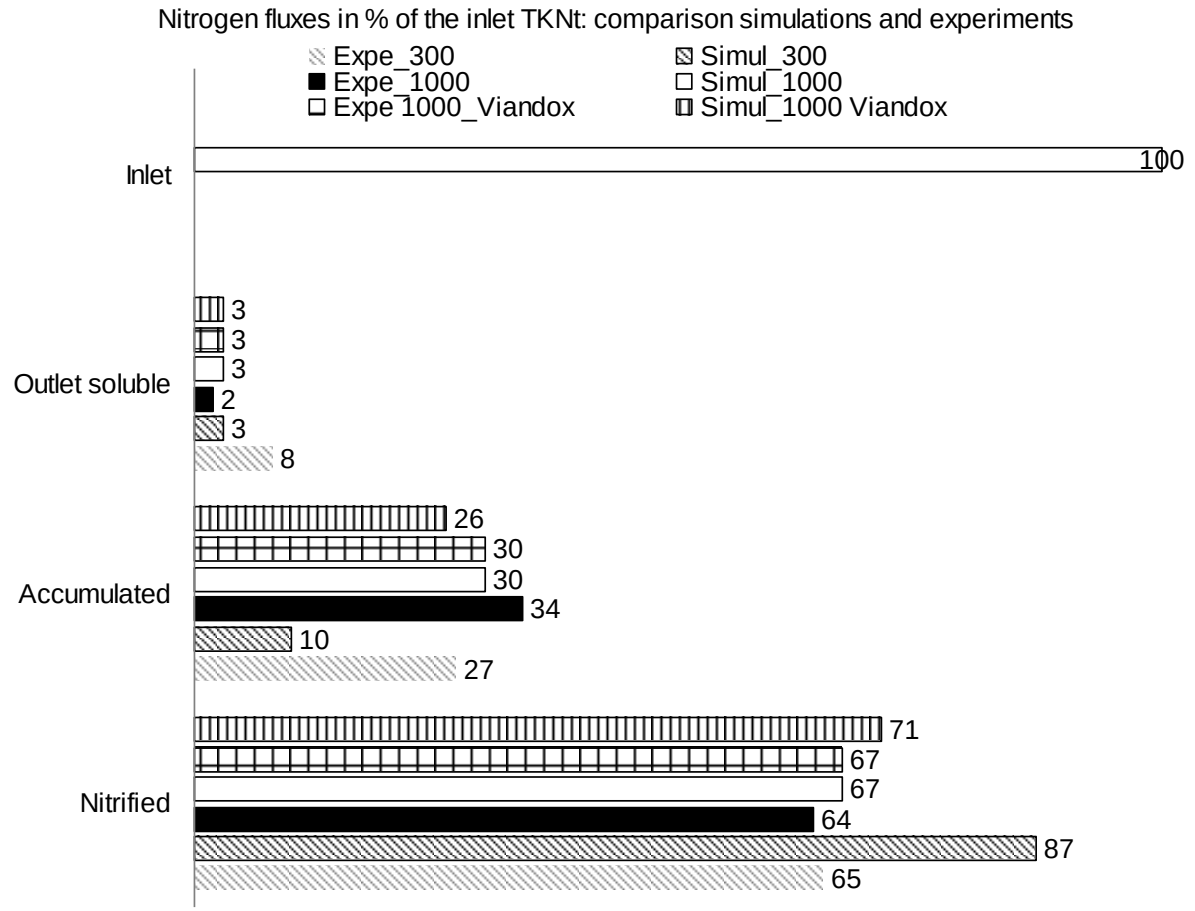

Figure V- 25: General simulation results comparison of ammonia removal and nitrite & nitrate production under various conditions, both simulation and biological experiments

From the nitrogen mass balance, the simulations represent little higher nitrified fractions than in the biological experiments, the lower OLR simulations in particular. However, confrontation between simulations and experiments show that high nitrification capacity can be achieved if oxygen transfer rate is high enough to provide oxygen for the two microbial populations.

6.4 Partial Conclusion

Simulations of 3 tests with similar influent conditions, physical conditions and hydrodynamic conditions but at different OLR and NLR have been performed and compared to the experimental concentrations profiles.

COD biodegradation along the depth of bioreactor was similar to the trend observed in biological experiments. It is confirmed that biodegradation and entrapment of COD mainly occurred in section 1; particularly on the top of section 1under low OLR, in deeper location of

section 1 under high OLR. Increasing the OLR and thus particulate COD concentration, resulting in decreasing in porosity and increasing in cell biomass, leads to better COD removal performance than only with soluble COD, which is in good agreement with the conclusion found in biological experiments.

TKN and ammonia removal is well represented by simulations either for the TF model or by the MSB model. On the contrary, N-NO_X profile is over estimated for TF model. This is due to the long term simulations that reach the steady-state in the TF model, but not in the case of the MSB model nor in the experiments.

7. Conclusion of the chapter

This chapter aims at testing the model of TF developed in the Biowin 4.0 software. The approach used included: (i) a comparison of simulations results for COD and N removal at a same OLR but using two combinations of flow rate/COD concentration, (ii) an analysis of the effect of oxygen transfer rate on COD removal and nitrification performances, (iii) the comparison, for the COD fraction concentrations and for ammonia, nitrite and nitrate concentrations, of simulated and experimental profiles along the filter.

By the use of two simulations at the same OLR and NLR but with two different combinations of COD inlet concentration and flow rate, a first evaluation of the TF and MSB models from Biowin 4 software has been done. COD degradation and entrapment into the filter has been quantified and mass balances on TKN and N has allowed quantifying nitrification yield. No difference due to a change in the values of the couple (flow rate/concentration) in the removal performances has been detected.

The difference between the MSB and the TF simulation configurations results from the ammonification processes that are further achieved when the duration of simulation is not limited (pseudo steady state reached). Hence, the majority of the biodegradable inlet nitrogen is converted to nitrate. These results point out the importance of the dynamic of the ammonification processes in a trickling filter.

Oxygen transfer rate is of crucial importance to allow a good nitrification and COD removal. It determines the maximal removal capacity of a TF. In our case, over an air flow rate of 0.006 m^3/h, the COD removal feature inside the filter is not affected. On the contrary, at an air flow rate of 0.0022 m^3/h, oxygen limitation in the first two sections leads to a slower COD

degradation that is displaced to the following sections. In the case of nitrification, the decrease in the air flow rate systematically leads to a spatial shift in ammonia removal.
Based on simulation with different DO input concentrations, increasing the input oxygen concentration decreases the height where ammonia is completely removed.
This work confirms the importance of oxygen transfer on the removal performances of a TF and gives quantitative values for optimal air flow rates depending on the OLR and NLR applied. These values should be compared to the air flow rate values of the industrial processes. However these latter values are not available. This is an aspect to be developed in future researches.

Confrontation between simulated results obtained for a fixed high oxygen concentration in the liquid film COD and experimental results has been performed. The model allows a rather good prediction of the global COD removal and of nitrification. Some improvement could be done to better match all concentration values along the filter depth. This calibration work has not been performed in this work. .
Model and experiments are in good agreement for the following conclusions:

- It is confirmed that biodegradation and entrapment of COD mainly occurred in section 1; particularly on the top of section 1 under low OLR, in deeper location of section 1 under high OLR. Increasing the OLR and thus particulate COD concentration, resulting in decreasing in porosity and increasing in cell biomass, that leads to better COD removal performance than only with soluble COD.

- High nitrification capacity can be achieved if oxygen transfer rate is high enough to provide oxygen for the two microbial populations. In that case nitrification can occur in the first sections of the filter together with the COD removal.

Using the Biowin software much can be learned about the behaviour of microbial populations in a TF.

General conclusion

Treatment for rural wastewater or for small communities is of growing interest. Various technologies can be chosen (SBR, RBC, ponds, wetlands, biofilter…). The use of a trickling filter combined with a polishing system can be an appealing solution because the energy consumption and need for maintenance are limited. However, this technology is difficult to design because numerous processes involving biofilm spatially distributed and complex hydrodynamics are occurring in parallel. The nature of the media and the distribution of the biofilm generate a specific hydrodynamic which governs mass transfer. Competition between heterotrophic activity and nitrification is often described but only scarcely deeply analysed. Competition for space or for oxygen is obviously a key mechanism determining the TF performances but very few works report on this aspect. It depends on many factors: the material carrier chosen, the oxygen mass transfer, the hydrodynamic of the reactor, the OLR, NLR, etc.

It is the reason why the main objective of this PhD work focused on the study of the COD removal and nitrification in a new designed Multi-Section Bioreactor (MSB), applied for rural wastewater treatment but also for small communities in the large cities. This MSB has been developped in China in order to treat urban WW with a compact and close technology. It is now widely encountered in the suburbs of Shanghai city for example. In order to improve the treatment performances and to decrease cost, optimization of the MSB is required. It has been decided to study the MSB with the following approach:

- Firstly, a characterization of the hydrodynamic of the MSB has been performed. Indeed, hydrodynamic determines liquid distribution in the column, the contact time for substrat consumption, the shear stress applied to the biofilm resulting in bioflm detachment, and the oxygen mass transfer. One originality of our work has been to performed the hydrodynamic characterization both in presence and in absence of biofilm and at different operating conditions.
- Secondly, the MSB was operated at different OLRs and NLRs to study its capacity for COD and reduced N removal. Work on reconstituted urban WW (based on real primary sludge) ensured the representativity of our study. Mass balances were used to characterized the becoming of the COD and of the TKN, nitrite and nitrate along the filter depth and versus time. The presence of air space between the five sections of the reactor allowed representative sampling at various depth of the column that is helpful to get a better knowledge on the processes occurring at each depth.

- Thirdly, an existing but never tested trickling filter dynamic model has been used in order to get more insights on the biomass distribution in the pilot and to assess the limitated process in each section of the bioreactor. Special attention has been paid on oxygen limitation of heterotrophic and autotrophic activities. Confrontation between results from the previous experiments and the results obtained from the simulations has been performed.

Therefore, the study of the MSB combined hydrodynamic and biological experiments with modelling.

With the ultimate aim of optimizing TF design and operation, the main objective of Chapter 3 was to characterize the hydrodynamic behavior of two types of TF (TFC and MSB) filled with the same porous medium but differing in its spatial organization (the TFC is a close structure without interval spaces, the MSB is of an open structure with interval spaces). The impact of the properties of the medium and its organization in the reactor on the overall hydrodynamics is characterized. Such impact is measured in term of liquid holdup fractions, liquid film thickness under the regimes with and without biofilm (two organic loading rates cultivation conditions were applied) all along the column. A further objective was using RTD experiments and modeling to investigate the changes in liquid flow pattern and liquid residence time due to the presence of biofilm in the MSB. Additionally, the study attempted to verify whether the configuration of the bioreactor (TFC or MSB, mainly focus on the close/open structure and presence of the interval spaces) would affect its hydrodynamic characteristics.

The static experiments with biofilm indicate that most of the liquid is retained by the carrier particles coated with biofilm, increasing static retention and, consequently, reducing dynamic retention. It is also found that the liquid static holdup makes a greater contribution than the dynamic holdup to total liquid holdup, on account of the high adsorption potential of the concrete block medium and biofilm, resulting from its porous structure. Moreover, the static holdup does not correlate with the configuration of TF, but dependent on the type of medium.

The effective liquid volumes represented in the Residence Time Distribution (RTD) curves are not only the dynamic holdup, but also partial static holdup volume, resulting from the sustained release of partial static holdup in the biofilm. Increasing the flow rates, the effective liquid volume involved in RTD first increases. However, when the flow rate was too low or too high, the effective volume decreases, resulting from low flow and short liquid residence

time, respectively. RTD experiments also show that at lower flow rates, the mass dispersion and diffusion between the liquid and biofilm was better than that at higher flow rates. Increasing the hydraulic load resulted in the flow approaching plug flow in the bioreactor, resulting in less mass dispersion and diffusion. The Liquid Residence Time (LRT) estimated from RTD models shows that the presence of biofilm will lead to a longer LRT in the filter, and thus promote the dispersion of mass in the bioreactor. Comparing the drainage and RTD methods allows us to show that dispersion and diffusion can occur in the biofilm, increasing the contact time between liquid and biofilm. Too low (less than 9 L/h) or too high (greater than 23 L/h) flow rates will not make advantages to the bioreactor performance, resulting from low effective liquid volume and short liquid residence time.

The presence of biofilm was also found to decrease the thickness of the liquid film compared to the cases without biofilm under the same hydraulic conditions, on account of the greater surface area and smaller dynamic holdup volume.

The estimation of oxygen volumetric mass transfer coefficient, based on the estimated liquid film thickness, shows that at lower flowrate, oxygen transfer is better than at higher flowrate. When biofilm was present, oxygen transfer was promoted compared to without biofilm, resulting from thinner liquid film. Within a reasonable range, increasing the biofilm thickness under a same hydraulic conditions leads to better oxygen transfer.

Furthermore, the physical properties of MSB and medium, liquid film thickness, Liquid Residence Time, and also the estimated oxygen transfer coefficient obtained in this chapter is applied to Biowin simulator of Chapter 5 in order to improve the representativeness of the simulations.

In term of prediction, the hydrodynamic studies may lead to the use of the LRT to appreciate the percolation in the bioreactor as well as the fraction of dead zones. Laters studies should be conducted to determine the shear forces and the transfer of oxygen in the liquid in the biological experiments.

Biological experiments in Chapter 4 investigate the performances of nitrification together with COD removal, and hence the competition between nitrification and heterotrophic growth. The capacity of MSB is also evaluated regarding clogging. Our experiments provide data to help understanding the various processes occurring in the biofilter, i.e. biological transformations, attachment, detachment, oxygen transfer, liquid repartition. They also provide information for a better design and operation of this type of TF (removal efficiencies against OLR and NLR).

By biological experiments run during 240 days, it appears that a rather conventional feature for COD removal is observed for the MSB compared to a TF. High removal efficiency is achieved in the upper part of the reactor, the removing capacity decreasing gradually with depth. Therefore, sections 4 and 5 played only a “polishing” role for the COD removal. High COD removal capacities (>93%) is obtained for the pilot under all the operating conditions tested. A settler is of course required in order to recover the released CODp.
More surprisingly, under a high OLR, the COD removal capacity is promoted. This promoted performance is explained by the better entrapment of particulate COD and the longer liquid residence time (as found in the hydrodynamic studies).
Nitrification mainly occurs in sections 1 and 2 where more than 70% of inlet ammonia is removed. With no limitation of oxygen, nitrification should achieve a realistic efficiency, even under conditions where the COD removal is promoted. Nitrite is detected in the first section, which indicates that under high OLR, not enough oxygen is supplied to ensure COD removal and complete nitrification. Even under high OLR, nitrification mainly occurred in the first section. From section 4 to section 5, less nitrification occurs due to lack of ammonia resource.

For designing the MSB reactor, our studies show it is able to treat the highest loading rate applied in this study. However, mass balances on COD and on nitrogen point out the accumulation of biomass inside the filter. Therefore, no steady state is reached in our experiments even after 260 days of operation. Even if no clogging is observed during the experimental time, this problem should occur if the duration of operation is increased. That behavior is confirmed at the full scale for which clogging is observed after two years of operation. In that case, the solution consists in inter changing the last basket with the first one (section five for section one).

The performances of our pilot are compared to that obtained at a full scale plant in China. Under similar organic loading rate but with a much lower flow rate, better COD removal efficiencies are obtained in our pilot. This implies that the Multi-Section Bioreactor (MSB) can sustain high organic loading, but to optimize the COD removal performance, a low flow rate is better. The nitrification performance in our study is also better than in the full-scale MSB reactor though the inlet concentration of ammonia is much higher than that in the full-scale MSB reactor. Lower hydraulic flowrate applied in our study could lead to longer Liquid Residence Time (LRT) and thinner liquid film thickness, and accordingly better mass and oxygen transfer into the biofilm. Higher oxygen transfer rate on the pilot due to a better

renewal of air in the void space due to the highly open structure may be thus responsible for the better performances.

Chapter 5 intends to describe the behavior of a MSB through simulation using the commercial Biowin® software. The effect of hydraulics and mass transfer on the MSB performances for the COD removal and nitrification is briefly studied. Simulations are very helpful for understanding the functional population distribution inside the biofilter and hence to understand the local removal capacities for COD removal and nitrification. Accumulation of biomass is however not well represented by the model. The effect of oxygen limitation on nitrification and then on COD removal efficiencies is characterized for the MSB reactor. The results, giving values of air flow rate, can help improving the design of a MSB reactor. However, as air is blown up from the upper part of the biofilter, it is not representative of a TF.

Confrontation between simulated results obtained for a fixed high oxygen concentration in the liquid film COD and experimental results has been performed. The model allows a rather good prediction of the global COD removal and of nitrification. Some improvement could be done to better match all concentration values along the filter depth. This calibration work has not been performed in this work.

Model and experiments are in good agreement for the following conclusions:

- It is confirmed that biodegradation and entrapment of COD mainly occurred in section 1; particularly on the top of section 1under low OLR, in deeper location of section 1 under high OLR. Increasing the OLR and thus particulate COD concentration, resulting in decreasing in porosity and increasing in cell biomass, that leads to better COD removal performance than only with soluble COD.
- High nitrification capacity can be achieved if oxygen transfer rate is high enough to provide oxygen for the two microbial populations. In that case nitrification can occur in the first sections of the filter together with the COD removal.

The perspectives of this work are numerous:

- Firstly, oxygen transfer rate should be studied because it is the limiting step that determines the short term performances of the reactor. To do that, the air renewal capacity depending on the temperature gradient between the air inside the reactor and the air outside the reactor must be determined. The geometric configuration and the size of the MSB reactor must be considered. Indeed it may have a huge effect on the air flow renew.
- Secondly, clogging must be studied but this is a hard task because long term experiments must be run. Hydrolysis of the biomass accumulated must be analysed. May be some resting period should be envisaged for part of the reactor in order to restore the reactor porosity.
- Thirdly, entrapment of particulate COD must be better characterized
- Finally, using the Biowin® software much can be learned about the behaviour of microbial populations in a TF.

Reference

Albertson, O. E. (1989). "Discussion of: Trickling Filter/Solids Contact Performance with Rock Filters at High Organic Loadings." Journal (Water Pollution Control Federation) 61(3): 369-372.

Alleman, J. E. and T. B. S. Prakasam (1983). "REFLECTIONS ON 7 DECADES OF ACTIVATED-SLUDGE HISTORY." Journal Water Pollution Control Federation 55(5): 436-443.

Alpkvist, E., C. Picioreanu, M. C. M. van Loosdrecht and A. Heyden (2006). "Three-dimensional biofilm model with individual cells and continuum EPS matrix." Biotechnology and Bioengineering 94(5): 961-979.

Aryan, A. F. and S. H. Johnson (1987). "Of: A Comparison of Trickling Filter Media." Journal (Water Pollution Control Federation) 59(10): 915-918.

A. Ohashi, D.G.V. deSilva, B. Mobarry, J.A. Manem, D.A. Stahl, and B.E. Rittmann, Influence of substrate C/N ratio on the structure of multi-species biofilms consisting of nitrifiers and heterotrophs, in Water Science and Technology, 1995, pp. 75-84.

Bakke, R., R. Kommedal and S. Kalvenes (2001). "Quantification of biofilm accumulation by an optical approach." Journal of Microbiological Methods 44(1): 13-26.

Behrens, M., Z. Olujic & P. J. Jansens (2006) Combining reaction with distillation - Hydrodynamic and mass transfer performance of modular catalytic structured packings. Chemical Engineering Research & Design, 84, 381-389.

Brunazzi, E., U. Di Festa, C. Galletti, C. Merello, A. Paglianti & S. Pintus (2002) Measuring volumetric phase fractions in a gas-solid-liquid stirred tank reactor using an impedance probe. Canadian Journal of Chemical Engineering, 80, 688-694.

Brunazzi, E., R. Macias-Salinas & A. Viva (2009) CALCULATION PROCEDURE FOR FLOODING IN PACKED COLUMNS USING A CHANNEL MODEL. Chemical Engineering Communications, 196, 330-341.

Bakke, R., M. G. Trulear, J. A. Robinson and W. G. Characklis (1984). "ACTIVITY OF PSEUDOMONAS-AERUGINOSA IN BIOFILMS - STEADY-STATE." Biotechnology and Bioengineering 26(12): 1418-1424.

Baojiu Xu and Tengyue Long (2000). Contemporary Principles of Water and Wastewater Treatment. Beijing, High Education Press (HEP).

Behrens, M., Z. Olujic and P. J. Jansens (2006). "Combining reaction with distillation - Hydrodynamic and mass transfer performance of modular catalytic structured packings." Chemical Engineering Research & Design 84(A5): 381-389.

Behrens, M., Z. Olujic and P. J. Jansens (2007). "Liquid flow behavior in catalyst-containing pockets of modular catalytic structured packing katapak SP." Industrial & Engineering Chemistry Research 46(12): 3884-3890.

Beyenal, H., S. Seker, A. Tanyolac and B. Salih (1997). "Diffusion coefficients of phenol and oxygen in a biofilm of Pseudomonas putida." Aiche Journal 43(1): 243-250.

Bird, R. B. (1979). "CITATION CLASSIC - TRANSPORT PHENOMENA." Current Contents/Engineering Technology & Applied Sciences(38): A12-A12.

Boller, M. (1997). "Small wastewater treatment plants -- A challenge to wastewater engineers." Water Science and Technology 35(6): 1-12.

Boller, M., W. Gujer and M. Tschui (1994). "PARAMETERS AFFECTING NITRIFYING BIOFILM REACTORS." Water Science and Technology 29(10-11): 1-11.

Bouwer, E. J. and G. D. Cobb (1987). "MODELING OF BIOLOGICAL PROCESSES IN THE SUBSURFACE." Water Science and Technology 19(5-6): 769-779.

BRENTWOOD-INDUSTRIE. "Trickling Filter Systems Design & Application."

Brunazzi and Viva (2006). Experimental investigation of reactive distillation packing Katapak-SP11:Hydrodynamic aspects and size effects. IChemE: 554-562.

Bryers, J. D. (1984). "BIOFILM FORMATION AND CHEMOSTAT DYNAMICS - PURE AND MIXED CULTURE CONSIDERATIONS." Biotechnology and Bioengineering 26(8): 948-958.

Burkhard, R., A. Deletic and A. Craig (2000). "Techniques for water and wastewater management: a review of techniques and their integration in planning." Urban Water 2(3): 197-221.

Catherine Boutin and A. Lienard. (2003). Constructed wetlands for wastewater treatment: the French experience. 1st international seminar on the use of aquatic macrophytes for wastewater treatment in constructed wetlands. Lisbonne : Portugal.

Chang, H. T. and B. E. Rittmann (1987). "MATHEMATICAL-MODELING OF BIOFILM ON ACTIVATED CARBON." Environmental Science & Technology 21(3): 273-280.

Clifford W. Randall, James L. Barnard and H. D. Stensel (May 6, 1998). Design and retrofit of wastewater treatment plants for biological nutrient removal. Lancaster, PA., CRC.

Cornier J.C., C. Fayoux, A. Lesouef and D. Villessot (1994). Les nouvelles contraients d'exploitation des usines d'épuration, Bruxelles. TSM89: 392-406.

Coustumer, S. L., T. D. Fletcher, A. Deletic and M. Potter (2008). Hydraulic performance of biofiltersystems for stormwater management: lessons from a field study. D. o. C. E. Facility for Advancing Water Biofiltration, Institute for Sustainable Water Resources, Monash University. Melbourne, Australian Government: 28.

Crites, R. and G. Tchobanoglous (1998). Small and Decentralized Wastewater Management Systems. The McGraw-Hill Companies. Boston, Massachusetts.

Crine, M., P. Marchot and G. Lhomme (1992). "STATISTICAL HYDRODYNAMICS IN TRICKLE FLOW COLUMNS." Aiche Journal 38(1): 136-147.

Daigger, G. T., T. A. Heinemann, G. Land and R. S. Watson (1994). "PRACTICAL EXPERIENCE WITH COMBINED CARBON OXIDATION AND NITRIFICATION IN PLASTIC MEDIA TRICKLING FILTERS." Water Science and Technology 29(10-11): 189-196.

Darakchiev, R. D. and N. N. Kolev (1996). "Packed bioreactor: Hydrodynamic behavior and mass transfer." Theoretical Foundations of Chemical Engineering 30(2): 144-147.

Desbos, G., F. Rogalla, J. Sibony and M. M. Bourbigot (1990). "BIOFILTRATION AS A COMPACT TECHNIQUE FOR SMALL WASTE-WATER TREATMENT PLANTS." Water Science and Technology 22(3-4): 145-152.

D. Elenter, K. Milferstedt, W. Zhang, M. Hausner, and E. Morgenroth, Influence of detachment on substrate removal and microbial ecology in a heterotrophic/autotrophic

biofilm, in Water Research, 2007, pp. 4657-4671.

Don, E. B., G. H. Teletzke and F. G. Pohland (1959). "Fundamental Hydraulic Principles of Trickling Filters." Sewage and Industrial Wastes 31(3): 243-253.

Eberl, H. J., C. Picioreanu, J. J. Heijnen and M. C. M. van Loosdrecht (2000). "A three-dimensional numerical study on the correlation of spatial structure, hydrodynamic conditions, and mass transfer and conversion in biofilms." Chemical Engineering Science 55(24): 6209-6222.

Eckenfelder, W. W., Jr. and E. L. Barnhart (1963). "Performance of a High Rate Trickling Filter Using Selected Media." Journal (Water Pollution Control Federation) 35(12): 1535-1551.

Eckenfelder, W. W. and R. F. Weston (1956). Kinetics of biological Oxidation. Biological Treatment of Sewage and Industrial Wastes. N. J. Horan. Reinhold, New York. Vol I: New York.

Elenter, D., K. Milferstedt, W. Zhang, M. Hausner and E. Morgenroth (2007). "Influence of detachment on substrate removal and microbial ecology in a heterotrophic/autotrophic biofilm." Water Research 41(20): 4657-4671.

EPA (1980). Converting rock trickling filters to plastic media: Design and performance. U. S. E. P. Agency. Cincinnati, U. S. EPA. 600280120: 192.

EPA (2000). Wastewater-Technology Fact Sheet: Nitrifying reactor. U. S. E. P. Agency. Cincinnati, U. S. EPA.

Trickling Filter Nitrification. E. P. Agency. Washington, D.C., Office of Water. EPA 832-F-00-015.

Fan, L. S., R. Leyvaramos, K. D. Wisecarver and B. J. Zehner (1990). "DIFFUSION OF PHENOL THROUGH A BIOFILM GROWN ON ACTIVATED CARBON PARTICLES IN A DRAFT-TUBE 3-PHASE FLUIDIZED-BED BIOREACTOR." Biotechnology and Bioengineering 35(3): 279-286.

France, M. o. A. o. (2003). L'assainissement des communes rurales.

Fruhen, M., E. Christan, W. Gujer and O. Wanner (1991). "SIGNIFICANCE OF SPATIAL-DISTRIBUTION OF MICROBIAL SPECIES IN MIXED CULTURE BIOFILMS." Water Science and Technology 23(7-9): 1365-1374.

Fujie, K., T. Sekizawa and H. Kubota (1977). "MASS-TRANSFER IN LIQUID-PHASE WITH TUBULAR WASTEWATER-TREATMENT CONTRACTOR." Journal of Fermentation Technology 55(5): 532-543.

G. Tchobanoglous (1972). Evaluation of the Progress of the City of Sacramento in Meeting the Discharge Requirements Established for the Main Wastewater Treatment Plant. Davis,State of California, Attorney General's Office.

Gordon, M. F., R. E. Fuhrman, C. C. Ruchhoft, H. A. Thomas, Jr. and F. W. Mohlman (1948). "Sewage Treatment at Military Installations: Summary and Conclusions." Sewage Works Journal 20(1): 52-95.

Gray, N. F. (1992). "How nature deals with waste." Biology of wastewater treatment Chapter 1.

Gujer, W. and M. Boller (1984). "OPERATING EXPERIENCE WITH PLASTIC MEDIA TERTIARY TRICKLING FILTERS FOR NITRIFICATION." Water Science and Technology 16(10-1): 201-213.

Gujer, W. and M. Boller (1986). "Design of a nitrifying tertiary trickling filter based on theoretical concepts." Water Research 20(11): 1353-1362.

Gönenç, E. and P. Harremoës (1990). "Nitrification in rotating disc systems--II. Criteria for simultaneous mineralization and nitrification." Water Research 24(4): 499-505.

Harrison, J. R. and G. T. Daigger (1987). "A Comparison of Trickling Filter Media." Journal (Water Pollution Control Federation) 59(7): 679-685.

Higbe, R. (1935). "The Rate of absorption of Pure Gas into a still liquid During Short Periods of Exposure." Inst. Chem. Engr 31: 365-389.

Hinson, R. K. and W. M. Kocher (1996). "Model for effective diffusivities in aerobic biofilms." Journal of Environmental Engineering-Asce 122(11): 1023-1030.

Horn, H. and D. C. Hempel (1997). "Substrate utilization and mass transfer in an autotrophic biofilm system: Experimental results and numerical simulation." Biotechnology and Bioengineering 53(4): 363-371.

Horn, H. and E. Morgenroth (2006). "Transport of oxygen, sodium chloride, and sodium nitrate in biofilms." Chemical Engineering Science 61(5): 1347-1356.

Horn, H., H. Reiff and E. Morgenroth (2003). "Simulation of growth and detachment in biofilm systems under defined hydrodynamic conditions." Biotechnology and Bioengineering 81(5): 607-617.

Howland, W. E. (1958). Flow Over Porous Media as in a Trickling Filter. Proc. 12th Ind. Waste Conf., Purdue Univiversity.

I. Mozo, G. Lesage, J. Yin, Y. Bessiere, L. Barna, and M. Sperandio, Dynamic modeling of biodegradation and volatilization of hazardous aromatic substances in aerobic bioreactor, in Water Research, 2012, pp. 5327-5342.

J. B.Wijffels, Verloop J. and Zuiderweg F. J. (1974). Wetting of Catalyst Particles under Trickle Flow Conditions.

Jaroszynski, M., I. Bylica, A. Kolodziej, A. Gorak & B. Janus (2008) EXPERIMENTAL STUDY ON LIQUID HOLD-UP FOR STRUCTURED CATALYTIC PACKINGS. Chemical and Process Engineering-Inzynieria Chemiczna I Procesowa, 29, 623-637.

Jaroszynski, M. & A. Kolodziej (2006) Diffusional and flow characteristics of column packing used in catalytic distillation. Przemysl Chemiczny, 85, 1113-1116.

Jaroszynski, M., A. Kolodziej & I. Bylica (2002) Mass transfer in columns equipped with structured reactive packing. Inzynieria Chemiczna I Procesowa, 23, 495-506.

Jaroszynski, M., A. Kolodziej, I. Bylica & W. Smolec (2000) Hydrodynamics of columns equipped with structured reactive packing. Inzynieria Chemiczna I Procesowa, 21, 691-705.

Jaroszynski, M. & A. S. Kolodziej (1993) LIQUID HOLDUP IN TRICKLE-BED COCURRENT REACTIONS. Inzynieria Chemiczna I Procesowa, 14, 359-373.

M. Jaroszynski, and A.S. Kolodziej (1994), CONVECTIVE HEAT-TRANSFER FOR THE CASE OF THE SOLAR HEATING DEVICES - THERMAL DIODES, in Inzynieria Chemiczna I Procesowa, 1994, pp. 379-392.

Kolodziej, A., M. Jaroszynski & I. Bylica (2003) Reactive column internals and their individual hydrodynamic characteristics. Przemysl Chemiczny, 82, 1214-1217.

Kolodziej, A., M. Jaroszynski, A. Hoffmann & A. Gorak (2001) Determination of catalytic packing characteristics for reactive distillation. Catalysis Today, 69, 75-85.

Kulkarni, A. A., A. K. Gorasia & V. V. Ranade (2007) Hydrodynamics and liquid phase residence time distribution in mesh microreactor. Chemical Engineering Science, 62, 7484-7493.

Kulkarni, A. A. & V. S. Kalyani (2009) Two-Phase Flow in Minichannels: Hydrodynamics, Pressure Drop, and Residence Time Distribution. Industrial & Engineering Chemistry Research, 48, 8193-8204.

Kulkarni, A. V. & J. B. Joshi (2006) Estimation of hydrodynamic and heat transfer characteristics of bubble column by analysis of wall pressure measurements and CFD simulations. Chemical Engineering Research & Design, 84, 601-609.

Kundu, A., K. D. P. Nigam & R. P. Verma (2003) Catalyst wetting characteristics in trickle-bed reactors. Aiche Journal, 49, 2253-2263.

Kornegay, B. H. and J. F. Andrews (1968). "Kinetics of Fixed-Film Biological Reactors." Journal (Water Pollution Control Federation) 40(11): R460-R468.

Kreikenbohm, R. and W. Stephan (1985). "APPLICATION OF A 2-COMPARTMENT MODEL TO THE WALL GROWTH OF PELOBACTER-ACIDIGALLICI UNDER CONTINUOUS CULTURE CONDITIONS." Biotechnology and Bioengineering 27(3): 296-301.

Kwok, W. K., C. Picioreanu, S. L. Ong, M. C. M. van Loosdrecht, W. J. Ng and J. J. Heijnen (1998). "Influence of biomass production and detachment forces on biofilm structures in a biofilm airlift suspension reactor." Biotechnology and Bioengineering 58(4): 400-407.

Laak, R. (1980). Wastewater Engineering Design for Unsewered Areas, Ann Arbor Science

Publishers.

Lackner, S., A. Terada and B. F. Smets (2008). "Heterotrophic activity compromises autotrophic nitrogen removal in membrane-aerated biofilms: Results of a modeling study." Water Research 42(4-5): 1102-1112.

Lekhlif, B., D. Toye, P. Marchot and M. Crine (1994). "INTERACTIONS BETWEEN THE BIOFILM GROWTH AND THE HYDRODYNAMICS IN AN AEROBIC TRICKLING FILTER." Water Science and Technology 29(10-11): 423-430.

Lesikar, B. and R. Persyn On-site wastewater treatment systems-Trickling Filter. T. A. M. University, Agricultural Communications. L-5345.

Levine, A. D., G. Tchobanoglous and T. Asano (1991). "Size distributions of particulate contaminants in wastewater and their impact on treatability." Water Research 25(8): 911-922.

Lijklema, L. (1987). "MODELING OF BIOLOGICAL PROCESSES IN THE SUBSURFACE." Water Science and Technology 19(7): 1144-1146.

Linping Kuai, Jiangping Qiu and Xudong Li (2003). Research and application on a novel combined trickling filter technology.

Logan, B. E., S. W. Hermanowicz and D. S. Parker (1987). "A Fundamental Model for Trickling Filter Process Design." Journal (Water Pollution Control Federation) 59(12): 1029-1042.

M. Sperandio, M.A. Labelle, A. Ramdani, A. Gadbois, E. Paul, Y. Comeau, and P.L. Dold, Modelling the degradation of endogenous residue and 'unbiodegradable' influent organic suspended solids to predict sludge production, in Water Sci Technol, 2013, pp. 789-96.

Manem, J. A. and B. E. Rittmann (1990). "SCALING PROCEDURE FOR BIOFILM PROCESSES." Water Science and Technology 22(1-2): 329-346.

Mascarau, G. (2008). Le service public d'assainissement non collectif.

Metcalf and Eddy (1991). Wastewater Engineering: Treatment, Disposal Reuse.

Metcalf and Eddy (1999). Wastewater Engineering: Treatment, Disposal Reuse.

Metcalf and Eddy (2003). Wastewater Engineering: Treatment, Disposal Reuse.

MOREL, A. and S. DIENER (2006). Greywater Management in Low and Middle-Income Countries, Review of different treatment systems for households or neighbourhoods. Duebendorf.

Morgenroth, E. and P. A. Wilderer (2000). "Influence of detachment mechanisms on competition in biofilms." Water Research 34(2): 417-426.

Morís, M. A., F. V. Díez and J. Coca (1997). "Hydrodynamics of a rotating disc contactor." Separation and Purification Technology 11(2): 79-92.

Muslu, Y. and L. Saltabas (1992). "A STUDY OF BIOLOGICAL FILTRATION USING FLOW-THROUGH TRACER TECHNIQUES." Journal of Chemical Technology and Biotechnology 54(4): 359-367.

Nengwang, C. (2004). Estimates of Household Wastewater Loads from Jiulong River Watershed.

Newbry, B. W., G. T. Daigger and D. Taniguchi-Dennis (1988). "Unit Process Tradeoffs for Combined Trickling Filter and Activated Sludge Processes." Journal (Water Pollution Control Federation) 60(10): 1813-1821.

Nicolella, C., M. C. M. van Loosdrecht and J. J. Heijnen (2000). "Wastewater treatment with particulate biofilm reactors." Journal of Biotechnology 80(1): 1-33.

Ohashi, A., D. G. V. deSilva, B. Mobarry, J. A. Manem, D. A. Stahl and B. E. Rittmann (1995). "Influence of substrate C/N ratio on the structure of multi-species biofilms consisting of nitrifiers and heterotrophs." Water Science and Technology 32(8): 75-84.

Okabe, S., K. Hiratia, Y. Ozawa and Y. Watanabe (1996). "Spatial microbial distributions of nitrifiers and heterotrophs in mixed-population biofilms." Biotechnology and Bioengineering 50(1): 24-35.

Okey, R. W. and O. E. Albertson (1989). "Diffusion's Role in Regulating Rate and Masking Temperature Effects in Fixed-Film Nitrification." Journal (Water Pollution Control Federation) 61(4): 500-509.

Ortiz-Arroyo, A., F. ç. Larachi and I. Iliuta (2003). "Method for inferring contact angle and for correlating static liquid hold-up in packed beds." Chemical Engineering Science 58(13): 2835-2855.

PAINTER, H. A., Ed. (1971). Chemical, physical and biological characteristics of wastes and waste effluents. Water and water pollution handbook. New York, Marcel Dekker, Inc.

Parker, D. S., T. Jacobs, E. Bower, D. W. Stowe and G. Farmer (1997). "Maximizing trickling filter nitrification rates through biofilm control: Research review and full scale application." Water Science and Technology 36(1): 255-262.

Peters, R. W. and J. E. Alleman. (1983). The history of fixed-film wastewater treatment systems. Fixed-film biological Pocesses for wastewater treatment. Y. C. Wu and E. D. Smith. Noyes, Park Ridge, NJ.

Peyton, B. M. and W. G. Characklis (1993). "A STATISTICAL-ANALYSIS OF THE EFFECT OF SUBSTRATE UTILIZATION AND SHEAR-STRESS ON THE KINETICS OF BIOFILM DETACHMENT." Biotechnology and Bioengineering 41(7): 728-735.

Picioreanu, C., M. C. M. van Loosdrecht and J. J. Heijnen (1998). "Mathematical modeling of biofilm structure with a hybrid differential-discrete cellular automaton approach." Biotechnology and Bioengineering 58(1): 101-116.

Picioreanu, C., M. C. M. van Loosdrecht and J. J. Heijnen (2000a). "A theoretical study on the effect of surface roughness on mass transport and transformation in biofilms." Biotechnology and Bioengineering 68(4): 355-369.

Picioreanu, C., M. C. M. van Loosdrecht and J. J. Heijnen (2000b). "Effect of diffusive and convective substrate transport on biofilm structure formation: A two-dimensional modeling study." Biotechnology and Bioengineering 69(5): 504-515.

Picioreanu, C., M. C. M. van Loosdrecht and J. J. Heijnen (2001). "Two-dimensional model of biofilm detachment caused by internal stress from liquid flow." Biotechnology and Bioengineering 72(2): 205-218.

Rampure, M. R., A. A. Kulkarni and V. V. Ranade (2007). "Hydrodynamics of bubble

column reactors at high gas velocity: Experiments and computational fluid dynamics (CFD) Simulations." Industrial & Engineering Chemistry Research 46(25): 8431-8447.

Richards, T. and D. Reinhart (1986). "Evaluation of Plastic Media in Trickling Filters." Journal (Water Pollution Control Federation) 58(7): 774-783.

Rittmann, B. E. and P. L. McCarty (1980). "MODEL OF STEADY-STATE-BIOFILM KINETICS." Biotechnology and Bioengineering 22(11): 2343-2357.

S. Ergun (1952). "Fluid flow through packed columns." Chemical Engineering Progress 48(2): 89-94.

Samb, F. M., M. Deront, N. Adler and P. Peringer (1996). "Dynamic liquid holdup and oxygen mass transfer in a cocurrent upflow bioreactor with small packing at low Reynolds numbers." Chemical Engineering Journal and the Biochemical Engineering Journal 62(3): 237-240.

Sarner, E. and S. Marklund (1985). "INFLUENCE OF PARTICULATE ORGANICS ON THE REMOVAL OF DISSOLVED ORGANICS IN FIXED-FILM BIOLOGICAL REACTORS." Water Science and Technology 17(2-3): 15-26.

Seguret, F., Y. Racault and M. Sardin (2000). "Hydrodynamic behaviour of full scale trickling filters." Water Research 34(5): 1551-1558.

Sharvelle, S., E. McLamore and M. K. Banks (2008). "Hydrodynamic characteristics in biotrickling filters as affected by packing material and hydraulic loading rate." Journal of Environmental Engineering-Asce 134(5): 346-352.

Shi Xiaoyan, Chen Mingxi and Y. Yunpeng (2005). "Research on Changing Rule of Campus Sewage Quality." JOURNAL OF CHINA THREE GORGES UNIVERSITY(NATURAL SCIENCES) 27(6)(X703).

Shigehisa Iwai, T. K. (1994). Wastewater treatment with microbial films, CRC Press.

Siebritz, I. P., G. A. Ekama and G. V. Marais (1983). "A PARAMETRIC MODEL FOR BIOLOGICAL EXCESS PHOSPHORUS REMOVAL." Water Science and Technology 15(3-4): 127-152.

Sivaguru, K., K. Begum and N. Anantharaman (2009). "Hydrodynamic studies on three-phase fluidized bed using CFD analysis." Chemical Engineering Journal 155(1-2): 207-214.

Smith, P. G. and P. Coackley (1984). "DIFFUSIVITY, TORTUOSITY AND PORE STRUCTURE OF ACTIVATED-SLUDGE." Water Research 18(1): 117-122.

Sorrels, J. H. and P. J. A. Zeller (1955). "Effect of Recirculation on Trickling Filter Performance." Sewage and Industrial Wastes 27(4): 415-430.

S. Okabe, K. Hiratia, Y. Ozawa, and Y. Watanabe, Spatial microbial distributions of nitrifiers and heterotrophs in mixed-population biofilms, in Biotechnology and Bioengineering, 1996, pp. 24-35.

Sperandio, M., Labelle, M.-A., Ramdani, A., Gadbois, A., Paul, E., Comeau, Y., Dold, P.L., 2013. Modelling the degradation of endogenous residue and “unbiodegradable” influent organic suspended solids to predict sludge production. Water Sci. Technol. J. Int. Assoc. Water Pollut. Res. 67, 789-796.

Speitel, G. E. and F. A. Digiano (1987). "BIOFILM SHEARING UNDER DYNAMIC CONDITIONS." Journal of Environmental Engineering-Asce 113(3): 464-475.

Spellman, F. R. (1999). Spellman's Standard Handbook for Wastewater Operators: Fundamental Level, Taylor & Francis Inc;.

State-Planning-Commission (1987). Outdoor drainage design Criterions. China. GBJ14-87.

Stenquist, R. J., D. S. Parker and T. J. Dosh (1974). "CARBON OXIDATION-NITRIFICATION IN SYNTHETIC MEDIA TRICKLING FILTERS." Journal Water Pollution Control Federation 46(10): 2327-2339.

Stewart, P. S. (1993). "A model of biofilm detachment." Biotechnology Bioengnieering 41: 111-117.

Sivaguru, K., K. Begum & N. Anantharaman (2009) Hydrodynamic studies on three-phase fluidized bed using CFD analysis. Chemical Engineering Journal, 155, 207-214.

Suess, P. & L. Spiegel (1992) HOLD-UP OF MELLAPAK STRUCTURED PACKINGS. Chemical Engineering and Processing, 31, 119-124.

Suess, P. and L. Spiegel (1992). "HOLD-UP OF MELLAPAK STRUCTURED PACKINGS." Chemical Engineering and Processing 31(2): 119-124.

SWILLEY, E. L. (1965). TRANSPORT PHENOMENA AND RATE CONTROL IN TRICKLING FILTER FLOW MODELS. PhD, Rice University.

Tang, W. T. and L. S. Fan (1987). "STEADY-STATE PHENOL DEGRADATION IN A DRAFT-TUBE, GAS-LIQUID-SOLID FLUIDIZED-BED BIOREACTOR." Aiche Journal 33(2): 239-249.

T.C. Zhang, Y.C. Fu, and P.L. Bishop, Competition for substrate and space in biofilms, in Water Environment Research, 1995, pp. 992-1003.

Tijhuis, L., M. C. M. Vanloosdrecht and J. J. Heijnen (1995). "DYNAMICS OF BIOFILM DETACHMENT IN BIOFILM AIRLIFT SUSPENSION REACTORS." Biotechnology and Bioengineering 45(6): 481-487.

Trulear, M. G. and W. G. Characklis (1982). "DYNAMICS OF BIOFILM PROCESSES." Journal Water Pollution Control Federation 54(9): 1288-1301.

V Tandoi, D Jenkins and J. Wanner (2006). Activated sludge separation problems: theory, control measures and practical experience. London, IWA. 9781900222846: 216.

Viva, A. and E. Brunazzi (2009). "The influence of modular structure on the hydrodynamics of catalytic structured packings for reactive separation processes." Icheap-9: 9th International Conference on Chemical and Process Engineering, Pts 1-3 17: 1519-1524.

Vogelpohl, A. (1975). "EFFECTIVE INTERFACIAL AREA IN IRRIGATED PACKED-COLUMNS." Chemical Engineering Science 30(4): 452-452.

Wanner, O. and W. Gujer (1985). "COMPETITION IN BIOFILMS." Water Science and Technology 17(2-3): 27-44.

Wanner, O. and P. Reichert (1996). "Mathematical modeling of mixed-culture biofilms." Biotechnology and Bioengineering 49(2): 172-184.

O. Wanner, and E. Morgenroth (2004), Biofilm modeling with AQUASIM, in Water Sci Technol, 2004, pp. 137-44.

Wasche, S., H. Horn and D. C. Hempel (2002). "Influence of growth conditions on biofilm development and mass transfer at the bulk/biofilm interface." Water Research 36(19): 4775-4784.

WEF (2000). Aerobic Fixed-Growth Reactors, Water Environment Federation.

Wentzel, M. C., G. A. Ekama, P. L. Dold and G. V. Marais (1990). "BIOLOGICAL EXCESS PHOSPHORUS REMOVAL - STEADY-STATE PROCESS DESIGN." Water Sa 16(1): 29-48.

Wentzel, M. C., G. A. Ekama and G. V. Marais (1992). "PROCESSES AND MODELING OF NITRIFICATION DENITRIFICATION BIOLOGICAL EXCESS PHOSPHORUS REMOVAL SYSTEMS - A REVIEW." Water Science and Technology 25(6): 59-82.

Wentzel, M. C., L. H. Lotter, G. A. Ekama, R. E. Loewenthal and G. V. R. Marais (1991). "EVALUATION OF BIOCHEMICAL-MODELS FOR BIOLOGICAL EXCESS PHOSPHORUS REMOVAL." Water Science and Technology 23(4-6): 567-576.

West, G. (2008). Biofilter Media Review, Hatchery international. 9: 38-39.

Westrin, B. A. and A. Axelsson (1991). "DIFFUSION IN GELS CONTAINING IMMOBILIZED CELLS - A CRITICAL-REVIEW." Biotechnology and Bioengineering 38(5): 439-446.

Williamson, K. and P. L. McCarty (1976). "MODEL OF SUBSTRATE UTILIZATION BY BACTERIAL FILMS." Journal Water Pollution Control Federation 48(1): 9-24.

Woolard, C. R. (1997). "The advantages of periodically operated biofilm reactors for the treatment of highly variable wastewater." Water Science and Technology 35(1): 199-206.

Xavier, J. D., C. Picioreanu and M. C. M. van Loosdrecht (2005). "A general description of detachment for multidimensional modelling of biofilms." Biotechnology and Bioengineering 91(6): 651-669.

Xin, Z., F. Yong-sheng, F. Xing-jian and H. Shuai (2008). "The sewage of village life disposal rule and processing method research." GUANGDONG AGRICULTURAL SCIENCES (8)(X824).

Xu, B. and T. Long (2000). Contemporary Principles of Water and Wastewater Treatment. Beijing, High Education Press (HEP).

Yano, T., T. Kodoma and K. Yamada (1961). "Fundamental studies on aerobic fermentations. Part III: Oxygen transfer within a mold pellet." Agriculture Biological Chemistry 25((7)): 580-584.

Yingqing, G., HUANG Xiangfeng, ZHANG Yuxian, QWI Yong, C. Yizhong and P. Mingguo. (2010). Study on selection of treatment technology pattern for rural municipal wastewater demonstration project in Taihu Lake Region. Proceedings of the 2010 Rural Wastewater Treatment Practical Technologies Conference.

Zelong, M., H. Zhirong and Z. Yun (2010). "Rural wastewater treatment technologies employed in Sichuan." Water Industry and Markets 703(2).

Zhang, T. C. and P. L. Bishop (1994). "DENSITY, POROSITY, AND PORE STRUCTURE OF BIOFILMS." Water Research 28(11): 2267-2277.

Zhang, T. C. and P. L. Bishop (1994). "EVALUATION OF TORTUOSITY FACTORS AND EFFECTIVE DIFFUSIVITIES IN BIOFILMS." Water Research 28(11): 2279-2287.

Zhang, T. C., Y. C. Fu and P. L. Bishop (1994). "COMPETITION IN BIOFILMS." Water Science and Technology 29(10-11): 263-270.

Zhang, T. C., Y. C. Fu and P. L. Bishop (1995). "Competition for substrate and space in biofilms." Water Environment Research 67(6): 992-1003.

Zhen, Y., S. Yang-cai, Q. Jiang-ping and K. Lin-ping (2006). "TREATMENT OF RESTAURANT WASTEWATER BY NOVEL BIOTRICKLING FILTER." TECHNOLOGY OF WATER TREATMENT 32(7)(X703.1).

Équip., B. O. M. (1997). l'assainissement collectif des communes- Ouvrages de capacité inférieure à 120 kgDBO5/jour. d. l. d. t. e. d. t. Ministère de l'Equipement, AIDA. 399-97/8.

Appendix

Appendix 1 - Dimensioning a lab-scale pilot set-up and Discussion of the interval space

1. Dimensioning trial based on COD removal

We tried to design a pilot in purpose to remove BOD, the modified Velz method and organic loads formula (Metcalf and Eddy, 1991) were taken into account as in previous discussion.

$$\frac{S_{out}}{S_{in}} = e^{\frac{-k\ D}{q^n}}$$

$$k_2 = k_1(\frac{D_1}{D_2})^{0.5}(\frac{S_{1,in}}{S_{2,in}})^{0.5}$$

$$E = \frac{100}{1+0.505\times\left(\frac{C_{vBOD}}{F}\right)^{0.5}}$$

where

k_1=0.21(L/s)$^{1/2}$/m²

S1=150 gBOD/m³

The dimensioning of the pilot was carried out as follows:

C_{vBOD} is the volumetric BOD loads where we take the classic value of **0.2** kgBOD/m³d proposed by (EPA, 1980); so the BOD removal efficiency E=82%.

The ratio of outlet BOD/inlet BOD in Velz equation=1-E=1-0.82=0.18;

Take classic value n=0.5 of the media constant

Take classic value k=0.7 of the reaction constant

Hydraulic loads= 4 m/d for a low-rate Trickling Filter (EPA, 1980)

Hence, packing depth D is calculated as 2.4 m

Volume of filter=0.075m³

Cross-section area=0.031m²

Hence, diameter of section≈0.2m

Column height (m)	Inner Diameter (m)	Packing Depth (m)	Volume (m³)
>2.4	0.2	2.4	0.075

To choose the feasible feeding flowrate, (Heijnen et al., 1984; Tijhuis et al., 1994) reported that biofilm will form when the dilution rate (shown in Eq.V-1) is greater than the observed

heterotrophic specific growth coefficient $D_H > \mu_{obs}$ in a packed-bed bioreactor; otherwise, the biofilm will not form before it is washed out from filter, with the hydraulic retention time τ_H.

$$D_H = \frac{1}{\tau_H} = \frac{Q}{V} > \mu_{obs} = \mu_{\max} - k_d$$

Since the classic values of μ_{max} are in the range of 0.6-13.2 d^{-1}, decay coefficient k_d is in the range of 0.05-0.2 d^{-1} (Metcalf and Eddy, 1991). Additionally, regarding the mean daily flow in rural areas as 100 m³/d (approximate 500P.E.×200L/P.E./d, see part 1), volume of liquid input V can be calculated in the range of 8-250 m³.

2. Dimensioning trial based on nitrification

For dimensioning a single-stage TF for nitrifying combine with BOD removal, amount of information is available. Sizing of the trickling filter is normally based on past experience and correlation with similar installations, particularly in the case of municipal wastewater treatment (Swilley, 1965). Technically, the equations based on the nitrification rate and Nitrogen removal for sizing a filter is as follows:

$$A_{TF} = \frac{P_{TAN}}{r_{TAN}}$$

$$V_{TF} = \frac{A_{TF}}{a}$$

$$A_{CS} = \frac{Q}{HSL}$$

$$D = 2 \times \sqrt{\frac{A_{CS}}{\pi}}$$

$$H = \frac{V_{TF}}{S_{CSA}}$$

where A_{TF} is the total surface area of trickling filter (m^2); P_{TAN} is total ammonia nitrogen load (g/day); r_{TAN} is maximum nitrification rate (g TAN/m^2/day); V_{TF} is the volume of Trickling Filter (m^3); a_p denotes the special surface area of media (m^2/m^3); A_{CS} is cross-sectional area (m^2); Q is the flow rate (m^3/day); H.S.L is hydraulic surface load (m^3/ m^2/day); D-The diameter of column (m); H- The height of column (m);

The mean ammonia nitrogen load $P_{tanload}$=1.19 kgTAN/d for rural wastewater;
Estimated nitrification rate r_{tan}-take 0.8 g TAN/m^2/d from Figure II-13;

V- Volume of Trickling Filter (m^3); calculated as 0.075

a- Special surface area of media (m^2/m^3); chose 500

Scross-sectional area-Cross-sectional area (m^2); calculated as 0.0375

Q -The flow rate (m^3/day); here take 100 m^3/d

HSL- Hydraulic surface loads (m^3/ m^2/day); take 4 m/d

Ddiameter-The diameter of trickling filter (m); as 0.11 m

Hheight- The height of the media (m); as 2 m

Column Height (m)	Inner Diameter (m)	Packing Depth (m)	Volume (m^3)
>2	0.22	2	0.075

The schema of the experimental pilot drawn by software AUTOCAD is shown in Figure A1-1.

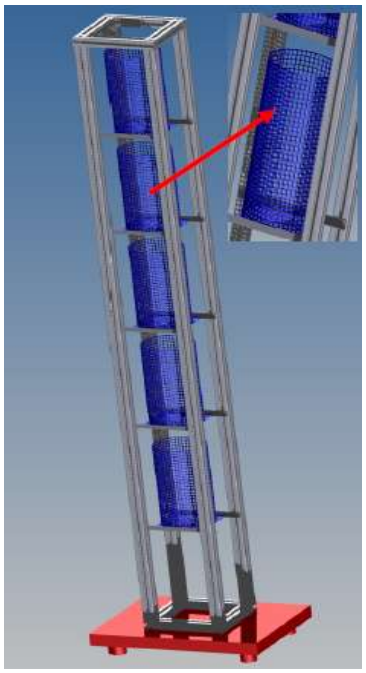

Figure A1- 1: Schematic diagram of the experimental pilot

3. Interval distance determination

The interval space/distance between the two adjacent sections was intentionally set up in order to improve the natural aeration, which was the same purpose of making the multi-section bioreactor into open structure with holes around the wall of the section frames. However, the principle of natural ventilation and the water transport were not well investigated even this bioreactor were already widely employed in rural wastewater treatment in some villages in Shanghai of China. The discussions of the interval space in terms of the

water-droplet spill/splashing natural ventilation and pressure drop aspects were hereafter carried out. In order to avoid the lose of the water droplet from the outside edge in the top of each section, the interval distance should be taken into discussion and the liquid splash exist in practical application when longer distance and greater hydraulic loads applied; however, the boundary interval distance do exist when considering the liquid transport between two adjacent sections.

Lots studies of the liquid droplet spread/splash have been reported; however two main types was taken into our concern: 1. liquid droplet onto liquid surface (Werner, 2007; Rein, 1993; Liu, 2003; Liu, 2009); 2.liquid droplet onto solid surface (Bowden, 1964; Rein, 1993; Chan, 2005); both the two cases existed in our study. However, their methods were not simplified because the first liquid droplet impact onto the dry particle surface and wet the solid surface due to the hydrophilic surface of our media, after the first droplet following by the droplet contacting on a liquid-solid surface, the phenomena is more complex when considering that the liquid film was formed .

In our case, we disregarded the influence of wind resistance, buoyancy and temperature such environmental factors; neither the loss of sound energy nor the dissipated energy loss during the liquid-surface impact were taken into account, only the basic conservation of momentum and kinetic energy were considered. The basic simplified principle is depicted in Figure A1-2.

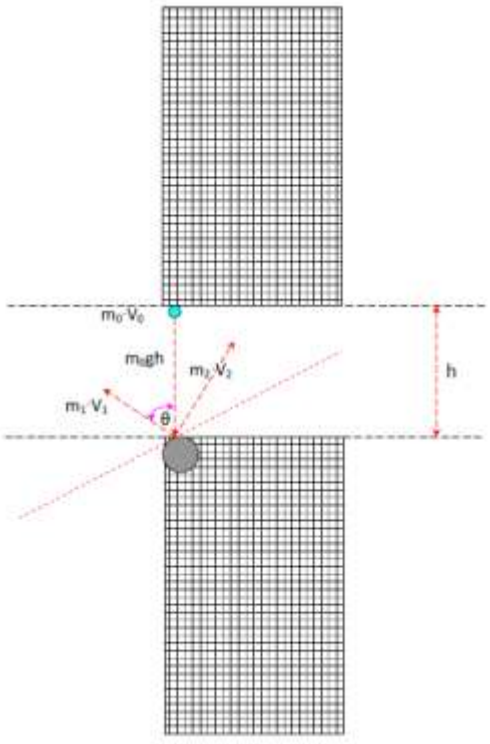

Figure A1- 2: Interval distance determination schema

Based on the principles of conservation of momentum and kinetic energy, the assumption of calculating the water droplet spilling at the edge of lower section was deduced by following dimensionless relations:

$$m_0 V^* = m_1 V_1 \cos\theta + m_2 V_2 \sin\theta$$

$$\frac{m_0 V_0^2}{2} + m_0 g h = \frac{m_0 (V^*)^2}{2}$$

$$m_1 V_1 \sin\theta = m_2 V_2 \cos\theta$$

$$m_0 = m_1 + m_2$$

$$m_0 = \rho \frac{4\pi}{3} \left(\frac{d_{droplet}}{2} \right)^3$$

where

m_0- The liquid droplet weight when leaving the bottom of upper section

m_1,m_2 –The weight of droplet separated into two direction after contacting with solid surface

θ- Projectile angle

V* is the instantaneous impact velocity of liquid droplet contacting the solid

V_1 and V_2 is the velocity in two direction after m_0 was separated into m_1 and m_2

Some researchers (Liu, 2003; Liu, 2009) investigated the diameter of liquid droplet and the initial velocity which are shown in Eq.

$$f(d) = \frac{1}{\lambda^{\alpha} \Gamma(\alpha)} d^{\alpha-1} \exp(-\frac{d}{\lambda})$$

$$f(V_0) = \frac{1}{\lambda^{\beta} \Gamma(\beta)} V_0^{\beta-1} \exp(-\frac{V_0}{\lambda})$$

Even the relations above hold true, some values are hard to be determined for calculating the interval distance ***h***. (Ortiz-Arroyo et al, 2003) investigated the contact angle with pure water and other kinds of liquid on numerous types of media. They found that θ≈30 ° is the mean contact angle of pure water droplet on porous ceramic; because the physical characteristics of the ceramic media are similar to our concrete block media, hence θ≈30 °can also be applied to our calculation.

In order to effectively wet the particle the θ<90° is necessary; and the loss weight m_1 should be the less the better. In our case, it was assumed the fraction of m_1 and m_2 equals 50% and the projectile angle θ≈30 °; substituting those values into the basic relations, H_{max}=0.1 m was acquired.

Generally, in order to maintain at least 50% of the liquid droplet at the splash edge, the interval distance H⩽0.1m is necessary.

In addition, the liquid droplet may splash from another edge of the section; the schema of the separated droplet projectile motion is depicted in Figure A1-3.

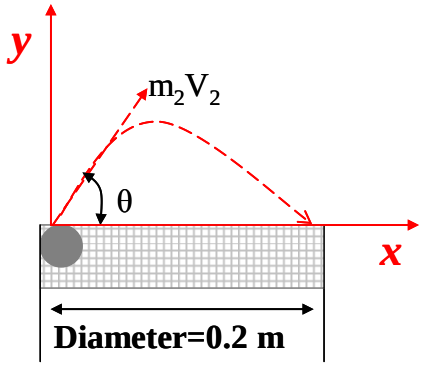

Figure A1-3: Schema of droplet paracurve splashing over another edge

Based on the principle of projectile motion and paracurve, the relations are present as follows:

$$V_x = V_2 \cos\theta$$

$$V_y = V_2 \sin\theta$$

$$t = \frac{2V_y}{g} = \frac{2V_2 \sin\theta}{g}$$

$$L = V_x t = V_2 \cos\theta \cdot \frac{2V_2 \sin\theta}{g} = \frac{V_2^2 \cdot 2\cos\theta \sin\theta}{g} = \frac{V_2^2 \cos 2\theta}{g}$$

The horizontal displacement of the separated droplet m_2 should theoretically be shorter than the diameter of the section equaling 0.2m to avoid splash loss.

When considering the projectile angle θ≈30 ° and the H_{max}=0.1 m, V_2=1,4 m/s.

Substituting those values into the energy conservation relations, L<0.2 m which implies the length is less than the diameter of section showing that the droplet won't projectile from another edge of section.

In general, the interval distance less than 10 cm is sufficient to avoid droplet splash from both edges of the section.

The pilot-scale MSB applied in this PhD study is presented in Figure A1-4.

Figure A1-4: Multi-Section Bioreactor pilot in experiments

Appendix 2- ASM1 model Matrix

Process	S_i	S_S	X_i	X_S	X_{BH}	X_{BA}	X_U	So	S_{NO}	S_{NH}	S_{ND}	X_{NO}	Process rate
Aerobic growth heterotrophy		$-\frac{1}{Y_H}$			1			$-\frac{1-Y_H}{Y_H}$		$-i_{XB}$			$\mu_H\left(\frac{S_S}{K_S+S_S}\right)\left(\frac{S_O}{K_{OH}+S_O}\right)X_{BH}$
Anoxic growth heterotrophy		$-\frac{1}{Y_H}$			1				$-\frac{1-Y_H}{2.86Y_H}$	$-i_{XB}$			$\mu_H\left(\frac{S_S}{K_S+S_S}\right)\left(\frac{K_{OH}}{K_{OH}+S_O}\right)\left(\frac{S_{NO}}{K_{NO}+S_{NO}}\right)\eta_g X_{BH}$
Aerobic growth autotrophy						1		$-\frac{4.57-Y_A}{Y_A}$	$\frac{1}{Y_A}$	$-i_{XB}-\frac{1}{Y_A}$			$\mu_{mA}\left(\frac{S_{NH}}{K_{NH}+S_{NH}}\right)\left(\frac{S_O}{K_{OA}+S_O}\right)X_{BA}$
Decay heterotrophy				$1-f_p$	-1		f_p					$i_{XB}-f_p i_{XP}$	$b_H X_{BH}$
Decay autotrophy				$1-f_p$		-1	f_p					$i_{XB}-f_p i_{XP}$	$b_A X_{BA}$
Ammonification										1	-1		$k_d S_{ND} X_{BH}$
Hydrolysis organic compounds		1		-1									$k_H \frac{X_S / X_{BH}}{K_X + X_S / X_{BH}}\left[\left(\frac{S_O}{K_{OH}+S_O}\right)+\eta_A\left(\frac{K_{OH}}{K_{OH}+S_O}\right)\left(\frac{S_{NO}}{K_{NO}+S_{NO}}\right)\right]X_{BH}$
Hydrolysis organic N											1	-1	$\rho_T\left(\frac{X_{ND}}{X_S}\right)$

S_i-unbiodegradable soluble matter (gCOD/m^3); S_S-Readily biodegradable substrate (gCOD/m^3); X_i-Particulate unbiodegradable matter (gCOD/m^3); X_S-Enmeshed slowly biodegradable substrate (gCOD/m^3); X_{BH}-Active heterotrophic biomass (gCOD/m^3); X_{BA}-Active autotrophic biomass (gCOD/m^3); X_U-Unbiodegradable particulates from cell decay (gCOD/m^3); S_O-Oxygen (gCOD/m^3); S_{NO}-Nitrate and Nitrite nitrogen (gN/m^3); S_{NH}-Ammonia nitrogen (gN/m^3); S_{ND}-Soluble biodegradable organic nitrogen (gN/m^3); X_{NO}-Particulate biodegradable organic nitrogen (gN/m^3)

Appendix 3-Diameter of medium estimation

To determine the particle diameter, different methods have been employed. The simplest method is to choose certain number of pieces randomly and measured their diameter by Calipers. The particle diameter distribution reported is shown in Figure A3-1 versus the sampling number.

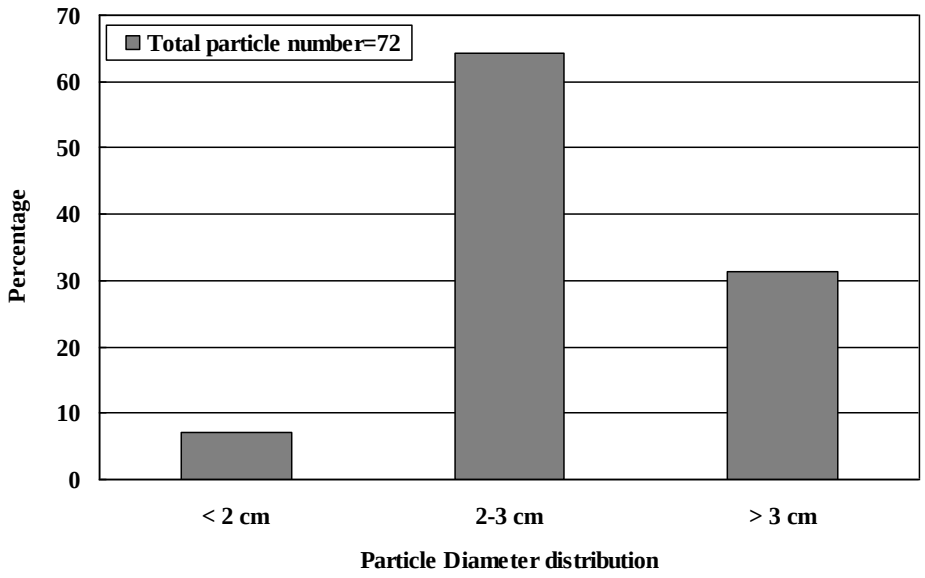

Figure A3- 1: Particle diameter distribution by random selection

In Figure A3-1, random selection of particle shows most particle diameter range of 2-3 cm. However, to more accurately measure the particle distribution, differential distribution and cumulative distribution were employed. Differential distribution represents the percentage of the particles mass in certain diameter range versus the total mass. The cumulative distribution represents the cumulative mass from the minimum diameter up to the larger one versus the total mass. Differential and cumulative distributions versus mass percentage are presented in Figure A3-2:

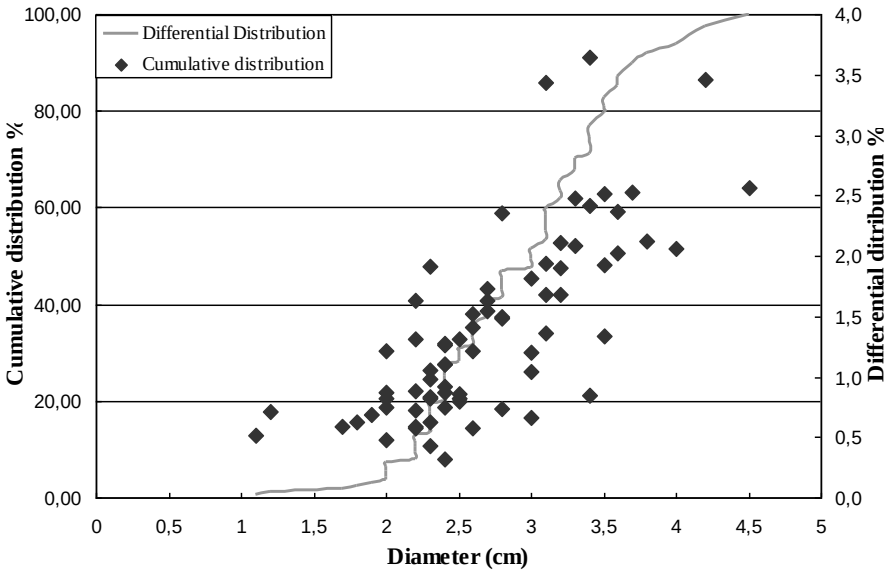

Figure A3- 2: Differential and cumulative distributions of particle diameters reported versus mass percentage

In Figure A3-2, differential distribution shows diameter of particles distribute in range of 2–4 cm with mean diameter 2.7±0.65 cm. Cumulative distribution shows that 60% particle diameter in the range of 2-3 cm. The particles were assumed as a sphere shape and using an individual particle mass together with particle density to estimate the volume of single particle. By using this obtained volume to calculate the theoretical diameter of an individual particle, the results were modified as shown in Figure A3-3.

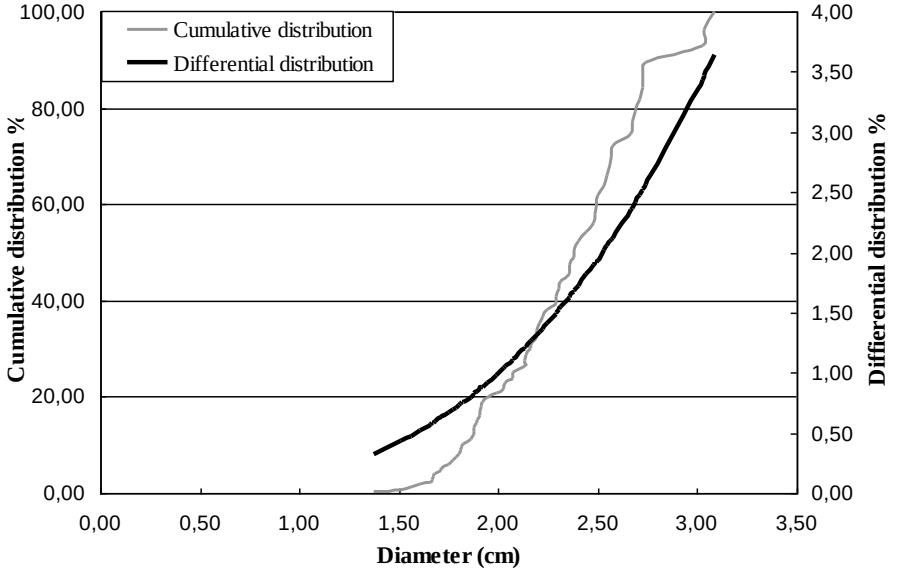

Figure A3- 3: Differential and cumulative distribution of particle diameter correlation

From Figure A3-3, the particle density of 586.4 kg/m^3 was applied to calculate the realistic diameter of particle with the assumption that all the particles were the sphere shape. Subsequently, the particle diameter distribute was calculated in the range 1.5-3.0 cm. Average particle diameter could be calculated as 2.17 ± 0.4 cm. In addition, in the static holdup experiments, 10-1000 pieces of particle were weighed and the average mass of single particle was 0.0034 kg. Nevertheless, with this assumption, using the particle density, the average diameter is about 2.2 cm which is in good agreement with the results in Figure A3-2.

Figure A3-4 represents the photo of one Concrete Brick medium particle, when we measured the diameter of particles by squared paper.

Figure A3- 4: Photo of Concrete Brick medium particle

Appendix 4 - Composition of primary sludge from GIENSTOUS and Viandox

The pilot filled with particles of porous concrete block media was fed by the primary sludge from a wastewater treatment plant-GINESTOUS after sifted on 1mm sieve and mixing with tap water to fulfil the influent composition requirements (300 mgCOD/L and 1000 mgCOD/L, respectively) for biological experiments during Inoculation to phase 3. The components concentrations of primary sludge from Ginetous are shown in Table A4-1.

Table A4-1: Components concentrations of primary sludge from GINESTOUS

CODt (g/L)	TSS (g/L)	VSS (g/L)	TKN (g/L)	Ammonia (mg/L)
69	82	72	4	170

Viandox (composition shown in Table A4-2) was employed during the high organic loads PHASE 4, components measurements indicated nearly no particulate COD exist in Viandox.

Table A4-2: Composition of Viandox

Components: Water, salt, yeast extract, coloring: caramel (E150c); soy sauce (water, soybeans, wheat, salt); flavor enhancers: monosodium glutamate, inosinate and disodium guanylate; acidifying: citric acid and lactic acid, extract of beef extract, spices (fenugreek, lovage), flavorings (including celery).

CODt (g/L)	CODs (g/L)	TSS (g/L)	VSS (g/L)	TKN (g/L)	$N\text{-}NH_4^+$ (mg/L)
160-185	160-180	0	0	11-12.5	800-900

Appendix 5-Static models without biofilm

For TFC:

First it is necessary to calculate the external capillary effect on to the solid

$$h_{externalcap} = \frac{6(1-\varepsilon)\sigma}{d_p \varepsilon \rho_L g}\cos 62° = 0.00029m$$

where ε = 0.61 is the particle porosity used in the trickle fix-bed column, σ= 72.8×10^{-3} $N.m^{-1}$ is the surface tension of water, d_p = 0.0217 m as the average particle diameter, ρ_L = 1000 kg/m^3 is mass density of water, θ = 62° proposed for the solid liquid contact angle and g = 9.8 $m.s^{-2}$ is gravity acceleration.

Secondly it is necessary to calculate the internal capillary effect into the solid

$$h_{internalcap} = \frac{6(1-\varepsilon)\sigma}{d_p \varepsilon \rho_L g}\cos 62° = 0.013m$$

where d_p = 0.001 m as the estimated pore diameter.

It can be observed from these calculated data that the internal capillary effect is more important than the external one.

The second part of the model must be applied to the holdup of the particle and then to the bed one. For a single particle, the external capillary holdup is defined as:

$$hl_{externalcap} = \frac{h_{externalcap}\varepsilon}{h_{cb}} = 0.004$$

For a single particle, the internal capillary holdup is defined as:

$$hl_{internalcap} = \frac{h_{internalcap}\varepsilon}{h_{cb}} = 0.39$$

where h_{cb} = 0.0217m is the particle height and ε= 0.61 is the fraction of the packing element.

So the total capillary holdup into the bed is deduced from:

$$hl_{cap} = hl_{internalcap} + hl_{externalcap} = \left(\frac{h_{internalcap}\varepsilon}{h_{cb}} + \frac{h_{externalcap}\varepsilon}{h_{cb}}\right).\varphi_{cb} = 0.176$$

where φ_{cb} is equal to the apparent bed porosity.

Correspondingly, the total residual water mass into the bed is calculated as:

$$m = hl_{cap} * V_{column} * \rho_{water} = 41.9\ kg$$

41 kg account for internal capillary water and only 0.9 kg for the external capillary water.

It was thus found that a 62° reliable solid-liquid contact angle allows matching with 42kg residual water mass obtained into the static holdup experiments in a TFC.

For MSB:

In this reactor the solid particles are the same but the dimensions of the reactor are changed. These differences do not modify the capillary holdup relate to a single particle properties but they change the entire bed properties and the corresponding residual quantities which are related to a new apparent bed porosity and a new column volume.
So the total capillary holdup into the bed was deduced from:

$$hl_{cap} = hl_{internalcap} + hl_{externalcap} = \left(\frac{h_{internalcap}\varepsilon}{h_{cb}} + \frac{h_{externalcap}\varepsilon}{h_{cb}}\right).\varphi_{cb} = 0.159$$

where φ_{cb} is the apparent bed porosity measured in the multi-section bioreactor.

Correspondingly, the total residual water mass in the packing bed was calculated:

$$m = hl_{cap} * V_{column} * \rho_{water} = 14.2\ kg$$

with 13.9 kg for internal capillary water and only 0.3 kg for external capillary water.

It was thus found that a 56° reliable solid-liquid contact angle allows matching with 14.2 kg residual water mass obtained into the static holdup experiments.

Appendix 6 -Calculated RTD curves comparing with experimental RTD

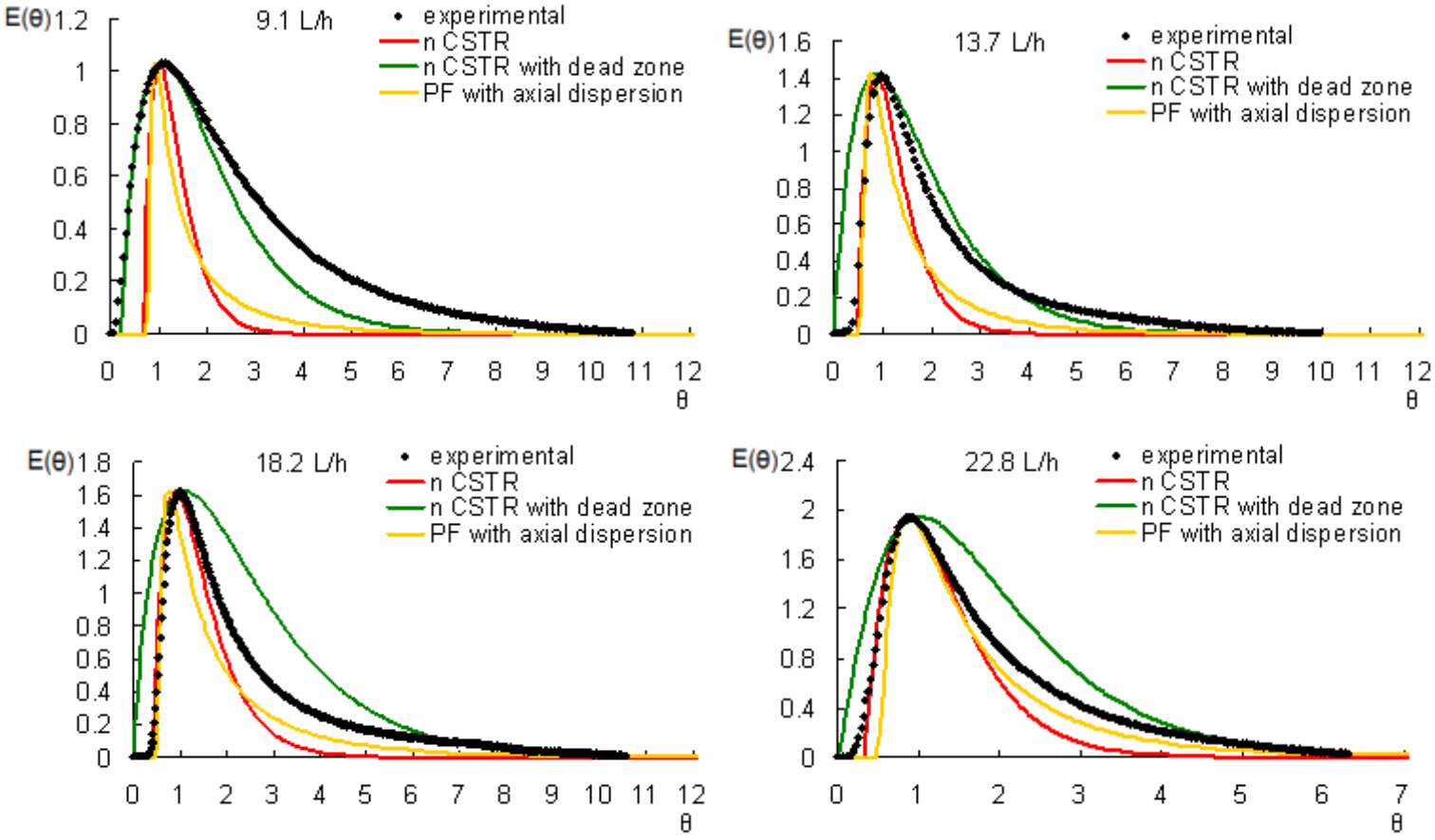

Figure A6-1: Experimental RTD and RTD models in the cases without biofilm

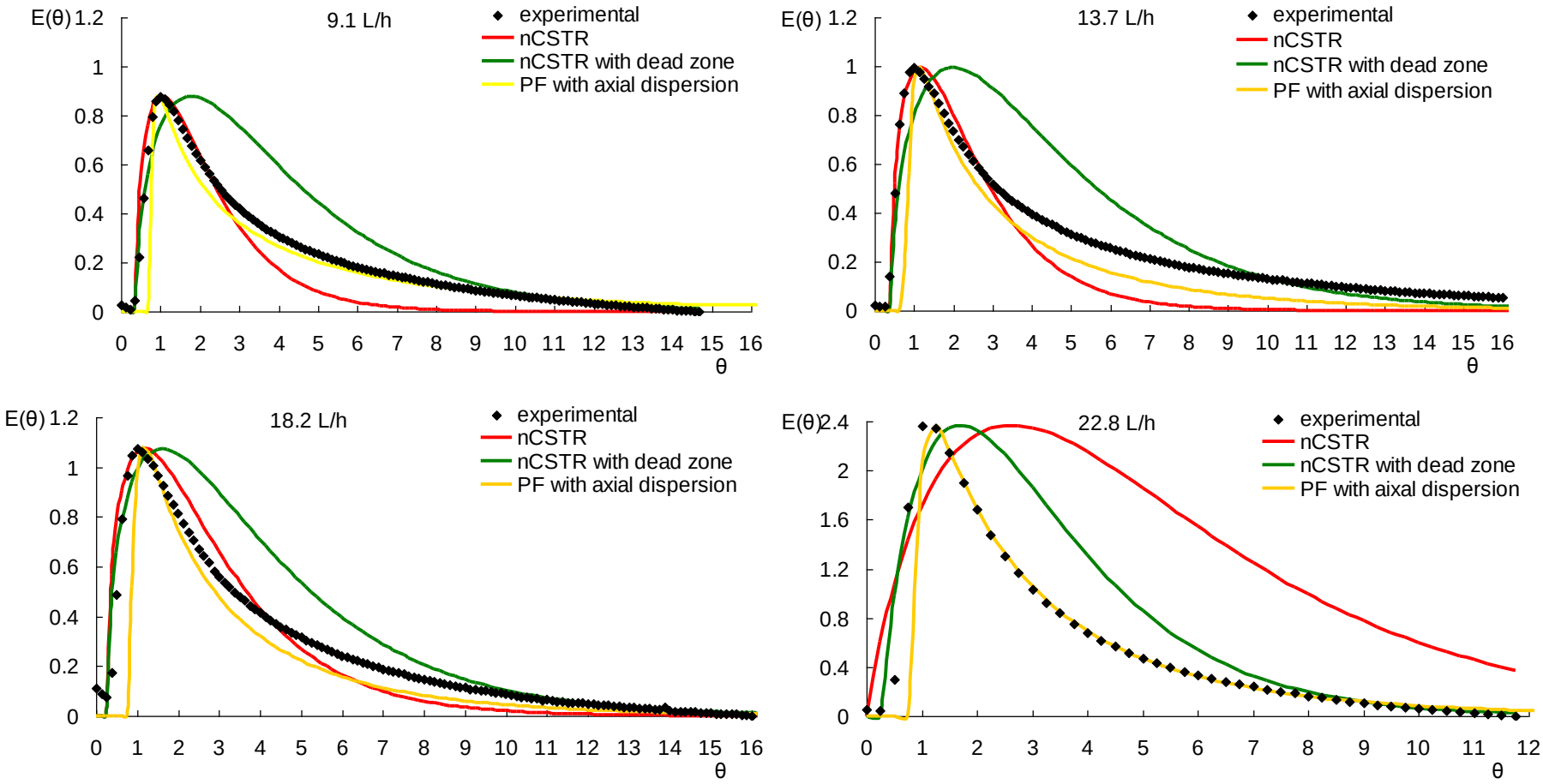

Figure A6-2: Experimental RTD and RTD models in the cases with thick biofilm

Figure A6-3: Experimental devices for RTD measurements

Appendix 7 - COD fractions and TKN fractions evaluation

Based on the measurements of ultimate BOD fraction, the soluble COD fraction and the filtered COD of total COD, the compositions of total COD can be estimated. An example of the relation between soluble COD and total COD is shown in Figure A7-1.

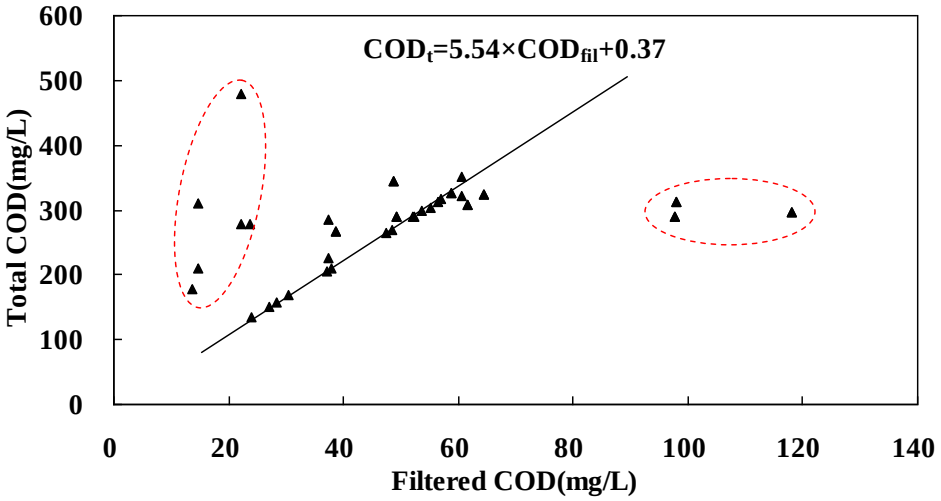

Figure A7-1: Relation between total COD and soluble COD

From Figure A7-1, a relation between soluble COD and total COD was obtained as follows:

$$(S_S + S_i + X_S + X_i) = 5.54(S_S + S_i) + 0.37$$

The fraction of soluble COD (Si+Ss) of total COD was measured about 0.18 after centrifugation. In addition, (Daigger et al., 1997) proposed a relation between ultimate BOD and biodegradable COD for a primary sludge as follows:

$$(S_S + X_S) = biodegraddble\,COD = \frac{BOD_U}{0.88}$$

Moreover, ultimate BOD was measured as about 70% of total COD.

The fraction of inert soluble COD (Si) was calculated as proposed by (Orhon et al., 1999a, b):

$$\frac{S_i}{COD_t} = \frac{Effluent\,COD_s}{Influent\,COD_t}$$

From the equations above, the fractions of total COD were obtained as shown in Table A7-1(literature data and in this study).

Table A7-1: Fractions of total COD in the primary wastewater after screening from Ginetous WWTP and other sources

Country, region	S_I %	S_S %	X_I %	X_S %	X_H %	$X_S(+X_H)$** %	VFA %	References
Japan	14.3*	26.7	8.20	41.0	9.8	50.8	16.0	Satoh *et al.*, 2000
Sweden							12.5	Lie and Welander, 1997
Denmark	7.7	24.3	19.4			48.6		Henze *et al.*, 1987
Switzerland	11.4	31.8	11.4			45.4		Henze *et al.*, 1987
Hungary	8.5	28.6	20.0			42.8		Henze *et al.*, 1987
Germany	5.4	27.4	19.2			48.0	8.70	Makinia *et al.*, 2005
	11.5	19.3	9.60	48.1	11.5	59.6	7.60	Henze *et al.*, 1999
Japan	14.0*	14.0*	10.0*	54.0*	8.0*	62.0*	10.80*	Funamizu *et al.*, 1997
Denmark	3.0	29.0	11.0	43.0	14.0	57.0		Henze, 1992
Switzerland	10.0	16.0	9.0	40.0	25.0	65.0		Solfrank, 1988
France	7.9	57.3	10.5	21.0	3.5	24.5		Lesouef *et al.*, 1992
South-Africa	8.0	28.0	4.0			60.0		Ekama *et al.*, 1986
Netherlands	4.6	41.50	16.6			37.2	13.0	Vanveldhuizen *et al.*, 1999
Netherlands	6.6	31.8	19.00			42.5	9.80	Brdjanovic *et al.*, 1999
Average	8.7	28.9	12.9	41.2	12.0	49.5	11.10	

* Estimate based on the article; ** Biomass COD is included in the slowly biodegradable substrate fraction

Source of data	Fraction of total COD (%)				
	Si	Ss	Xs	Xi	X_{bH}
(Henze et al., 1995)	5-10	12-30	30-60	10-15	5-15
(Makinia et al., 2000)	3-15	16-33	40-60	4-17	Not estimated
Our study	2-10(5)*	10-30(13)*	40-68(57)*	12-30(25)*	0

()* represents the mean value

TKN fractions estimation

The total organic nitrogen was determined by total TKN minus the S_{NH}. Furthermore, soluble biodegradable organic nitrogen S_{ND} was estimated by soluble TKN minus S_{NH}. X_{NI} is usually estimated as 0.1-0.15 of particulate inert organic material Xi (Metcalf and Eddy, 1991). The fractions of TKN were thereafter calculated based on these relations and shown in Table A7-2.

Table A7-2: Fractions of TKN

Source of data	Fraction of TKN (%)				
	SNH	SND	SNI	XND	XNI
GPS-X	65	3.5	0	21.9	9.6
Our study	65±6	4±2	1±1	20±2	10±1

Appendix 8 - Biomass accumulation and sludge production estimation

Based on the method of weighing the mass difference in each section, the mass of liquid static holdup should be extracted from the measured mass. As described in Chapter 3, at the end of period 2, the liquid static holdup accounts approximately for 12% of solid volume, at flowrate of 0.08m³/d; and the static holdup was about 17% at the end of period 3. Though the static liquid holdup was found increasing with the biofilm thickness development, we assumed at the pseudo steady state, the liquid static holdup mass was constant. Thus mass of the liquid static holdup was calculated as 2.1 and 2.6 kg, respectively. Using the measured mass of each section minus the liquid static holdup mass, the estimated mass of wet biomass can then be obtained.

The estimated mass of wet biomass in each section is shown in Table A8-1:

Days	Wet biomass (kg)				
	Section 1	Section 2	Section 3	Section 4	Section 5
			Period 2		
7	0.559	0.508	0.477	0.435	0.346
14	0.720	0.654	0.615	0.560	0.446
21	0.643	0.585	0.549	0.501	0.398
28	0.795	0.722	0.678	0.619	0.492
35	0.748	0.679	0.638	0.582	0.463
42	0.734	0.667	0.626	0.571	0.454
49	0.981	0.891	0.837	0.763	0.607
56	0.814	0.740	0.695	0.634	0.504
63	0.871	0.792	0.744	0.678	0.540
70	1.016	0.923	0.866	0.790	0.629
77	1.059	0.962	0.903	0.824	0.655
84	1.059	0.962	0.903	0.824	0.655
91	1.386	1.259	1.182	1.078	0.858
98	1.075	0.977	0.917	0.837	0.666
105	1.193	1.084	1.018	0.928	0.739
112	1.304	1.184	1.112	1.014	0.807
119	1.241	1.127	1.058	0.965	0.768
Average fraction	24%	22%	21%	19%	15%
			Period 3		
126	1.496	1.359	1.276	1.164	0.926
133	1.383	1.256	1.180	1.076	0.856
140	1.361	1.237	1.161	1.059	0.843
147	1.365	1.240	1.165	1.062	0.845
154	1.399	1.271	1.194	1.089	0.866
161	1.506	1.368	1.285	1.172	0.932
168	1.529	1.389	1.305	1.190	0.947
175	1.901	1.727	1.622	1.479	1.177
179	2.201	1.527	1.484	1.320	1.317

182	2.194	1.522	1.479	1.316	1.313
186	2.050	1.423	1.382	1.230	1.227
189	2.149	1.491	1.449	1.289	1.286
193	2.003	1.389	1.350	1.201	1.198
196	2.097	1.455	1.413	1.257	1.255
200	2.456	1.704	1.656	1.473	1.470
203	2.162	1.500	1.458	1.297	1.294
207	2.810	1.950	1.895	1.686	1.682
210	2.118	1.469	1.428	1.270	1.267
214	2.138	1.483	1.441	1.282	1.279
217	2.248	1.560	1.516	1.348	1.345
221	2.174	1.509	1.466	1.304	1.301
224	2.184	1.515	1.473	1.310	1.307
Average fraction	28%	20%	19%	17%	16%

*Average fraction is calculated by the average mass of wet biomass in each section divided by the sum of that in 5 sections.

From Table A8-1, it can be found that the biomass accumulation in the 1st section was always higher than that in other 4 sections, the biomass accumulation decreased along the filter. Under low OLR, the biomass accumulation distribution was more even. Under high OLR, the biomass accumulation in the 1st section accounted for 28% of total biomass accumulation in the filter; it made the biomass accumulation in other 4 sections was less.

The time-course wet biomass + static liquid holdup is shown in Figure A8-1.

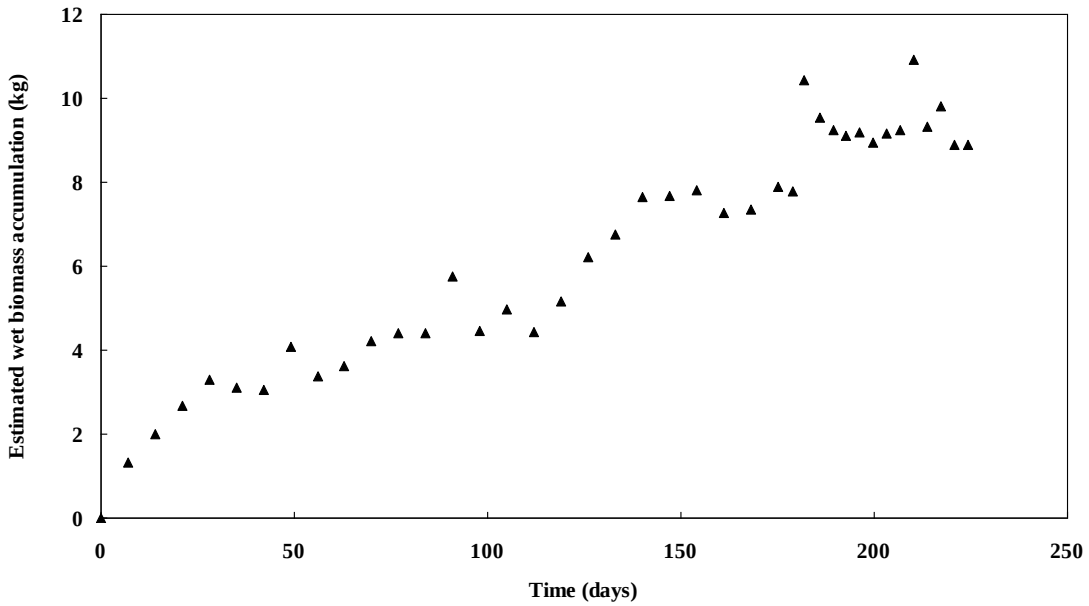

Figure A8-1: Time-evolution of wet biomass and static liquid holdup

From Figure A8-1, after about 30 days, the system achieved the pseudo steady-state. However, the wet biomass contained not only the synthesized biomass but also the

cellular water inside the biofilm. The fraction of dry biomass in the biofilm should be determined by the biofilm measurement.

The estimation of dry biomass fraction over the wet biomass is shown in Figure A8-2.

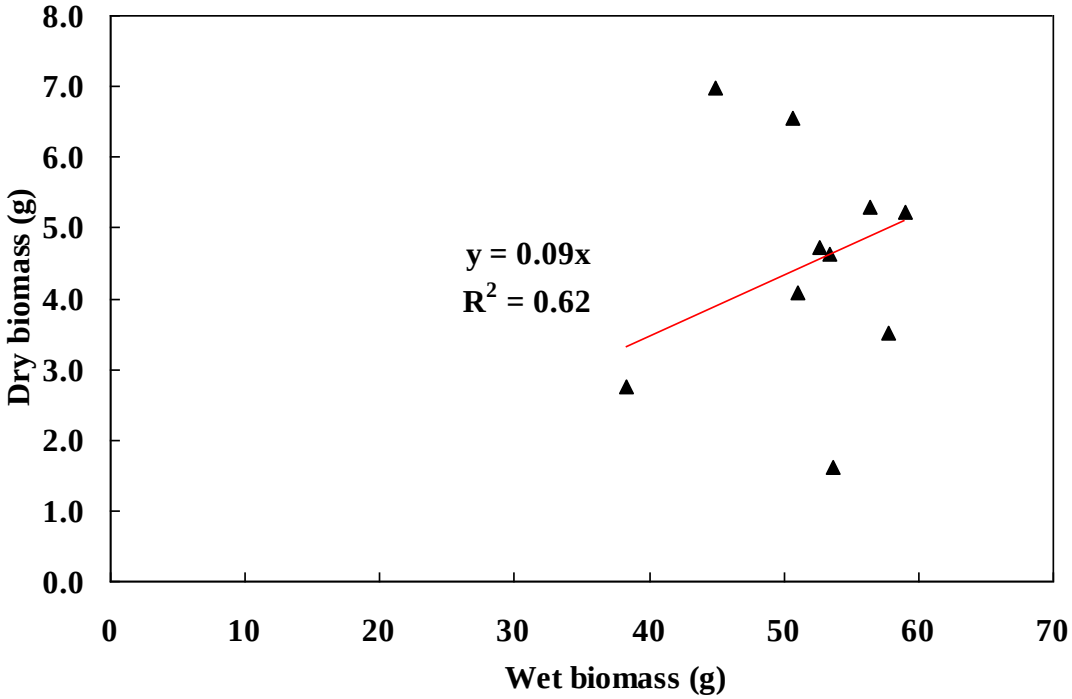

Figure A8-2: Dry biomass fraction estimation versus wet biomass

From Figure A8-2, though the measured data was with great uncertainty, the fraction of dry biomass was estimated as 0.1 of total biofilm (wet biofilm), which was in good agreement with the studies of (Metcalf and Eddy, 1991) that the dry biomass from bacterial synthesis accounted for about 0.1-0.15 of total biofilm mass. Similarly, the dry biomass fraction under high OLR was found close to 0.2 of total biofilm mass.

Therefore, we assumed the biomass from bacterial synthesis accounted for 10% and 20% of the estimated wet biomass in Figure A8-1, under low and high OLR, respectively. The total produced biomass was estimated based on the COD mass balance. The estimated biomass production and net biomass accumulation was plotted in Figure A8-3.

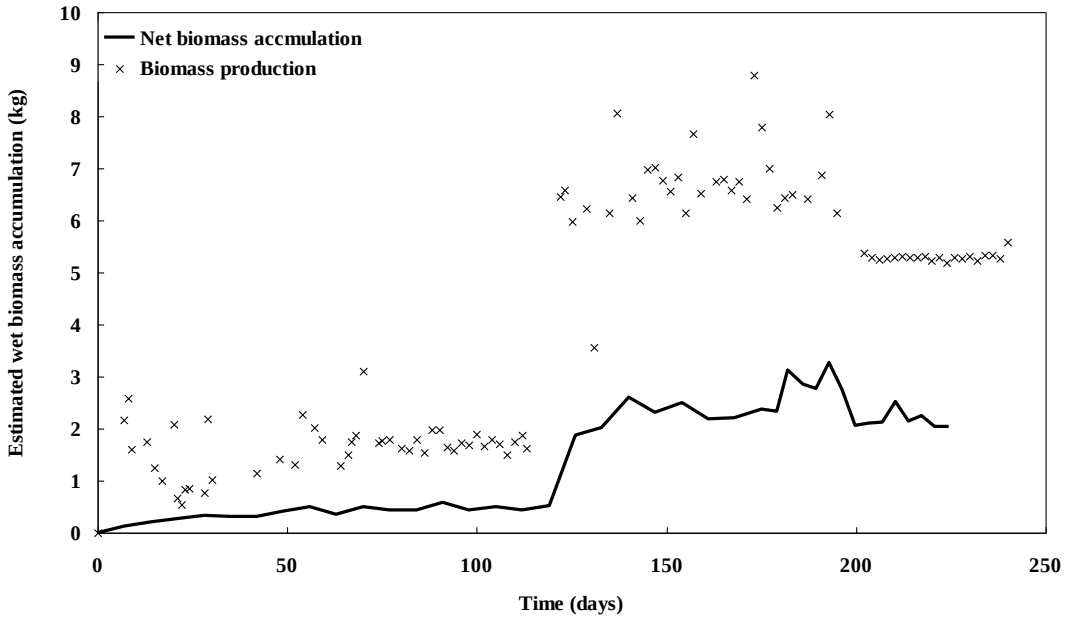

Figure A8-3: Time evolution of estimated biomass production and net biomass accumulation

In Figure A8-3, the difference between the produced biomass and the net biomass accumulation was the detached biomass. The detached biomass under high OLR was higher than that under low OLR. However, due to the entrapment by thicker biofilm in the packing bed, under high OLR, even the detached biomass was higher; majority of the detached biomass was still captured by the packing bed.

Moreover, another manner to estimate the sludge production is applied in this study. Though the estimation of $\mathbf{Y_{g,obs}}$ of 0.11 gCOD/gCOD was acquired in Chapter 4, by the particulate COD measurements at the outlet over the total consumed COD of period 4, similar estimation of this observed yield coefficient is also performed for other periods, but for the final effluent CODp over consumed COD mass. The cumulated CODp mass in final effluent of 3 periods is shown in Figure A8-4 against the cumulated consumed COD mass.

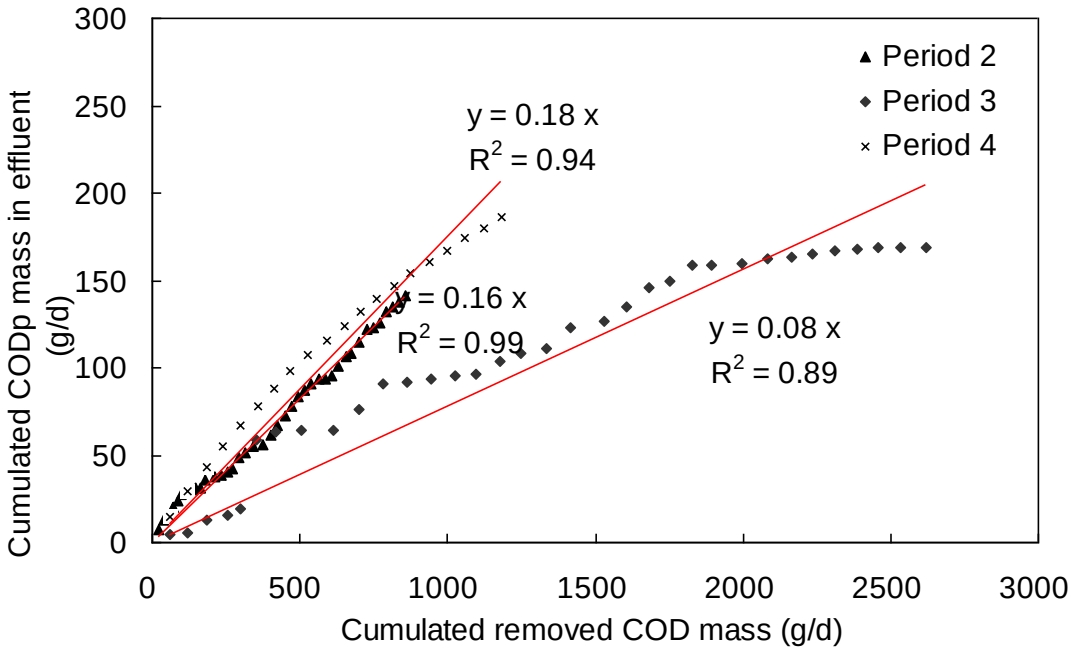

Figure A8-4: Time evolution of estimated biomass production and net biomass accumulation

Figure A8-4 shows higher Yg,obs value than we obtained of 0.11 gCOD/gCOD by section 1 of period 4 as mentioned in Chapter 4. We believe that this estimation could be influenced by the input particulate COD in period 2 and 3, when the particulate COD was applied in the influent, also the detached biomass will influence this Yg,obs value. The Yg,obs of 0.11 gCOD/gCOD was thus used to estimate the sludge production during 3 periods of biological experiments.

This calculation is carried out based on Eq. II- 39; the total sludge production comes from the biomass accumulation and inert particulate COD, when the system achieves the pseudo steady-state. The net biomass accumulation is thus 0.11*consumed COD mass, inert particulate COD accounts for 10% of total inlet COD from the experiments which estimate the fractions of COD components. The sludge production is thus calculated by 0.11* consumed COD mass (CODt,in mass – CODs, out mass) + inert particulate COD mass (0.1* total COD mass).

Figure A8-5 represents the estimated sludge production during period 2 to period 4, compared to the CODp mass in the final effluent of pilot.

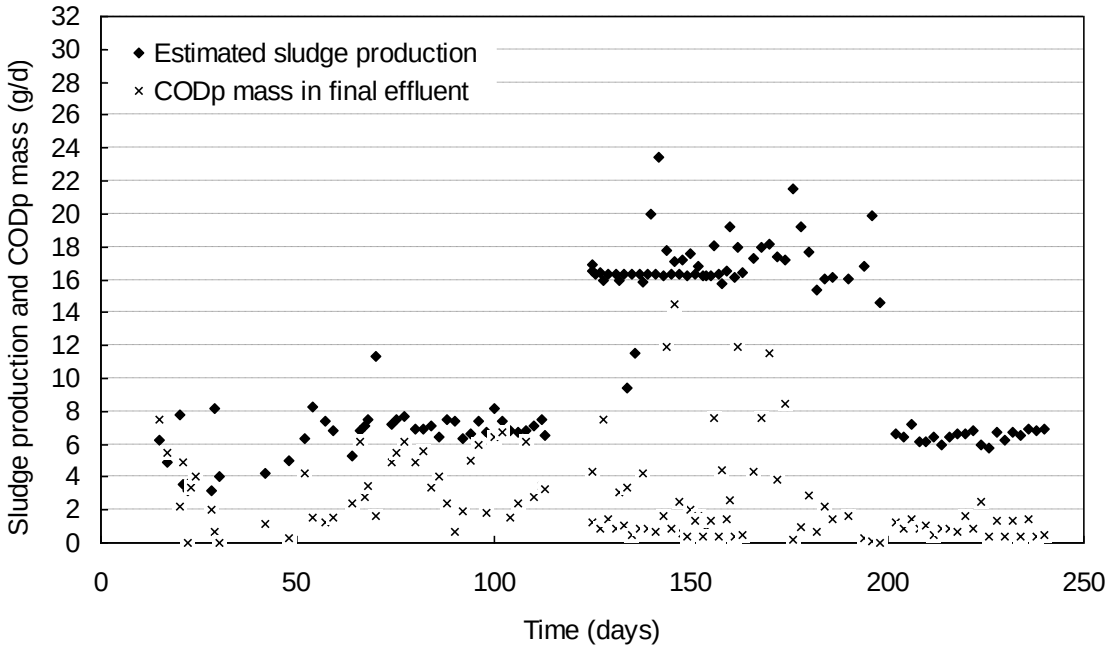

Figure A8-5: Time evolution of estimated biomass production and effluent CODp mass

In Figure A8-5, estimated sludge production based on Yg,obs of 0.11 gCOD/gCOD is much higher than the measured CODp mass in final effluent of pilot. In period 2, the difference is less than that in period 3 and 4, this implies that under lower OLR, sludge production could be influenced by the inlet particulate fractions. During period 3, even at high OLR and with particulate substrate influent; measured CODp in final effluent are much lower than the estimated sludge production. We believe the entrapment of the particulate substrate is more significant than other periods, because particulate substrate formed thicker biofilm. However, there is risk of clogging during period 3.

Appendix 9 - Estimation of $K_L a$ for both COD oxidation and nitrification under high OLR

$$COD_{biomassaccumulation} = Y_{obs} \times Q \times (COD_{t,in} - COD_{s,out})$$

=0.12*0.08 m^3/d*(1000-34) g/m^3=9.27 gCOD/d

In theory, $COD_{inlet} + COD_{accumulated} - COD_{oxidized} = COD_{outlet}$

$COD_{oxidized}=COD_{in}-COD_{outlet}+COD_{accumulated}$

= 1000*0.08-64*0.08+9.27=84.15gCOD/d

SO DO_{demand}= 84.15 gCOD/d *0.44 gO_2/gCOD=37.03 gO_2/d

It is known that the timely contribution AH of oxygen for dimensioning.

$$AH = k_L a C_S V$$

Assuming the temperature is 20 ºC and at 1atm, Cs of saturated oxygen is 9.08 mg/L and V is the packing volume as 0.044 m³. Oxygen transfer coefficient $K_L a$ is calculated as:

$$k_L a = \frac{AH}{VC_S} = 92.7\ d^{-1}$$

Furthermore, for nitrification use.

$N_{assimilated}$(kg/d)=0.1gN/gVSS*1.42gVSS/gCOD*0.12gCOD/gCOD*9.27gCOD/d *0.08m³/d=1.2 gN/d

$N_{nitrifiable}=TKN_{inlet}-N_{assimilated}$ =162*0.08 gN/d-1.2 gN/d=11.76 gN/d

$N_{nitrified}=TKN_{nitrifiable}-TKN_{outlet}$ =11.76 g N/d-6 gN/m^3*0.08m^3/d=11.28 gN/d

It is also known that to oxidize 1mol NH_4^+, 1.87mol O_2 is needed.

So to oxidized 1mg NH_4^+, 4.3 mg O_2 is needed.

The demand of O_2 for the oxidizing NH_4^+ is calculated as:

DO=4.3 gO_2/gN*11.28 gN/d=48.5 gO_2/d

Hence the total oxygen demand is the sum of oxidizing COD and nitrogen as follows:

Total DO_{demand}=37.03+48.5=85.53 gO_2/d

It is known that the timely contribution AH of oxygen for dimensioning.

$$AH = k_L a C_S V$$

Assuming the temperature is 20 ºC and at 1atm, Cs of saturated oxygen is 9.08 mg/L and V is the packing volume as 0.044 m³. Oxygen transfer rate $K_L a$ for both COD biodegradation and nitrification is calculated as: $k_L a = \frac{AH}{VC_S} = 214\ d^{-1}$

Appendix 10 - Estimation of biofilm thickness by optical method

Besides the mechanic method of estimating the biofilm thickness reported in Chapter 2, optical method proposed by (Bakke and Olsson, 1986) was also employed to compare with the results of mechanic method. Figure A10-1 shows the conceptual diagram of the optical method for measuring the biofilm thickness. The disadvantage of this method is that the biofilm samples were cut from the outside surface of carrier which is destructive to the biofilm integrity. Consequently, the measurement of biofilm thickness may deviate from the real biofilm thickness attaching on the media particles' surface.

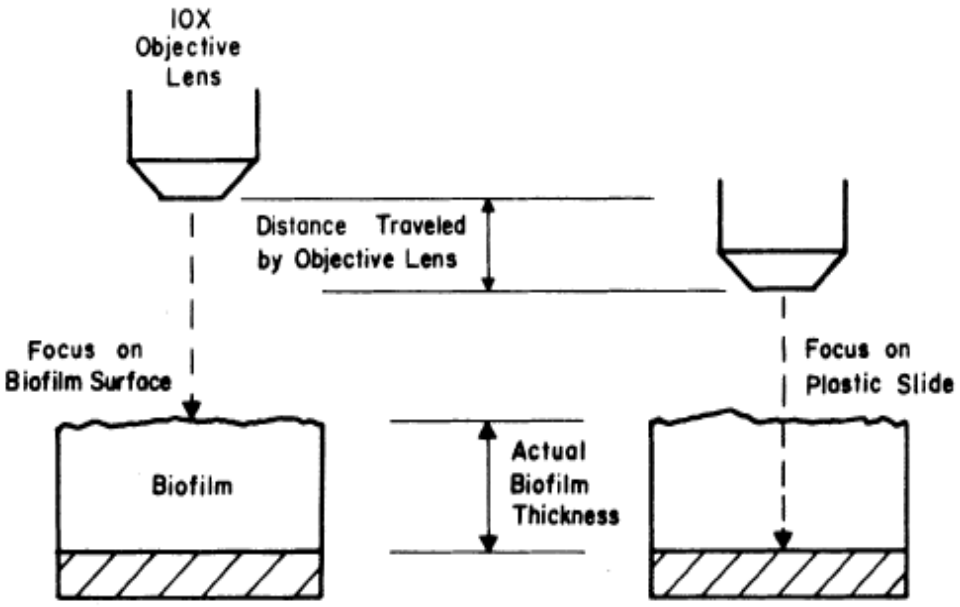

Figure A10-1: Schematic diagram of microscopic observation to determine L_f

An empirical relation was given:

$$L_f = k_f y_f = \frac{n_f}{n_a} y_f$$

$$k_f \approx 1.33$$

where n_f is biofilm refractive index and n_a is the refractive index of the medium interfacing the film between the film and the objective lens (n_a = 1.474 for the glass in this study). L_f denotes the biofilm thickness, y_f is the observed thickness, k_f is the reflective index.

In addition, photos of medium particles coated with biofilm and the packing bed were taken during different experimental periods. Figure A10-2 shows an example of one medium particle coated by biofilm of period 3, before the biofilm thickness measurement by optical method.

Figure A10-2: Medium particle coated with biofilm, in period 3 of biological experiments, high OLR, 1000 CODt input from real WW.

During period 3, with high OLR input, filter flies and worms were observed in the packing bed as shown in Figure A10-3.

Figure A10-3: Photos of filter fly and worms observed in the packing bed and surface of biofilm during period 3, high OLR, real WW.

During period 2 and 4, neither filter flies nor worms were observed. The appearance of flies and worms may due to the high OLR cultivation during period 3 but with particulate substrate, which may cause the partial clogging inside the packing bed. Another reason may be due to high temperature during period 3, because experiments were carried out in summer, at an average indoor temperature of 25ºC.

Résumé

Traitement des eaux usées en milieu rural ou dans les petites collectivités est d'un intérêt croissant. Différentes technologies peuvent être choisies (SBR, RBC, étangs, zones humides, biofiltre ...). L'utilisation d'un filtre d'écoulement combiné avec un système de polissage peut être une solution intéressante, parce que la consommation d'énergie et les besoins de maintenance sont limités. Cependant, cette technologie est difficile à concevoir, car de nombreux procédés faisant intervenir un biofilm répartis dans l'espace et l'hydrodynamique complexes se produisent en parallèle. La nature des médias et de la distribution du biofilm génèrent une hydrodynamique spécifique qui régit le transfert de masse. La concurrence entre l'activité et la nitrification hétérotrophe est souvent décrit, mais seulement à peine profondément analysé. Compétition pour l'espace ou de l'oxygène est évidemment un mécanisme clé qui détermine les performances de TF mais très peu d'œuvres rapport sur cet aspect. Il dépend de nombreux facteurs : le support matériel choisi, le transfert de masse d'oxygène, l'hydrodynamique du réacteur, les charges OLR, NLR, etc.

C'est la raison pour laquelle l'objectif principal de ce travail de thèse a porté sur l'étude de l'élimination de la DCO et de la nitrification dans une nouvelle Multi-Section bioréacteur conçu (MSB), appliqué pour le traitement des eaux usées en milieu rural, mais aussi pour les petites communautés dans les grandes villes. Cette MSB a été développé en Chine afin de traiter des eaux usées urbaines avec une technologie compacte et étroite. Il est maintenant largement rencontré dans la banlieue de la ville de Shanghai par exemple. Afin d'améliorer les performances de traitement et de diminuer les coûts, l'optimisation du MSB est nécessaire. Il a été décidé d'étudier le MSB avec l'approche suivante :

- 1. Une caractérisation de l’hydrodynamique du MSB a été effectuée. En effet, hydrodynamique détermine la distribution du liquide dans la colonne, le temps de contact pour la consommation de Substrat, la contrainte de cisaillement appliquée au biofilm entraînant le détachement de biofilm, et le transfert de masse d’oxygène. Une originalité de notre travail a été effectué à la fois la caractérisation hydrodynamique en présence et en l'absence de biofilm et à différentes conditions de fonctionnement.

- 2. Le MSB a été opéré à différents OLRs et NLR pour étudier sa capacité de remboursement et le retrait d’azote réduite. Travail sur des eaux usées urbaines reconstitué (basé sur les véritables boues primaires) a assuré la représentativité de notre étude. Bilans de masse ont été utilisés pour caractérisé le devenir de la DCO et de la NTK, nitrites et nitrates sur la profondeur du filtre et en fonction du temps. La présence de l'espace aérien entre les cinq sections du réacteur a permis un échantillonnage représentatif à différentes profondeurs de la colonne qui est utile pour obtenir une meilleure connaissance des processus qui se produisent à chaque profondeur.

- 3. Une existante mais jamais testé ruissellement modèle dynamique de filtre a été utilisé afin d'obtenir plus d'idées sur la répartition de la biomasse dans le pilote et d'évaluer le processus limitante dans chaque section du bioréacteur. Une attention particulière a été portée sur la limitation de l'oxygène des activités hétérotrophes et autotrophes. Confrontation entre les résultats des expériences précédentes et les résultats obtenus à partir des simulations ont été effectuées.

Ce travail de recherche a été effectué sous la direction du Professeur E. PAUL dans le

cadre d'une collaboration franco-chinoise entre Shanghai Jiaotong University (SJTU) et l'INSAT. La problématique de ce travail est centrée sur l'analyse des performances d'un lit bactérien à ruissellement pour traiter les eaux usées domestiques de communautés rurales, l'originalité du système repose sur (i) l'utilisation d'un garnissage original de type matériau aggloméré et (ii) une distribution verticale, étagée et disjointe du garnissage dans le lit.

Par conséquent, l'étude de la MSB combiné expériences hydrodynamiques et biologiques avec la modélisation.

Le premier chapitre (environ 50 pages) est dédié à l'état bibliographique de la problématique ciblée. On aborde successivement les points suivants : (i) les principaux systèmes de traitement des eaux usées en milieu rural dont les lits bactériens à ruissellement appartenant à la famille des procédés à culture fixée présentant l'intérêt majeur d'une aération naturelle du milieu réactionnel, (ii) la description d'un biofilm et des mécanismes biologiques associés, (iii) les processus physiques de transfert/transport, (iv) les outils sommaires de quantification des performances et dimensionnement, (v) l'outil de modélisation Biowin et (vi) des données caractéristiques des eaux usées en zones rurales, notamment chinoises.

Le deuxième chapitre (30 pages) est dédié à la présentation des matériels et méthodes. Sont présentés successivement (i) les systèmes pilotes, (ii) les outils de mesure de l'activité biologique et (iii) les relations et grandeurs cinétiques de l'outil de simulation Biowin.

Le troisième chapitre (30 pages) est consacré à la caractérisation de l'hydrodynamique

des réacteurs. Les mesures de différentes grandeurs ont été effectuées sur les deux systèmes pilotes en faisant varier la charge hydraulique, en absence ou présence d'un biofilm mince ou épais. Il est ainsi montré que la rétention statique représente la plus grande fraction d'eau retenue dans le système, du fait essentiellement de la porosité interne conséquente du garnissage, que la rétention dynamique est une fonction croissante de la charge hydraulique et qu'elle diminue en présence d'un biofilm. Les mesures de DTS par injections impulsion d'une solution saline permettent le calcul de temps de séjours moyen et l'analyse de la dispersion au sein du milieu garni. Les résultats mettent clairement en avant une dynamique d'échange entre rétention dynamique et statique très dépendante de la charge hydraulique et de la rétention statique, montrant alors un temps de séjour moyen lié aussi au volume interne du matériau. Par ailleurs, il est bien souligné le rôle du biofilm qui accroît la rétention hydraulique et le temps de séjour moyen. Les mesures de capacité d'oxygénation au travers du paramètre k_La montrent aussi des capacités d'échange importantes au regard de valeurs mesurées sur d'autres systèmes.

Dans le but ultime d'optimiser la conception et l'exploitation TF, l'objectif principal du chapitre 3 était de caractériser le comportement hydrodynamique de deux types de TF (TFC et MSB) rempli avec le même milieu poreux mais différant dans son organisation spatiale (le TFC est un structure proche sans espaces intervalle, le MSB est une structure ouverte avec des espaces d'intervalle). L'impact des propriétés du milieu et de son organisation dans le réacteur sur l'hydrodynamique globale est caractérisé. Cet impact se mesure en terme de fractions rétention de liquide, l'épaisseur du film liquide dans les régimes avec et sans biofilm (conditions deux taux de charge organique de culture ont été appliqués) tout le long de la colonne. Un autre

objectif a été utilisé expériences de DTS et de modélisation pour étudier les changements dans le modèle d'écoulement de liquide et le temps de séjour du liquide due à la présence de biofilm dans le MSB. En outre, l'étude a tenté de vérifier si la configuration du bioréacteur (TFC ou MSB, se concentrent principalement sur la structure de fermeture / ouverture et la présence des espaces d'intervalle) devait modifier ses caractéristiques hydrodynamiques.

Les expériences statiques avec biofilm indiquent que la plupart du liquide est retenu par les particules de support revêtues d'un biofilm, l'augmentation de la rétention statique et, par conséquent, la réduction de la rétention dynamique. Il est également constaté que le hold-up statique liquide permet une plus grande contribution de la rétention dynamique de rétention de liquide au total, en raison du potentiel d'adsorption du milieu de blocs de béton et biofilm, résultant de sa structure poreuse. De plus, le taux de rétention statique n'est pas en corrélation avec la configuration de TF, mais dépend du type de milieu.

Les volumes de liquide efficaces représentés dans la distribution de temps de séjour (DTS) de courbes ne sont pas seulement la rétention dynamique, mais aussi partielle volume de rétention statique, résultant de la libération prolongée de hold-up statique partielle dans le biofilm. L'augmentation des débits, le volume de liquide efficace impliqué dans la DTS première augmente. Cependant, lorsque le débit est trop basse ou trop élevée, le volume effectif réduit, résultant d’un faible débit et à court temps de séjour du liquide, respectivement. DTS expériences montrent également que pour des débits inférieurs, la dispersion et la diffusion de masse entre le liquide et le biofilm est meilleure que celle à des débits plus élevés. L'augmentation de la charge hydraulique

entraîné dans le flux d'écoulement de bouchon s'approche dans le bioréacteur, ce qui entraîne moins de masse dispersion et la diffusion. Le Temps de séjour du liquide (LRT) estimée à partir de modèles de DTS montre que la présence d'un biofilm se traduira par un LRT plus dans le filtre, et donc de favoriser la dispersion de la masse dans le bioréacteur. En comparant le drainage et méthodes DTS permet de montrer que la diffusion et la dispersion peuvent avoir lieu dans le biofilm, ce qui augmente le temps de contact entre le liquide et le biofilm. Trop faible (moins de 9 L / h) ou trop élevée (supérieure à 23 L / h) les débits ne feront pas des avantages de la performance du bioréacteur , résultant de faible volume de liquide efficace et peu de temps de séjour du liquide .

La présence du biofilm a aussi été trouvée pour diminuer l'épaisseur du film liquide par rapport au cas sans biofilm dans les mêmes conditions hydrauliques, en raison de l'aire de surface plus grande et plus petite du volume de rétention dynamique.

L'estimation du coefficient volumétrique de transfert de masse d’oxygène, en fonction de l'épaisseur du film de liquide estimée, montre que, à débit plus faible, le transfert de l'oxygène est meilleur que le débit plus élevé. Lorsque biofilm était présent, le transfert d'oxygène a été promu par rapport à sans biofilm, résultant de film liquide mince. Dans une fourchette raisonnable, augmentation de l'épaisseur du biofilm sous une même condition hydraulique conduit à un meilleur transfert d’oxygène.

En outre, les propriétés physiques du MSB et moyennes, l'épaisseur du film liquide, liquide Temps de résidence, ainsi que le coefficient de transfert d'oxygène estimée obtenue dans ce chapitre est appliqué à Biowin simulateur du chapitre 5 afin d'améliorer la représentativité des simulations.

En termes de prédiction, les études hydrodynamiques peuvent conduire à l'utilisation de la LRT d'apprécier la percolation dans le bioréacteur ainsi que la fraction des zones mortes. Des études futures doivent être effectuées pour déterminer les forces de cisaillement ainsi que le transfert d'oxygène dans le liquide dans les expériences biologiques.

Le chapitre 4 (40 pages) rassemble les résultats illustrant les performances épuratrices du lit étagé au travers notamment de l'élimination des fractions organiques et l'oxydation des composés azotés. Le choix du lit segmenté MSB est de plus très utile pour analyser les performances en fonction de la profondeur du lit par des bilans matières effectués à chaque étage. Les résultats obtenus sur l'unité pilote ont par ailleurs été comparés à ceux obtenus sur une unité industrielle et une unité pilote mises en place sur des sites en Chine et suivies par les équipes partenaires chinoises. Les résultats mettent en avant le rôle majeur dans l'épuration du premier étage recevant l'eau à traiter. Les deux étages suivants ont des performances variables en présence d'une fraction particulaire organique importante dans l'eau d'entrée mettant ainsi en avant le rôle des réactions d'hydrolyse qui libèrent de la DCO soluble. L 'élimination de l'azote Kjeldahl est majoritairement liée à la nitrification et d'une façon moindre à la croissance des espèces hétérotrophes oxydant la matière organique. Les performances de l'unité industrielle fonctionnant dans des conditions assez proches (malgré une charge hydraulique plus importante) apparaissent sensiblement plus faibles que sur les unités pilotes, ces dernières étant favorisées par le transfert d'oxygène offert par l'ouverture des parois latérales des colonnes de laboratoire sans doute conséquent au regard du diamètre des colonnes. Dans tous les cas, les

performances sont importantes avec un abattement de DCO suffisant pour répondre à une norme de rejet de 125 mg/l (en supposant une séparation liquide solide efficace en aval du lit). Les deux derniers étages des colonnes ne servent généralement que de traitement d'affinage. Les calculs de production de boues ne sont pas aisés en raison de la difficulté de quantifier l'accumulation de matière au sein des lits. De même, l'évaluation de l'épaisseur de biofilm reste assez illusoire dans un milieu où l'écoulement des phases reste très hétérogène.

Les expériences biologiques dans le chapitre 4 enquêté sur les performances de nitrification avec élimination de la DCO, et donc la concurrence entre la nitrification et la croissance hétérotrophe. La capacité de MSB est également évaluée en ce qui concerne le colmatage. Nos expériences fournissent des données pour aider à comprendre les différents processus qui se produisent dans le biofiltre, c'est à dire des transformations biologiques, l'attachement, détachement, transfert d'oxygène, liquide répartition. Ils fournissent également des informations pour une meilleure conception et le fonctionnement de ce type de TF (de rendement d'élimination contre OLR et NLR).

Par des expériences biologiques pendant 240 jours, il semble qu'une caractéristique assez classique pour la DCO est observée pour le MSB rapport à un lit bactérien. Une grande efficacité d'élimination est réalisée dans la partie supérieure du réacteur, la capacité de retirer progressivement décroissante avec la profondeur. Par conséquent, les articles 4 et 5 ne jouaient qu'un rôle de " polissage " pour l'élimination de la DCO. Les capacités d'élimination de la DCO élevée (> 93%) sont obtenues pour le pilote sous toutes les conditions opératoires testées. Un colon est bien sûr nécessaire pour récupérer la DCO particulaire.

Plus surprenant, sous haute OLR, la capacité de la DCO est promue. Cette performance promue s'explique par le meilleur piégeage de DCO particulaire et le temps de séjour plus long liquide (que l'on trouve dans les études hydrodynamiques).

Nitrification se produit principalement dans les sections 1 et 2 où plus de 70 % de l'entrée de l'ammoniac est éliminé. Sans limitation d'oxygène, la nitrification atteindre une efficacité réaliste, même dans des conditions où l'élimination de la DCO est promu. Le nitrite est détecté dans la première section, ce qui indique que, sous haute OLR, pas assez d'oxygène est fourni pour assurer l'élimination de DCO et de la nitrification complète. Même sous haute OLR, nitrification principalement eu lieu dans la première section. De la section 4 de l'article 5, moins nitrification se produit en raison d'un manque de ressources de l'ammoniac.

Pour la conception du réacteur MSB, nos études montrent qu'il est en mesure de traiter le taux de charge le plus élevé appliqué dans cette étude. Cependant, les bilans de masse sur la DCO et de l'azote sur soulignent l'accumulation de la biomasse à l'intérieur du filtre. Par conséquent, aucun état d'équilibre n'est atteint dans nos expériences, même après 260 jours de fonctionnement. Même si aucun encrassement n'est observé pendant le temps d'expérimentation, ce problème doit se produire si la durée de fonctionnement est augmentée. Ce comportement est confirmé lors de la pleine échelle pour lesquels l'obstruction est observée après deux années de fonctionnement. Dans ce cas, la solution consiste à changer entre le dernier panier de la première (section de cinq pour un article).

Les performances de notre pilote sont comparées à ceux obtenus dans une usine à grande échelle en Chine. Sous taux similaire de la charge organique mais avec un débit beaucoup plus faible, de meilleures DCO efficacité d'élimination sont obtenus dans notre pilote. Cela implique que le Multi- Section bioréacteur (MSB) peut supporter la charge organique élevée, mais pour optimiser le rendement de la DCO, un faible débit est meilleur. Le rendement de la nitrification dans notre étude est également préférable que dans le réacteur à pleine échelle MSB mais la concentration à l'entrée de l'ammoniac est nettement plus élevée que celle dans le réacteur à pleine échelle MSB. Débit hydraulique inférieur appliqué dans notre étude pourrait conduire à plus Temps de Séjour du liquide (LRT) et plus mince épaisseur du film de liquide, et donc un meilleur transfert de masse et de l'oxygène dans le biofilm. Plus le taux de transfert d'oxygène sur le pilote grâce à un meilleur renouvellement de l'air dans l'espace vide en raison de la structure très ouverte ne peut être ainsi responsable des meilleures performances.

Le cinquième et dernier chapitre (40 pages) est dédié à l'utilisation du logiciel Biowin pour simuler les performances de telles unités. Cette approche intègre (i) une comparaison des performances pour l'élimination de la DCO et de l'azote NTK à charge volumique identique mais avec deux couples « concentrations – débits » différents, (ii) une analyse du rôle du transfert d'oxygène dans le milieu et (iii) une comparaison des profils de concentration entre simulations et expériences. Pour le premier point, les simulations ne montrent pas de différences notables de performances que ce soit par l'emploi d'un lit continu ou d'un lit segmenté (pour lequel la durée de calculs est réduite et permet d'atteindre des conditions stationnaires de fonctionnement, ce qui n'est pas le cas pour le lit segmenté pour lequel les résultats

sont donc minimisés). Les résultats les plus originaux sont sans aucun doute ceux montrant le rôle dominant de la dynamique de transfert d'oxygène au sein du lit au travers de l'intensité du flux d'air circulant. Cette dynamique génère en fait la distribution de l'activité au sein du lit. Cette approche, par méthode inverse, pourrait en fait être utile pour analyser la circulation d'air au sein d'un lit à ruissellement en suivant les performances en différents points d'échantillonnage sur la hauteur du lit. La dernière partie est consacrée à la comparaison de simulations, basées sur les conditions opératoires fixées dans la colonne de laboratoire, avec les résultats obtenus. Dans l'ensemble, l'adéquation entre simulation et résultats est correcte.

Chapitre 5 l'intention de décrire le comportement d'un MSB par simulation en utilisant le logiciel Biowin. L'effet de l'hydraulique et de transfert de masse sur les performances MSB pour la DCO et de nitrification est brièvement étudié. Les simulations sont très utiles pour comprendre la répartition de la population fonctionnelle à l'intérieur du biofiltre et donc de comprendre les capacités d'élimination locales pour élimination de la DCO et de la nitrification. L'accumulation de la biomasse n'est cependant pas bien représentée par le modèle. L'effet de la limitation de l'oxygène sur la nitrification puis sur DCO efficacité d'élimination est caractérisé pour le réacteur MSB. Les résultats, donnant des valeurs de débit d'air, peuvent aider à améliorer la conception d'un réacteur MSB. Cependant, comme l'air est soufflé vers le haut à partir de la partie supérieure du biofiltre, il n'est pas représentatif d'une TF.

Confrontation entre les résultats simulés obtenus pour une concentration élevée en oxygène fixe dans le film liquide DCO et les résultats expérimentaux a été effectuée.

Le modèle permet une assez bonne prédiction de l'élimination de DCO et de nitrification. Une certaine amélioration pourrait être fait pour mieux correspondre à toutes les valeurs de concentration le long de la profondeur du filtre. Ce travail de calibrage n'a pas été effectué.

Modèle et expériences sont en bon accord pour les conclusions suivantes :

- Il est confirmé que la biodégradation et le piégeage de DCO principalement eu lieu dans la section 1, notamment sur le sommet de la section 1under bas OLR, dans un endroit plus profond de l'article 1 sous charge organique haute. L'augmentation de la concentration de OLR et DCO particulier, résultant dans la réduction de la porosité et l'augmentation de la biomasse cellulaire, qui conduit à une meilleure DCO performances d'élimination de DCO soluble seulement avec.

- Grande capacité de nitrification peut être atteinte si le taux de transfert d'oxygène est suffisamment élevé pour fournir de l'oxygène pour les deux populations microbiennes. Dans ce cas, la nitrification peut se produire dans les premières sections du filtre avec la DCO.

Les perspectives de ce travail sont nombreuses :

- 1. Le taux de transfert d'oxygène devrait être étudié parce qu'elle est l'étape limitante qui détermine les performances à court terme du réacteur. Pour ce faire, la capacité de renouvellement de l’air en fonction du gradient de température entre l'air à l'intérieur du réacteur et de l’air à l'extérieur du réacteur doit être déterminée. La configuration géométrique et la taille du réacteur MSB doivent être considérées. En effet, il peut avoir un effet énorme sur le flux d'air à renouveler.

- 2. Le colmatage doit être étudié, mais il s'agit d'une tâche difficile parce que les expériences à long terme doivent être exécutées. L'hydrolyse de la biomasse accumulée doit être analysée. Peut-être une période de repos doit être envisagée pour une partie du réacteur, afin de rétablir la porosité du réacteur.

- 3. Le piégeage de COD de particules doit être mieux caractérisé

- Finalement, ce logiciel peut en apprendre beaucoup, enfin, en utilisant la Biowin sur le comportement des populations microbiennes dans un TF